ERDC/CHL TR-15-14

Coastal and Hydraulics Laboratory

US Army Corps of Engineers®
Engineer Research and Development Center

ERDC
INNOVATIVE SOLUTIONS for a safer, better world

North Atlantic Coast Comprehensive Study (NACCS) Coastal Storm Model Simulations: Waves and Water Levels

Mary A. Cialone, T. Chris Massey, Mary E. Anderson, Alison S. Grzegorzewski, Robert E. Jensen, Alan Cialone, David J. Mark, Kimberly C. Pevey, Brittany L. Gunkel, Tate O. McAlpin, Norberto C. Nadal-Caraballo, Jeffrey A. Melby, and Jay J. Ratcliff

August 2015

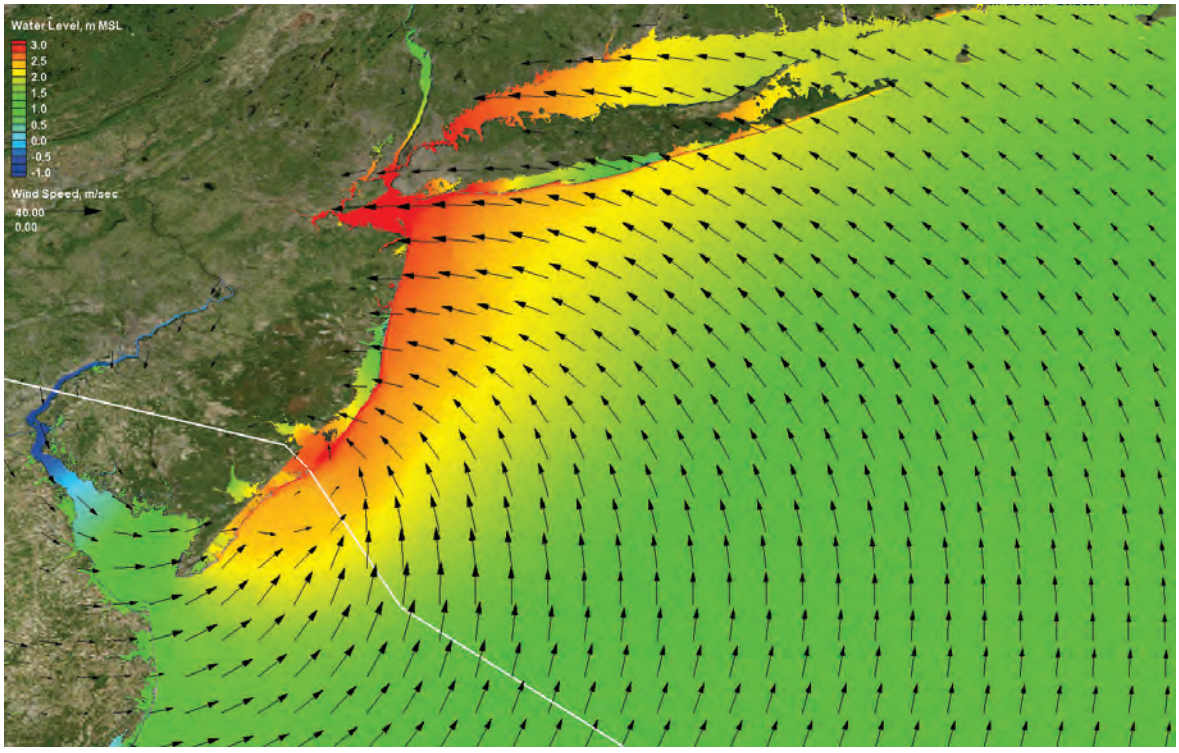

The U.S. Army Engineer Research and Development Center (ERDC) solves the nation's toughest engineering and environmental challenges. ERDC develops innovative solutions in civil and military engineering, geospatial sciences, water resources, and environmental sciences for the Army, the Department of Defense, civilian agencies, and our nation's public good. Find out more at www.erdc.usace.army.mil.

To search for other technical reports published by ERDC, visit the ERDC online library at http://acwc.sdp.sirsi.net/client/default.

ERDC/CHL TR-15-14
August 2015

North Atlantic Coast Comprehensive Study (NACCS) Coastal Storm Model Simulations: Waves and Water Levels

Mary A. Cialone, T. Chris Massey, Mary E. Anderson, Alison S. Grzegorzewski, Robert E. Jensen, Alan Cialone, David J. Mark, Kimberly C. Pevey, Brittany L. Gunkel, Tate O. McAlpin, Norberto C. Nadal-Caraballo, Jeffrey A. Melby, and Jay J. Ratcliff

Coastal and Hydraulics Laboratory
U.S. Army Engineer Research and Development Center
3909 Halls Ferry Road
Vicksburg, MS 39180-6199

Final report

Prepared for U.S. Army Engineer District, Baltimore
City Crescent Building 10, South Howard Street
Baltimore, MD 21201

Under Project 401426, North Atlantic Coast Comprehensive Study

Abstract

This document summarizes the coastal storm wave and water level modeling effort performed in support of the North Atlantic Coast Comprehensive Study (NACCS). This effort involved the application of a suite of high-fidelity numerical models within the Coastal Storm Modeling System (CSTORM-MS). The study was conducted to provide information for computing the joint probability of coastal storm environmental forcing parameters for the U.S. North Atlantic Coast (NAC) because this information is critical for effective flood risk management project planning, design, and performance evaluation. CSTORM-MS modeling produced nearshore wind, wave, and water level estimates and the associated marginal and joint probabilities. Documentation of the statistical evaluation is provided in the companion report *North Atlantic Coast Comprehensive Study (NACCS) Coastal Storm Hazards from Virginia to Maine* (Nadal-Caraballo et al. 2015). In this study, both tropical and extratropical storms were strategically selected to characterize the regional storm hazard. CSTORM-MS was then applied with the wave generation and propagation model WAM, providing offshore, deep-water waves to apply as boundary conditions to the nearshore steady-state wave model STWAVE, ADCIRC to simulate the surge and circulation response to the storms, and STWAVE to provide nearshore wave conditions including local wind -generated waves. Products of this study are intended to close data gaps required for flood risk management analyses by providing statistical wave and water level information for the NAC within the Coastal Hazards System (CHS). The CHS is expected to provide cost and study time efficiencies and a level of regional standardization for project studies.

Contents

Figures and Tables

Figures

Tables

Preface

This study was conducted for the North Atlantic Division under Project Number 401426, North Atlantic Coast Comprehensive Study. The technical monitor for the modeling and statistical analysis was Lynn M. Bocamazo.

The work was performed by the Coastal Processes (HF-C), Harbors, Entrances, and Structures (HNH), Estuarine Engineering (HFE), and Coastal Engineering (HNC) Branches of the Flood and Storm Protection (HF) and Navigation (HN) Divisions, U.S. Army Engineer Research and Development Center, Coastal and Hydraulics Laboratory (ERDC-CHL). At the time of publication, Mark Gravens, James Gutshall, Dr. Robert McAdory, and Tanya Beck were Branch Chiefs, respectively; Dr. Ty Wamsley and Dr. Jackie Pettway were Division Chiefs, respectively; and Mr. William Curtis was the Technical Director for the Flood and Coastal Research Program. The Deputy Director of ERDC-CHL was Dr. Kevin Barry, and the Director was José E. Sánchez.

At the time of publication of this report, LTC John T. Tucker III was the Acting Commander of ERDC, and Dr. Jeffery P. Holland was the Director.

Unit Conversion Factors

Multiply	By	To Obtain
feet	0.3048	meters
miles per hour	0.44704	meters per second

1 Introduction

The goal of the North Atlantic Coast Comprehensive Study (NACCS) modeling effort was to ultimately compute the joint probability of coastal storm forcing parameters for the North Atlantic Coast of the United States as this information is essential for effective flood risk management project planning, design, and performance evaluation. The main focus of the modeling was to generate storm winds, waves, and water levels along the coast for both tropical and extratropical storms. The area of interest (based on U.S. Army Corps of Engineers [USACE] North Atlantic Division areas affected by Hurricane Sandy) was coastal watersheds in the Mid- to North-Atlantic region, from Maine to Virginia. In this region, flood and wind damage from coastal storms have caused negative impacts to the national economy with combined direct costs of over $350 billion for the top seven most-damaging hurricanes. Six of these seven storms have occurred since 2004. In 2012, Hurricane Sandy alone, which made landfall in northern New Jersey as a post-tropical cyclone, accounted for approximately $66 billion in damages and over 200 deaths. With more than 52% of the U.S. population living in coastal watershed counties and the coastal population expected to increase 10% by 2020, the *potential* for damages from future storms is expected to increase as a result of the rise in population density and the accompanying added infrastructure. Potential changes in relative sea level and storm frequency may or may not exacerbate the vulnerability of these coastal communities, depending on future climate conditions.

This study employed modern atmospheric, wave, and storm surge modeling and extremal statistical analysis techniques. The study was performed using the high-fidelity models within the Coastal Storm Modeling System (CSTORM-MS), the Joint Probability Method with Optimal Sampling (JPM-OS) (applied in recent USACE studies [USACE 2006; IPET, 2009]) together with traditional joint probability techniques applied recently in a Federal Emergency Management Agency (FEMA) Risk MAP study (FEMA 2012). The NACCS study produced nearshore wind, wave, and water level estimates and the associated marginal and joint probabilities. This study did not include engineering calculations, such as wave runup, nearshore morphology change, sediment transport, probabilistic analysis of riverine stage, or overland flooding.

For coastal storm forcing, the standard of practice is to estimate the joint probability distribution representing the likelihood of occurrence for combinations of nearshore waves, water levels, winds, overland flooding, river flow, and any other parameters of interest. For recent similar regional USACE and FEMA studies, planetary boundary layer numerical models have been utilized to generate wind and pressure fields that are then used to drive high-fidelity storm surge and wave hydrodynamic models. Waves and water levels were simulated to the nearshore area for historical storm events and/or synthetic events to define a robust statistical population of project storm forcing. The details vary for each of the recent regional studies completed by FEMA and the USACE but generally follow the approach outlined herein. These and other regional studies conducted for hurricane-prone areas have utilized ERDC-CHL-developed hydrodynamic and statistical techniques and numerical models. The NACCS study also exercised these proven strategies.

Prior storm characterization work along the eastern seaboard of the United States is extensive. Storm surge was modeled, and resulting stage-frequency relations were generated for the Fire Island to Montauk Point, NY, area as part of the Fire Island to Montauk Point, NY (FIMP), study (Irish et al. 2005). The study was conducted with the prehurricane-Katrina wave and storm surge numerical models as well as pre-Katrina statistical methods. The modeling methods have since been greatly improved. The statistical approaches for estimating the joint probability of coastal storm response, such as surge and waves, have also been greatly improved within USACE studies as well as FEMA Risk MAP studies. Present approaches include the JPM-OS technique for hurricanes (Resio et al. 2007; Toro 2008) and more traditional joint probability techniques for extratropical storms (Nadal-Caraballo et al. 2012; FEMA 2014). FEMA Region II and III are currently updating base flood elevation maps as part of the Risk MAP program, which has direct parallels to the NACCS study. FEMA has performed a JPM-OS-based analysis of tropical storm surge hazards and an empirical simulation technique (EST)-based analysis of extratropical storm surge hazards. They have applied both a highly detailed and geographical-extensive ADvanced CIRCulation (ADCIRC) mesh and corresponding parameter estimation information for that area. The ADCIRC model for the FEMA study was validated for a series of historical storms, both tropical and extratropical for those regions (FEMA Regions II and III). Because of these extensive, recent studies by FEMA, the modeling grids, bathymetry, and joint probability models available from the FEMA

Region II and III studies were used as a starting point for the central and southern portions of this study and will be described in the grid development section of this report. The northern portion of this study reach (Maine to New York) is part of FEMA Region I where another methodology was applied, and therefore, no JPM-OS-based analysis exists for this region. FEMA Region I therefore required more development for storm selection, forcing conditions, and grid development.

Historical water level and meteorological measurements extend back approximately 100 years along the area of interest. Also, relatively long-term wave measurements extend back into the 1970s while continuous wave and wind hindcasts extend back to 1954. As such, there are considerable supporting data already available that were used to develop comprehensive and accurate joint probability models of coastal storm response. The Joint Probability Method (JPM), JPM-OS, and the development of coastal storm forcing parameters conducted as part of this study are documented in a companion report entitled *North Atlantic Coast Comprehensive Study (NACCS) Coastal Storm Hazards from Virginia to Maine* (Nadal-Caraballo et al. 2015) and characterize the coastal storm hazard for the East-coast region from Virginia to Maine. The primary focus was on storm winds, waves, and water levels along the coast for both tropical and extratropical storm events. Winds, waves, and water levels were computed by applying a suite of high-fidelity numerical models within CSTORM-MS. Products from this work include simulated winds, waves, and water levels for 1050 synthetic tropical events and 100 extratropical events computed at over three million computational locations. A smaller number of save points (18,000) archived the same information at higher frequency for more convenient and concise data handling. The simulated storm events were determined to span the range of practical storm probabilities. The water levels were modeled in such a way that the contribution to total water level from storm surge, tide, and sea level change can be assessed.

The products of this work are intended to close gaps in data required for flood risk management analyses by providing statistical wave and water level information for the entire North Atlantic coast within the Coastal Hazards System (CHS). The CHS is expected to provide cost and study time efficiencies and a level of regional standardization for project studies compared to developing individual, project-specific coastal storm hazard information as is the current practice. The statistical database can potentially be revised based on estimates of future climatology. The CSTORM-

MS platform provides the raw model data (winds, waves, and water levels) as well as processed data (visualization products and statistics) and is available through the internet-based CHS. These data are available for engineering analyses and project design for coastal projects from Maine to Virginia.

This report documents the storm selection process, development of wind and pressure fields, model development and validation, production system development, and modeling of production storms.

2 Storm Selection

2.1 Introduction

This chapter provides a summary of the storm selection process as detailed by Nadal-Caraballo et al. (2015). Storm-induced damages and the economic impact to the NACCS coastal region are primarily due to tropical, extratropical, and transitional storms. It is standard practice to group the storms into statistical families of tropical and extratropical with transitional storms that were once tropical being mostly categorized as tropical. Extreme value theory requires any given population of extreme events being analyzed to be homogeneous. Tropical and extratropical storms are independent, nonidentically distributed populations, and when practical, they must be analyzed separately. For the NACCS, storms were strategically selected for both populations or groups (tropical and extratropical) to characterize the regional storm hazard. Extratropical storms were selected using the method of Nadal-Caraballo and Melby (2014) with an observation screening process. The result was an efficient sample of historical extratropical storms that were then simulated using climate and hydrodynamic numerical models as described in Chapters 4 through 7. The tropical storm suite (consisting of synthetic events) was developed using a modified version of the JPM methodology (Ho and Myers 1975) with optimized sampling JPM-OS methods from Resio et al. (2007) and Toro et al. (2010). In this process, synthetic tropical storms are defined from a joint probability model of tropical cyclone parameters. The cyclone parameters describe the storm size, intensity, location, speed, and direction. These storms are also simulated using climate and hydrodynamic models. This approach to statistical sampling is specifically designed to produce coastal hydrodynamic responses that efficiently span practical parameter and probability spaces specific to the study area.

2.2 Storm selection process for extratropical cyclones

The screening and sampling of extratropical cyclones was limited to screening from water level and meteorological observations. As part of this process, the storm surge response (nontidal residual) was estimated as the difference between the verified observed water level and the astronomical tide. Approximately 40 National Oceanic and Atmospheric Association (NOAA) water level stations were initially identified, but ultimately 23 sta-

tions were retained based on the criterion of having at least 30 years of verified hourly measurements. The preliminary screening of the 23 NOAA stations resulted in the sampling of approximately 250 extratropical storms for the entire NACCS region. This number was reduced to an optimal amount using the Composite Storm Set (CSS) method (Nadal-Caraballo et al. 2012). Employing this approach, storms were screened and sampled using the peaks-over-threshold (POT) technique from the 23 NOAA gages, and the highest ranked storms (largest water level values) among all stations were retained to constitute the CSS. The storms list from screening water level observations was cross checked with atmospheric observations to further identify storms.

Based on sensitivity analyses, it was determined that a CSS of 100 storms was adequate to capture the extratropical cyclones response statistics in the NACCS region. Therefore, the number of sampled storms was reduced to an optimal set of 100 historical extratropical cyclones. These storms are listed in Appendix A: NACCS Historical Extratropical Cyclones.

2.3 Storm selection process for tropical cyclones

Storm selection for tropical storms, or transitional storms that were previously tropical, began by assembling historical data from authoritative sources, such as the HURDAT2 database distributed by NOAA (Landsea and Franklin 2013). Although the entire HURDAT2 data set dating from 1851 to 2013 was used to discern parameter ranges, the data used for the quantitative analysis corresponded to the period 1938–2013, roughly corresponding to the period of modern aircraft reconnaissance missions. Using the entire 1851–2013 record would have resulted in underestimation of storm recurrence rates of up to 45% (Nadal-Caraballo et al. 2015). Tropical cyclone parameters for storms that impacted the region from Virginia to Maine were collected. The primary parameters considered were

- landfall or reference location, x_o
- heading direction, θ
- central pressure deficit, Δp
- radius of maximum winds, R_{max} or RMW
- translation speed, V_f.

Holland B is a secondary parameter that is also considered in the joint probability analysis. It is a function of R_{max} and latitude. These storm parameters were required as inputs to the planetary boundary layer (PBL) model used for the generation of wind and pressure fields used to force the

hydrodynamic models. Storms were segregated into three spatial regions and by landfalling and bypassing criterion (Figure 2-1). Spatial discretization is essential for characterizing the variability of storm parameters as a function of latitude. Storm parameter marginal distributions from the above list of parameters were developed and discretized and combined into regional joint probability models. The joint probability model was critical to the storm selection process because storms are synthesized from the discrete joint probability distribution.

Figure 2-1. Three regions identified for selecting storms.

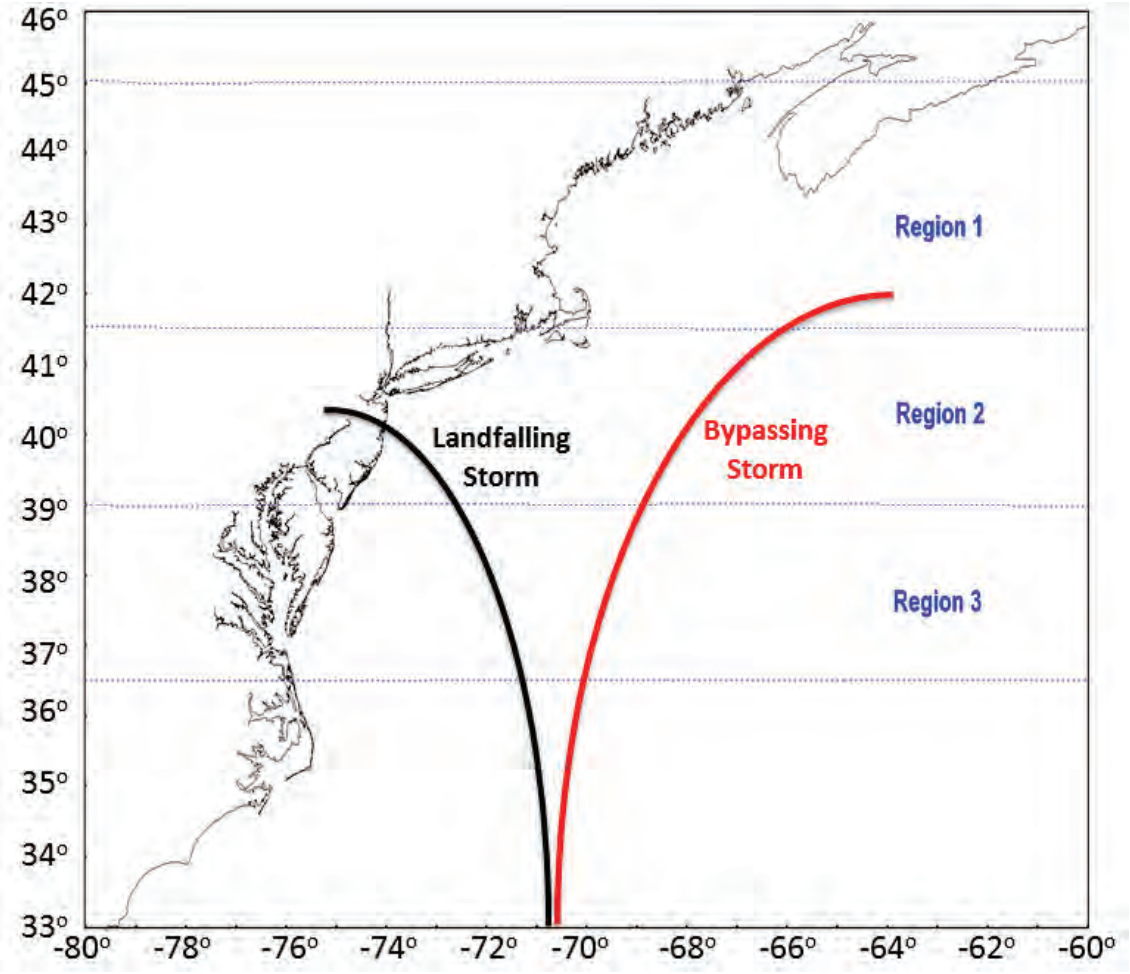

The product of the probability model discretization is a suite of storm parameter combinations listed in Table 2-1. The parameter ranges exceed the historical record but reasonably represent extreme potential storms.

Table 2-1. Discrete values of synthetic tropical cyclone parameter marginal distributions.

Tropical Cyclone Parameters	NACCS Subregion 3	NACCS Subregion 2	NACCS Subregion 1
θ	-60°, -40°, -20°, 0°, +20°, +40°	-60°, -40°, -20°, 0°, +20°, +40°	-60°, -40°, -20°, 0°, +20°, +40°
Δp	From 28 to 98 hPa at 5 hPa intervals	From 28 to 88 hPa at 5 hPa intervals	From 28 to 78 hPa at 5 hPa intervals
R_{max}	From 25 to 145 km, median of 54 km	From 25 to 158 km, median of 62 km	From 26 to 174 km, median of 74 km
V_t.	From 12 to 59 km/h, median of 27 km	From 14 to 88 km, median of 45 km	From 16 to 83 km, median of 49 km
Holland *B*	From 0.45 to 1.32	From 0.56 to 1.35	From 0.66 to 1.37

Landfalling storms have track headings of -60, -40, -20, and 0 deg (positive angles are clockwise from North) at the point of landfall. At landfall, storms had linear tracks with a starting location of 35.0 deg N, 76 deg W, with parallel track spacing determined by the landfall region location. In all, 130 master tracks were developed. Of these, 89 were landfall track paths. All landfalling tracks applied a constant heading from 250 km prior to and post landfall. A natural spline fit was applied prior to (farther offshore of) the 250 km offshore reference location to result in track path consistent with climatology. Bypassing storms had track headings of 20 deg and 40 deg (clockwise from North). The bypassing storm set applied storm parameters specified over the entire latitudinal range of each region (i.e., NACCS subregions 3, 2, and 1). Bypassing storms had linear tracks with parallel track spacing starting from each region's southern latitude. Forty-one bypassing track paths were developed. All bypassing tracks applied a constant heading within each region and transitioned using a spline fit to climatologically consistent track paths outside the region latitudinal limits. For NACCS, the track path spacing was varied across the three NACCS subregions. The final master track spacing used for subregions 3, 2, and 1 were 60 km, 67 km, and 74 km, respectively. The resulting 130 master tracks are listed in Appendix B: Synthetic Tropical Cyclone Master Tracks.

In the landfall set, the storm parameters were constant until a reference location 250 km from the point of landfall was reached. Then, prelandfall filling of the storm parameters was applied. The prelandfall filling rates were determined based on HURDAT2 data for 45 historical storms. This same set of historical storms was used in the development of the JPM parameter set.

To reflect infilling, a 5% reduction in central pressure was applied from the 250 km offshore point to the coastline. This reduction profile was applied to the central pressure deficit prior to landfall for the JPM storm set. Since both Holland's B and RMW depend on central pressure deficit, these parameters were also recomputed during the prelandfall filling. An example of prelandfall filling of storms is shown in Figure 2-2.

The combination of parameter variations resulted in a total of 1050 tropical storms as listed in Appendix C: NACCS Synthetic Tropical Cyclones. Three variations of the 1050 tropical and 100 extratropical storms were modeled for this study.

- The first set, or base condition, was modeled on mean sea level with wave effects but without astronomical tides or long-term sea level change.
- The second set consisted of the same base condition as described in the first set but with each storm modeled on a unique randomly selected tide phase.
- The third set was the same as the second set except that it was modeled with a static water level adjustment of 1.0 m to simulate a potential future global sea level rise (GSLR) scenario.

An additional set of results was developed by linear superposition of 96 randomly selected tide phases to the base condition set. The main differences between this and the second set of results are that for this set, the tides were linearly added to the base condition water levels while in the second set, the tide was modeled along with the base condition processes as part of the hydrodynamic simulations. Also, a total of 96 random tide phases per storm were incorporated into the additional set whereas just one random tide phase storm was included in the second set.

Figure 2-2. Example of along-track variations for landfalling tropical cyclones.

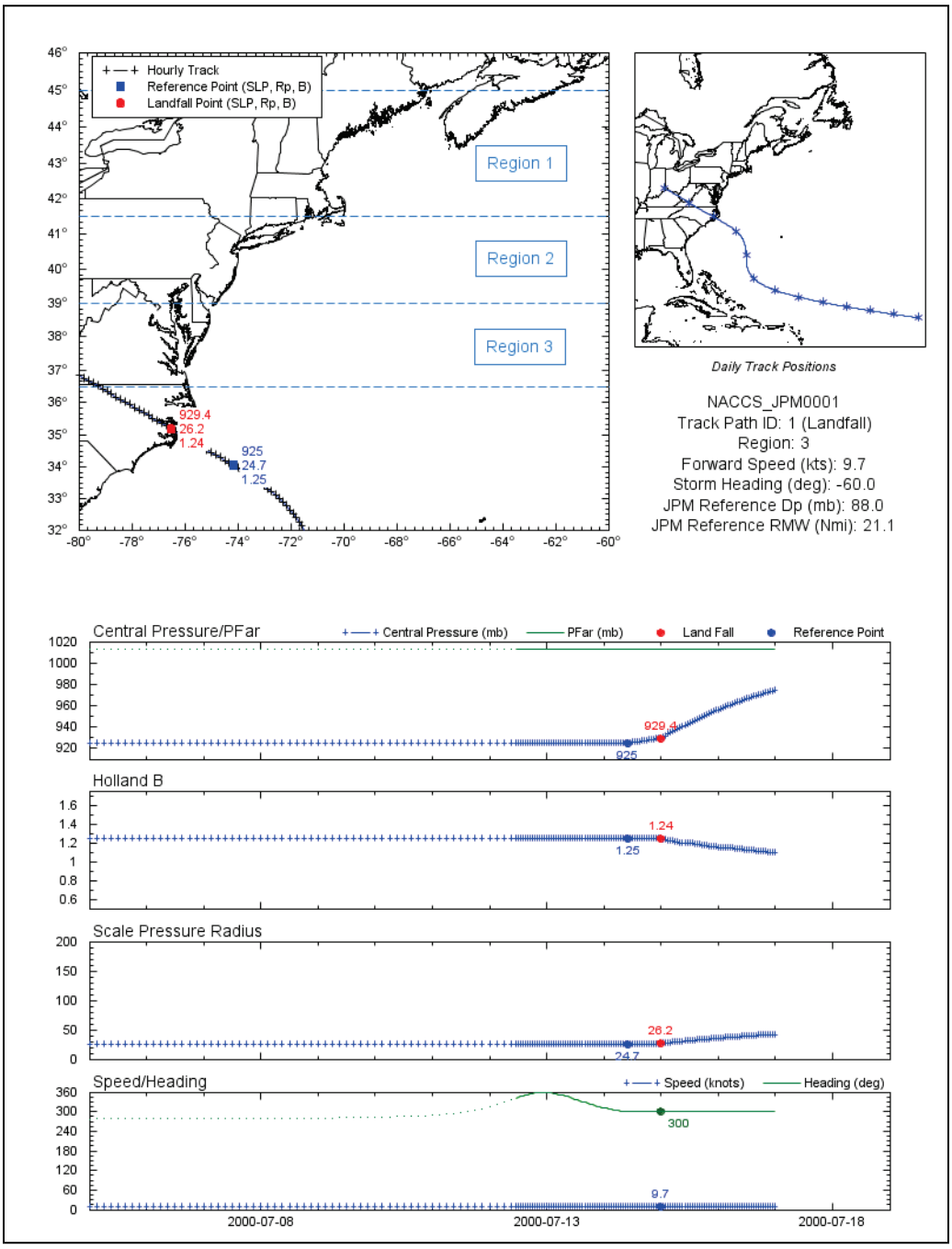

Note: The variables depicted in Figure 2-2 are defined as follows: *SLP* is the sea level pressure, equivalent to far-field pressure (PFar); *Rp* is the scale pressure radius, analogous to R_{max} or RWM; *B* is Holland *B*; *Dp* is the central pressure deficit, equivalent to Δp; Forward Speed is the translation speed; and Storm Heading is the heading direction.

3 Coastal Storm Modeling System (CSTORM-MS)

The CSTORM-MS is a comprehensive methodology and system of highly skilled and highly resolved numerical models used to simulate coastal storms. Analysis of CSTORM-MS model results can be used to assess flood damage risk to coastal communities. With physics-based modeling capabilities, CSTORM-MS integrates a suite of high-fidelity storm modeling tools that can support a wide range of coastal engineering needs for simulating tropical and extratropical storms, wind, wave, and water levels and for representing the coastal response, including erosion, breaching, and accretion due to the storms (Figure 3-1). CSTORM-MS rigorously represents the underlying physical processes involved in coastal storm modeling and makes use of a powerful and user-friendly graphical user interface (GUI) within the SurfaceWater Modeling System (SMS). The CSTORM-MS GUIs within SMS allow for efficient configuration of models that are generally applicable to a wide range of modeling scenarios and are required for accurate risk assessment of coastal storms. For the NACCS numerical modeling study, the primary modeling emphasis was to produce wind, surge, and wave frequencies in the coastal zone. Accordingly, the CSTORM-MS was applied with the following models:

- WAM for producing offshore deep water wave boundary conditions for the nearshore steady-state wave model STWAVE.
- ADCIRC model to simulate the surge and circulation response to the storms. The ADCIRC and STWAVE models were applied in a tightly coupled mode using the CSTORM-MS coupling framework.
- STWAVE to provide the nearshore wave conditions including local wind generated waves.

Figure 3-1. Schematic of CSTORM-MS workflow.

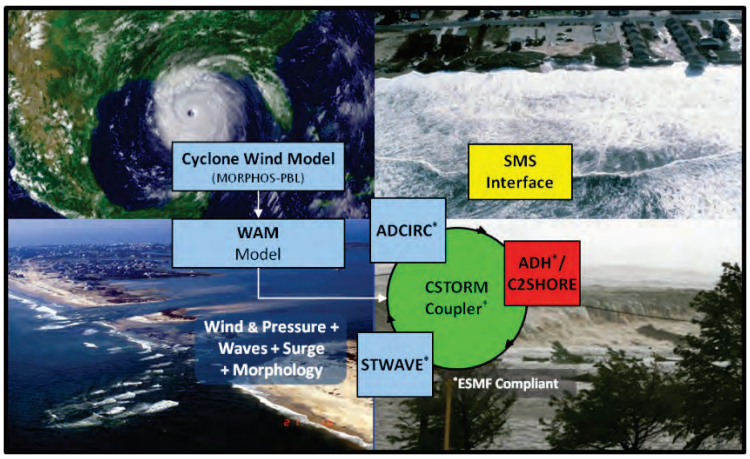

The CSTORM-MS coupling framework options used for the NACCS numerical modeling study tightly linked the ADCIRC and STWAVE models in order to allow for dynamic interaction between surge and waves. The ADCIRC model provided the STWAVE model with updated water surface elevations along with wind fields, and in turn, the STWAVE model provided ADCIRC gradients of wave radiation stresses. The execution of each model and the interchange of information between the models were controlled by the CSTORM-MS coupling framework. This type of coupling system is referred to as being tightly coupled. The information exchange between models takes place via computer memory to allow for fast and efficient sharing of information. ADCIRC and STWAVE can each produce a file record of the input conditions that were supplied to them by the coupler. These records are useful for quality control purposes and for performing additional simulations in a noncoupled mode.

A description of the winds and pressure fields is provided in Chapter 4. An overview of the offshore wave model WAM is given in Chapter 5. The applications of ADCIRC and STWAVE are found in Chapter 6 and 7, respectively. The Coastal Storm Modeling Production System (CSTORM-PS) is described in detail in Chapter 8.

4 Wind and Pressure Field Generation

4.1 Historical extratropical storms wind and pressure fields

Oceanweather Inc. (OWI) generated extratropical wind and pressure fields for the 100 historical extratropical events identified in the storm selection process for the NACCS effort (Appendix A: NACCS Historical Extratropical Cyclones). A summary report detailing this effort was produced by OWI and provided to ERDC for review and reference (Oceanweather Inc. 2014). As mentioned in Chapter 2, the list of storm dates provided to OWI for generation of extratropical wind and pressure fields was identified by ERDC based on a peaks-over-threshold process. A second list of 25 substitute storms was identified by ERDC in the event that any of the selected storms were later determined by OWI to be a nonevent (convective [rain] storm). Three such nonstorm events were identified by OWI during their analysis (Storms 71, 3, and 9); therefore, OWI generated wind and pressure fields for Storms 101, 102, and 103, respectively, in place of the nonevents (Appendix A: NACCS Historical Extratropical Cyclones).

Prior to the NACCS Study, OWI developed the WIS (Wave Information Study) Level II wind fields on a 0.25 deg grid, covering the domain 22–48 deg N, 82–52 W for the 1980–2011 time period. These wind fields applied adjusted National Center for Environmental Research (NCER)/National Center for Atmospheric Research (NCAR) reanalysis wind fields as a base, then assimilated NDBC* buoy/C-MAN† stations and manually reanalyzed storm events using the Interactive Objective Kinematic Analysis (IOKA) methodology (Cardone and Greenwood 1993; Cox et al. 1995). Storm analysis for the WIS Study was primarily offshore (wave driven) rather than nearshore/coastal, which is an essential component of the NACCS storm surge modeling.

Wind fields for the NACCS study were developed for the 100 storm set on two working grids: the original WIS Level II domain as well as a 0.125 deg domain covering 36–45 deg N, 78–66 deg W (NACCS domain covering Virginia to Maine) (Figure 4-1). Storm analysis consisted of re-evaluation

* National Data Buoy Center

2 Coastal-Marine Automated Network

of the storm core of winds generating the maximum ocean response and included the assessment and assimilation of coastal station data such as National Weather Service reporting stations and National Ocean Service stations not considered as part of the WIS effort. Background wind fields were sourced from the NCEP/NCAR reanalysis for the 1948–2012 periods, preserving the enhancements applied in the WIS effort. Storms prior to 1948 were developed from the NCEP 20th Century Reanalysis project. Matching pressure fields on both grids were sourced from reanalysis products and interpolated onto the WIS/NACCS grids. Each storm event produced by OWI contains 8 days of wind/pressure fields with the core of manual reanalysis (8 hours of meteorologist time per storm) spent on the coastal domain of the storm with high wind forcing. The reader is referred to contractor report *Development of Wind and Pressure Forcing For the North Atlantic Coast Comprehensive Study (NACCS)* (Oceanweather Inc. 2014) for more information.

Figure 4-1. WIS Level II and NACCS wind and pressure domains.

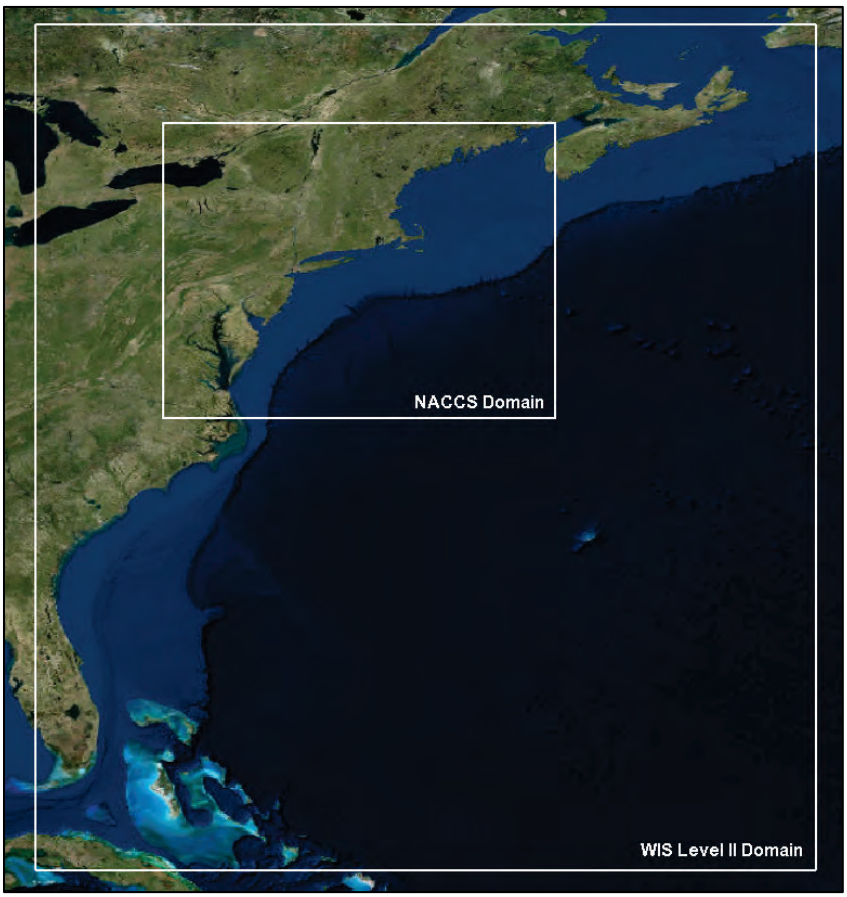

4.2 Synthetic tropical storm development

In addition to the extratropical storm wind and pressure fields developed by OWI for the NACCS study, OWI provided development support and analysis associated with the generation of synthetic tropical storm wind and pressure fields. Data provided to OWI by ERDC for this task included the landfall/closest approach location (latitude/longitude), central pressure (C_p), radius of maximum winds (R_{max}), and storm heading and forward speed for approximately 1050 synthetic events. OWI was responsible (with input from ERDC) to expand these landfall parameters into a full track time history to drive the ERDC Tropical Planetary Boundary Layer (PBL) Model developed by OWI as part of the MORPHOS (now CSTORM-MS) project. OWI required additional data from ERDC including the HURDAT storm parameters applied by ERDC for the development of the landfall statistics to ensure that the analysis done by OWI was based on a consistent set of input data.

Parameters supplied by ERDC for the 1050 synthetic set were evaluated by OWI to ensure that they were consistent with real storms previously designed and applied by OWI with the tropical PBL model. This task was not intended as a full evaluation (which would entail repeating the full analysis) but rather a check on the inputs provided to identify combinations of parameters that may fall outside previous modeling experience.

The development of a track path both pre- and postlandfall followed the same basic methodology as was applied in OWI's contribution to the FEMA Region IV Georgia/North Florida Surge study. Storm speed remained constant for the storm duration by applying the landfall speed specification supplied by ERDC. Postlandfall, the storm heading was preserved for a suitable amount of time (usually 24 hours) to allow sufficient spin-down time for the response (surge and wave) models. Prior to landfall, an analysis of mean track paths for three regional stratifications supplied by ERDC was evaluated to recommend a suitable turning rate (by stratification, if needed) of storm heading so that synthetic track paths were consistent with the historical record. Typically, the storm was modeled 3–5 days prior to landfall or the closest approach to land to allow sufficient spin-up time for the ADCIRC model.

An analysis of *high intensity* (C_p < 965 mb) and *low intensity* (965 < C_p <=985) HURDAT storms (intensity thresholds defined by ERDC) was performed to evaluate if a prelandfalling C_p algorithm should be applied. The

extent and application of prelandfall filling was subject to approval by ERDC. Storm conditions well away from the study area remained steady state as has been applied in previous FEMA work. The Vickery filling model was applied postlandfall. The Vickery model relates the weakening of a storm at landfall to its translation speed, pressure deficit, and radius of maximum winds at landfall. ERDC provided algorithms to OWI to set the appropriate Holland's B and RMW values for any prescribed change in C_p so each synthetic storm was consistent with the methodology applied by ERDC at landfall. Additional model parameters, such as the conversion from RMW to the scale pressure radius (R_p), were determined with approval from ERDC.

Generation of synthetic tropical storm wind and pressure fields from 3–5 days prior to landfall or closest approach to land to 1 day postlandfall was accomplished with the tropical PBL model. Wind (WIN) and pressure (PRE) output files of 10 m wind and sea level pressures were made on two target grids. The same WIS Level II and NACCS domains described in the extratropical wind and pressure field development were applied with the synthetic tropical storms.

Sample images of wind and pressure fields for Storm 1050 for the NACCS domain are shown in Figure 4-2 and Figure 4-3, respectively. In addition, quality control figures for both the model inputs and outputs were produced and are documented in the contractor report *Development of Wind and Pressure Forcing For the North Atlantic Coast Comprehensive Study (NACCS)* (Oceanweather Inc. 2014). Data were delivered from OWI* to ERDC and uploaded to the ERDC high-performance computer (HPC) for application to the NACCS modeling study.

* Contract No. W912BU-10-D-0002/0014

Figure 4-2. Wind field snapshot for Storm 1050 for the NACCS domain.

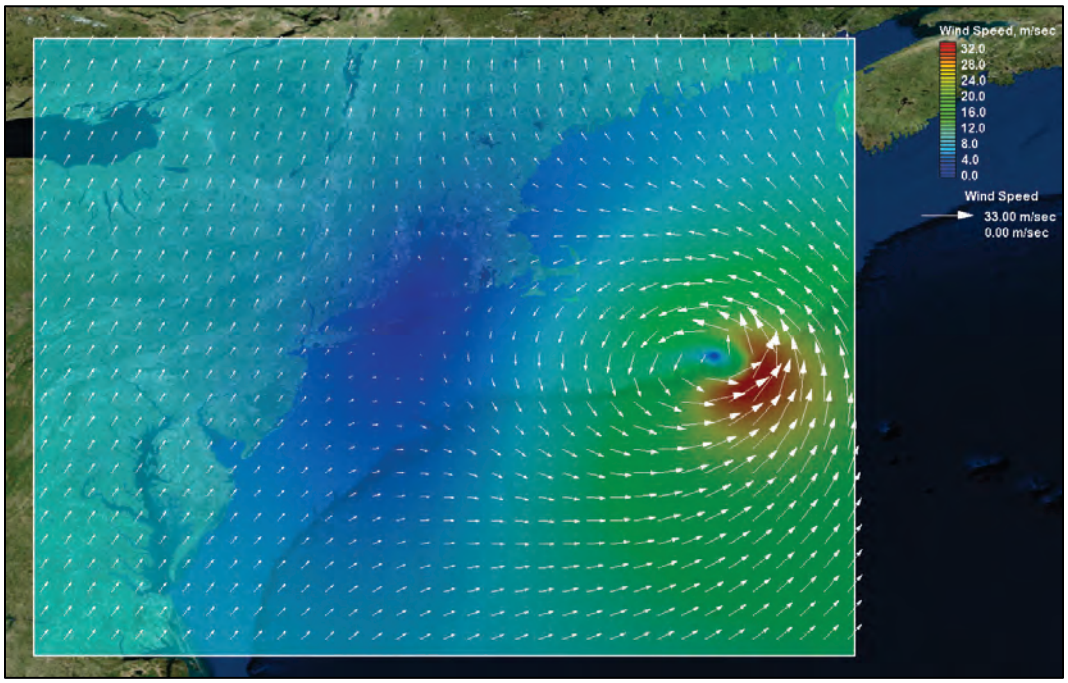

Figure 4-3. Pressure field snapshot for Storm 1050 for the NACCS domain.

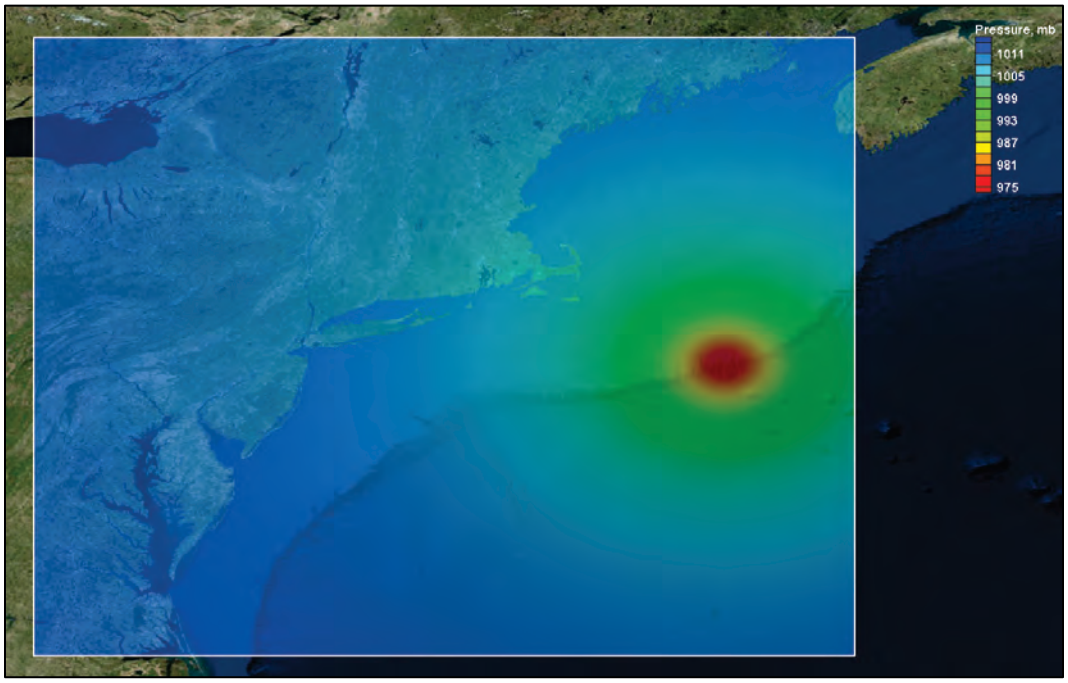

5 Offshore Wave Generation

5.1 Introduction

The primary motivation of the Offshore Wave Generation task in NACCS was to estimate offshore wave conditions during the extratropical extreme storm events (100 selected events) and synthetic tropical storm events (1050 individual events) to be used by STWAVE (Massey et al. 2011b) in assessing the net impact of the contribution of waves on the overall water level estimates.

The NACCS domain (Figure 5-1) spans from the U.S.-Canadian border to just south of the Chesapeake Bay. To properly account for active wave generation derived from model simulations, the wave model domain is defined to the southern tip of Florida and accompanied with higher-resolution coastal domains extending to the South Carolina-Georgia border. The wave climate in the NACCS domain can be generalized as a mixed, locally generated, wind-sea component and swell environment. Extratropical storm systems in the NACCS are dominated by Nor'easters that develop in response to the large temperature gradient resulting from the Gulf Stream and cold air masses coming from Canada. The larger the temperature gradient between the two air masses, the greater the turbulence and instability and more severe the storm can become. As the migration of these low-pressure centers move in a northeasterly direction, they can intensify or attenuate based on the loss of cold air that is the energy source for the development of these storm systems. These events can originate as far away as the Gulf of Mexico as in the case of the Storm of the Century (Cardone et al. 1996). These storms elevate the offshore waves, increase water levels along the coast, and produce an abundance of precipitation on land. In some instances as these Nor'easters lift toward the northeast, they lose intensity, resulting in a very different, and generally lower wave climate north of Cape Cod in the Gulf of Maine as compared to the New Jersey-south shore of Long Island. Nor'easters can also form from the merging of several weaker storms as in the case of the Perfect Storm (October 1991) (Cardone et al. 1996) in which warm air from a low-pressure system coming from one direction, a flow of cool dry air generated by a high-pressure system from another direction, and tropical moisture resulting from Hurricane Grace combined forming a massive, extreme storm affecting the New England coast. A Nor'easter generally reaches its

maximum intensity while off the Canadian coast and can meander in the North Atlantic for weeks at a time. Through the lifecycle of a Nor'easter, the resulting wave climate along the coast is initially dominated by local wind-seas increasing in magnitude as the winds increase; then, as the storm lifts to the northeast, the local wave climate would transition to long-period swell energy. Conversely, tropical systems are rare events, but they do exist in the NACCS domain and can have a devastating effect along a coastline. In general, as a tropical system moves north of Cape Hatteras, NC, there is a tendency for the forward speed to increase. In addition, the tropical systems are also modulated by synoptic-scale systems (e.g., combining with low-pressure centers, picked up by fronts) and affected by the jet stream. These systems are rare and follow random track positions. Landfalling and bypassing tropical events can have an impact on the NACCS domain, elevating the offshore wave climate, increasing the water levels along the coast, and producing an abundance of precipitation on land.

Figure 5-1. Offshore wave model regional and subregional domains and NOAA NDBC sites used for extreme-wave storm analysis.

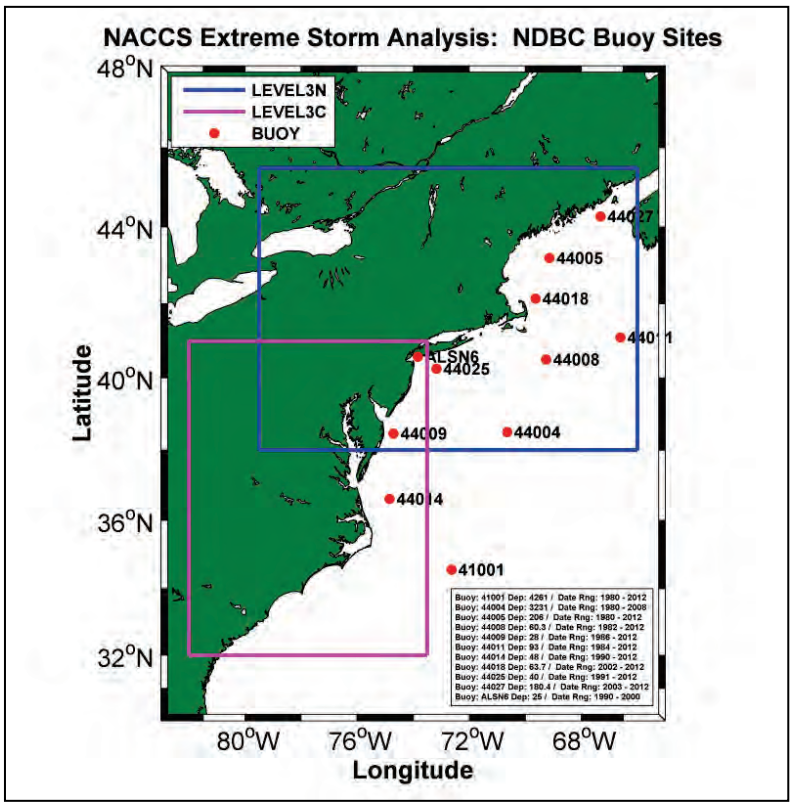

The local wave climate of the NACCS becomes more complex with distance into the Atlantic Ocean basin. Thompson (1980) indicated from a series of

wave gages positioned along the Atlantic coast that the wave climate is dominated (65%) by multiple wave systems occurring at the same time. For the evaluation of extreme storm events, especially the extratropical events, special care is required to account for far-field wave energy. In general, one primary storm will stand out over all other events; however, selective coastal areas will be impacted by all energy in the large-scale domain. For example, during the migration of Superstorm Sandy, Hurricane Rafael (Cat-1) was making landfall along the Portugal coastline, and Tropical Storm Tony was developing in the central Atlantic Ocean, radiating swell energy to the U.S. coastline along with the locally generated wind-seas from Superstorm Sandy (Figure 5-2). To a lesser degree, a similar combination of energy was evident during the Halloween Nor'easter (or the Perfect Storm) with evidence of the No-Name Storm just south of Long Island, Tropical Storm Grace, and Tropical Storm Fabian east of Florida (Figure 5-3). Wave energy contained in these systems by virtue of their respective storm tracks created swells that impacted the Atlantic coast.

Focusing on the local wave conditions will provide a part of the solution; however, accounting for all wave energy, even if the levels are minute compared to the major system, will impact the final results. Indications from Smith and Vincent (1992) suggest swell energy in the presence of a high-frequency wind-sea component will be unaffected in the decay stages of a primary storm as energy is transmitted to the coast. The degree to which swell can be assumed to be unaffected in the NACCS study could only be accomplished with proper estimation of the winds, spatial and temporal scaling of the meteorology, and application of a wave-modeling technology that would properly simulate the complex extratropical systems (100 extreme events) identified in the NACCS.

The simulation of the 1050 synthetic tropical events was more straightforward. The tropical wind fields were derived from a PBL model (Thompson and Cardone 1996), and the winds appear as a moving vortex (Cardone et al. 1992), with prescribed central pressure, radius to maximum wind, forward speed, Holland B parameter (Holland 1980), and the inflow angle. Local (to the tropical system) wind-seas develop, and as downshifting in frequency of the spectral energy takes place, swell energy will radiate outward forward of the storm system. There will be no resulting far-field wave energy (derived from the Atlantic Ocean basin) to consider. The storm's simulation length is fixed where the duration of the storm is estimated

based on the time of entrance into the Regional NACCS domain extending to 1 day after landfall.

Figure 5-2. Maximum wave height envelope during Superstorm Sandy 26-day simulation, where five tropical systems were evident in the Atlantic Ocean domain.

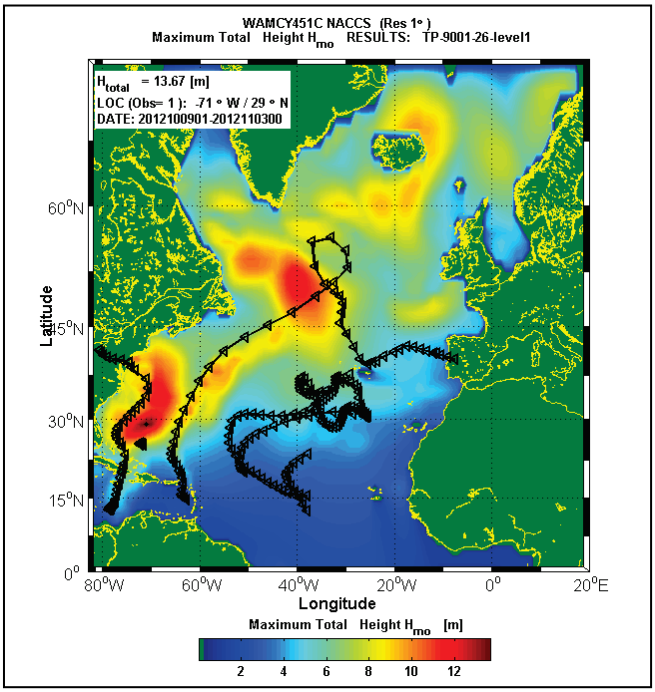

Figure 5-3. Maximum wave height envelope during Halloween Nor'easter (ET0058-8) 8-day simulation, where three tropical systems were evident in the Atlantic Ocean domain.

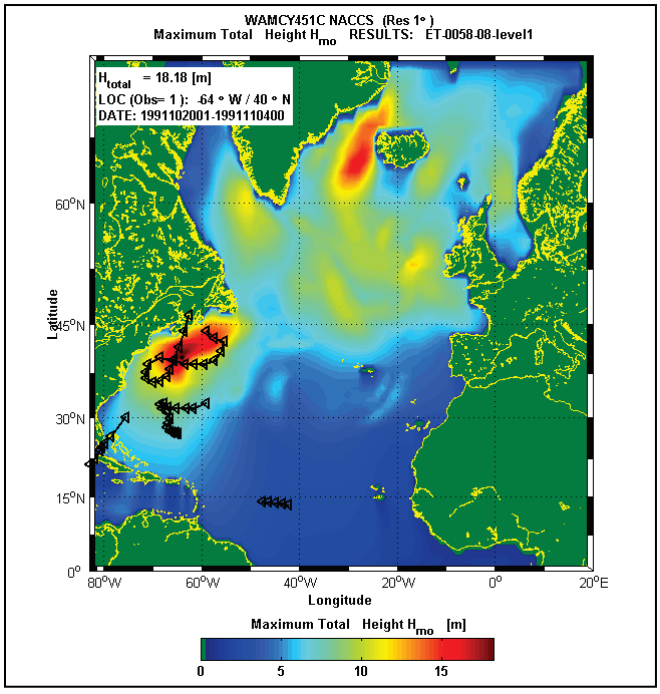

Proper testing and evaluation were required prior to generating offshore wave conditions for NACCS. Checking ensures that the grid systems and bathymetry, model set-up (grid resolutions, model resolutions-frequency/direction intervals, time-steps for propagation and source term integration, and optional mechanisms identified), and storm duration are properly defined. Storm duration is more critical to the extratropical events because they represent real conditions but also contain wave energy derived from distant storm events in the coastal region.

A synopsis of these steps is provided in the following sections. In addition, selected examples from the evaluation analysis and production procedures were documented. The final sections summarize the results from producing the extratropical and synthetic tropical event storms.

5.2 Wave model selection.

The wave modeling technology used to generate the offshore wave estimates for NACCS was the Wave Model (WAM) model (Komen et al. 1994). The model is a third-generation wave model, where there are no a priori assumptions governing the spectral shape, and the source terms are solved and consistent with the wave model's frequency and directional spectral resolution. WAM was developed by a consortium of wave theoreticians and modelers over a 10-year period specifically intended for use by weather prediction centers (the European Center for Medium Range Weather Forecasts, ECMWF), researchers, and in the private sector. WAM is similar to other third-generation wave models like WaveWatch III (Tolman 2014) or Simulating Waves Nearshore (SWAN) (SWAN Team 2014).

The model solves the action balance equation (Equation 1) for the temporal and spatial change in wave action. Wave action is selected because the model could be used in an area containing surface current fields given by

$$\frac{DN}{Dt} = \frac{1}{\omega}\left[S_{in} + S_{nl} + S_{ds} + S_{w-b} + S_{br} + \sum_{i=1}^{N} S_i\right] \quad (1)$$

where:

N = wave action ($N=E(x,y,t,f,\theta)/\omega$)
t = time

ω = radial frequency (ω=2πf)
Sin = atmospheric input source term (wind forcing)
Snl = nonlinear wave-wave interaction source term (transmits energy across the frequency domain)
Sds = high frequency dissipation sink term (energy loss due to white-capping)
Sw-b = wave bottom (e.g., bottom friction energy loss)
Sbr = depth-induced, wave-breaking sink term
E (x,y,t,f,θ) = spectral energy
X = longitude (geographic position)
Y = latitiude (geographic position)
F = frequency
θ = wave angle.

S_{br} represents additional source or sink mechanisms that some of the third-generation wave models retain (Tolman 2014; SWAN Team 2014).

In deep water the above equation reduces to

$$\left\{\frac{\partial}{\partial t} + \overrightarrow{c_g} \cdot \frac{\partial}{\partial \vec{x}}\right\} E\left(\vec{k}, \vec{x}, t\right) = \sum_{i=1}^{N} S_i \quad (2)$$

where:

$\overrightarrow{c_g}$ = vector group speed (dependent on frequency)
k = vector wave number (related to frequency, f and direction, θ)
S_i = S_{in}, S_{nl}, S_{ds}, $S_{w\text{-}b}$, and S_{br} identified above.

WAM solves the action balance equation (Equations 1 and 2) in two steps. In deep water, the first step is propagation or advection of energy over the model grid domain (the second term on the left side of Equation 2). The second step is to solve for the source terms, adding energy from the wind forcing (S_{in}), transferring energy across frequency bands (S_{nl}), compensating for energy losses due to white-capping (S_{ds}), removing energy (where applicable) from wave-bottom effects ($S_{w\text{-}b}$, bottom friction), and then in very shallow water (Equation 1), collapse of the spectrum resulting from depth-induced wave breaking (S_{br}). The result after one time-step is the spatial and temporal change of $E(x,y,t,f,\theta)$. For the NACCS offshore wave climate generation, the WAM frequency range is defined by

$$f_{n+1} = 1.1 \cdot f_n \text{ where } f_0 = 0.03138428\text{-}s^{-1} \mid n = 1, 28$$

where:

s = seconds

n = number of frequency bins

and the direction range is defined by

$$\theta_m = 7.5 + 5.0 \cdot (m - 1) \mid m = 1,72$$

where m is the number of direction bins.

5.3 WAM grid development.

The accuracy of the WAM model's results is dictated by the accuracy in the bathymetric grid used in the simulations. These grids are tailored to maximize grid resolution while accounting for spatial gradients in the water depths, identifying coastal geometry, and accounting for offshore islands. The designation of these spatial features is balanced to minimize the computational requirements in implementing these grid systems. The grid resolution selection is also dependent on the relative size of the meteorological systems (e.g., wind fields) that are applied as forcing conditions to the wave model. The method used in WAM to account for features and forcing conditions, while optimizing use of computational resources, is to build unique grid systems at various resolutions, increasing the resolution where it is warranted. Three grid levels ranging from 1.0 deg, to 0.25 deg and 0.083 deg are used in all NACCS offshore wave simulations. This maximizes the grid resolution in the coastal domain and reduces the resolution in the far field, which optimizes the computational load for each simulation. All point source wave measurement sites used in the model evaluation are identified by the red symbols identified in Figure 5-4 and Figure 5-5. The final model grid domains, resolutions used, time-steps, and the wind field boundaries (spatial and temporal resolutions) for all evaluation testing are identified in Table 5-1.

Figure 5-4. WAM multilevel grid system used in NACCS. Note Level 1 covers the entire domain illustrated.

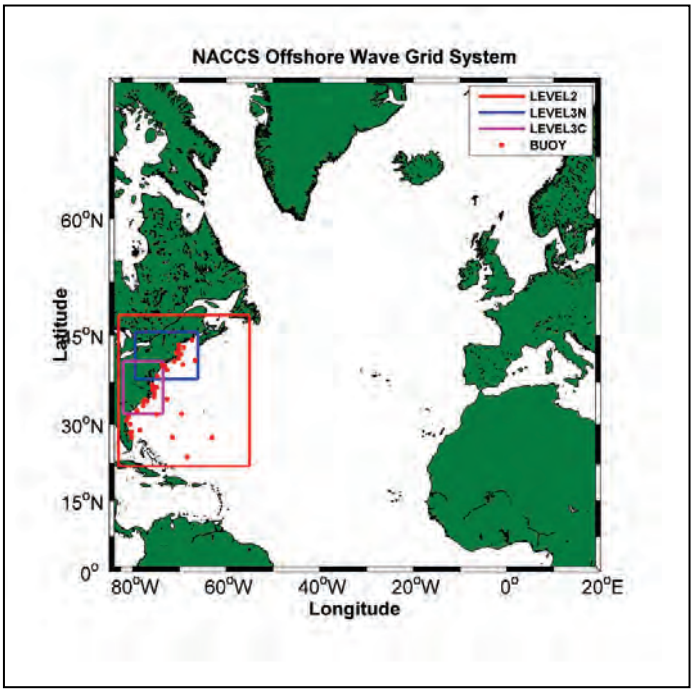

The three multilevel grid system identified in Figure 5-4 and Figure 5-5 were used for all evaluation tests and all extratropical extreme storm simulations. The role of the Level 1 simulations is only to resolve the far-field wave energy providing that information at the Level 2 boundaries (Figure 5-4, red box). Two-dimensional (2D) spectral estimates defined the boundary condition information provided at a 900 s interval. Following the Level 1 simulation, the Level 2 domain was run, creating boundary conditions for Level 3N and Level 3C. Once the Level 2 simulation completed, the Level 3N and Level 3C simulations commenced creating boundary condition information to be used in the STWAVE simulations.

Figure 5-5. WAM multilevel grid system used in NACCS. Note Level 2 covers the entire domain illustrated.

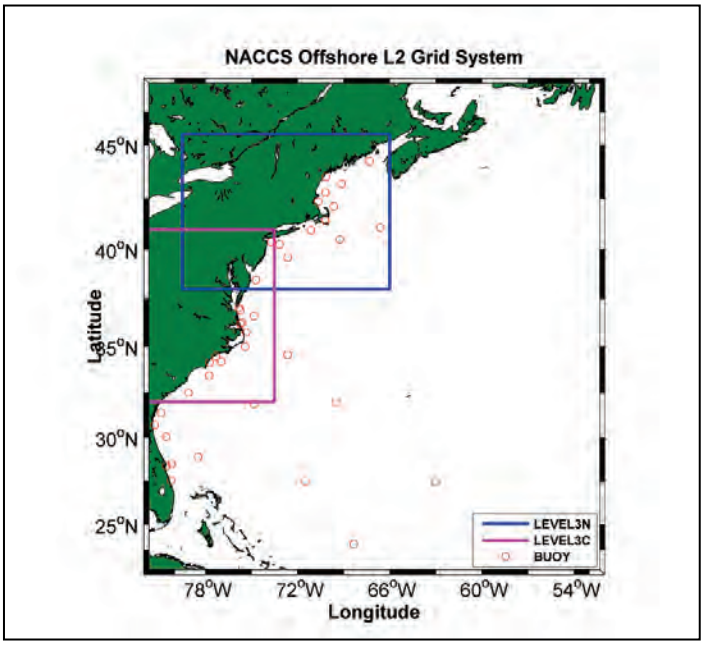

Table 5-1. Model grid information evaluation testing.

Domain	WAM Boundary Extent				WAM Grid Size, deg Δx/Δy	Wind Data		WAM Time-Steps (s)		Relative Grid Depth**
	Longitude		Latitude							
	West	East	South	North		Spatial Resolution, deg*, Δx/Δy	Temporal Resolution, Δt (hr)	ΔPrp	ΔST	
Level 1	-83.33	+20.83	0.00	75.625	1.0 / 1.0	.833/ .625	6	900	900	Deep
Level 2	-82.00	-52.00	22.00	48.00	.25 / .25	.25 / .25	1	400	400	Shallow
Level 3N	-79.50	-66.00	38.00	45.50	.083 / .083	.25 / .25	1	200	200	Shallow
Level 3C	-82.00	-73.50	32.00	41.00	.083 / .083	.25 / .25	1	200	200	Shallow

*Winds used in all evaluation tests were derived from the WIS archive.

ΔPrp: Propagation time-step (s)

ΔST: Source Term Integration time-step

**Deep > 200 m and Shallow < 200 m

5.4 WAM model evaluation

Evaluation testing is a requirement in any study such as NACCS. It is necessary to test and evaluate the wind forcing, wave modeling technology, grid systems, and the operational system implemented during the produc-

tion phase. The evaluations were based on time, scatter, Quartile-Quartile graphics (Q-Q), and a battery of statistical tests (bias, root-mean-square-error [RMSE], regression, correlation, symmetric correlation, scatter index, and skill score). The principal focus of the wave-model evaluation is on the extreme storm period of record and the storm peak condition. The wind fields are also assessed at the same sites used for the WAM comparisons. These results provide sufficient information to determine the causes of any differences found in the wave model results compared to the measurements. The evaluation analysis also provides the basis to test all operational production shells, to determine the run times required for each simulation, and to serve as a presetting check for consistency in the model output locations when compared to point-source measurements (also over time) and boundary condition locations in the Level 3N and Level 3C regions used for input to the STWAVE (Massey et al. 2011b) nearshore wave simulations. Finally, the analysis provides additional quality control of available point-source wave and meteorological data and their availability.

A series of extreme storm events was initially selected for these tests. The list of five tropical storms (Figure 5-6) and seven extratropical events is given in Table 5-2. These events were chosen based on long-term archival water-level measurement sites in the NACCS domain.

The original tests were started at least 1 month prior to the storm eventually affecting the NACCS domain. It was assumed that a 1-month time period was sufficient to capture all far-field wave energy from the Atlantic Ocean basin.

Table 5-2. Baseline extreme storm events.

Storm Type	Yr/Month	Storm Name	Peak Date	Storm No.	Winds Used
Tropical	2012-09	Sandy	20121029	TP-9001	WIS* / L1-L2
	2012-10				WIS / L1-L2
	2012-11				WIS / L1-L2
Tropical	2011-07	Irene	20110828	TP-9002	WIS / L1-L2
	2011-08				WIS / L1-L2
	2011-09				WIS / L1-L2
Tropical	2003-07	Isabel	20030918	TP-9003	WIS / L1-L2
	2003-08				WIS / L1-L2
	2003-09				WIS / L1-L2
Tropical	1996-08	TS-Josephine	19961009	TP-9004	WIS / L1-L2

Storm Type	Yr/Month	Storm Name	Peak Date	Storm No.	Winds Used
	1996-09				WIS / L1-L2
	1996-10				WIS / L1-L2
Tropical	1985-08	Gloria	19850927	TP-9005	WIS / L1-L2
	1985-09				WIS / L1-L2
	1985-10				WIS / L1-L2
Extratropical	1996-10	ET-0073	19961206	ET-0073	WIS / L1-L2
	1996-11				WIS / L1-L2
Extratropical	1995-10	ST-0069	19951115	ST-0069	WIS / L1-L2
	1995-11				WIS / L1-L2
Extratropical	1994-02	ET-0066	19940303	ET-0066	WIS / L1-L2
	1994-03				WIS / L1-L2
Extratropical	1993-12	ET-0065	19940104	ET-0065	WIS / L1-L2
	1994-01				WIS / L1-L2
Extratropical	1991-11	ET-0058	19911211	ET-0058	WIS / L1-L2
	1991-12				WIS / L1-L2
Extratropical	1986-12	ET-0054	19870123	ET-0054	WIS / L1-L2
	1987-01				WIS / L1-L2
Extratropical	1984-02	ET-0050	19840329	ET-0050	WIS / L1-L2
	1984-03				WIS / L1-L2

*WIS: Wave Information Study long-term hindcast wind fields were used for all evaluation tests.

Figure 5-6. Five tropical storm tracks used in evaluation tests. Level 3N and Level 3C domains are identified by the black boxes; black dots represent hurricane intensities of Cat-1 and higher.

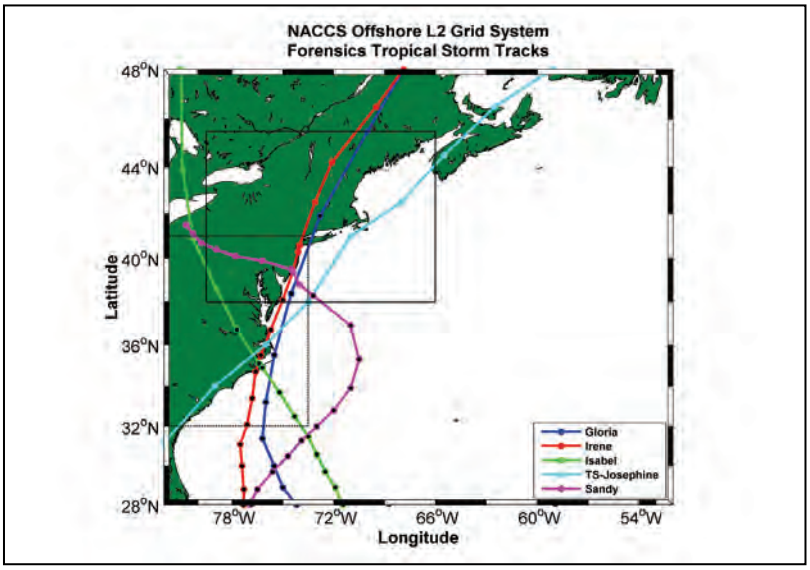

A preliminary validation data set developed as part of this study was derived from water level and local (coastal) meteorological measurements. In many cases, these data did not represent major wave events; hence, an independent data set was utilized for the purpose of evaluating WAM for large wave events. Eleven NDBC sites were selected for this purpose (Figure 5-1) because they had the longest record lengths available for this region. This technique is somewhat flawed because any wave measurement record contains gaps, from missing hourly, monthly, or at times, yearly records. In addition, there is a strong likelihood of a buoy transmission failure in or around high winds and/or wave conditions. Hence, there is a high probability that major storm conditions are missing from the wave record. Despite these potential flaws, each buoy record was evaluated based on a POT (mean plus 2 times the standard deviation, σ^2) to determine a storm condition.

The evaluation process isolated all tropical and extratropical events; tropical events were omitted from the extratropical list. The final top 10 extratropical storms were selected based on

- availability of wind fields (1980 through 2012) derived from the WIS (Oceanweather Inc. 2014, wind fields)
- maximum number of available buoy sites (of the 11 selected) with data during the storm period.

The list of added extratropical storms selected for the model evaluation study of WAM is presented in Table 5-3. As noted in Table 5-3, there were four extreme wave events found in this analysis that were not part of the extreme storm population. This most likely was due to the buoy locations residing offshore (50–100 km from shore) rather than close to the coast.

These additional 10 extreme wave events provided the means to fully test the wave model as well as procedures used in the production, isolated any wind field deficiencies, and identified distinct grid problems or other factors that could contaminate the final wave estimates.

Table 5-3. Extratropical extreme wave events utilized for evaluation testing.

Storm Type	Yr/Month	Storm Name	Peak Date	Storm No.	Winds Used	BCS Gen
Extratropical	2011-12	N/A	20120114	ET-9304	WIS / L1-L2	YES
	2012-01				WIS / L1-L2	YES
TP-Noel*	2007-11	N/A	20071103	ET-9303	WIS / L1-L2	YES

Storm Type	Yr/Month	Storm Name	Peak Date	Storm No.	Winds Used	BCS Gen
	2007-11				WIS / L1-L2	YES
Extratropical	2007-03	ET-0086	20070416	ET-0086	WIS / L1-L2	YES
	2007-04				WIS / L1-L2	YES
Extratropical	2005-02	N/A	20050309	ET-9302	WIS / L1-L2	YES
	2005-03				WIS / L1-L2	YES
Extratropical	2004-11	N/A	20041227	ET-9301	WIS / L1-L2	YES
	2004-12				WIS / L1-L2	YES
Extratropical	2003-11	ET-0080	20031206	ET-0080	WIS / L1-L2	YES
	2003-12				WIS / L1-L2	YES
Extratropical	1995-12	ET-0070	19960108	ET-0070	WIS / L1-L2	YES
	1996-01				WIS / L1-L2	YES
Extratropical	1993-02	ET-0062	19930305	ET-0062	WIS / L1-L2	YES
	1993-03				WIS / L1-L2	YES
Extratropical	1992-11	ET-0060	19921211	ET-0060	WIS / L1-L2	YES
	1993-12				WIS / L1-L2	YES
Extratropical	1991-12	ET-0059	19920104	ET-0059	WIS / L1-L2	YES
	1992-01				WIS / L1-L2	YES

*It was assumed this storm was extratropical (from the November date); however, it was later identified as Hurricane Noel.

A total of 22 extreme storms were simulated (5 tropical and 17 extratropical) using WAM with the multilevel grid nesting and domains defined in Table 5-1 (and shown in Figure 5-4). All wind fields used in these tests were derived from the WIS wind field archive (see Table 5-1 for domains and resolutions). All runs were started from an initial condition based on simple wave growth approximations. From that point they were run for the entire storm period identified in Table 5-2 and Table 5-3. The Level 1 simulation-fed boundary condition information 2D spectral estimates) to the Level 2 region; the Level 2 simulation fed boundary condition information to both the Level 3N and Level 3C domains. The Level 3 domains were run, and 2D spectral estimates were saved at STWAVE (Massey et al. 2011b) boundary locations (Figure 5-7) at a time-step between 5 and 30 min.

Figure 5-7. STWAVE boundary condition save points (open circles)and buoy sites (solid points). Initialization analyses used both STWAVE boundary points and measurement sites.

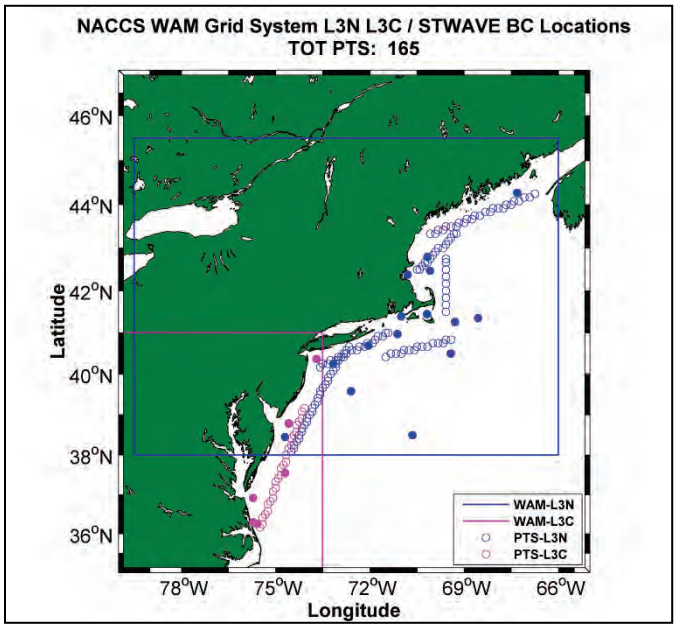

Approximately 30 wave measurement sites were used (Level 1, Level 2, Level 3N, and Level 3C) for these storms; however, at times not all buoys were fully operational during a given simulation. Model performance was evaluated based on comparing the model-simulated waves to the wave measurements. Preliminary results were generated, and examples are provided from the Superstorm Sandy simulation for Level 3N and Level 3C grids (Figure 5-8 and Figure 5-9, respectively). Results for the remaining four tropical simulations compared well to the measurements; however there was a slight net increase in errors (based on bias, RMSE, scatter index, and correlation) for storms occurring in the more distant past. This is due to the quantity (and quality) of wind measurements, from point-source to satellite-based scatterometer estimates, have improved with advancements in technology. In addition, the number of wave measurement sites have increased with time, thus expanding the population size. Both of these factors will impact the wave model results and validity of the statistical testing, progressing from past (largest errors) to recent events (smallest errors).

Compendium time plots are provided for the Level 3N (Gulf of Maine, Figure 5-8; Long Island, Figure 5-9) to illustrate the temporal and spatial quality of the model results spanning the region. For the southern domain (Level 3C), the number of active buoy sites was limited, and for illustration

purposes, one location is shown (Figure 5-10). WAM replicated the measurements well at the five northern region sites (Figure 5-8). There are some phasing and elevated conditions at 44005 prior to the peak of the storm. Most of these errors are derived from the wind field being slightly high (2–4 m/s) during that time period. The remaining sites show excellent agreement, from the initial growth, through the storm peak, and then decaying at the same rate as the observations. Moving to the five Long Island sites, the WAM results also produce high-quality estimates (Figure 5-9). The model tracks the measurements from growth through the storm peak and decay. Capturing peaks ranging from over 9 m offshore to 3 m at 44020 (Nantucket Sound) in a water depth of 9.8 m provides evidence that WAM can replicate Superstorm Sandy-like storms. These results also demonstrate the high quality of wind forcing derived from the OWI winds fields that was previously applied in the WIS and is now applied to the NACCS WAM simulations.

Figure 5-8. Evaluation of the WAM Level 3N grid, northern region results for five wave measurement locations during Superstorm Sandy.

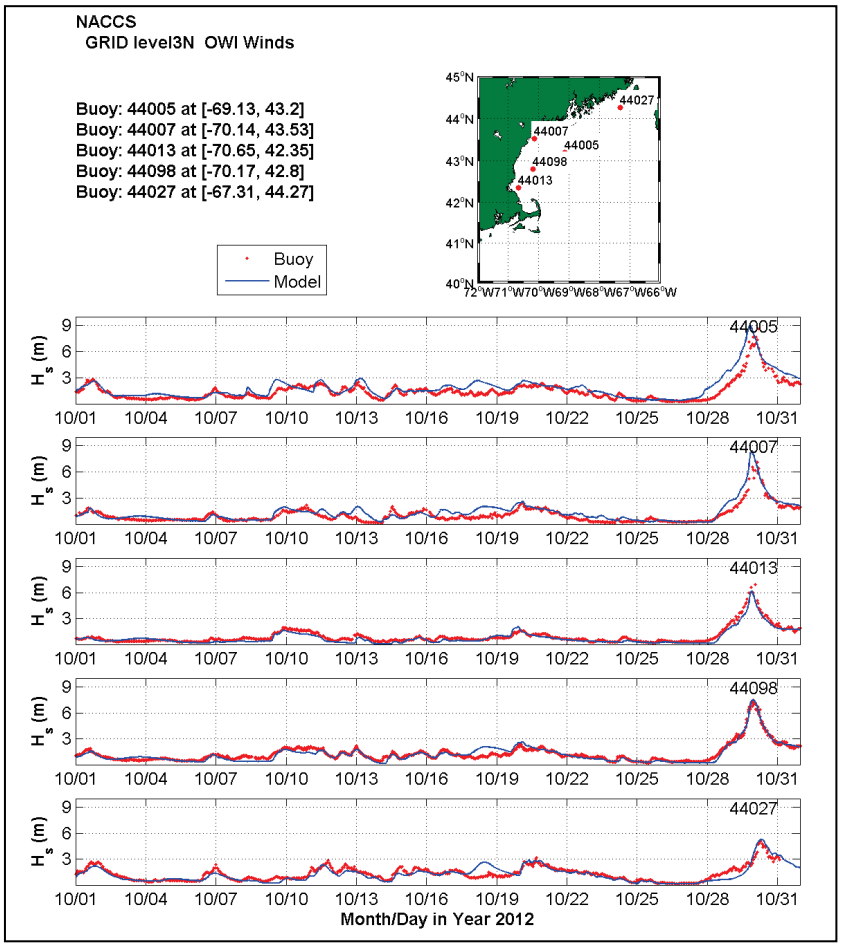

Figure 5-9. Evaluation of the WAM Level 3N grid, Long Island region results for five wave measurement locations during Superstorm Sandy..

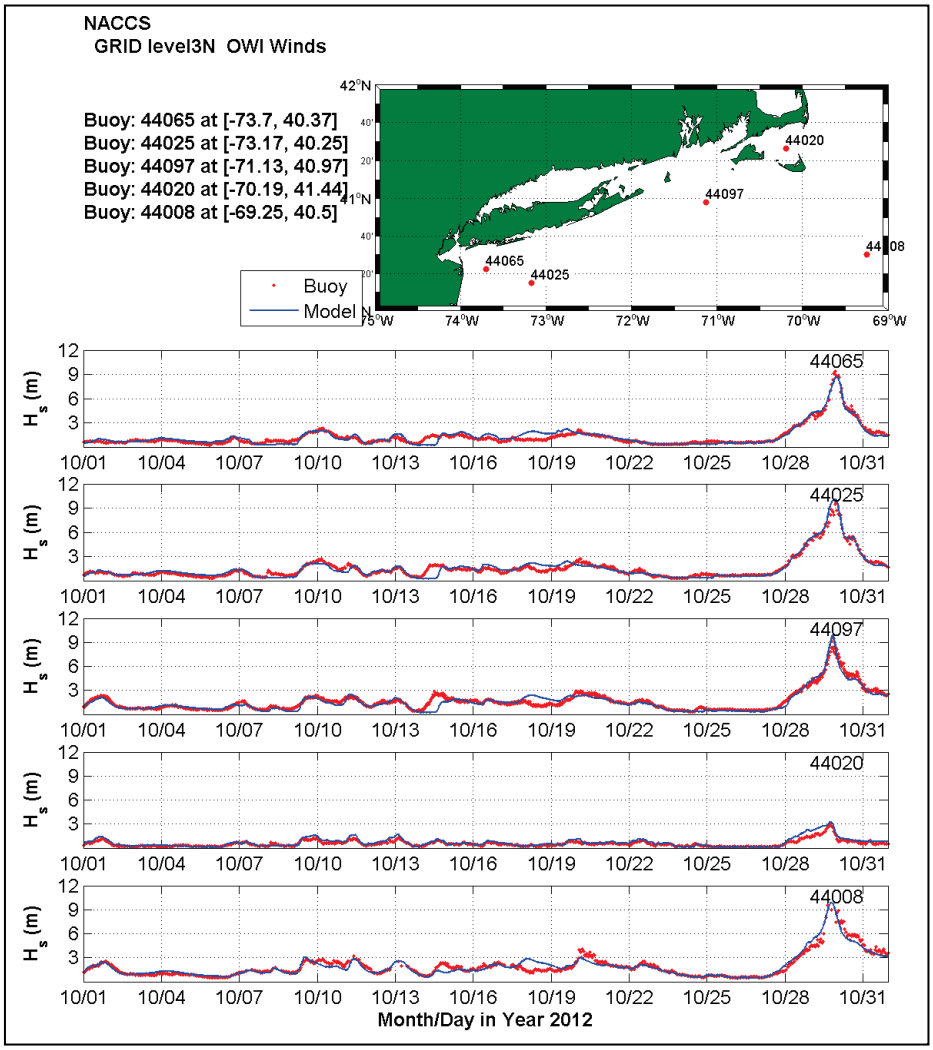

Of the seven sites in the southern portion of the NACCS region, only three were actively recording wave data during Superstorm Sandy. Buoy 44099 is just offshore of Chesapeake Bay and shows a vastly different wave height trace compared to the other 10 sites shown for the Long Island and northern domains (Figure 5-10). The storm peak for 44099 is only 4 m (compared to 9 m for buoys 44065, 44025, and 44097) and does not show the rapid intensification of the storm peak that is observed at the Long Island and northern domains. Buoy 44095 (in the southern domain) was also recording and shows a similar trend to Buoy 44099. These results clearly demonstrate the rapid intensification of Superstorm Sandy as it migrated up the U.S. coastline and also the dramatic spatial variation in the significant wave heights.

Figure 5-10. Evaluation of WAM results at NDBC 44099, the significant wave height, parabolic-fit wave period, the mean wave period, and the vector mean wave direction during Superstorm Sandy.

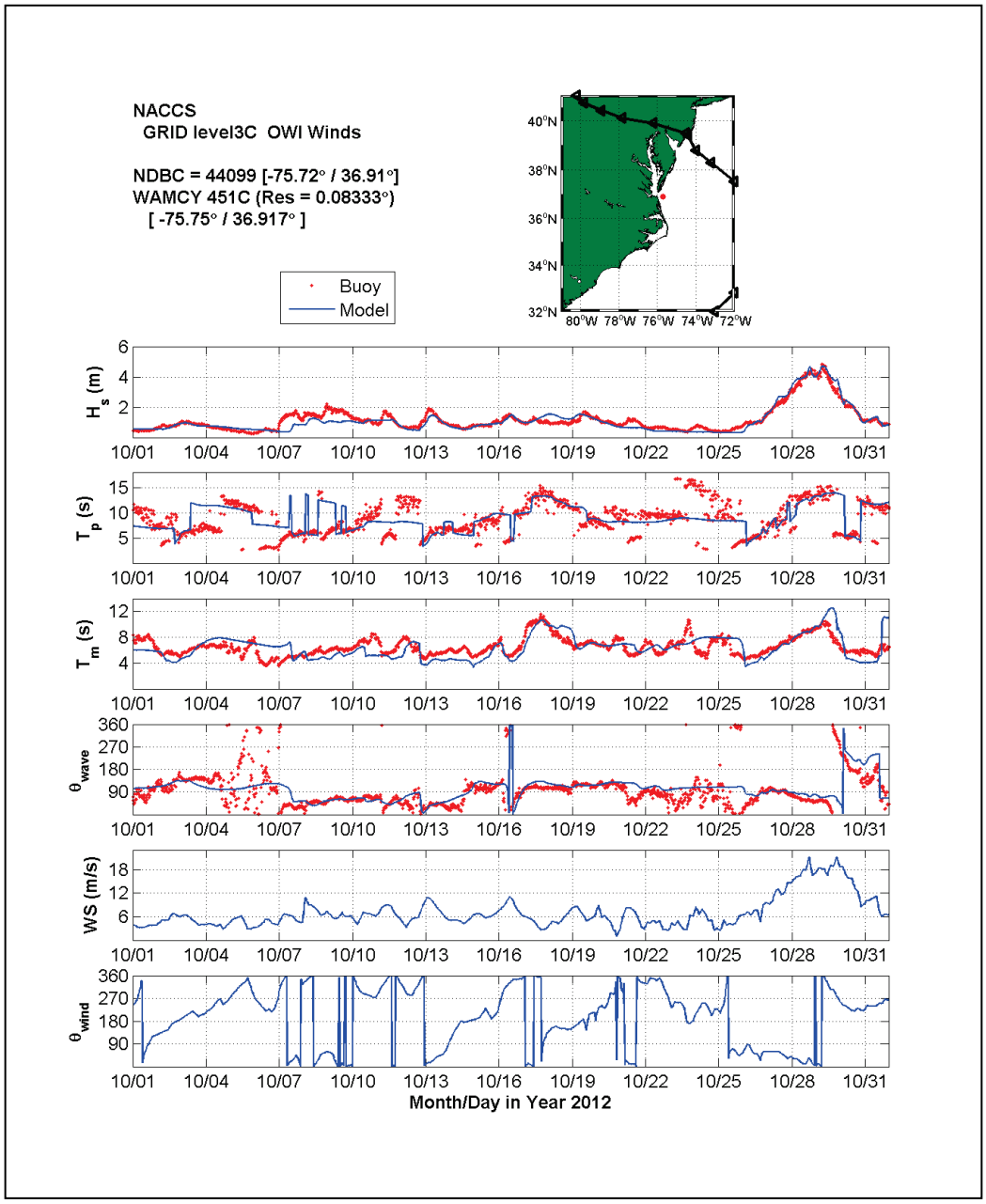

WAM performed well for Superstorm Sandy. Modeled wave heights emulated the measurements, and both mean and peak wave period estimates followed the measurement trends. There is a slight difference in the mean wave period results soon after the storm peak (Figure 5-10) when WAM tends to increase the low-frequency energy, whereas the measurements follow a newly formed wind-sea. This slight difference is also evident in the peak wave period results, showing a phase difference between the two

model results and measurements. The modeled wave direction also follows the measurements from the growth and peak sequences. Soon after the storm peak, there is a divergence between the modeled and measured wave direction. WAM tends to incorporate the swell energy longer before moving to the new wind-seas as is apparent in the measurements.

5.5 Model sensitivity to simulation length

In order to minimize computation time while retaining quality of the wave estimates during the extreme storm event peaks, sensitivity tests of the simulation length were made. Simulation duration was varied and compared to the base condition. Starting the simulation prior to the storm peak is required to ensure that far-field wave energy has sufficient time to propagate into the study domain. The WAM evaluation is based on comparisons between the base-line runs (initialized one month prior to the storm peak) versus the 5-, 10-, 15-, and 20-day initializations. For brevity, two examples are provided for the L3N domain: one tropical storm (Superstorm Sandy) and one extratropical event (ET-0062, Storm of the Century, March 1993), and comparisons were made at 165 special output locations (Figure 5-11 through Figure 5-14).

The first event was a rapidly moving extratropical storm that occurred over a 3-day period. Plotting all individual time-series provides a wave height envelope as found in Figure 5-11. The temporal change in all 165 special output locations was plotted, essentially defining the range of conditions for the entire data set. Analysis of these time series showed that the differences in results between the 20-, 10-, and 5-day initializations around the storm peak were negligible (identified by the green curve and less than 0.1 m). The maximum differences occurred immediately after the initiation of the simulation and during transitions between growth and lull sequences in the wave records. Though the focus is on one principal event (in this case, the peak just prior to 15 March), there are additional meteorological events in the Atlantic Ocean that have an impact on the local NACCS study area. In addition, the start of the simulation may have occurred during the growth sequence of a minor event (e.g., Figure 5-11, approximately 4 March) that generated the largest differences. However the time period around the selected storm event is well replicated even with a 5-day initialization (Figure 5-12). Investigating further, Figure 5-13 shows the results from time-pairing the baseline wave height estimates with the 5-, 10-, and 20-day initialization results. Two obvious trends emerge from this analysis. The first is that the 10-day initialization wave estimates dis-

played larger differences than in any other simulation, including the 5-day initialization. Most if not all of these differences are a result of when the start of the simulation occurs (see Figure 5-11) relative to when a minor event occurs. In this case, a minor event begins to develop approximately 4 March and rapidly evolves to approximately 5 m wave heights. This storm sequence was well replicated in the 20-day initialization and occurred prior to the initiation of the 5-day initialization simulation. Looking closely at the scatter plot (Figure 5-14) and the wave height trace for the selected storm (14 March), there is very little observable difference in wave heights greater than approximately 5 m to the peak of the storm of nearly 14 m.

Figure 5-11. Time plot envelope of 165 special output locations for 20-day initialization test, Storm of the Century.

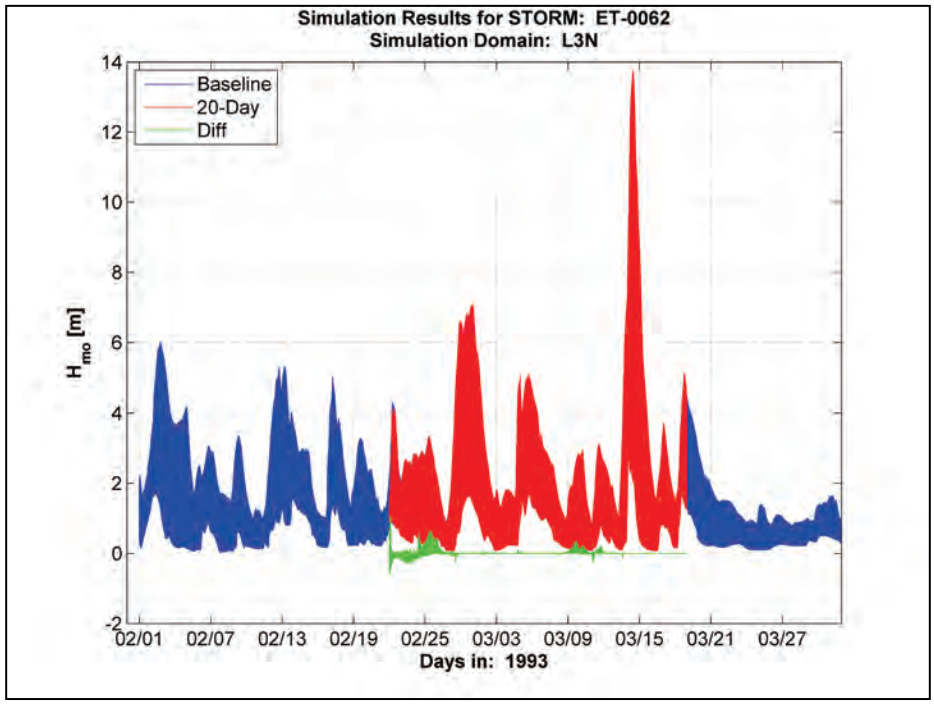

Figure 5-12. Time plot envelope of 165 special output locations for 10-day initialization test, Storm of the Century.

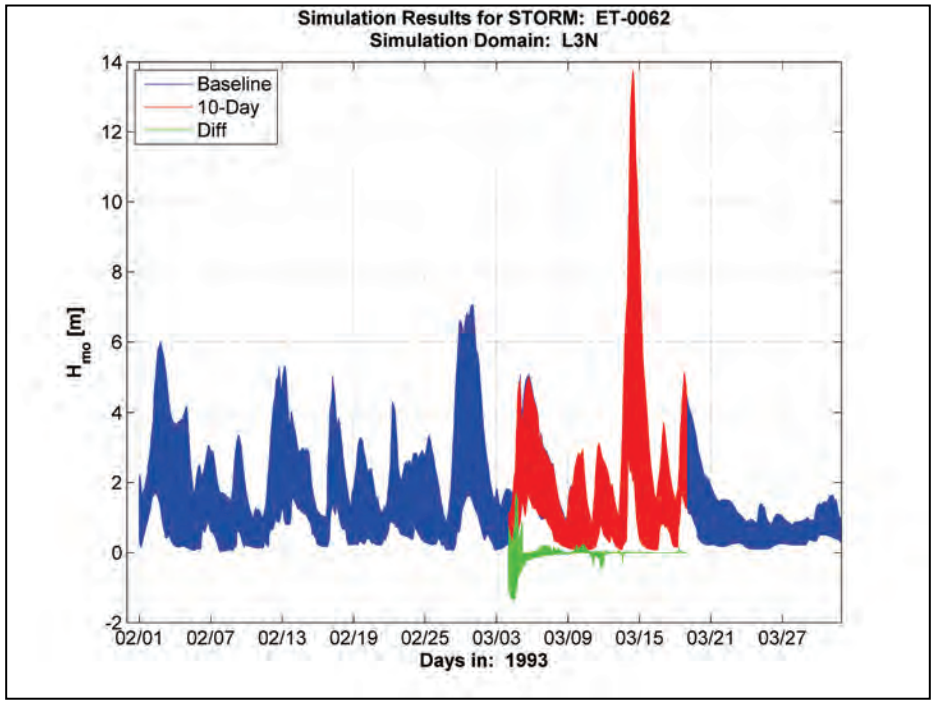

Figure 5-13. Time plot envelope of 165 special output locations for 5-day initialization test, Storm of the Century.

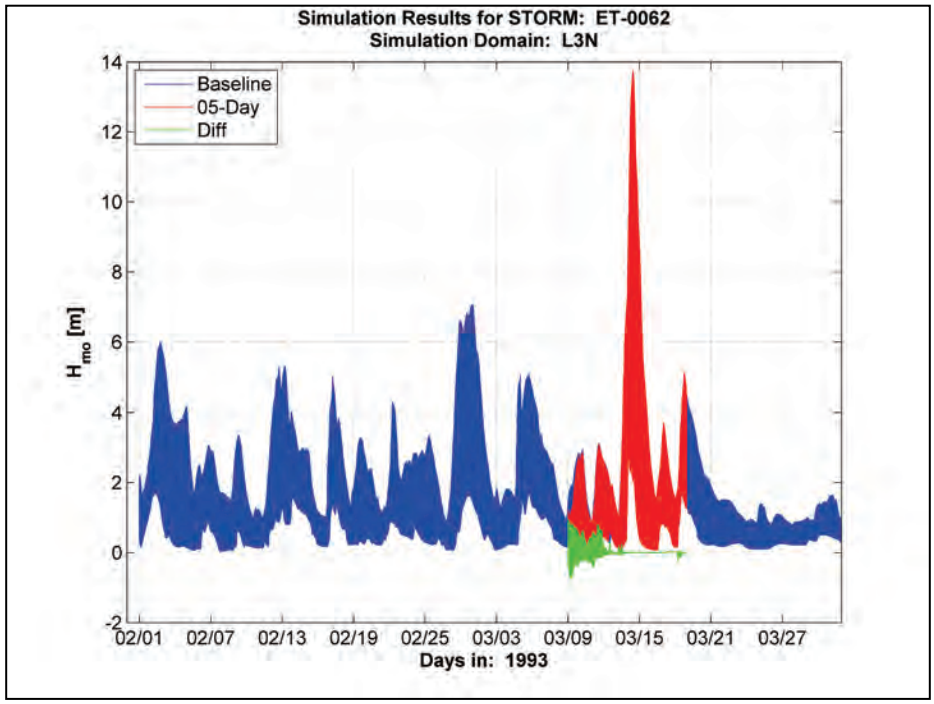

Figure 5-14. Scatter plot of time-paired results of 165 special output locations compared to base-line (30-day initialization), Storm of the Century.

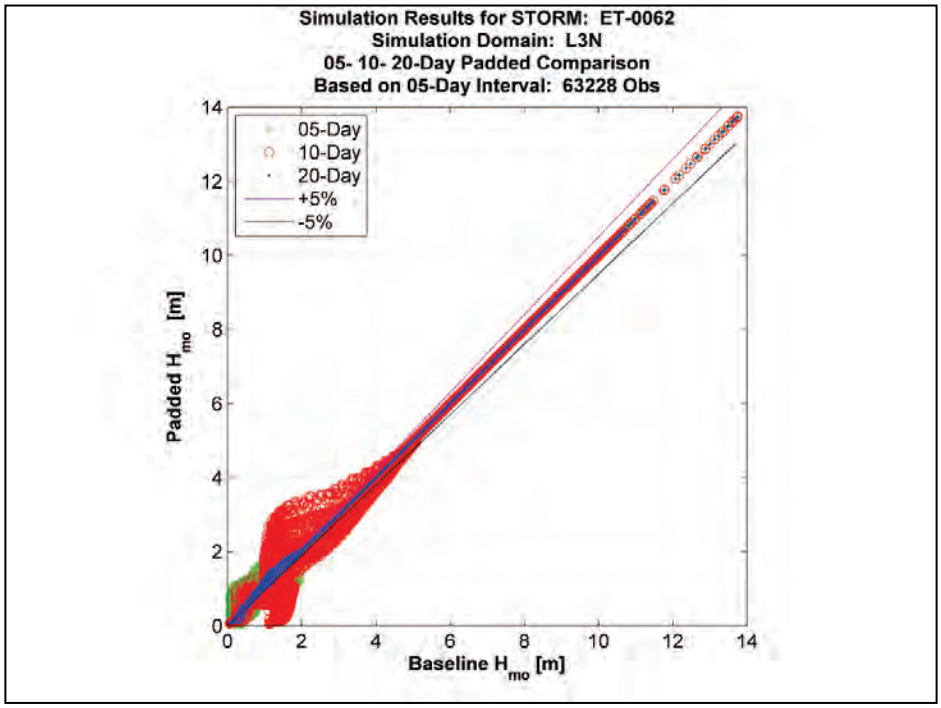

The results from Superstorm Sandy (Figure 5-15 through Figure 5-18) show a similar trend to what was described in the previous example. There are very small differences between the 20- and 10-day initialization results (Figure 5-15 and Figure 5-16) during the growth, peak, and decay sequences of Superstorm Sandy, and the two simulations compare well at all locations. However, the 5-day initialization results clearly show approximately a 0.5 m difference at the initial growth stages of the storm sequence (Figure 5-17). These differences are small compared to the peak estimates of 10 m, but they still represent a 5% discrepancy relative to the storm peak. The scatter plot derived from the time-paired estimates between the base-line simulation and the three initialization results (Figure 5-18) showed little or no differences above a 4 m wave height.

This analysis indicated the need for some criteria to be selected in order to set the initialization of the deep-water WAM simulations. For brevity, and to introduce a certain degree of conservatism, all simulations used a 10-day initialization for the starting date in the Atlantic Ocean Basin Simulations (Level 1). The boundary conditions generated from these simulations should be sufficient to define the far-field wave energy in the higher resolution simulations. All finer resolution domains were initiated at the start times defined in the wind field. Despite shortening the spin-up for these

domains, the boundary condition information (2D wave spectra) contained most if not all of the far-field wave energy derived from distant storm events.

Figure 5-15. Time plot envelope of 165 special output locations for 20-day initialization, Superstorm Sandy.

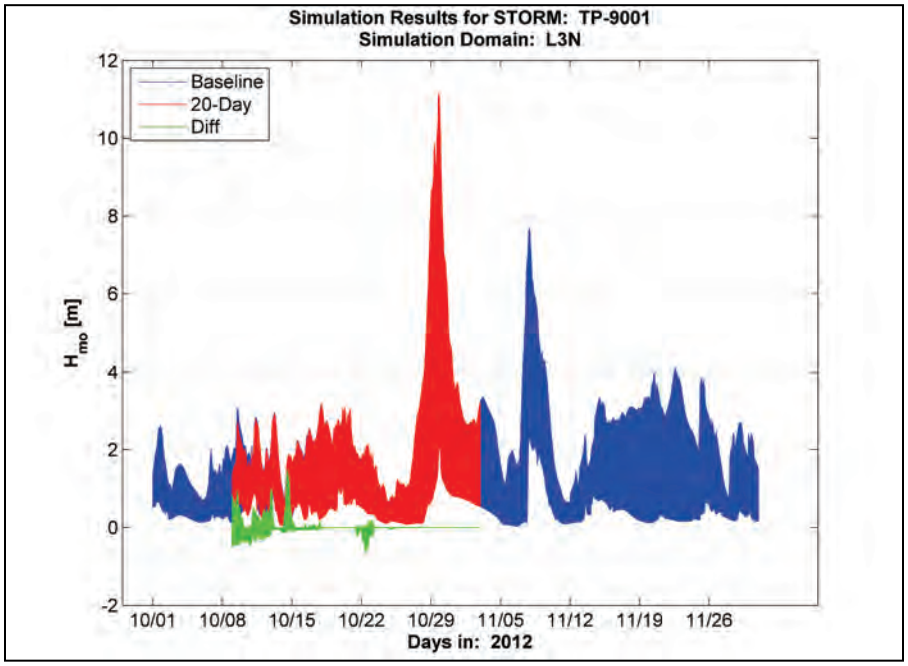

Figure 5-16. Time plot envelope of 165 special output locations for 10-day initialization, Superstorm Sandy.

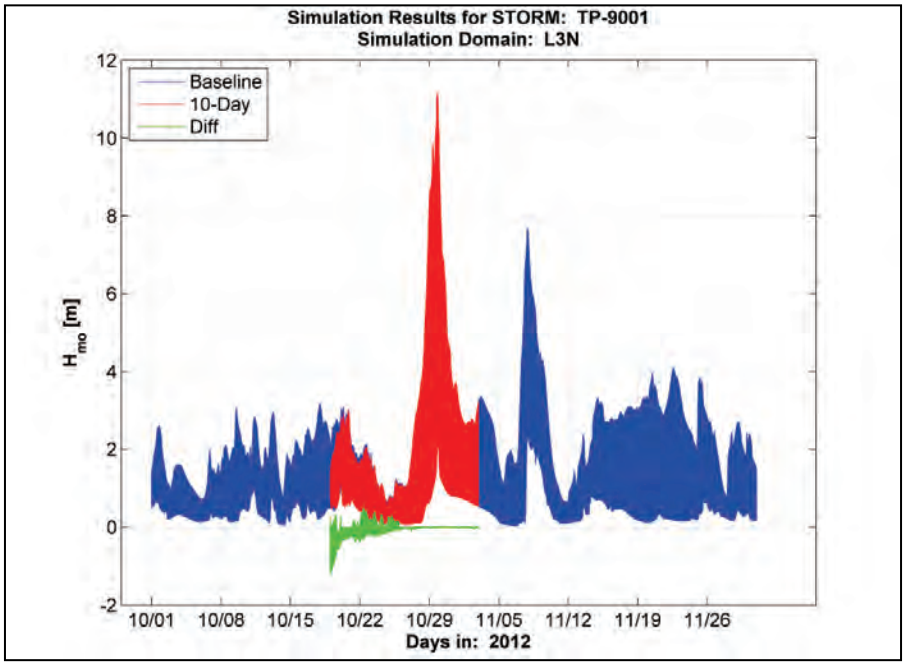

Figure 5-17. Time plot envelope of 165 special output locations for 5-day initialization, Hurricane Sandy.

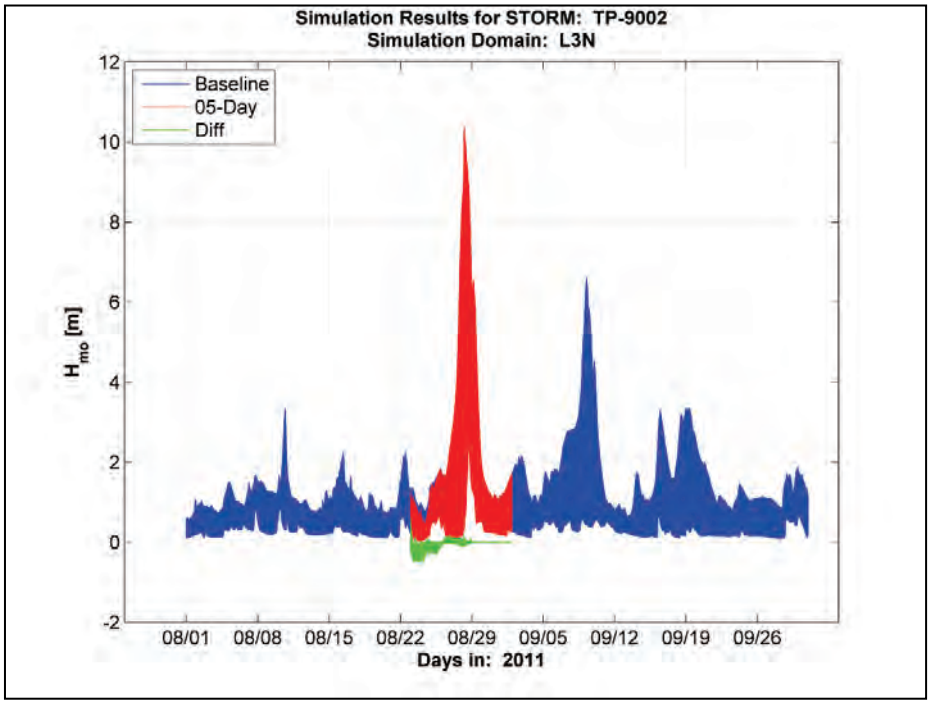

Figure 5-18. Scatter plot of time-paired results of 165 special output locations compared to base line (30-day initialization), Hurricane Sandy.

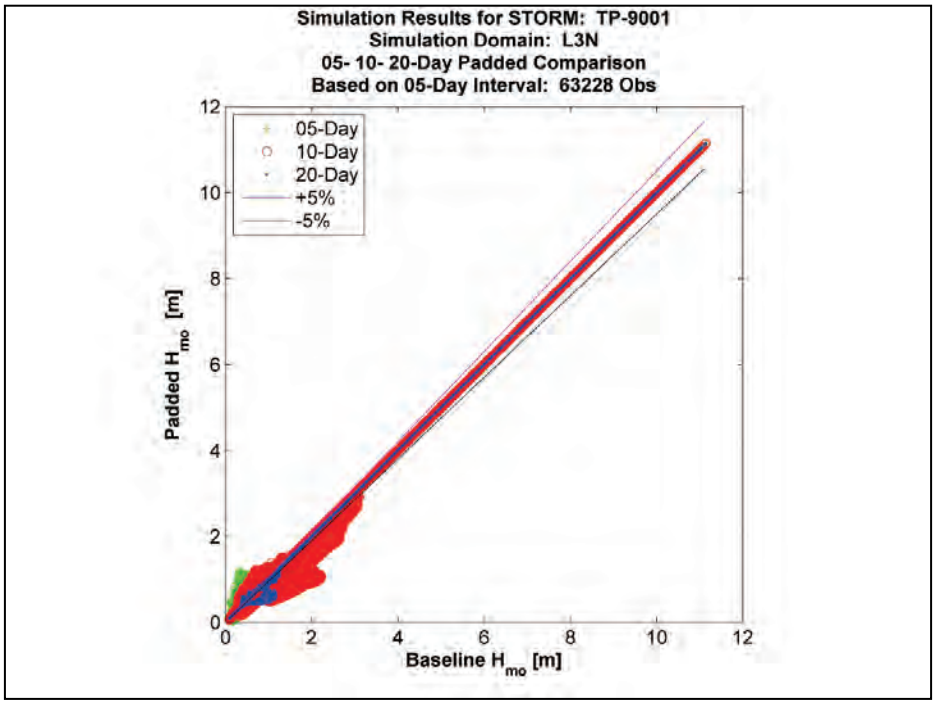

5.6 Summary of model evaluation and testing

Twenty-two extreme storm (17 extratropical and 5 tropical) event simulations were run using the three level grid systems, initiating the Level 1 grid (Atlantic Ocean) 10 days prior to the storm peak. The Level 2, Level 3N, and Level 3C grids were run according to the final extreme storm simulation period of 8 days, in which the start date was 4 days prior to landfall, and the end date was 3 days after landfall. WAM simulations used the WIS wind fields for all levels, as noted in Table 5-1. All storm simulations were individually evaluated based on time series, scatter, Q-Q graphics, and a battery of statistical tests. Each evaluation storm simulation and the number of point-source measurement sites used in the evaluation are presented in Table 5-4. The total number of sites for all extratropical events tested is 353, and for the tropical events, a total of 141 locations. In most instances, the sites found in Level 3N and Level 3C grids were also tested in Level 2 and Level 1 grids (i.e., double or triple counted). These results provided the means to compare the effect of increased grid resolution as well as increased wind-field resolution. Summary information related to the wave model evaluation is provided and discussed below and focuses on the Level 2, Level 3N, and Level 3C results.

Most importantly, the tropical storm simulations used in the evaluation portion of the study were derived from actual historical events with available field measurements for comparison purposes and are not synthetic events as in the 1050 tropical storm population production data set.

Table 5-4. Number of point-source measurement sites utilized in model evaluation testing.

Storm No.	Date	Description	WAM Grid Levels				Total	Cumulative Total
			Level 1	Level 2	Level 3N	Level 3C		
Extratropical Storms								
ET-0050-08	1984-03	-	3	1	0	1	5	
ET-0054-08	1987-01	-	3	0	0	1	4	
ET-0058-08	1991-02	-	10	5	1	3	19	
ET-0059-08	1991-01	-	9	5	1	2	17	
ET-0060-08	1992-12	-	7	5	1	2	15	
ET-0062-08	1993-03	Storm of Century	7	5	1	2	15	
ET-0065-08	1993-01	-	7	5	1	2	15	
ET-0066-08	1994-03	-	5	4	1	1	11	

Storm No.	Date	Description	WAM Grid Levels				Total	Cumulative Total
			Level 1	Level 2	Level 3N	Level 3C		
ET-0069-08	1995-11	-	7	5	1	2	15	
ET-0070-08	1995-01	-	7	4	1	1	13	
ET-0073-08	1996-12	-	6	4	1	1	12	
ET-0080-08	2003-12	-	10	7	2	2	21	
ET-0086-08	2007-04	-	16	10	2	3	31	
ET-9301-12	2004-12	Added	10	7	1	2	20	
ET-9302-12	2005-03	Added	9	8	2	2	21	
ET-9303-12	2007-11	Added (Noel)	19	11	1	3	34	
ET-9304-12	2012-01	Added	37	29	10	9	85	353
Tropical Storms								
TP-9001-16	2012-10	Sandy	24	17	6	5	52	
TP-9002-16	2011-08	Irene	26	16	4	7	53	
TP-9003-16	2003-09	Isabel	9	7	2	0	18	
TP-9004-16	1996-10	TS-Josephine	6	4	1	2	13	
TP-9005-16	1985-09	Gloria	3	1	0	1	5	141
TOTAL			**240**	**160**	**40**	**54**	**494**	**494**

A set of graphical products depicting summaries of the various statistical, direct model-measurement comparisons, and skill indicators was generated for each of the WAM model evaluation and testing simulations. Given the total number of buoy locations, it was prudent to summarize the results in a concise fashion. The results are based on time-paired, wave-height calculated and measured data sets and combined into four graphics: bin averaged scatter plot, color contour plot, Q-Q plot, and a Taylor Diagram (Taylor 2001). The latter graphic provides a concise statistical summary of how well model and measurements matched in terms of their correlation, RMSE, and the ratio of their standard deviation. The WAM results for all 22 evaluation storm events are shown in Figure 5-19.

Nearly 84,000 time-paired, observation-model points generated these results. The bin averaged plot shows the distribution of all individual time-paired model and measurements (open circle is the mean; the vertical lines identify the ± standard deviation, σ); the color contour plot shows the population density of the distribution with the linear fit line defined (results forced to a 0. intercept) and the 95% confidence limits; the Q-Q plot represents a cumulative distribution comparison where extreme values

(tail of the wave height probability density function where the rightmost point is the 99.99 percentile) are clearly identified. The Taylor Diagram is slightly more difficult to interpret. Three different statistical measures are plotted in the same graph. The correlation coefficient (statistic derived from least squares linear fit to the data) is represented by the blue-dashed radial lines. The higher the correlation, the better the model fits the measured data. The dashed-green contours (centered about the value of 1 along the *x*-axis) indicate the RMSE or a measure of the spread in the model results relative to the measurements. The lower the RMSE the lower the spread about the mean, and the lower the error in the model estimates. The last statistical variable plotted is the normalized standard deviation (solid black contours, centered on the origin). The standard deviation of the model results are normalized by the observations and thus the closer to (1,0) the better the results. There is an "X" identified in the figure representing a perfect fit to all variables: correlation of 1.0, RMSE of 0., and a normalized standard deviation of 1.

Figure 5-19. Bin average scatter diagram (top left), color contour (top right), Q-Q plot (lower left) and Taylor diagram (lower right) for WAM Level 2 calculated waves derived from the extra- and tropical storm set.

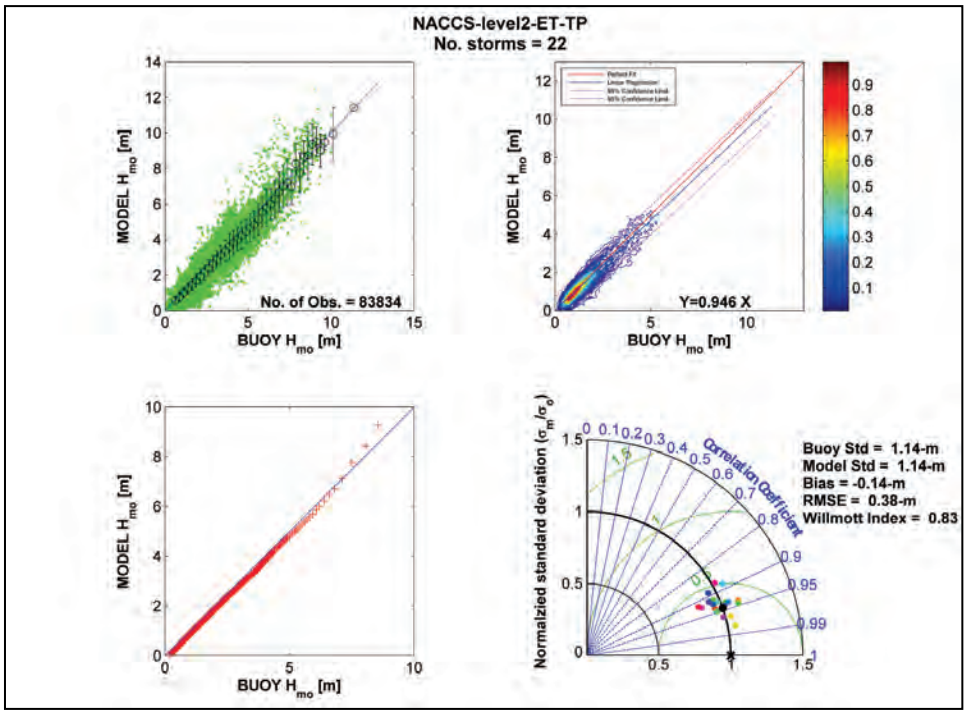

In general, these results are very good. The trend in the WAM results (bin average) compares favorably to the measurements; however, there is a slight underestimation in the calculated H_{mo} estimates between 3 to 7 m,

but that difference is less than 0.25 m (3% to 8% of the measured wave height). Looking at the top of the scatter plot, there are signs of the model overestimating the larger wave height conditions. The color contour plot (Figure 5-19, upper right panel) shows a similar trend. The color contours do not identify all time-paired model and measurement points. The distribution shows a limit approximately 5 m despite containing data greater than this 5 m threshold as shown in the bin-averaged scatter diagram. However, the contoured model results remain in the 95% confidence band, and from the linear fit (using a zero intercept), it is shown that on average the model results are approximately 5% lower than the measurements. This result (despite overestimating the high H_{mo} values) is weighted heavily on the larger population of low (less than 2 m) wave height values contained in the data set. The Q-Q plot emulates the previous two graphics: a modest negative bias in wave heights less than approximately 7 m, then an increasing positive bias in the larger wave heights peaking at the 99.99 percentile at approximately 0.5 m for nearly 9 m conditions. The results plotted in the Taylor Diagram are found in a very small area of the plot, where the individual storm simulation results are consistent. The correlation ranges from 0.97 to 0.87, the RMSE is approximately 0.5 m, and the normalized standard deviation is close to 1.0. Over the mean of all storm simulations (solid, larger black symbol) the correlation is approxmately 0.94, with a RSME less than 0.5 m and normalized standard deviation of 1.0. Overall, the WAM results are quite good, replicating the H_{mo} conditions derived from the 17 extreme extratropical and 5 tropical events.

The summary continues with the Level 3N domain, plotting the WAM results for all 22 events in the four-panel plot (bin average, color contour, Q-Q, and Taylor Diagram) found in Figure 5-20. The number of time-paired observations is over a factor of four lower for the Level 3N compared to Level 2 WAM evaluation; however, 20,000 points is sufficiently large to carry out a meaningful assessment of the model's performance. The Level 3N bin average graphic is very similar to that of Level 2. The distribution of the data is nearly uniform on either side of the 45 deg line (perfect fit); however, WAM again tends to underestimate H_{mo} values for heights greater than 5 m (indicated by the open symbols). The divergence does not grow and remains at approximately 0.25 to 0.5 m (5% to 10% of the measured wave height). The series of six point locations where WAM does poorly correspond to ET-9304-16 (January 2014), where a very local coastal jet emerged in close proximity to NDBC 44005. This event elevated the wave height to a maximum of nearly 9 m, while the remaining three

point source measurement sites recorded H_{mo} values from 4 to 6 m. From the data, it appears the modeled winds were biased low by 6 m/s, and the directions were rotating to the south while the buoy recorded nearly constant easterlies. This event was not selected as an extreme extratropical event, so the wind forcing in the Level 3N domain (0.083 deg) used a bilinearly interpolated 0.25 deg WIS Level 2 wind field, strongly suggesting a wind error.

Figure 5-20. Bin average scatter diagram (top left), color contour (top right), Quartile-Quartile plot (lower left) and Taylor diagram (lower right) for WAM Level 3N results derived from the extratropical and tropical storm set.

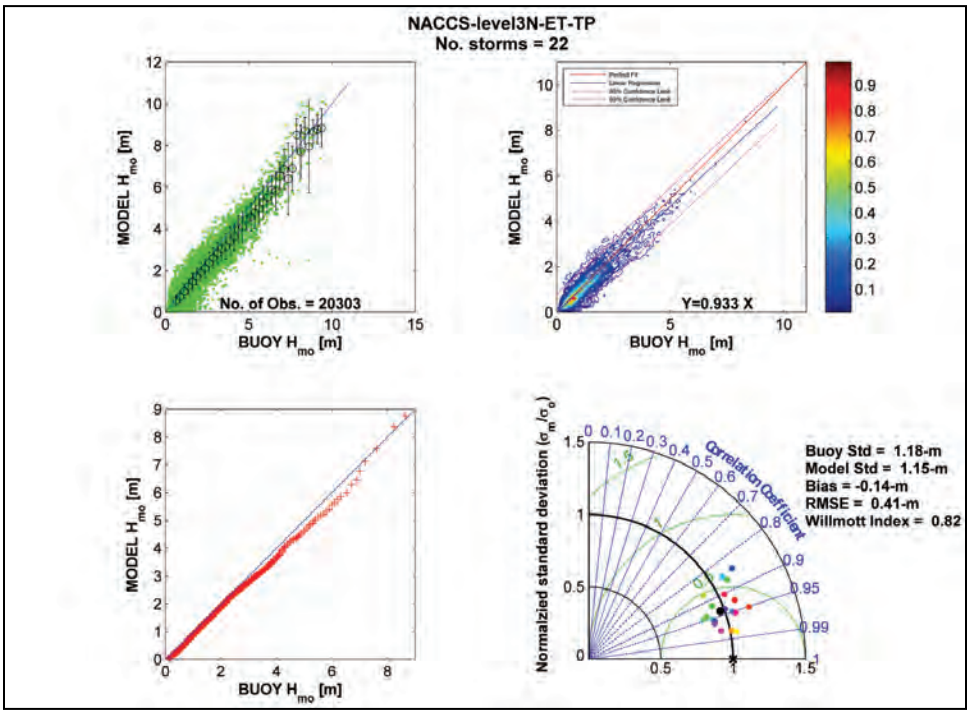

The Level 3N color contour plot (Figure 5-20, upper right panel), emulates the Level 2 results. The distribution generally falls within the 95% confidence limits, with exception of the lobe of relatively low wave heights (2 m and less), where WAM is biased low. The linear fit (symmetric fit) indicates the model results on average are biased low by approximately 7%. This is a result of the large population of extremely low wave heights (red lobe) residing below the 45 deg line (perfect fit). The Q-Q graphic (Figure 5-20, lower left panel) supports the preceding two results. The slight underestimation of the WAM-generated wave heights (between 3 to 7 m) is very obvious in the plot. However, for the larger H_{mo} values, WAM performance tends to recover and only slightly overestimates conditions of approximately 9 m. Last are the results shown in the Taylor diagram

(Figure 5-20, lower right panel). The cloud of data points is larger compared to Level 2, indicating a greater spread in the statistical results. The range of correlation coefficients is between 0.85 to approximately 0.97; the RMSE is between 0.75 to 0.30 m while the normalized standard deviation is between 0.75 and 1.25. Despite the modest increase in errors, the overall result (large black symbol) is only slightly lower than that represented in the Level 2 (Figure 5-19, lower right panel) results. These results are indicative of wind resolution deficiencies used in the nine (five tropical and four added extratropical storms) evaluation storm event population. In general, for a very complicated meteorological and wave climate domain, WAM did very well estimating these extreme events.

Level 3C had nearly 26,000 time-paired model and measurement data points, reflecting a slightly larger population size for the 22 storm events simulated as compared to the Level 3N. The first obvious difference found in the Level 3C results is the scatter of time-paired model to measurement data shown in the bin average (Figure 5-21, upper left panel). As the H_{mo} increases, the over- and underestimation in modeled results increases. In addition, the σ^2 (vertical lines) are longer than Level 2 or Level 3N even for low wave height estimates, indicating the WAM results for the Level 3C domain show a greater variability compared to the measurements.

Figure 5-21. Bin average scatter diagram (top left), color contour (top right), Q-Q plot (lower left) and Taylor diagram (lower right) for WAM Level 3C results derived from the extratropical and tropical storm set.

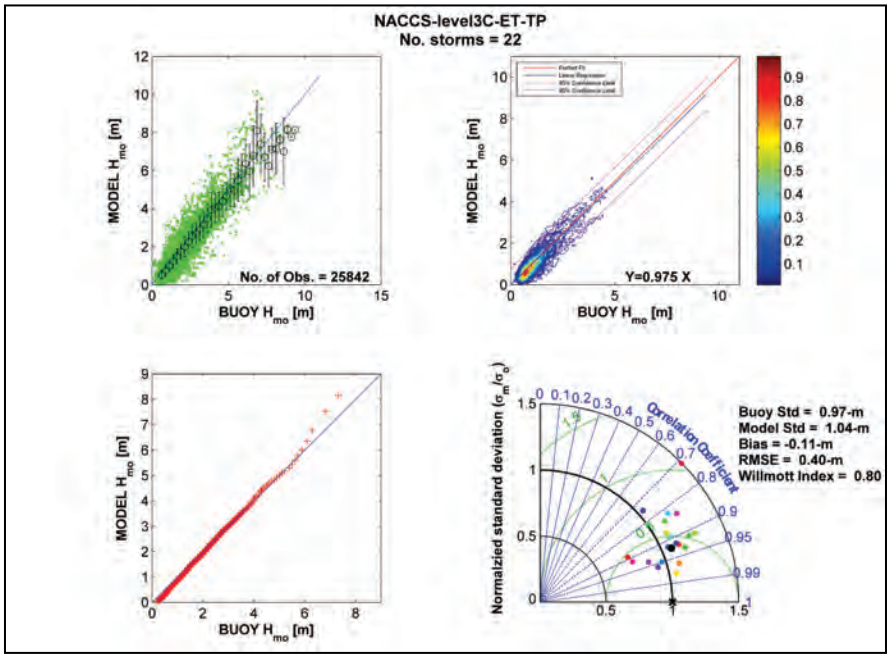

The bin average also displays an increase in the number of overestimations in the WAM estimates (i.e., higher than the line of perfect fit). Embedded in the Level 3C data are measurements obtained from the USACE Field Research Facility (FRF) 17 m Waverider buoy located approximately 3 km offshore. The bathymetry in this region consists of straight and parallel contours with some local variation. However, the WAM grid resolution was 5 min (or approximately 7.5 km for this latitude) and would be difficult to co-locate the FRF Waverider in the grid. The grid resolution at this location was a dominant source of error and dependent on the direction of the wave climate, the local winds, and other site-specific factors in and around the buoy site. It is quite possible that this one site contaminated the summary statistics. Removing this set of data would improve the statistics but would significantly reduce the population size. The color contour plot (Figure 5-20, upper right panel) shows that a high population of low (< 1.5 m) H_{mo} results where WAM is negatively biased. However, throughout the range of wave heights, the model replicates the measurements quite well, remaining within the 95% confidence limits. The linear fit indicates over the mean that WAM has a 2.5% error (again reflecting the negative bias), which is an improvement compared to the results found in Level 2 and Level 3N. The Q-Q graphic clearly reflects quality in the WAM results for H_{mo} values slightly less than 6 m, following the line of perfect fit. However, above this threshold, WAM results diverge yielding a positive bias as H_{mo} increases to a maximum of approximately 0.5 m for a 7.5 m wave height (approximately a 6.5% error). Analysis of the Taylor diagram indicates a larger range in the statistics for the time-paired model and measurements data set for Level 3C. The poor results in the correlation (less than approximately 85%) are primarily based on limited data (despite the near 26,000 individual points) for the more historical events selected (e.g., ET-0050, ET-0054), and the uncertainty in spatially co-locating the FRF Waverider to the WAM grid. The number of active wave measurement observation points contained in the Level 3C grid varied between zero and nine for each storm event (Table 5-3). Of the limited number of sites, the FRF Waverider was one and thus negatively weighed (or skewed) the results. Despite these inherent errors, the majority of the WAM results have an RMSE less than 0.5 m, the correlation is generally 90% or greater, and the normalized σ^2 values range from 0.75 to 1.25 with a mean bias of -0.11 m, RMSE of 0.40 m; overall, these results are very acceptable.

In summary, from the results of the evaluation tests, it was concluded the modeling technology WAM provided good estimates of wave height for tropical and extratropical storm events. The multilevel grid system (Level 1: Atlantic Ocean basin; Level 2: Atlantic coastal regional domain; Level 3N and Level 3C: Atlantic coastal subregional domains) were well positioned accounting for the spatial variability in the geographic features in the NACCS area. The winds used for these tests were derived from the WIS Atlantic Hindcast developed by OWI and were very accurate accounting for the multiple meteorological scales of the weather patterns (both tropical and extratropical events) associated with the Atlantic. Last, noting that all extratropical storm simulations used an 8-day storm duration, it was concluded initializing the Atlantic Ocean Level 1 by 10 days was sufficient to account for all distant wave energy capable of reaching the NACCS domain. From this work, production of the 100 extreme extratropical storm events and the 1050 extreme synthetic tropical storm events could be simulated. Note that for the 100 extratropical storm event simulations, WAM (and OWI wind fields) were evaluated for the full duration of the point-source measurement data.

5.7 WAM production 100 extratropical storm events

The motivation of the WAM simulation of the 100 extratropical and 1050 synthetic tropical storm events is to provide offshore and input boundary condition information to drive the nearshore STWAVE model (Massey et al. 2011) simulations as part of the NACCS. The only change between the input conditions defining the production and that of the evaluation tests are the areal coverage of the

- Level 2 Wind Fields
- Level 3 Wind Fields
- Level 3N and Level 3C WAM domains.

There may be slight confusion between the winds used in the WAM and CSTORM-MS (notably ADCIRC) simulations. The offshore wave estimates are based on three grid levels for all extratropical simulations and two grid levels (Level 2 and Level 3) for the synthetic tropical events. The CSTORM-MS wave and surge estimates are based on only two sets of winds, omitting the Atlantic Ocean Level 1 fields. In this section there is a continuation of the three level naming conventions for consistency. The domains for these new definitions are listed in Table 5-5 and graphically represented in Figure 5-22.

Table 5-5. Model grid information production.

Domain	WAM Boundary Extent				WAM Δx/Δy	Wind*		WAM Time-Steps (s)		Depth Effects
	Longitude		Latitude							
	West	East	South	North		Δx/Δy (deg)	Δt (hr)	ΔPrp	ΔST	
Level 1	-83.33	+20.83	0.00	75.625	1.0 / 1.0	.833/ .625	6	900	900	Deep
Level 2	-82.00	-58.00	22.00	48.00	.25 / .25	.25 / .25	.083	400	400	Shallow
Level 3 Wind	-78.00	-66.00	36.00	45.00		.125 / .125	.083			
Level 3N	-78.00	-66.00	38.00	45.00	.083 / .083			200	200	Shallow
Level 3C	-78.00	-73.50	36.00	41.00	.083 / .083			200	200	Shallow

*Shading reflects changes from evaluation (see Table 5-1) to production.

The simulation of the 100 extreme extratropical and 1050 synthetic tropical events was initiated during the production phase of the offshore wave generation task for NACCS. The WAM simulations were purposefully run independent of the CSTORM-MS workflow and were treated as input similar to the wind and pressure fields. Under this paradigm, the WAM simulations were completed in advance of the start of the CSTORM-MS processing.

Figure 5-22. WAM multilevel grid system used in NACCS Production. Note Level 2 covers the entire domain illustrated (compare to Figure 5-5 displaying evaluation test grid systems).

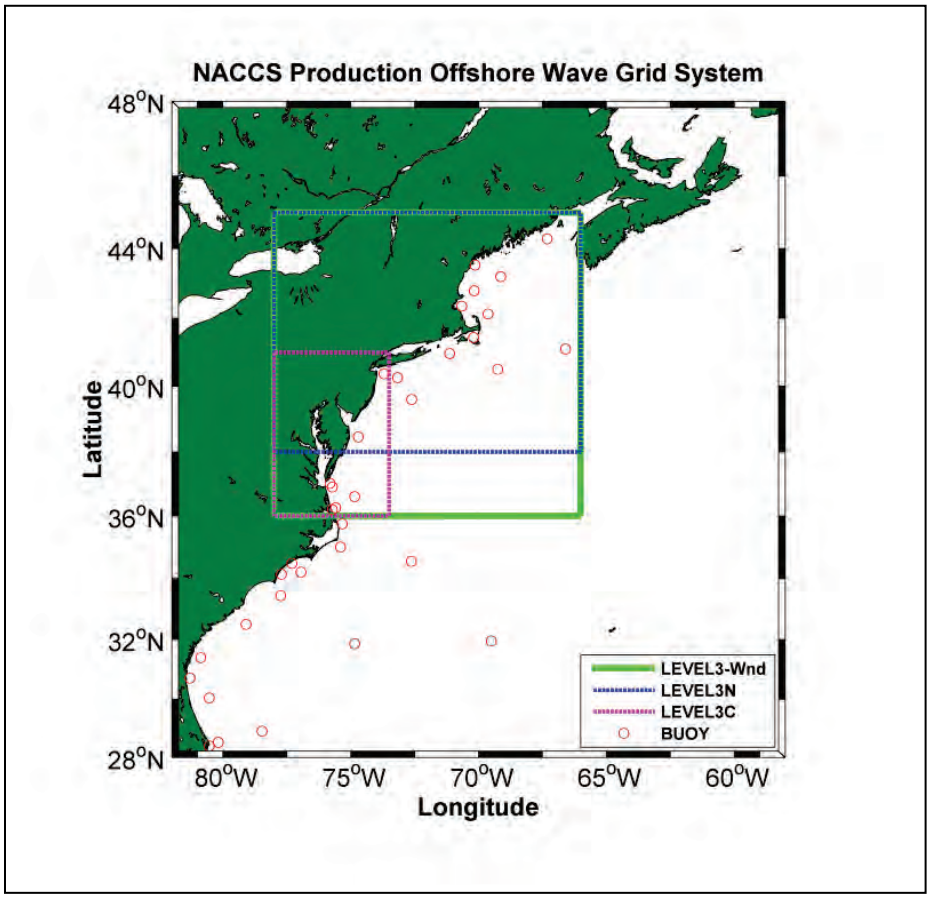

The procedure was automated to maximize the utility of the computational platform while minimizing wall clock time and staff support. All general input files derived from the evaluation tests were used in the production phase. These included the WAM-specific general input files (including postprocessing) and the grid/bathymetry file. For the NACCS offshore wave climate generation the WAM frequency range was defined by

$$f_{n+1} = 1.1 \cdot f_n \text{ where } f_0 = 0.03138428\text{-s}^{-1} \mid n=1, 28$$

$$\theta_m = 7.5 + 5.0 \cdot (m - 1) \mid m=1,72$$

and identical to that used in the evaluation tests.

Sets of wind fields were uploaded, and the simulations were initiated. For the 100 extratropical extreme storm events, the WAM Level 1 was run, dropping boundary condition (2D wave spectra) every 900 s. Upon com-

pletion of the Level 1 storm simulation, Level 2 was initiated building boundary condition information every 400 s for Level 3N and Level 3C domains. Once Level 2 completed, Level 3N and Level 3C commenced where boundary condition information for the STWAVE locations was created (Figure 5-7). When Level 3N and Level 3C completed, the postprocessing phase of the storm simulation was started. Output files consisting of fields defined as integral wave parameters (height, period, direction for total, wind-sea, and swell components) were created at each active grid point in a given region. Point-source integral wave parameters as well as 2D wave spectra were saved at wave measurement sites. The naming convention of all files followed the construct defined by the NACCS workflow procedures defined prior to the production phase of the NACCS. The STWAVE boundary condition information (two files) were created and made accessible for the ensuing STWAVE simulations. The raw binary files were tarred and automatically sent to the mass storage facility for permanent archiving, also defined by the NACCS workflow construct. In addition, a set of files (oneline, spectra, and field files) were automatically transferred to local computer platforms for quality assurance/quality control (QA/QC) processing. Final graphic products including color contours of the maximum and mean wave height envelopes were generated and evaluations performed. The graphic products were reviewed for consistency and quality assuring the WAM simulation performed correctly. For each simulation, a total of eight mean/maximum color contour graphics was generated for each of the four WAM domains (Level 1, Level 2, Level 3N, and Level 3C). Graphic products were also generated to evaluate the STWAVE boundary condition input for each of the STWAVE grids defined in the coastal region of NACCS described in Chapter 7. For each active measurement site (Table 5-4) residing in a given region, three graphic products were produced. The synthetic tropical and historic extratropical event simulations were handled differently and will be summarized in the next section.

To illustrate the similarities and differences between the 100 extreme extratropical events*, the overall maximum (derived from the maximum wind speed and maximum wave height envelope graphics) wind speed and H_{mo} values are plotted as a function of storm number (examples are shown

* Note that three original *storms* (ET_0003, ET_0009, and ET_0071) were replaced with ET_0101, ET_0102, and ET_0103. The original storms selected due to an indication of high surges were actually caused by rain events and outflow past various water level gauges. These three storms were replaced because they were not actual extratropical events.

in Figure 5-2 and Figure 5-3). The estimates of all three levels (i.e., Level 1, Level 2, and Level 3 [North and Central]) are shown in Figure 5-23, where the upper panel contains the maximum wind speed estimates and the bottom panel displays the maximum significant wave height estimates for the 100 extreme extratropical event simulations (8-day storm length).

Evident from Figure 5-23 is a fairly consistent record of maximum wind speeds from approximately 20 to upwards of 40 m/s. Proceeding from the large-scale domain of Level 1 (L1) into Level 3N and 3C (target NACCS area of interest), the maximum winds tend to range between 20 and 30 m/s. The vast majority of the Level 1 wind speed maxima occur in the upper north Atlantic, where the Nor'easters track, or where tropical events dissipate and re-form into large, intense, extratropical systems migrating in an easterly direction toward the United Kingdom and the European coast. Differences between the Level 2 (L2) and Level 3N (L3N) and Level 3C (L3C) are generally modest, indicating the intensity and magnitude of these storms are preserved from the offshore domain to the coastal area as defined by NACCS. However, results derived from Level 3C are generally lower caused in part by the domain size relative to the other three regions. Based on these results, it is evident that relatively intense extreme events were selected appropriately.

The model estimates of H_{mo} maximums range from 5 m to slightly over 20 m (primarily derived from Level 1). Influence of these Level 1 events will at best transport low-frequency energy into the NACCS domain, assuming the wave directions are translating from the proper quadrant. There are times when the Level 1 and Level 2 coalesce toward similar values (e.g., the Perfect Storm, October 1991, ET_0058, January 2000) indicative of a western Atlantic Coastal storm. These results persist throughout the extreme storm record length where Level 3N is in close agreement (slightly less) to the Level 2 H_{mo} estimates. The Level 3C maximum wave height estimates are generally lower than other levels, akin to the wind speed results. Overall, the range in results from Level 3N and Level 3C is variable and consistent with estimating the wave climate for extreme extratropical events.

Figure 5-23. Maximum wind speed and H_{mo} estimates for 100 extratropical historical storm simulations. Decades are indicated by the red vertical lines.

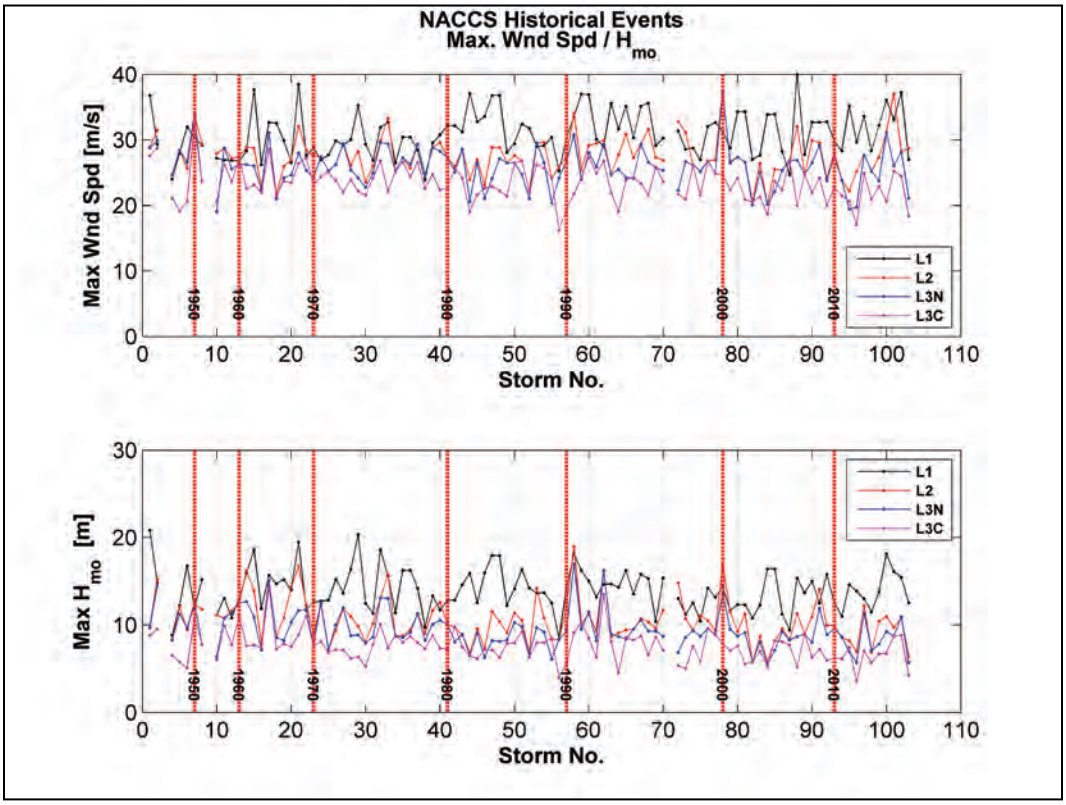

The spatial variation of the maximum wind speed and significant wave height estimates are shown in Figure 5-24. The 100 extreme extratropical event results are plotted; however, some locations will have multiple entries. The wind speed maxima fall in the offshore region, which is expected given the potential for these storms to be spatially large with relatively slow forward motion of the storms. There are, however, many cases of wind speed maxima found along the seaward boundaries between the Level 2 and Level 3 domains. In addition, there are a few cases in Level 3N and Level 3C where the wind speed maxima are located at or relatively close to the land/water boundary. Considering that these events are dominated by Nor'easters, there is a strong southwest to northeast distribution of the wind maxima (indicating storm path). For the significant wave height maxima, there is a much different distribution. It is apparent that the significant wave height maxima are not spatially co-located with maximum wind speed location but are temporally concurrent (illustrated in Figure 5-23). There is generally a temporal phase shift between a wind speed maximum and H_{mo} maximum at a point location. The majority of maximum H_{mo} estimates fall on or in close proximity to the boundary between Level 2 and the two Level 3 domains. This is an indication that both

Level 3N and Level 3C maximum wave climate is a result of wave energy entering the region and rapidly attenuating rather than continuing to grow under the wind forcing. However, there are some cases where local generation occurs. The pockets of maximum wave heights near the coastline reside in the Gulf of Maine and offshore of the New Jersey-Maryland-Virginia-North Carolina coastline. There is a void of H_{mo} maxima south and east of the south shore of Long Island, continuing to east of Cape Cod. This is the transition region for many of the Nor'easters, where they would attenuate and track well to the east, amplify and lift up in a northeasterly direction, or be blocked by high pressure to the north. In the latter case, the winds will continue to blow in a counterclockwise direction, and local wind-seas would continue to develop off the northwesterly quadrant. Concurrently, to the south of the low-pressure system, the swells radiate southeast and eastward.

Figure 5-24. Location of wind speed and significant wave height maxima derived from the 100 extreme extratropical simulations.

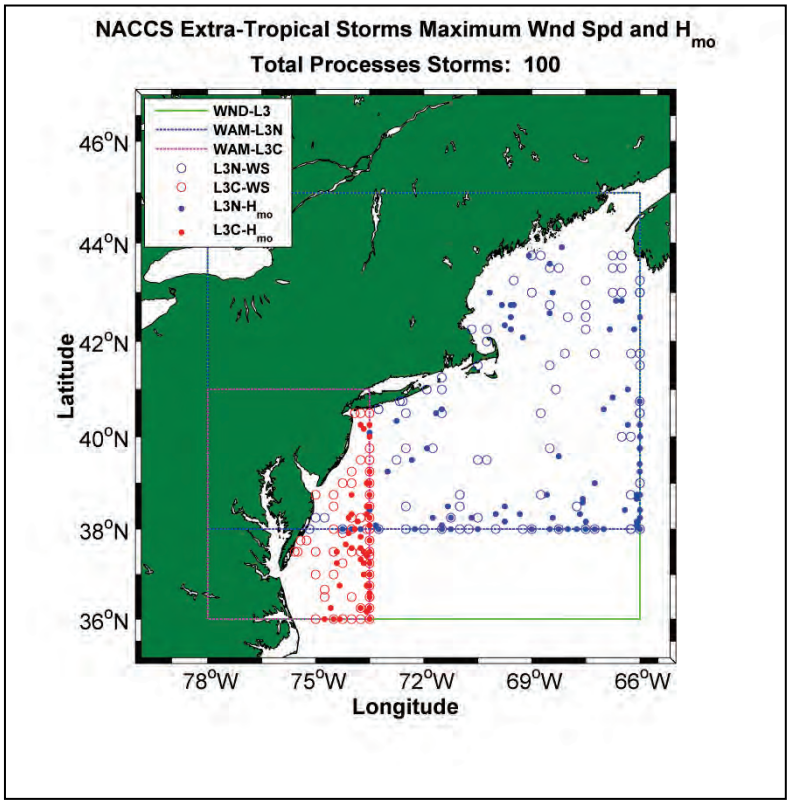

During the production of the 100 extreme extratropical storm event simulations, the evaluation of WAM continued. Graphic products were generated (time, scatter, and Q-Q plots), and statistical testing was performed at all point-source wave measurement sites in the three model production

levels. The number of point-source measurement sites for these analyses is illustrated in Figure 5-25, where the storm number is labeled along the abscissa and the number of point-source sites labeled along the ordinate. Any storm simulation below ET_0040 (Storm 40 in Figure 5-25) had no point-source measurement sites available, and no evaluation could be performed. For all extratropical storm simulations, the Level 3C domains contained no more than four sites compared to a maximum of eight in Level 3N. This limited population size will have an impact on the overall assessment of WAM. The limited data used for comparisons also contained the FRF Waverider data and as previously noted, could not be sufficiently co-located in the Level 3C grid domain, producing false negative results. Last, the evaluation testing was based on simulation lengths (i.e., initiated at least 1 month prior to the storm maximum) that were considerably longer than the extratropical extreme event durations of 8 days. Despite comparing the number of evaluation storm events (22) versus the extreme extratropical events (100, approximately 60 containing data) used in the production, the actual number of time-paired observation to model results was similar in some comparisons.

Figure 5-25. Number of point-source measurement sites available during the production of the 100 extreme extratropical storm events. Decades are indicated by the red vertical lines.

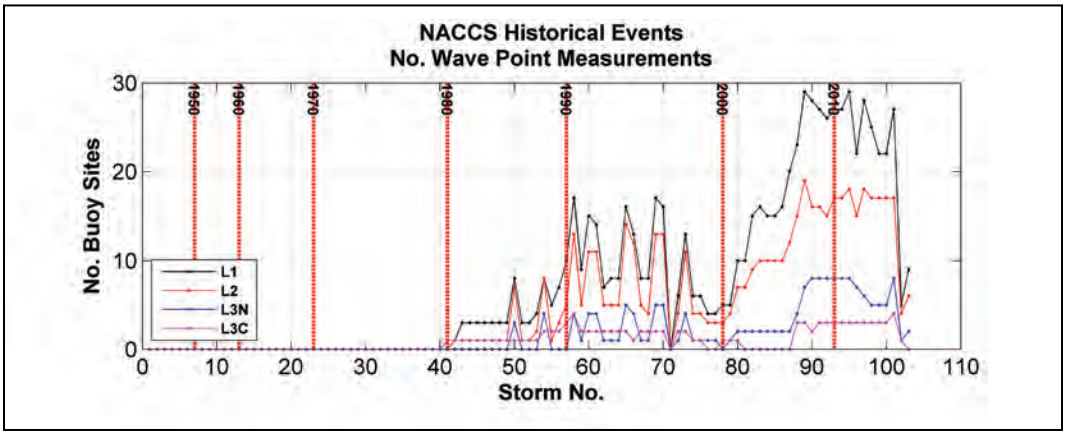

The Level 2 WAM results from the 100 extreme extratropical storm simulations are presented in Figure 5-26. The results are expected to emulate those found in the evaluation testing because most if not all of the simulated extratropical storms were incorporated in the extreme storm population. The number of time-paired observation/model results compared to the evaluation test set increased by approximately 40,000 (Figure 5-19), and the peak H_{mo} results increased by about 4 m (bin average, upper left panel). The bin average plot indicates a region where WAM is negatively

biased (from 5 to 7.5 m) to a greater extent than in the evaluation testing. This is contrary to a visual inspection of the cloud of results which appears to be greater than the 45 deg line (i.e., positively biased). The positive bias is more obvious for wave conditions greater than approximately 10 m; however, the population size is restricted to a very small population size. The color contour plot is similar to the results derived from the evaluation tests. The WAM results generally fall within the 95% confidence bands, and the linear regression (slope of 0.964) indicates approximately a 3.6% negative bias over the mean (actually, -0.13 m shown in the lower right panel). These errors reflect the persistency in WAM to slightly underestimating the large population (red color contours) of low wave conditions. As the wave heights increase, there is a near uniform distribution of relative errors above and below the 45 deg perfect fit line. The Q-Q analysis and graphic (lower left panel) clearly illustrate the reliability of WAM in estimating the entire wave height distribution found in the point source measurements. This includes up through the 99.99th interval for wave heights of 8.75 m. The last 1% has not been accounted for; however, based on the bin average, WAM does show a slight overestimation (approximately 1 m) of the peak conditions for H_{mo} values above 10 m.

The Taylor diagram provides a very good representation of multiple statistical tests in one graphic and reflects the quality in the WAM results for the 100 extreme extratropical events (note that there are approximately 60 events containing wave measurements). The RMSE generally falls below 0.5 m, and the correlation is between 0.90 to 0.97, signifying quality in the model estimates. The normalized σ estimates are between 0.75 and 1.25, suggesting the scatter in the model emulated that of the measurements. This is true for all but three points (individual storms) that show slightly less quality, where the RMSE falls above 0.5 m and the correlation coefficient is near 0.80.

Figure 5-26. Bin average scatter diagram (top left), color contour (top right), Q-Q plot (lower left), and Taylor diagram (lower right) for WAM Level 2 results derived from the 100 extreme extratropical storm events.

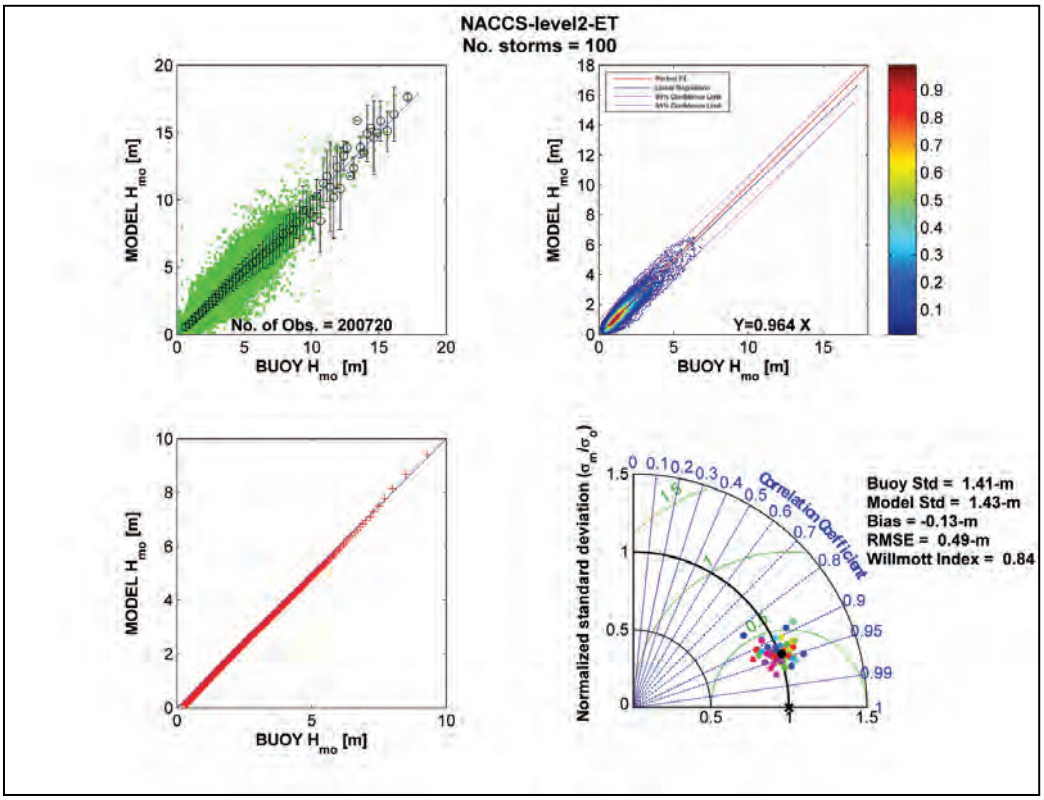

The Level 3N summary results are displayed in Figure 5-27. With the additional storm simulations, there is an increase in scatter of the bin average (upper left panel) above and below the 45 deg line of perfect fit, which appears to be relatively uniform. However, the binned mean H_{mo} model results diverge approximately 5 m from the perfect fit. These results are derived from one storm event (ET-0061-08, the Storm of the Century; Cardone et al. 1996) where an emerging Nor'easter entered the Level 2 domain early into the hindcast. Wave measurements from multiple sites were on the order of 6 to 7 m compared to WAM estimates of 2 to 4 m generating the obvious underestimations (lack of sufficient spin-up in the L2 domain). WAM did relatively well at the selected storm of 6 m later in the simulation. With the limited population size, WAM does replicate the peak storm wave heights (> 12 m) rather well. The overall quality in the WAM estimates (upper right panel) is provided in the color contour plot, where WAM estimates run approximately 7.5% lower than the wave measurements.

Figure 5-27. Bin average scatter diagram (top left), color contour (top right), Q-Q plot (lower left), and Taylor diagram (lower right) for WAM Level 3N results derived from the 100 extreme extratropical storm events.

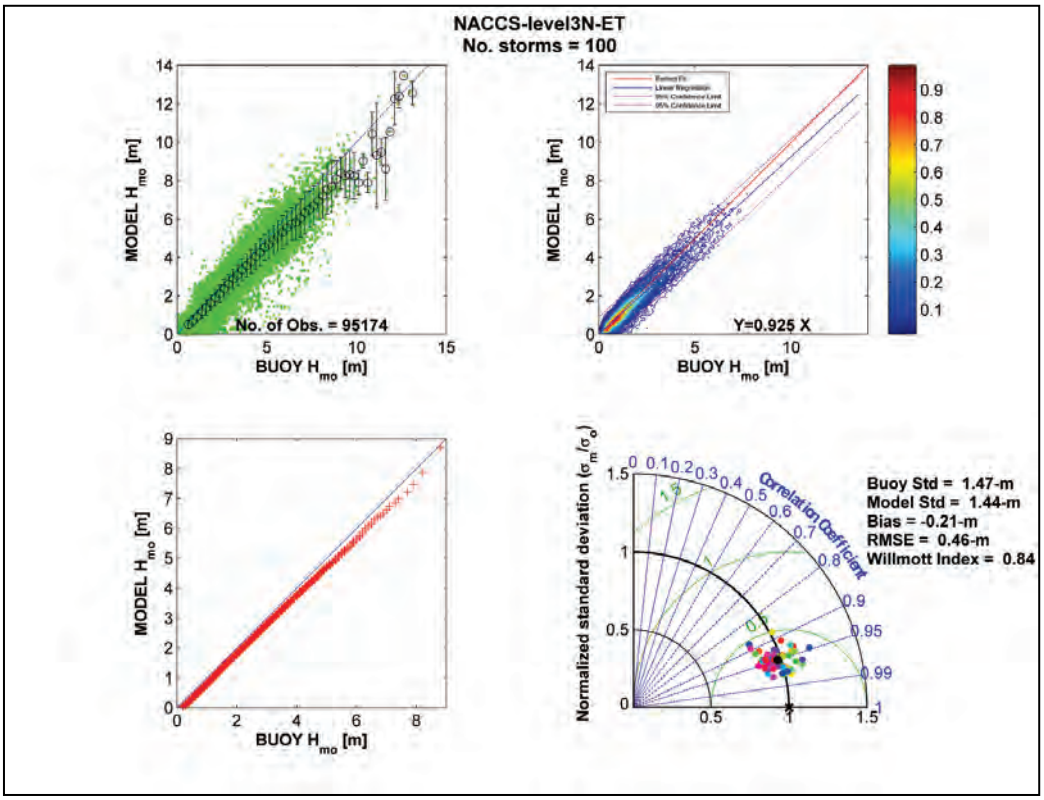

As found in the Level 2 results, the Level 3N WAM estimates fall within the 95% confidence limits for the wide range of wave conditions in the 100 extratropical extreme events. It does appear a significant component of the error resides in underestimating the low H_{mo} conditions (i.e., < 2 m) indicated by the red region falling below the perfect fit.

The Q-Q analysis (Figure 5-27, lower left panel) reveals the trend found in the bin average and color contour diagrams. For low significant wave heights (< 2 m), WAM tends to underestimate these conditions. This underestimation increases slightly through the remaining range in the wave climate. However, this error is only approximately 0.25 m at its maximum, or approximately 3% for wave heights of 8 m. The last analysis, displayed in the Taylor diagram (lower right panel of Figure 5-27) summarizes the previous results. The overall bias for the 95,000 time-paired observations was -0.21 m, with an RMSE of 0.46 m and correlation generally falling above 0.9, which is a good indication of the quality in the WAM estimates in multiple locations when compared to multiple storm scenarios. These results would be improved, if the selected storm period of record would

have been used, as this would essentially eliminate evaluations based on the spin-up deficiencies previously noted existing in the Level 2 and Level 3N regions.

The Level 3C domain WAM evaluation results are provided in Figure 5-28. As previously indicated, the number of wave measurement sites compared to Level 2 and Level 3N was much lower (Figure 5-25). Hence, the results do not indicate the true quality in the WAM estimates especially at locations such as the FRF WaveRider (the longest wave record of all measurement sites) where there were issues of co-locating the WAM estimates to the true buoy site. The bin-average scatter plot (upper left panel, Figure 5-28) displays a lower overall wave climate relative to the Level 2 and Level 3N domains, where the maximum recorded wave height is on the order of 8 m (compared to 17 m and 12 m for Level 2 and Level 3N, respectively). This may in part be attributed to the number of sites available, the relative size of the domain, or a natural condition. There is also a larger scatter in the WAM results that lies above the line of perfect fit. Nevertheless, over the binned means, WAM generally performs well until approximately 5 m where there is a tendency to underestimate H_{mo} conditions. The model errors (given adequate population size) are approximately -0.25 m and acceptable for these types of simulations. The distribution of the 34,000 time-paired observations (upper right panel, Figure 5-28) displays a similar trend in the WAM results as found in the scatter plot. There is a tendency for some contours to fall outside the 95% confidence limits for wave heights between 2 to 4 m; however, the WAM results are approximately 5.5% lower than the measurements. The majority of these errors (yellow to red colors in distribution) again reside in the low H_{mo} range (< 1.0 m) where WAM consistently underestimates wave height. These results are also evident in the Q-Q analysis where the data fall below the line of perfect match for significant wave heights less than 1.0 m, follow the line up to approximately 3.5 m where again there is a small underestimation, and finally track on the line until the extreme case (> 7 m), which is slightly above the line. The Taylor diagram (lower right panel, Figure 5-28) displays a much larger scatter in the WAM results compared to Level 2 and Level 3N. Again, the scatter is mainly attributed to the population size of time-paired model and measurements and the inability to co-locate the FRF WaveRider site in the WAM grid. These two conditions tend to drive the analyses producing substandard results. The five greatest outliers shown in the Taylor diagram (Correlation < 0.9 and RSME > 0.5 m) are based on the limited sites for the evaluation or were based on only the FRF

WaveRider data. However, most of the WAM results for Level 3C do fall above a correlation of 0.9, an RMSE of 0.5 m, and normalized σ^2 between 0.75 and 1.25 m. The overall bias was -0.17 m with an RMSE of 0.42 m, results that are very similar to those found in Level 2 and Level 3N.

Figure 5-28. Bin average scatter diagram (top left), color contour (top right), Quartile-Quartile plot (lower left) and Taylor diagram (lower right) for WAM Level 3c results derived from the 100 extreme extratropical storm events.

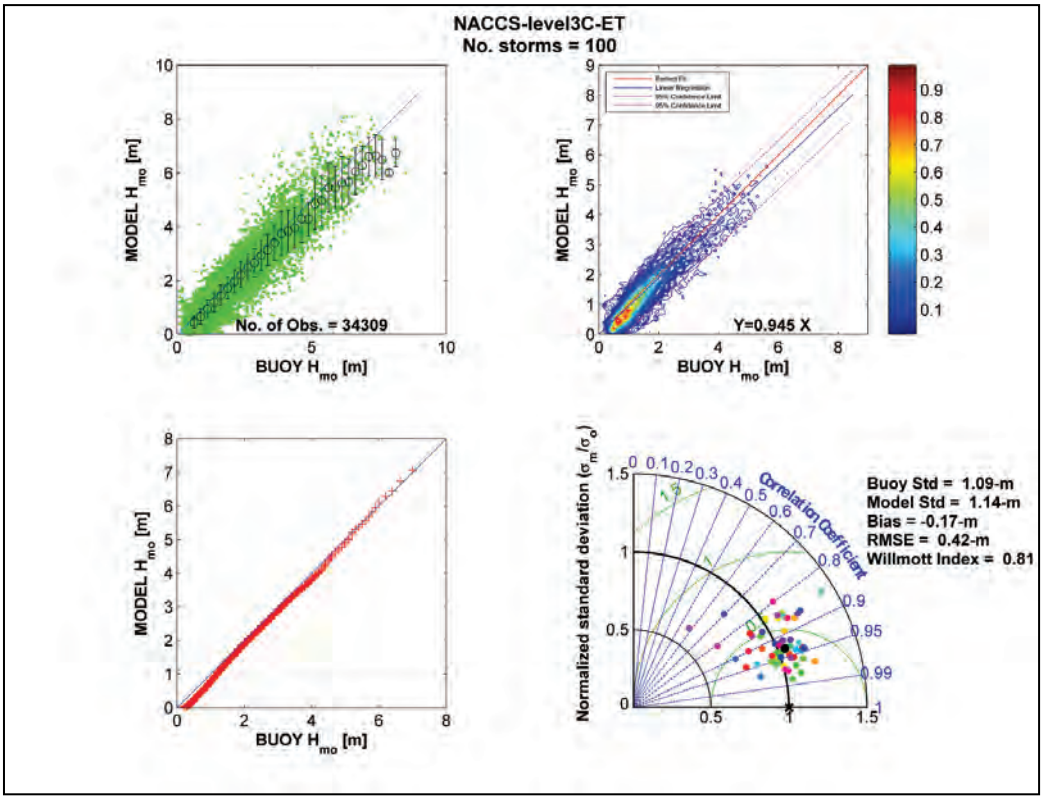

In summary, a total of 100 extreme extratropical events were simulated using a multilevel WAM grid system. Evaluations of WAM were performed for approximately 60 of those storm events at upwards of 30 measurement sites along the Atlantic coast (Level 2) and in the NACCS domain (Level 3N and Level 3C). The summary of results indicated that in general, WAM performed well for the extreme storm events where measurements were available. The overall trends showed high-quality results given sufficient data for the evaluation. Only when there were limited point-source sites available, or in some cases pre-emerging meteorological events prior to the designated storm peak, did the WAM performance indicators decline. The remaining WAM estimates for the extreme extratropical simulations selected in the NACCS produced high-quality results.

5.8 WAM production 1050 synthetic tropical storm events

As in all wave modeling applications, accuracy in the wind field specification is the most critical factor influencing the quality of the resulting wave estimates. The wind fields used in the production of synthetic tropical storm event were generated from a planetary boundary layer model (Thompson and Cardone 1996) that solves the vertically averaged equations of motion subject to horizontal and vertical shear. The model is an application of a theoretical estimate of the horizontal airflow in a boundary layer of a moving vortex. The model (TC96) has been used successfully for the past 4 decades in the generation of wind fields (and pressure fields) resulting from a tropical storm system (Thompson and Cardone 1996). This methodology has been successfully used in the construction of all WIS wind fields used in its long-term wave hindcasts, in the Interagency Performance Evaluation Task Force report on Hurricane Katrina, and in follow-up studies by the USACE ERDC and the Federal Emergency Management Agency work on the Louisiana and Texas coasts. For the NACCS production of the synthetic storm events, these are the only meteorological systems occupying the model domain, and the results should be interpreted in a manner consistent with the generated wind fields.

The 1050 storm events consisted of sets of storms with one of four landfalling track headings, two bypassing track headings, variations in central pressure deficit (Δp), storm speed (V_f), and radius of maximum winds (RMW) along the track. Note that Δp, V_f, and RMW were held constant along the storm track until prelandfall filling would occur. A prelandfall filling value was selected based on an assessment of 45 historical storm events defined in the NACCS domain. The prelandfall filling takes place approximately 250 km from the point of landfall. For the bypassing storm set, Δp, V_f, and RMW were held constant and a postregion filling over the ocean was defined along the storm track. In the special case of bypassing storms which make landfall prior to entering the NACCS domain, the JPM parameters were specified at and prior to landfall after which the Vickery (2005) postlandfall filling model was applied. Three regions (Figure 5-30) were preselected for the construction of the synthetic tropical storm events and designated for unique track spacing. These regions are defined by

- Region 3 36.5 deg to 39.0 deg
- Region 2 39.0 deg to 41.5 deg
- Region 1 41.5 deg to 45.0 deg.

The generation of the offshore boundary condition wave estimates (2D spectral estimates provided at 15 min intervals along the nine offshore STWAVE domains) was treated as input (as in the case of the wind and pressure fields) to the CSTORM-MS production system. This required the WAM simulations to be performed prior to the initiation of the CSTORM-MS system.

The production for the 1050 synthetic tropical storm events varied slightly from the extratropical simulations. The first difference restricted all storm events to be contained in the Level 2 (and for the WAM simulations, the Level 3N and Level 3C grid) domain. The second, more obvious change was the removal of the evaluation step in postprocessing (i.e., model to measurement tests performed). During the simulation of these events, the WAM results underwent QA/QC by visual inspection. The maximum and mean wave height and wind speed envelope graphics were examined to ensure consistency (eight graphical products). Boundary condition wave estimates used to drive the STWAVE model simulations were also evaluated graphically to assure the results derived from WAM were consistent with the forcing conditions. Upon completion of the QA/QC, the results (i.e., the boundary condition files) were saved for the CSTORM-MS simulations. All other output files were merged and archived on the ERDC HPC mass storage facility.

An assessment of the WAM results for the 1050 synthetic tropical events is provided below. The information presented summarizes the maximum conditions generated for these storms, the relative location of these conditions, and the degree to which Level 3N and Level 3C compare to the Level 2. Placing these storms in the context of real events, the following are maximum wind speed estimates* occurring the life cycle of each event.

- 2012 SuperStorm Sandy: 46 m/s
- 2011 Hurricane Irene: 54 m/s
- 2003 Hurricane Isabel 72 m/s
- 1996 Tropical Storm Josephine 31 m/s
- 1991 Hurricane Bob 51 m/s
- 1985 Hurricane Gloria 64 m/s.

* Wind speed estimates were found on http://weather.unisys.com/hurricane/.

As previously indicated, the assessment is based on overall maxima for a storm event. These results were derived from the maximum wind speed and maximum significant wave height envelope generated during the QA/QC evaluation process. The values represent the overall maximum condition that was generated at any grid point in the WAM domain for the duration of each storm simulation. Figure 5-29 is a graphic presentation of the maximum wind speed (top panel) and the maximum H_{mo} estimates for the 1050 storm events. The lines are color coded for the Level 2 (black), Level 3N (blue), and Level 3C (red) results. The vertical lines indicate the various classifications of storm events and landfalling position relative to the three preselected regions in the initial generation of the events. Also, the regional storm systems were subdivided into landfalling and bypassing storm scenarios. Finally, for each of the subsets there are track numbers starting at a southern point and progressing in a northerly direction.

For the conditions presented in Figure 5-29, the Level 2 maximum wind speeds are generally higher as compared to the Level 3N and Level 3C results. Level 3N winds tend to be higher than Level 3C. The variation (low to high wind speeds) falls into the range of the tropical storm maxima listed above. Hurricane Isabel's maximum wind speed was located farther east of the Level 2 domain and varied between 45 to 51 m/s once inside the Level 2 boundaries. The bulk of the maximum wind speeds falls between 25 to 50 m/s with a few storm conditions containing winds in excess of 60 m/s consistent with historical storms affecting the NACCS domain.

Figure 5-29. Overall maximum wind speed (top panel) and maximum significant wave height (bottom panel) estimates for each of the 1050 synthetic tropical storm simulations for the NACCS.

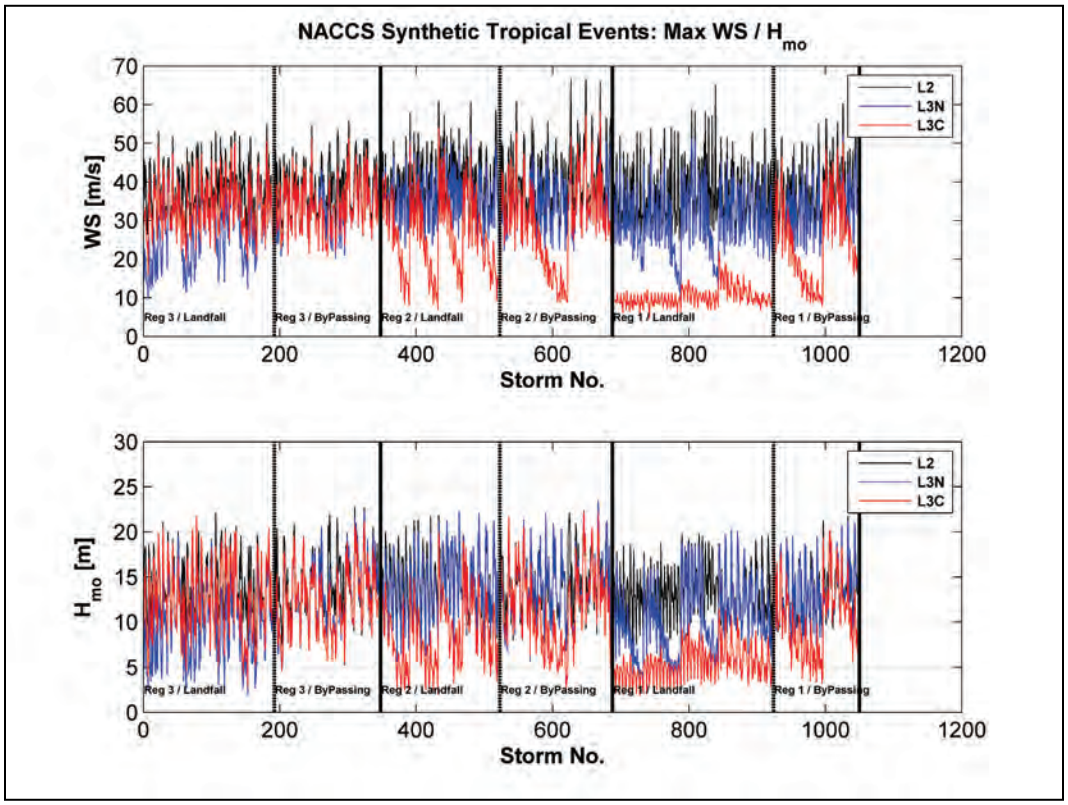

Level 3C shows greater variability in the maximum wind conditions for nearly all subsets (by region, landfalling, or bypassing) and is highly dependent on the track number and angle of attack at landfall. There are two primary reasons for large gradients in the maximum wind speed trace. The first is the relative position of the Level 3C domain as it is located in the southernmost area of the NACCS. Second, tropical systems and their accompanying wind fields rotate counterclockwise, with the core of the maximum winds of each storm located in the right front quadrant. This means for any track the maximum winds would fall to the right side of the track's position. The synthetic tropical systems are organized by type, (landfalling or bypassing), region, and track. For all cases in the population there will be one unique track that falls to the north of the Level 3C domain (Figure 5-22), and the maximum wind speed would fall further outside the defined area. Figure 5-29 reflects these conditions where the large gradients (functionally related to the storm) in wind speeds occur in Region 2 and Region 1 (for Level 3C). These gradients occur to a limited extent for the Level 3N model grid as found in Region 3. There is a similar pattern (storm dependent gradients) of Region 1 and Level 3N winds where there are sets of

storms with decreasing wind speeds as the new storm track location is translated in a more northerly position until it hits the Level 3N northerly boundary. Geographical considerations (protrusion of Cape Cod to the east), storm track position, and tropical system parameters (e.g., Δp,V_t, and RMW) for landfalling systems occurring in Region 1 will nearly eliminate any wind forcing effect on the Level 3C domain.

The results from bypassing tropical systems are similar to the conditions found in the landfalling systems. Maximum wind speeds for all three model domains (Level 2, Level 3N, and Level 3C) are very similar in magnitude. There are limited cases where the Level 3C results depart from the other two domains. The storm tracks generally follow the coastline and will have a net impact on all three of the wave model domains. The sequencing of the individual storm tracks now runs from north to south and west to east. As Figure 5-29 (top panel) indicates, the variation in the storm track location is nearly invariant relative to the maximum wind speed magnitudes. The bypassing storms for Region 2 again show a variation in maximum wind speeds observed in the Level 3C domain. The storm tracks for these bypassing events translate from west to east and eventually falling outside the eastern boundary of the Level 3C domain and thus resulting in a low maximum values (approximately 10 m/s). The return of the storm track position to the western edge of Level 3C occurs at TP-0624-06 and is reflected by the step increase in the wind maximum. The Level 3N results remain generally unaffected by the tropical storm track position because of the wider expanse of the domain. A similar trend exists for bypassing events in Region 1. The results reflect the track position relative to the Level 3C domain that was evident in the Region 2 storm set (Figure 5-29). The initial storm track is positioned near the Atlantic coast (TP-0925-04). Each successive storm track moves in an easterly direction through TP-0996-02) and then repeats the sequence again starting along the Atlantic coastline. The results from Level 3N again show very little changes over the track position subset. Maximum winds vary between 20 and 40 m/s for Level 3N although the Level 3C results include winds as low as 10 m/s.

Scaling principles (Phillips 1957) state that the significant wave height is proportional to the wind speed squared; hence, the results found in Figure 5-29 (bottom panel) should reflect the maximum wind speed variations. In part this is true. For increasing wind speed maxima, the H_{mo} maxima follow a similar trend. As wind speed maxima decrease, the significant wave

height decreases. There is an added component of the wave field that will also affect the coastal reaches of NACCS. The complexities of mapping the wave climate in the presence of a tropical system have been precisely measured (Walsh et al. 2002) showing migration of swell energy across the core of a tropical system.

Certain variables of a tropical storm system are important in the development of the wave field including the wind speed, forward speed, and storm track. Local wind-waves are developed by the specified wind fields. There is a dynamic balance between the atmospheric input (S_{in}), the transfers of energy (downshifting in the frequency range) by the nonlinear wave-wave interaction (S_{nl}), and whitecapping or dissipation (S_{ds}), which occurs when the energy level exceeds a threshold and breaking will commence. This balance will continue; however, if the phase speed of wave systems exceeds the wind speed, the relative energy is transformed to swell. As this is taking place, the storm is moving at a given forward speed. As the tropical system translates along a given storm track, energy will escape from the system because its group speed is greater than the system's forward speed. There are occurrences when the translation speed of the storm system matches the group speed. When this occurs, the local wave climate will continue to develop and potentially become trapped or saturated (e.g., Pierson and Moskowitz 1964; Resio et al. 1999). Extratropical systems have similar characteristics representing the local and distant wave field. However, tropical systems are smaller, fairly well defined, more rapidly moving, and contain wind speeds of higher intensity.

There are similarities in the H_{mo} maxima as observed in the wind speed maxima for the 1050 synthetic tropical storm simulations. For the landfalling conditions in Region 3, the similarities are apparent; Level 3N wave estimates are lower for lower wind speed maxima, and Level 2 H_{mo} results increase and decrease with the winds. Results from the Level 3C maximum significant wave heights in general follow the winds; however, at times they do exceed the results from Level 2. The wave energy is carried farther into this region with a combined effect of the local wind-seas surrounding the tropical storm core and the swell energy radiating outward toward the coast. For Region 2 a similar situation exists for the landfalling events; however, the roles of Level 3C and Level 3N are reversed, and Level 3C maximum H_{mo} conditions follow the wind speeds. When individual storm tracks translate farther to the northern Level 3C boundary, the wave heights will diminish. Level 3N maximum significant

wave heights, despite a sometimes lower wind speed maxima, at times meet or exceed the maximum Level 2 wave heights. The similarities persist in the Region 1 landfalling storm set. The Level 3C domain H_{mo} conditions are nearly a factor of three lower than what is observed in Level 3N. There is an observable decreasing trend in the significant wave heights in the Level 3N results compared to its wind speed counterpart. The decrease in the wave heights is a result of the individual storm track position running into the Level 3N northern and eastern boundaries reducing the capability of any local wind-wave generation. For the bypassing events, the H_{mo} trends are similar to the winds. Occasionally Level 3N wave heights are equal to or exceed the Level 2 conditions. These tracks are slightly offshore and follow the coastline so that wind-wave generation will continue until the event makes landfall along Nova Scotia, Canada. In all cases, the results shown in Figure 5-29 follow an expected pattern for the types of conditions simulated. All of the outlier events are explained by either geographical constraints or by the bounding boxes defined by the Level 3N and Level 3C domains relative to the storm track positions.

The second summary graphic (Figure 5-30) displays the geographical location of the 1050 wind speed and significant wave height locations. The Level 2 grid domain is identified by the magenta box, the three Regions used in the tropical storm event set are defined (horizontal black dashed lines), and the maximum wind speed and H_{mo} estimates are plotted. Note, only one point is generated for each synthetic tropical storm event whether multiple locations exist in the domain for that simulation. The tropical winds were based on a moving vortex translating along a given storm track. The winds in the core of the storm system remained constant through the simulation until the filling routine was applied at approximately 250 km offshore from the land falling location. Hence, the wind maxima for landfalling storms will be positioned along the initial storm track starting at approximately 20 deg N latitude and 40 deg W longitude. All maximum wind speed estimates follow the initial arch of the storm suite. The distribution found in Figure 5-30 is a reflection of the original input wind field data set.

Figure 5-30. Maximum wind speed and significant wave height locations in Level 2 model domain for the 1050 synthetic tropical storm event simulations.

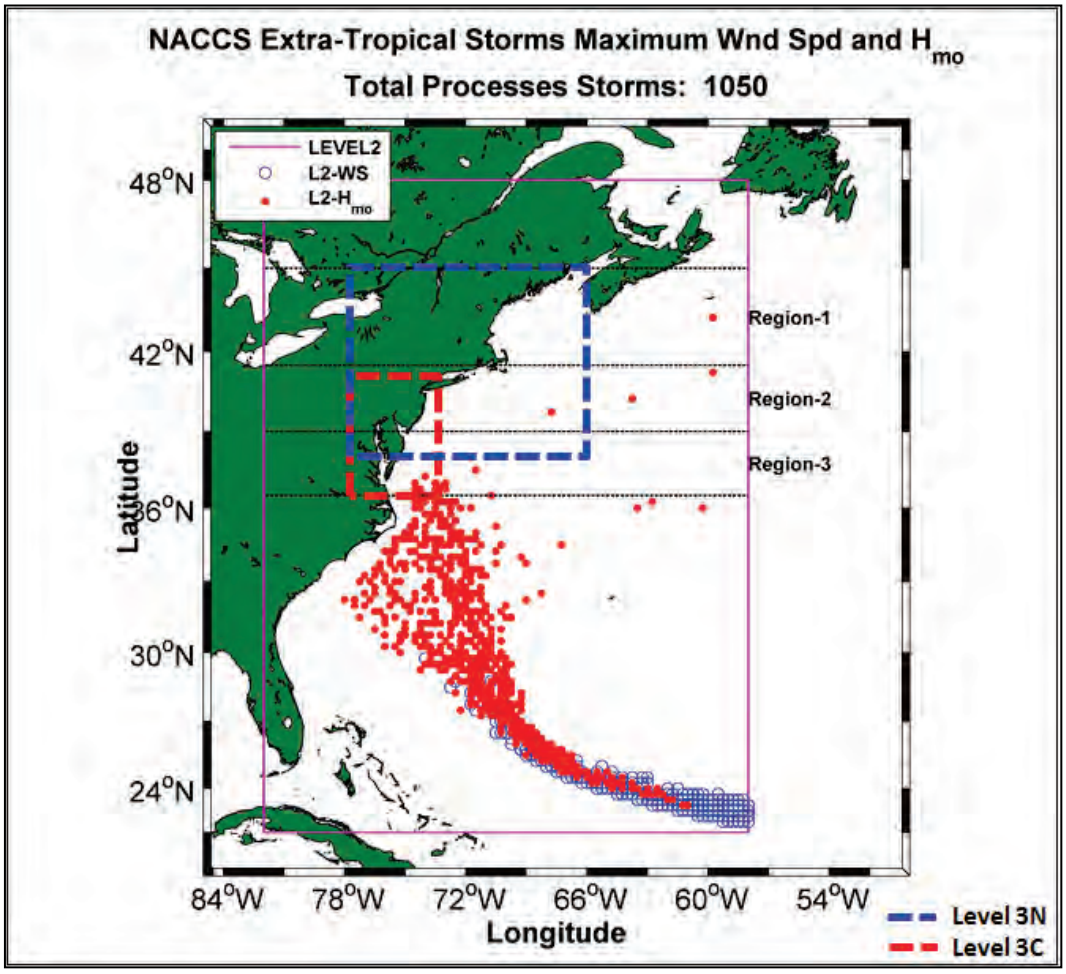

The maximum significant wave height locations require additional reasoning. First, nearly all of the designated locations fall well south of the NACCS domain (southern boundary around 36 deg N latitude. The maximum H_{mo} estimate locations are based (as is the wind speed) on an absolute value. If there are multiple values contained in the domain for a given simulation, only the initial location is tabulated. Hence, if the wind fields are constant over the track position, it is reasonable to expect these locations of maximum wave height to propagate into the NACCS region. Second, the magnitude of the wind speed falls to the range between 30 and approximately 65 m/s. For these winds, wave heights in wind-wave growth expressions can attain over 20 m as shown in Figure 5-29. Wind-wave growth is occurring from the initial storm track at the initial time-step and will continue to grow until the wave field becomes saturated. This is essentially what is occurring for nearly all of the synthetic tropical storm events. The fan-shaped pattern found in the H_{mo} maxima distribution is a result of

two mechanisms. The first is the transitional arc of all storm tracks originating at approximately 20 deg N, 40 deg W then following a specified track in an area defined approximately by

- Southern Boundary: 27 deg N
- Northern Boundary: 30 deg N
- Western Boundary: 74 deg W
- Eastern Boundary: 78 deg W.

The second mechanism is the turning of the storm system. When this occurs, the local wind-seas will transition into swell energy and radiate outward toward the west. These two effects and the east-west location of individual storm tracks will create the fan shape identified in Figure 5-30. Once the tropical system completes its transitional arc, local wind-wave growth will continue along the final section of the storm track.

Located in Figure 5-30 are approximately seven points that appear to be outliers. These results stem from bypassing storm conditions (Region 3 and 2) or from Region 1 landfalling conditions at -60 and -40 deg. In order to achieve the latter condition, the storm track must arch far to the east to meet the conditions (-40 and -60 deg) at the landfalling position. Three of the seven events were a product of these conditions while the remaining four storm simulations were bypassing events.

Similar analyses were performed for the Level 3N and Level 3C domains. These results are presented in Figure 5-31. The number of symbols may seem low (1050 potential symbols for the wind speed and H_{mo} maxima). It is because many of the maxima for an event are co-located with other storm simulation results. This is especially true for the Level 3C domain. In addition there are a number of maxima residing on the boundaries of Level 3N and Level 3C (Table 5-6). This is due to the selection procedure defining an absolute maximum value in the field files generated for a single synthetic tropical storm simulation. In general, the storm track initially enters the southern or eastern boundary, and the maximum value would be set despite achieving a similar value elsewhere in space and time. Infilling (resulting in a decrease in the wind speed) will occur within 250 km of coastline for landfalling systems. This will reduce the number of maxima residing landward from approximately 25 grid points in the model domain. More than half of the maximum wind speeds for the 1050 storms reside on both the Level 3N and Level 3C boundaries while more than half

of the maximum significant wave height estimates for the Level 3C region again reside on the boundary.

There is no discernible pattern in the wind speed maxima because most of the population lies along the boundaries of Level 3N and Level 3C. It is interesting to note that some of the maximum wind speed estimates for particular simulations fall near the coastlines of the NACCS. Most if not all of these locations are from landfalling systems with low heading angles or bypassing systems running parallel to the NACCS coastline.

Figure 5-31. Maximum wind speed and significant wave height locations in Level 3N and Level 3C model domains for the 1050 synthetic tropical storm event simulations.

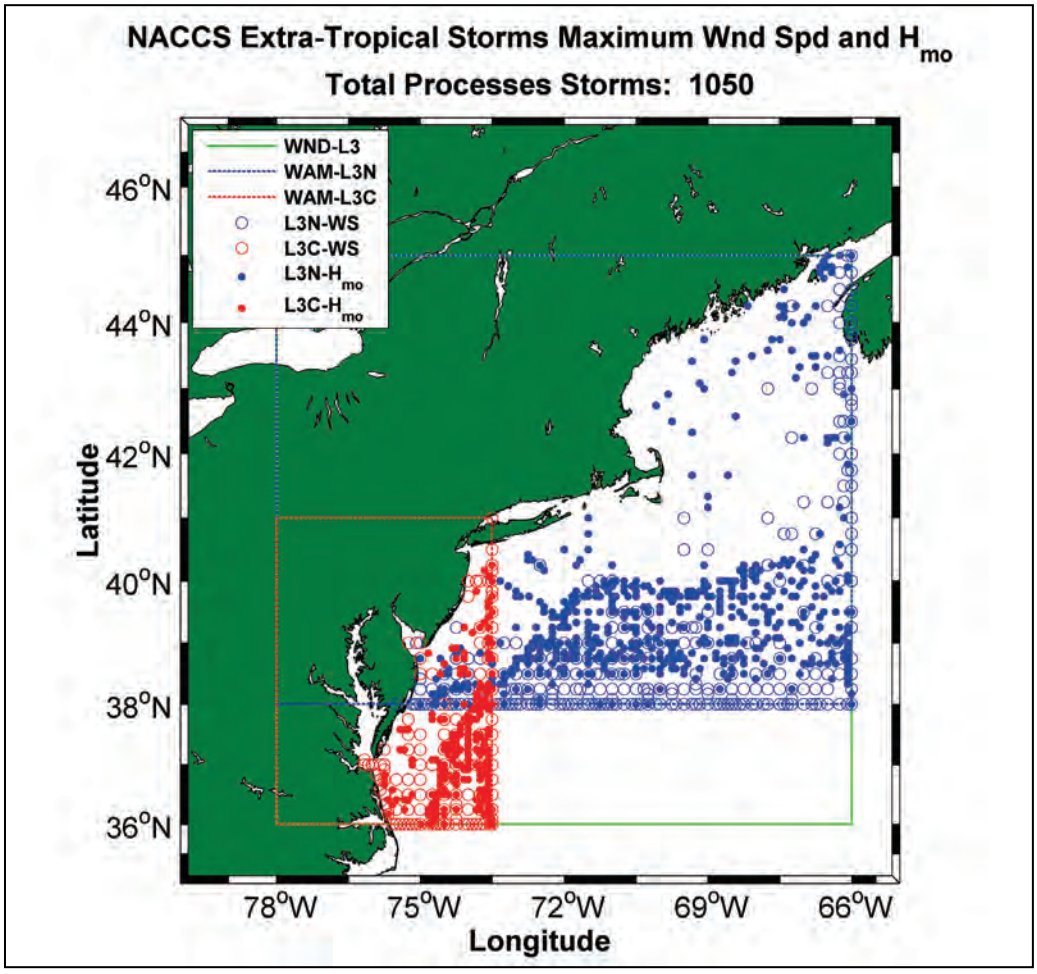

Table 5-6. Wind speed / H_{mo} maxima locations.

Domain	Number of Observations Positioned on Boundary		Number of Observations Positioned inside Domain	
	Wind Speed	H_{mo}	Wind Speed	H_{mo}
Level 3N	666	252	384	798
Level 3C	843	666	207	384

The distribution of the H_{mo} maxima is a different matter. There is an observable pattern in the solid blue and red symbols for the population offshore the NACCS domain. In general, there is a large grouping of significant wave height maxima in the southeast corner of Level 3N and Level 3C. Landward from this cloud, there is a well-defined line that extends from Level 3C southern boundary to the eastern boundary in the Level 3N domain. This *line* approximately follows the 200 m isobaths in the wave model's grid. Landward of this line, the water depth decreases slowly, arbitrary water depth effects (phase, group velocities) and wave-bottom effects will affect and generally attenuate the offshore wave climate. The patterns in the H_{mo} maxima from the 200 m isobaths may appear to be random; however, the relative location of these points falls in areas of deeper water. It is depth effects that control where the maximum significant wave height exists for these synthetic tropical storm simulations in the Level 3N and Level 3C domains defined in the NACCS.

5.9 Summary

The offshore wave climate defined in the NACCS domain is very complex and a result of meteorological events of various scales and intensities passing through the region. Storm events dominated by Nor'easters generally occur on an annual basis. These storms on land produce significant rainfall or massive snowfalls. Offshore it is not uncommon for these events to produce H_{mo} values in the range of 8 to 15 m. Tropical events also occur but less frequently than Nor'easters. These events are generally modified by other synoptic-scale systems once they pass Cape Hatteras and continue up the Atlantic seaboard. These systems, as in the case of Superstorm Sandy, can result in large-scale devastation of the coast and infrastructure. It is also not uncommon for tropical systems passing well to the east of the NACCS domain to have an impact on the coastal environment from radiating swell energy from the moving system. It is necessary to properly estimate not only a tropical system but also embed that system into synoptic- and meso-scale meteorological events. Defining the offshore

wave climate under these extreme storm events is a challenge; however, it is a tractable solution provided the wind forcing is well described. It is also critical for the wave modeling effort to be properly posed (grid systems, model resolutions, wave mechanisms) and to have a high-quality model that is capable of accurately simulating these complex conditions. For historical event simulations it is necessary to have high-quality wave measurements to evaluate not only the wind forcing but also the wave estimates.

The motivation for the generation of the offshore wave climate for the NACCS was to properly estimate the local and far-field wave energy in the form of 2D wave spectra defined at boundary locations used to force the STWAVE (Massey et al. 2011) nearshore wave simulations. WAM (Komen et al. 1994) was selected as the wave modeling technology to be used in the generation of the offshore wave climate for the NACCS. The model is a third-generation wave model solving the action balance equation for the advection and source terms that will describe the temporal and spatial variation of 2D wave spectra over a fixed grid system. A multilevel grid system (Level 1, Level 2, Level 3N, and Level 3C) was implemented for the NACCS to minimize computational requirements yet maximize the resolution along the outer boundary defined. This assured proper temporal and spatial scaling of the meteorological events occurring in the Atlantic Ocean basin and to local-scale conditions occurring offshore of the Atlantic seaboard.

Prior to the production phase for the offshore waves, evaluation testing was conducted to assess the quality of the wave model estimates for various extratropical and tropical events. The testing also provided a means to evaluate the grid system, model resolutions (in frequency and direction), and forcing functions (i.e., wind fields). Twenty-two storm simulations were conducted as part of the evaluation and testing phase: 5 tropical (Sandy, Irene, Isabel, Josephine, and Gloria) and 17 extratropical storms based on high water level measurements and extreme wave-dominated events. All evaluation test simulations used the WIS (http://wis.usace.army.mil/) archived wind fields. Those winds were developed by OWI. The wave model results were evaluated at as many as 30 point-source measurement sites contained in the Atlantic Basin derived from NOAA's NDBC, the Coastal Data Information Program, Canada's Meteorological Service, and the USACE FRF. The evaluation consisted of time-series, scatter, Q-Q graphics, and a battery of statistical tests performed at each site for each

grid level and for each of the 22 selected storm events. The summary of these results indicated that WAM provided high-quality wave estimates (low bias, low RMSE, high correlation) compared to the measurement sites. From these tests it was determined to be necessary to initiate the Level 1 WAM simulations at a minimum of 10 days prior to the occurrence of the storm peak. This assured the nearshore wave climate contained sufficient far-field wave energy generated by synoptic-scale events in the entire Atlantic Ocean basin. The evaluation testing also provided a means to develop and test (1) the fully automated system, (2) the generation of the boundary condition information for STWAVE, and (3) the tools for quality checking of the final model results to be used in the production portion of the work.

For production there were two sets of extreme storm events to be simulated: 100 extratropical events and 1050 synthetic tropical storms. The extratropical events were run on the three multilevel grid system (Level 1, Atlantic Basin; Level 2, Atlantic Region; Level 3N and Level 3C coastal NACCS domain) used in the evaluation study. The wind fields were developed by OWI. The duration of every event was 8 days, where the start date was set to 4 days prior to the coastally defined storm peak, 1 day during the peak condition, and 3 days subsequent of the peak. As noted, wind fields were also prepared for the Level 1 with an additional 6 days added to the front of the simulation to assure far-field wave energy was properly accounted. All model results were evaluated to point-source measurements when available. Of the 100 extratropical storm events, approximately 60 contained point-source measurements (from ET-0040-08 through ET-0103-08) and were evaluated using the same procedure developed during the evaluation testing. Time, scatter, Q-Q graphics, and statistical tests were performed at each site and for every storm. Summary results indicated WAM performed well (low bias, low RSME, high correlation); however, there were instances where the results were poor. For these events the errors were attributed to small sample size, poor measurements, or the inability to accurately co-locate the model to the measurement site.

The production of the 1050 synthetic tropical storm events commenced following the extratropical simulations. There was a slight modification to the operational paradigm previously implemented for the extratropical production. The tropical storm systems and accompanying wind fields were restricted to the Level 2 and Level 3N/Level 3C domains. Also, the simulation length was based on the various forward speeds of the tropical

systems and varied between 4 and 12 days. The results of these simulations were subject to QA/QC based on visual inspection of the maximum and mean wave height envelopes and the boundary condition estimates for all nine of the STWAVE coastal domains. The results were summarized for all 1050 events and evaluated based on maximum wind speed and significant wave height estimates. Discussions were limited to an overall consistency in the results. Maximum wind speeds were found to be between 30 to 65 m/s with accompanying H_{mo} values between 8 to 20 m, consistent with scaling principles of wind-generated wave estimates.

Generation of offshore wave estimates for extreme extratropical and tropical storm events can become very complex. However, given high quality wind field forcing, a third-generation, state-of-the-art wave model posed in a grid system that considers the spatial and temporal scales of these types of events, the outcome of the modeling effort will be successful as is the case in this project.

6 ADvanced CIRCulation (ADCIRC) Modeling

This chapter summarizes the storm surge modeling conducted for the NACCS using the ADCIRC long-wave hydrodynamic model (Luettich et al. 1992). The ADCIRC model has been applied extensively to simulate extreme water levels which are forced by winds, pressures, and waves, most recently in support of FEMA flood-risk map updates in the northern Gulf of Mexico region, the Great Lakes (Jensen et al. 2012; Hesser et al. 2013), FEMA Region II, FEMA Region III, and in support of USACE projects in Louisiana and Mississippi (USACE 2006; Bunya et al. 2010; Wamsley et al. 2013). A detailed description for the general application of ADCIRC is available at http://www.adcirc.org (ADCIRC 2014). The specific application of the model to the NACCS domain is described in this chapter. The ADCIRC modeling component of the NACCS supplies model-generated, water-surface elevations that are applied in the statistical analysis and are also made available through the CHS. This chapter describes the hydrodynamic model ADCIRC, the NACCS model development including mesh generation as well as the forcing mechanisms used to drive the model, the validation procedure for ensuring the model accurately depicts water-surface elevations in the study area, and application of the validated model for NACCS production.

6.1 Model description

The physics-based ADCIRC model was developed as part of the USACE Dredging Research Program (DRP) as a family of 2D and 3D finite element-based models (Luettich et al. 1992; Westerink et al. 1992). The model represents all pertinent physics of the 3D equations of motion including tidal potential, Coriolis, and all nonlinear terms of the governing equations as described in the following paragraphs. ADCIRC is capable of simulating tidal circulation and storm-surge propagation over very large computational domains while simultaneously providing high resolution in areas of complex shoreline configuration and bathymetry. The model provides accurate and efficient computations over time periods ranging from days to months to years.

ADCIRC has been successfully applied in a large number of coastal applications, including the Louisiana Coastal Protection and Restoration (LACPR) project (USACE 2006), the Mississippi Coastal Improvements

Program (MSCIP) (Wamsley et al. 2013), the Lake Michigan storm wave and water level study (Jensen et al. 2012), and the Lake St. Clair storm wave and water level study (Hesser et al. 2013). Because of the ADCIRC model capabilities and its applicability to large-scale storm surge studies, it was chosen for simulating waves and water levels for the NACCS study for the large suite of storms described in this report. Applying wind fields from OWI, the 2D, depth-integrated ADCIRC model predicts tidal- and wind-driven water-surface elevations for the study area.

In two dimensions, the model is formulated using the depth-averaged shallow water equations for conservation of mass and momentum. The formulation assumes that the water is incompressible, hydrostatic pressure conditions exist, and the Boussinesq approximation is valid. Using the standard quadratic parameterization for bottom stress and neglecting baroclinic terms and lateral diffusion/dispersion effects results in a set of conservation equations in primitive, nonconservative form (Flather 1988; Kolar et al. 1994; Westerink et al. 2008). The momentum equations are spatially differentiated and substituted into the time-differentiated continuity equation to develop the generalized wave-continuity equation (GWCE).

ADCIRC solves the GWCE in conjunction with the primitive momentum equations. The GWCE-based solution scheme eliminates several problems associated with finite-element programs that solve the primitive forms of the continuity and momentum equations, including spurious modes of oscillation and artificial damping of the tidal signal. Forcing functions include time-varying, water-surface elevations, wind-shear stresses, atmospheric pressure gradients, and the Coriolis acceleration effect. Also, the study area can be described in ADCIRC using either a Cartesian (i.e., flat earth) or spherical coordinate system.

The ADCIRC model uses a finite-element algorithm in solving the defined governing equations over complicated bathymetry encompassed by irregular sea/shore boundaries. This algorithm allows for extremely flexible spatial discretization over the entire computational domain and has demonstrated excellent stability characteristics. The advantage of this flexibility in developing a computational mesh is that larger elements can be used in open-ocean regions where less resolution is needed whereas smaller elements can be applied in the nearshore and estuary areas where finer resolution is required to resolve hydrodynamic details (Hagen et al. 2001).

6.2 Mesh development

6.2.1 General

The ADCIRC model domain developed for the NACCS encompasses the western North Atlantic, the Gulf of Mexico, and the western extent of the Caribbean Sea (Figure 6-1). The mesh consists of 3.1 million computational nodes and 6.2 million elements with an open-ocean boundary specified along the eastern edge (60 deg W longitude). The largest elements are in the Caribbean Sea, with nodal spacing of approximately 40 km. The smallest elements resolve detailed geographic features such as tributaries, where nodal spacing is approximately 10 m. The NACCS mesh boundary was aligned with the U.S. National Geospatial-Intelligence Agency (NGA) Digital Nautical Chart (DNC) coastline, and bathymetry was extracted from the NGA DNC database, except where specified in the following sections. Details of the mesh development are outlined herein.

Figure 6-1. ADCIRC mesh domain boundary (shown in red).

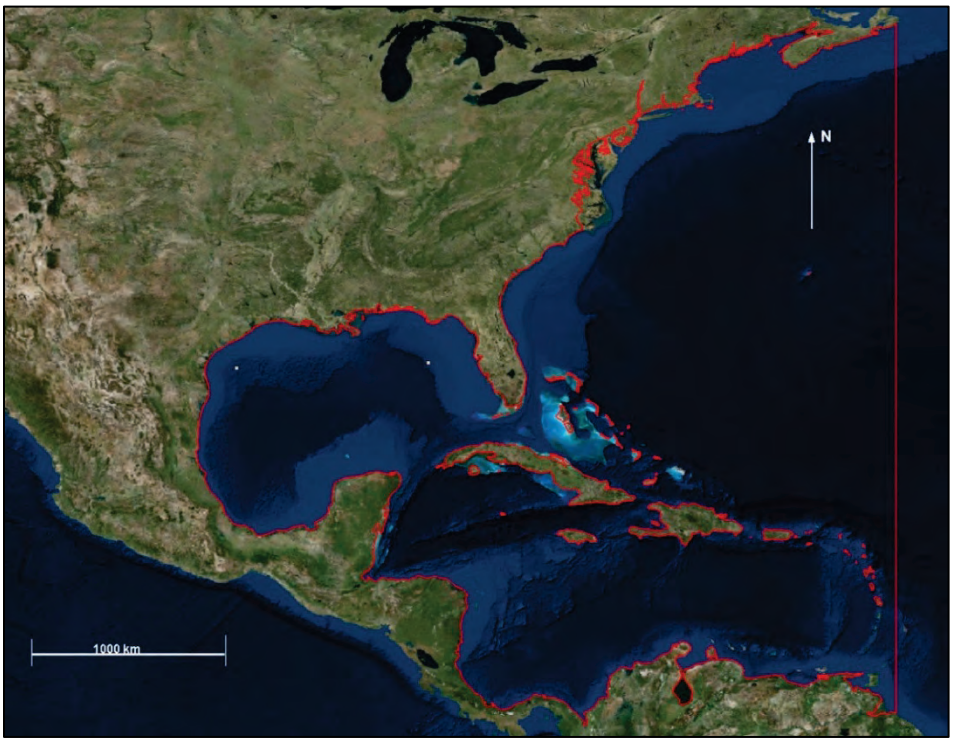

6.2.2 Details

The ADCIRC mesh developed and applied to the NACCS was adapted from a combination of two previously validated FEMA model meshes and the NOAA Vertical Datum Transformation (VDATUM) mesh. For the northern

reaches, the combined mesh was refined, expanded, and extended into areas not included in the existing meshes. The full NACCS finite element mesh included the upland areas to allow for flooding and drying of these areas during storms and to allow for overland wind reduction in the model simulations. The inland limit of the ADCIRC mesh was determined by querying the USGS National Elevation Dataset (NED) 10 m resolution database and extracting the 20 m topographic contour to allow for overland wind reduction in the model simulations. The 7 m topographic contour was also extracted from the database in order to incorporate low-lying areas into the ADCIRC mesh and to allow for flooding and drying of these areas during storms.

Two of the existing meshes used in the initial NACCS grid development were generated and applied by FEMA to perform updates to its flood maps. The first mesh was developed for FEMA Region II, with mesh resolution focused in the New York and New Jersey areas. The second existing mesh was developed for FEMA Region III, with mesh resolution detail focused in the Chesapeake-Delaware Bay region of the Atlantic coast. Areas south of and including Delaware Bay were extracted from the FEMA Region III mesh while areas north of Delaware Bay to New York Harbor were extracted from the FEMA Region II mesh. As noted in the review process, there is variable mesh resolution off the coast of New Jersey when transitioning from the FEMA Region III mesh to the FEMA Region II mesh. The average nodal spacing along the New York/New Jersey area is noticeably larger from one mesh to the other, and the nodal spacing normalized by the depth is also noticeably larger in this region. However, an examination of the bathymetry in the area shows that there is a continuous, smooth representation of the bathymetry. In addition, preliminary validation results with the combined NACCS mesh in the New York/New Jersey area show that the model is correctly capturing the physics because model and measurements compare well regardless of the larger nodal spacing in this area. Based on the smooth bathymetry and the reasonable validation results, a decision was made to maintain the integrity of the two (FEMA Region II and FEMA Region III) validated meshes.

East of New York Harbor, from approximately Flushing Meadows to the northern mesh limits, the initial NACCS mesh was derived from the NOAA VDATUM mesh. However, the north mesh area extracted from the NOAA VDATUM mesh was extensively revised for this study, primarily by increasing mesh resolution but also by optimizing the agreement between (1)

the mesh coastline definition and (2) Controlled-Image Base 5 (CIB5) satellite imagery published by the NGA and NOAA-published Electronic Navigation Charts (ENCs). This section of the mesh is referred to as the *North Mesh*. As with FEMA Region II and FEMA Region III, the full ADCIRC mesh developed for this study is referenced to NAD83* (horizontal) and mean sea level (MSL) (vertical) in meters. The final mesh contained over 6.2 million computational elements and over 3.1 million computational nodes (Figure 6-2).

Figure 6-2. ADCIRC mesh for NACCS.

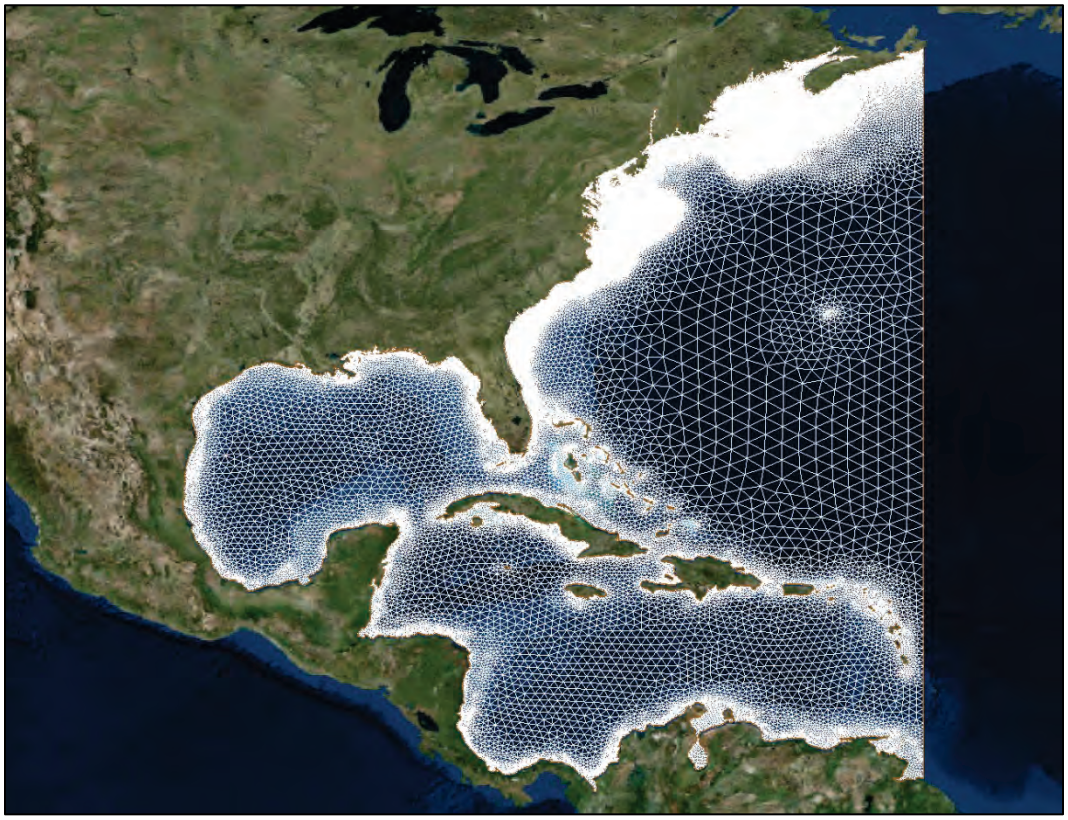

6.3 Bathymetric and topographic data sources

Sources of bathymetric and topographic data for the ADCIRC mesh were gathered from the existing meshes, published data sources, recent data

* The coastline representation in the North Mesh is based on the CIB5 satellite imagery (with a pixel size in the imagery of approximately 5 m) and is referenced to the WGS84 horizontal datum. This datum has only a 1 m displacement relative to the NAD83 datum, and the two datums are considered identical when the precision of the data is less than 2 m (i.e., the horizontal displacement between the datums is less than the precision of the data itself).

collection, and personal contacts. Contact was made with personnel at federal and state government agencies, as well as university professors and private consultants, to acquire bathymetry and topography to update the ADCIRC mesh. The primary goal was to obtain post-Sandy bathymetry and topography data where it existed so that the mesh could be updated to post-Sandy conditions. Pre-Sandy bathymetry and topography data were also gathered where more recent data did not exist.

6.3.1 Bathymetry

Bathymetry specified in the FEMA Regions II and III portions of the ADCIRC mesh remained unchanged and were applied directly in this study. Bathymetry specified in the North Mesh was obtained from NOAA-published ENCs and NGA DNCs. The NGA republishes NOAA-produced ENCs in NGA format, which is the preferred data source because NGA-formatted data are easier to extract from the databases. However, bathymetry values within the coastal zone were taken from NOAA-published ENCs where NGA DNC data values did not exist. Each bathymetric source provided data referenced to mean lower low water (MLLW). Bathymetry was subsequently converted to MSL using conversion values published by NOAA for stations that encompass the region of the North Mesh.

6.3.2 Topography

Topography specified in the FEMA Regions II and III portions of the ADCIRC mesh remained unchanged and were applied directly in this study. However, the NACCS did require external sources for topographic data for the NOAA VDATUM portion of the ADCIRC mesh (North Mesh segment). For New England, terrain data from the USGS NED 10 m resolution database were queried to determine inland limits for the ADCIRC mesh. The 7 m topographic contour was extracted from the database in order to incorporate low-lying areas into the ADCIRC mesh to allow for flooding and drying of these areas during storms. The 20 m topographic contour was extracted from the database in order to allow for overland wind reduction in the model simulations. A finite element mesh was developed for these upland areas and merged with the bathymetric mesh.

6.3.3 ERDC lidar

Post-Sandy lidar data collected by ERDC were used to update the ADCIRC mesh topography along the New Jersey, New York, and Connecticut

coastal areas. Bare-earth 1 m grids based on 2012 lidar data were provided by the Joint Airborne LIDAR Bathymetry Technical Center of Expertise, also known as JALBTCX (http://shoals.sam.usace.army.mil). The mission of JALBTCX is to perform operations, research, and development in airborne lidar bathymetry and complementary technologies to support the coastal mapping and charting requirements of the USACE, the U.S. Naval Meteorology and Oceanography Command, and NOAA. JALBTCX staff includes engineers, scientists, hydrographers, and technicians from the USACE Mobile District, the Naval Oceanographic Office (NAVOCEANO), the USACE ERDC, and NOAA National Geodetic Survey. JALBTCX data can be downloaded via the NOAA Digital Coast Data Access Viewer (http://www.csc.noaa.gov/dataviewer/).

JALBTCX provided the New York/New Jersey/Connecticut tri-state 2012 lidar as raster images with elevations referenced to NAVD88 (Figure 6-3). These data were converted from NAVD88 to MSL to be incorporated into the ADCIRC mesh and STWAVE grids. To perform the datum shift to MSL, differences between MSL and NAVD88 were taken at known points within the region using NOAA tide gauges and the VDATUM program. These differences were used to create a continuous triangulated irregular network (TIN) surface over the area of interest in ArcGIS. The TIN surface was then converted to a 1 m raster grid and added to each of the original NAVD88 rasters to create a new raster for each 2012 bare-earth grid file with elevations relative to MSL. The newly created MSL rasters were converted to ASCII text files in ArcGIS for ready implementation in the model grids.

Incorporation of the newly created MSL lidar data into the numerical model grids was achieved via the application of a computationally efficient, inverse-weighted residual interpolation technique. In total, over 149,000 node elevations were updated within the tri-state area (New York-New Jersey-Connecticut), including over 13,000 node elevation updates in Connecticut, over 17,000 node elevation updates in New Jersey, and over 118,000 node elevation updates in New York. An overview of the ADCIRC mesh that incorporated over 149,000 node elevation updates based on the JALBTCX 2012 lidar is shown in Figure 6-4. A comparison of a portion of the ADCIRC mesh for Long Island, NY, before and after the incorporation of 2012 lidar indicates an apparent dune lowering along the Atlantic coast of Jones Beach and Long Beach (Figure 6-5 and Figure 6-6).

Figure 6-3. 2012 lidar Coverage for New York, New Jersey, and Connecticut.

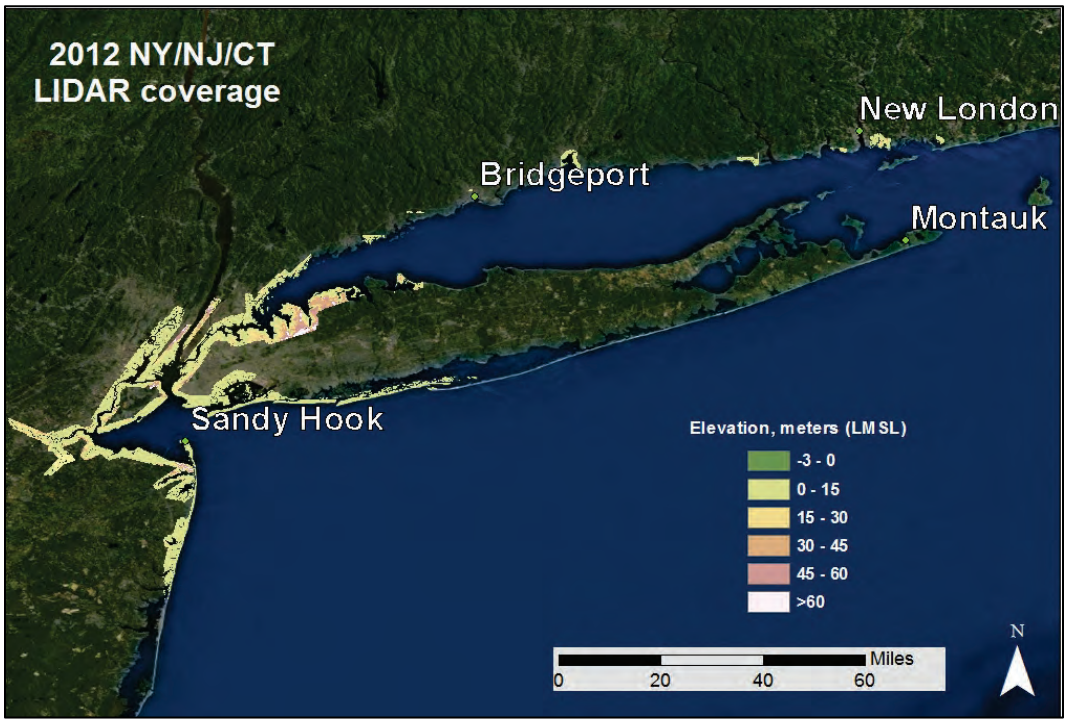

Figure 6-4. Portion of the ADCIRC mesh that incorporated over 149,000 node elevation updates based on the JALBTCX 2012 lidar.

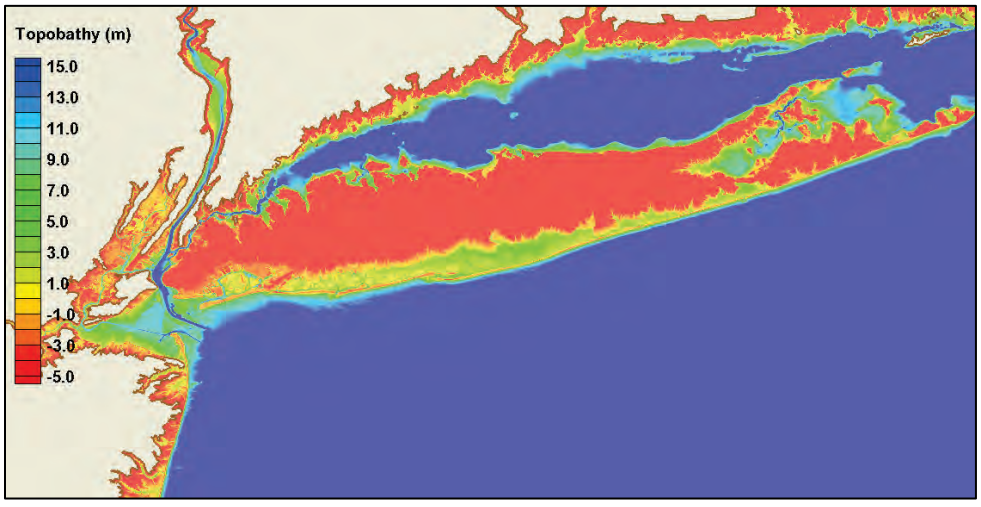

Figure 6-5. ADCIRC mesh topography/bathymetry for a portion of Long Island, NY, before 2012 lidar update.

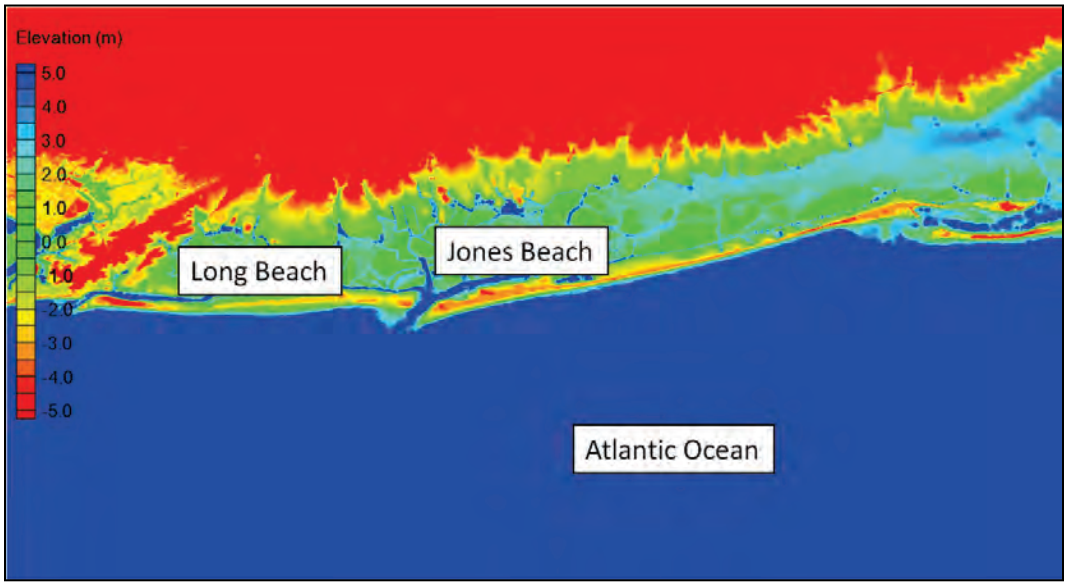

Figure 6-6. ADCIRC mesh topography/bathymetry for a portion of Long Island, NY, after 2012 lidar update.

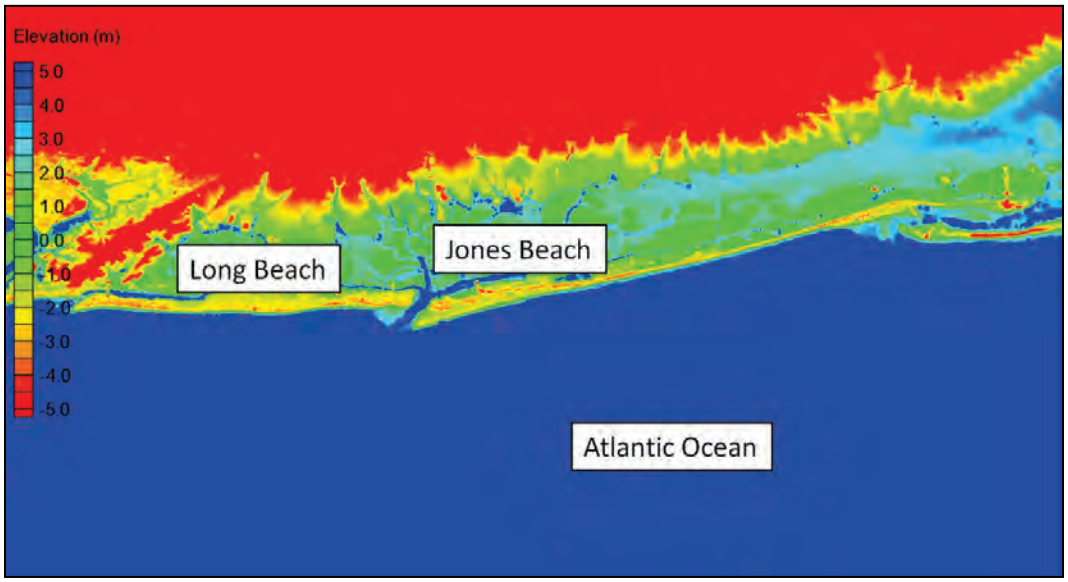

6.3.4 USGS lidar

The U.S. Army District, New York, was able to obtain and provide the USGS 2012 post-Sandy lidar data for Long Island, NY, to ERDC. All lidar data were processed and incorporated into ADCIRC and STWAVE model domains. As previously mentioned, this effort was achieved via the application of a computationally efficient, inverse-weighted residual interpolation technique updated for this project. These topographic changes have

been included in the validation sequence described below. Care was taken to ensure smooth transitions in topographic values between the newly updated areas and the existing surrounding data.

The ADCIRC mesh with the lidar incorporated showed breaches near Smith County Park, NY, (Figure 6-7) and east of Moriches Inlet, NY, (Figure 6-8) with the implementation of the lidar data. The U.S. Army District, New York (NAN), indicated that the two breaches were relatively quickly repaired to 8 ft NAVD88 (2.51 m MSL) following Hurricane Sandy, and NAN requested that ERDC *repair* the two breaches in the mesh. Figure 6-9 and Figure 6-10 show the breach-repaired conditions for Smith County Park, NY, and east of Moriches Inlet, NY, respectively. In addition, NAN noted that the breach at Old Inlet, NY, was being left in its natural state, and it was requested that the breach be widened to 200 m and deepened to 2 m MSL in the computational grid. This condition is shown in Figure 6-11.

Figure 6-7. Post-Sandy breach at Smith County Park, NY.

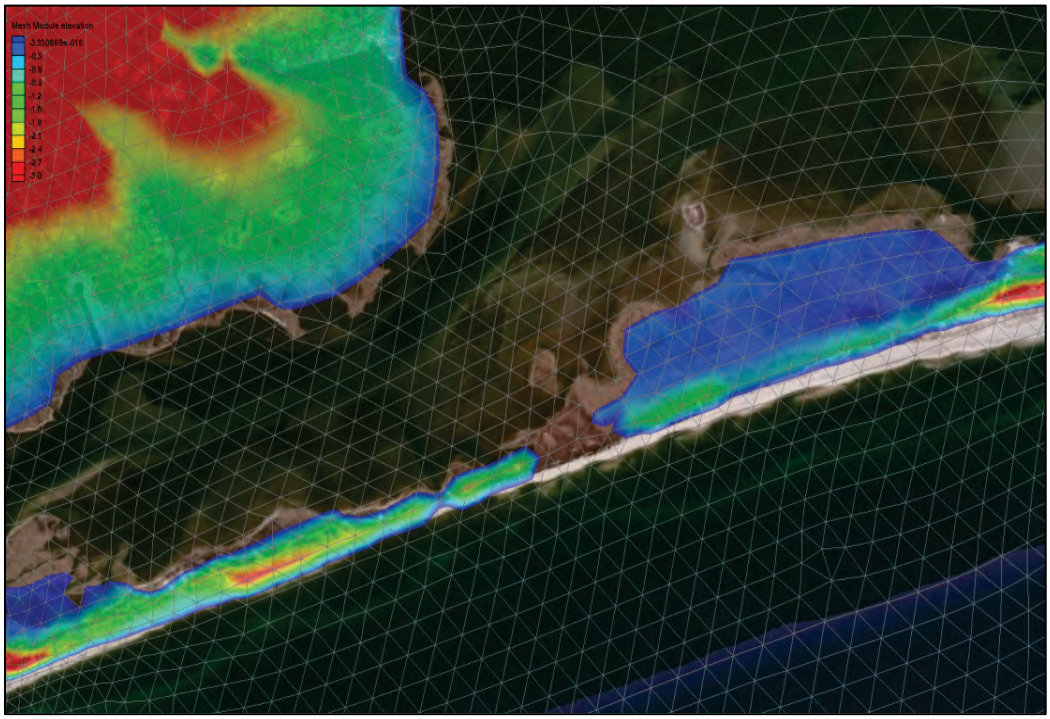

Figure 6-8. Post-Sandy breach east of Moriches Inlet, NY.

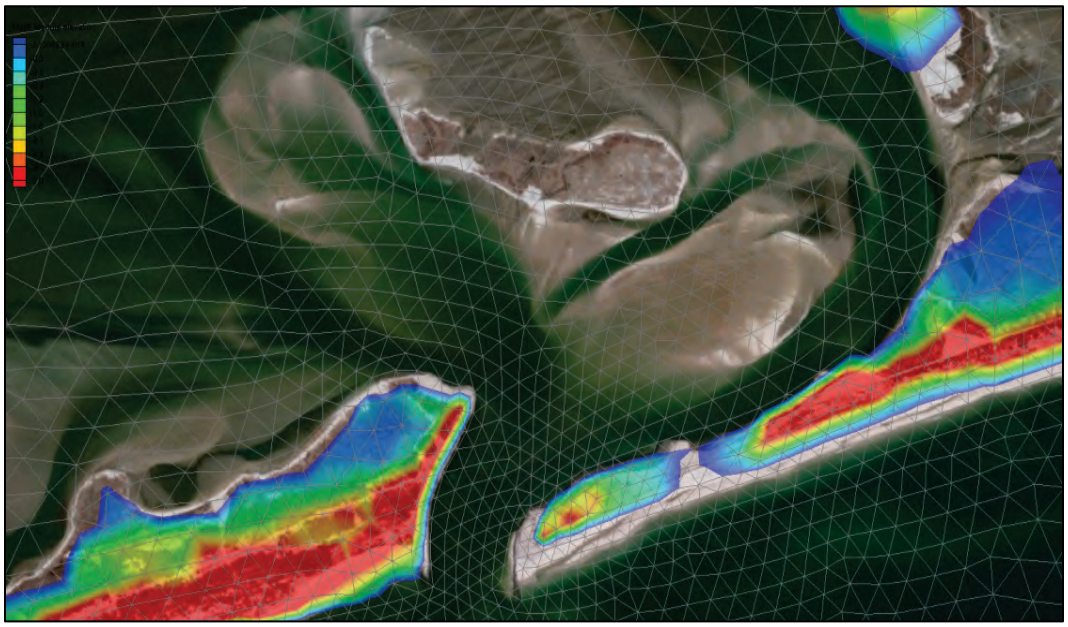

Figure 6-9. Breach repaired at Smith County Park, NY.

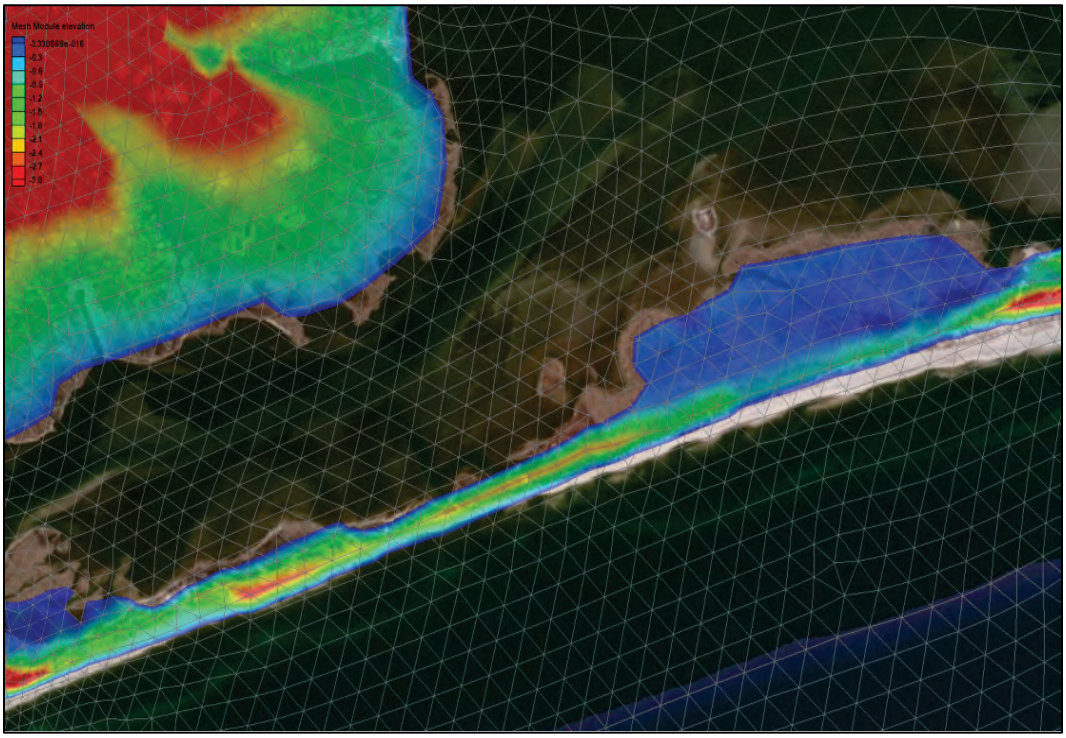

Figure 6-10. Breach repaired east of Moriches Inlet, NY.

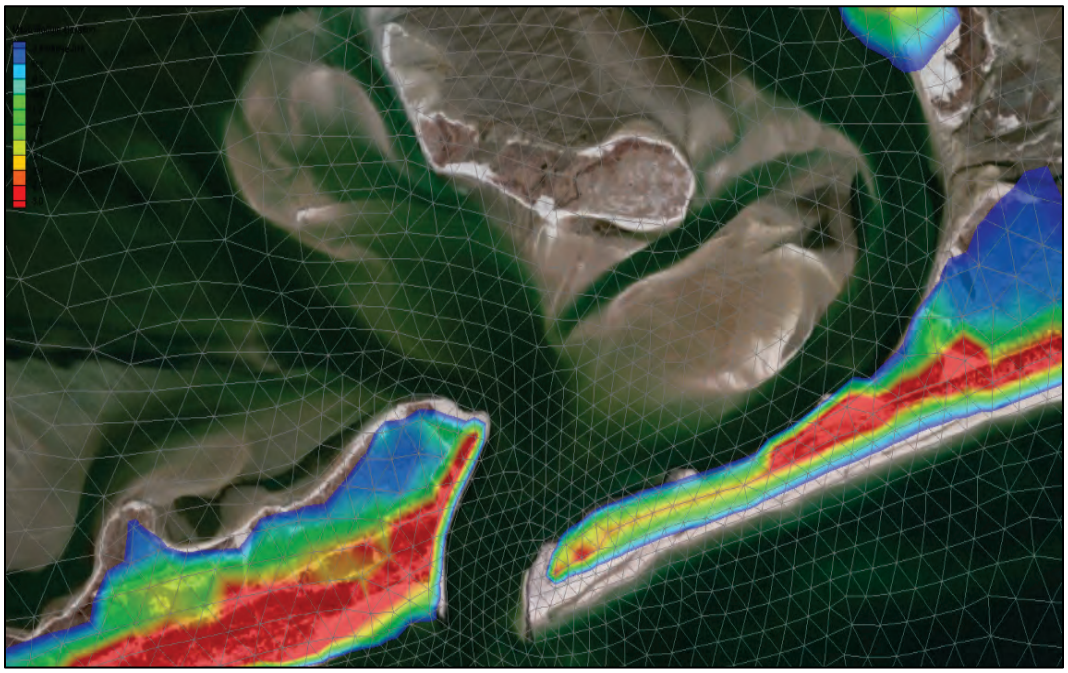

Figure 6-11. Breach at Old Inlet, NY.

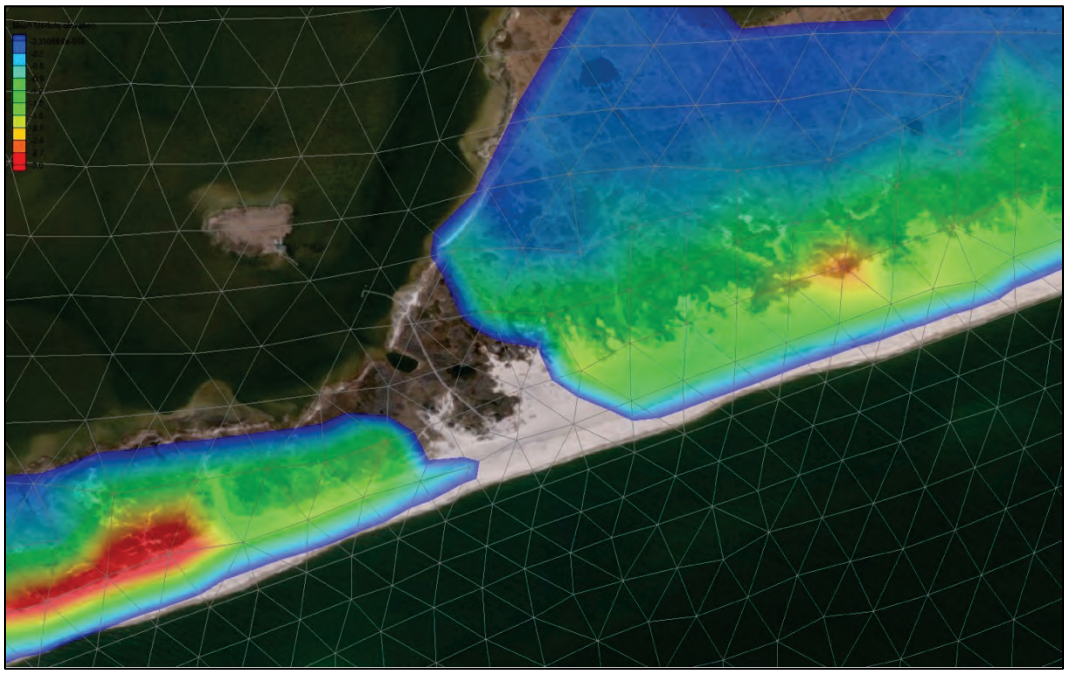

6.4 Forcing conditions

The hydrodynamic model ADCIRC was applied to the NACCS to estimate water level responses to astronomical and meteorological forcing conditions. Tidal forcing was applied at the open ocean boundary, river inflows

were applied at the river boundaries, and meteorological forcing (winds and pressures) were applied over the North Atlantic basin. A description of these forcing conditions is described in this section. In addition, wave forcing was applied to the model through coupling with STWAVE, details of which will be described in Chapter 7.

6.4.1 Tidal forcing

The open ocean boundary (60 deg west longitude) was forced with eight tidal constituents. Time-varying tidal elevations specified at nodes along the open ocean boundaries were synthesized using the M_2, S_2, N_2, K_1, O_1, Q_1, P_1, and K_2 tidal constituents. Constituent information was extracted from a database developed from the TOPEX 7 satellite measurements. Because the model domain is of sufficient size that celestial attraction induces tide within the mesh proper, tide-generating potential functions were included in the simulations and correspond to the constituents listed above.

6.4.2 River inflows

Fourteen rivers were included in the ADCIRC mesh (Table 6-1). The majority of these rivers had USGS gages (with mean daily flow rates) located either at upstream dam locations or at the head of tide with sufficient periods of record available for analysis (data began in the 1930s and 1940s for most gages). However, the Raritan and Passaic Rivers required NAN personnel to translate flow from a known gage measurement/location to the model boundary location through data manipulation.

The mean daily flow rate for each of these river inflow locations was obtained for the period from approximately 1930 to present. Initially, the impact of river inflows on water levels was investigated collectively by applying the flow of record for all 14 rivers in a single model simulation. From this analysis it was determined that if all rivers were simultaneously discharging at their maximum rate, the maximum potential change in water level due to river inflow was at most 0.2 m for the larger bays (Chesapeake, Delaware, etc.) with larger impacts observed near the river boundaries not considered part of the project study area. Though the effect of river inflow is not a significant factor, the inclusion of as many physical processes as possible provides a more conservative estimate of computed water levels. Flow rates for historical extratropical and tropical storms from this region were extracted from the measurements and were analyzed

in conjunction with the storm characteristics to determine if a correlation between storm characteristics (speed, pressure, etc.) and the measured river flow rate existed. This analysis indicated that the flow rate is independent of the storm and there is no discernable correlation.

6.4.2.1 Extratropical production inflows

Since the extratropical storms were historical events, USGS-measured flows were utilized to determine representative river flows for each storm. The USGS daily flow rates were extracted for +/- 3 days from the date of the peak water level as recorded by the NOAA gages in the region. An analysis was performed on these flow rates to determine the 90th percentile flow (for each river) that occurred during the corresponding storm. This 90th percentile flow was specified as a constant inflow in the model in an effort to obtain realistic flows for a particular extratropical event that would still result in slightly conservative water levels.

6.4.2.2 Tropical production inflows

The synthetic tropical storms used in this study had no historical flow rates making the previously used method for the extratropical storms infeasible. Also, from the previously discussed analysis, historical tropical storms exhibited no significant correlation between any of the storm forcing parameters and river inflows, making the creation of a regression/conversion using a storm characteristic(s) to flow rate infeasible. Therefore, a separate methodology was utilized to determine the tropical flow rates.

Since there were no correlation between storm characteristics and flow rate, determining storm specific flows was not feasible and as such, a single flow rate for each river was utilized for all synthetic tropical storms. This also resulted in significant time/computational savings as individual flows for each storm would require individual river spin-up simulations in ADCIRC thereby greatly increasing run times and computational burdens.

Although previous studies have applied mean discharge rates, from analysis conducted in this study it was found that mean discharges did not adequately represent the range of values sought in an extreme value analysis. Since a single flow rate for each river was needed to represent the discharges during all the historical tropical storm events, the study team recommended and an oversight committee approved the team's decision to

base the final inflows on each river's maximum discharge instead of the mean for the tropical storm simulations. These inflows were determined by examining flow rates during historical tropical storm events and performing a statistical analysis of those flow rates. The maximum flows +/- 3 days about landfall were extracted for 45 historical storms and analyzed to determine a representative flow rate to use in the model. Different statistics of the historical maximum flows were evaluated and indicated that, similar to the historical extratropical storms simulations, the synthesized storm flows would also result in slightly conservative water levels. It was found that for most rivers the 90th percentile of the maximum discharged resulted in comparable values to the "mean plus one standard deviation" discharges. Therefore, the production discharge used for tropical storms for each river was the greater of either the 90th percentile of the maximum discharge and a discharge equal to the mean plus one standard deviation. On average, the production discharge of each river is close to three times the mean discharge as can be observed in Table 6-1. This method was utilized to create reasonable inflows that would result in somewhat conservative water levels.

Additional analyses were done to examine the impact of production and maximum river inflows on water levels for specific storm events and the impact of each river on water levels when a maximum or production flow rate is applied. Details of this additional research and analysis are presented in a companion paper on the variability of water level response to river inflow rates (Gunkel et al. 2015).

Table 6-1. River flow rates determined from analyzing 100 historical tropical events.

River	Mean Flow (cms)	Production Flow (cms)	Maximum Flow (cms)
Brandywine River	70	255	405
Chester Creek	20	57	163
Connecticut	802	1954	6400
Delaware	829	2209	7900
James	589	1982	8382
Mattaponi	36	85	283
Pamunkey	93	311	708
Potomac	993	3794	9458
Rappahannock	228	736	2384
Schuylkill	358	934	2645
Susquehanna	2043	7617	31715

River	Mean Flow (cms)	Production Flow (cms)	Maximum Flow (cms)
Hudson	570	1444	4474
Passaic	76	283	615
Raritan	221	651	1969

6.4.3 Wind forcing

All wind and pressure fields applied to the NACCS were generated by OWI. Historical extratropical storm wind and pressure field generation was accomplished for 100 events selected based on the water level analysis described in Chapter 3. The OWI analysis of each event covered an 8-day period centered around the time of the peak water level for each event. NACCS wind and pressure fields for the 100 storm set were developed on two working grids: (1) the original WIS Level II domain and (2) a 0.125 deg domain covering 36–45 N, 78–66 W. Storm analysis included reanalysis of the storm core of winds generating the maximum ocean response and the assessment/assimilation of coastal station data such as National Weather Service reporting stations and National Ocean Service stations not considered as part of the WIS effort. Storm analysis was primarily offshore (wave driven) rather than the nearshore/coastal area, which is important in the NACCS ADCIRC modeling because model results in this region have potential application to coastal project design.

Storm wind and pressure fields developed for the 1050 synthetic storms selected in the storm selection process were a joint effort of ERDC and OWI as outlined in the OWI contractor report. ERDC specified the tropical storm parameters for each synthetic event, and OWI generated track paths and the modification of the basic storm parameter set along the tracks. The TC96 tropical wind and pressure model applied by OWI to generate the wind and pressure fields is the same modeling system applied by ERDC and also in many of the FEMA studies (Thompson and Cardone 1996). The overall storm duration for each synthetic event was a function of the storm's forward speed. The temporal spacing between wind and pressure snapshots for all storms was controlled by the fastest moving storms, which required a 5 min snap interval.

6.4.4 Steric adjustment and sea level change

Thermosteric and halosteric sea level changes occur in response to fluctuations in temperature and salinity, respectively. The cumulative effect of both thermosteric and halosteric changes is referred to herein as the total

steric adjustment. In order to account for the seasonal mean sea surface variability within the ADCIRC simulations, long-term NOAA stations (http://tidesandcurrents.noaa.gov/sltrends/sltrends.html) from Maine to Virginia were examined. For example, the steric adjustment or average seasonal cycle of mean sea level along with a 95% confidence interval is shown in Figure 6-12 for Station #8534720 Atlantic City, NJ. The steric adjustment varies both temporally and spatially. Two approaches were adopted for the ADCIRC simulations and are described below. Approach #1 was applied to historical extratropical storm events, and Approach #2 was applied to synthetic tropical storm events.

1. For historical extratropical storm events, a unique steric adjustment value was calculated using the spatial arithmetic mean steric values during the time of each historical event at NOAA Station #8418150 Portland, ME, and Station #8534720 Atlantic City, NJ. For example, a steric adjustment value of 0.04 m will be applied for the extratropical storm event that occurred on 1 October 2010 (i.e., the average of 0.013 m for Station #8418150 and 0.067 m for Station #8534720).

2. For synthetic tropical storm events, a temporal weighted mean value in addition to the spatial arithmetic mean value was used when computing the steric adjustment. Using Station #8534720 (Atlantic City, NJ) and Station #8638863 (Chesapeake Bay Bridge Tunnel, VA) (Figure 6-13), the spatial arithmetic means were computed for each month. Next, the temporal mean values were calculated for hurricane season. While hurricane season is from June through November, the relative frequency of storms occurring during the month of September is nearly double that of the next most frequent month (August). Monthly weights during hurricane season (weights provided in parentheses) are as follows: June (0.04), July (0.04), August (0.26), September (0.48), October (0.12), and November (0.06). Applying the temporal weighting factors to the arithmetic mean of the upper 95% confidence band resulted in a steric adjustment value of 0.1 m, which was applied for all synthetic tropical storm events.

Figure 6-12. Mean and 95% confidence band steric adjustment of mean sea level for Station #8534720 Atlantic City, NJ.

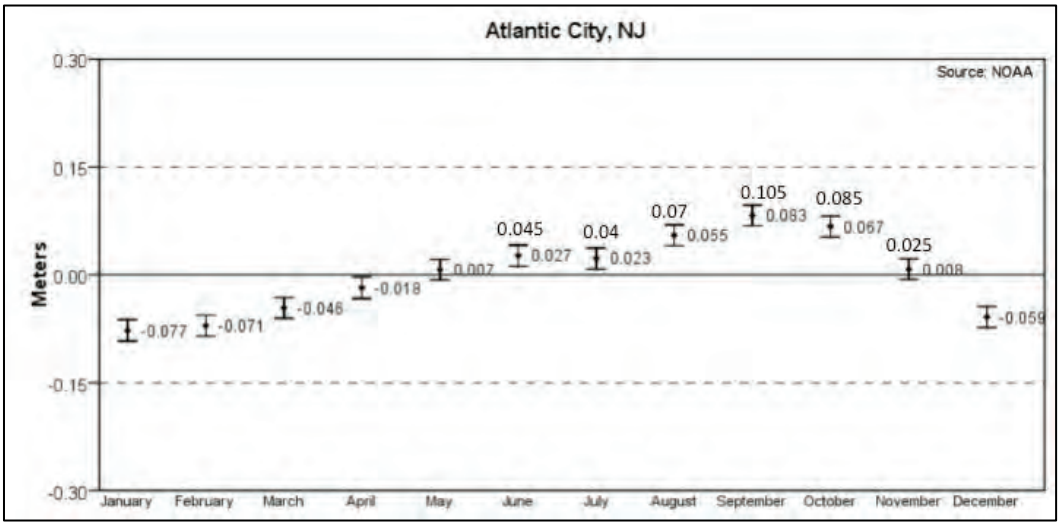

Figure 6-13. Mean and 95% confidence band steric adjustment of mean sea level for Station #8638863 Chesapeake Bay Bridge Tunnel, VA.

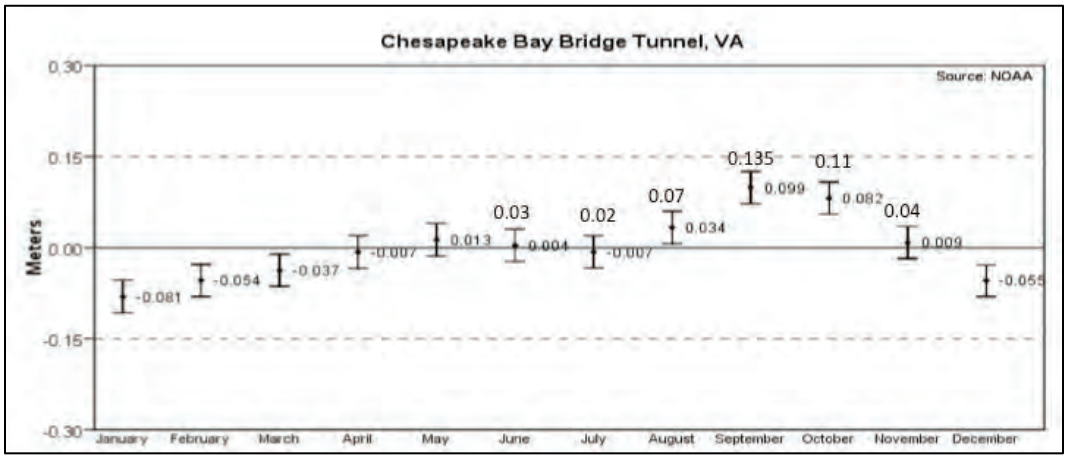

The goal of the steric height adjustment is to account for physics not represented in the model (baroclinic terms) by applying a single water level adjustment value to the entire mesh. Back bays may have more variability in temperature and salinity than the open coast; therefore, the selected steric height adjustment value may not be equally applicable in interior bays. However, the goal of the modeling effort was to provide a large-domain regional model that could be applied directly to projects or used as a driving condition for inset models. Additionally, a local datum adjustment could be applied to results at inland bay locations.

6.5 Nodal attributes

The ADCIRC model has the ability to specify certain quantities at location points (nodes) within the model's computational domain, and these quantities are referred to as nodal attributes. The nodal attributes used in this study include (1) Manning's *n* bottom friction coefficient, (2) lateral eddy viscosity, (3) land cover effects on winds (also referred to as canopy effect), (4) directional wind reduction factors which are derived from land use, and (5) primitive weighting in the model's continuity equation, also known as Tau0. Tau0 is the weighting factor in the GWCE that governs the relative contribution of the primitive and wave portions of the GWCE.

The nodal attributes of Manning's *n* bottom friction coefficients, canopy effects, and directional wind reduction factors applied in the FEMA Region II and FEMA Region III study areas were retained for this study. The FEMA Region III mesh used a lateral eddy viscosity of 10 m^2/s for land nodes and a value of 4 m^2/s for water nodes, while the FEMA Region II simulation used a constant lateral eddy viscosity of 50 m^2/s. Both sets of values have been used in other studies for storm surge modeling with ADCIRC. ERDC-CHL evaluated applying the strategy from the FEMA Region III mesh of 10 m^2/s for eddy viscosity for land nodes and 4 m^2/s for water nodes for the entire mesh. In addition, CHL tested the effect of locally smoothing the eddy viscosity values in order to avoid sharp gradients in the lateral eddy viscosity. The primitive weighting coefficient values for FEMA Region II and FEMA Region III generally follow the standard methodology for setting Tau0 based on depth and nodal spacing. For initial testing application by ERDC-CHL, the standard primitive weighting was applied to the entire domain for consistency.

Nodal attributes developed for the North Mesh are as follows.

6.5.1 Manning's *n* bottom friction coefficient

Separate land and water data sources for the Manning's *n* coefficients were used for the North Mesh. For land-based nodes, Manning's *n* values are based on the USGS-published land coverage types together with the Manning's n associated for a particular type as published in Bunya et al. (2010). For water-based nodes, the Manning's *n* is based on the bottom characteristic or type published in the NGA's DNCs, with distinct values assigned to areas of sand, gravel, clay, etc.

6.5.2 Lateral eddy viscosity

As with the FEMA Region III domain, water nodes were assigned a viscosity of 4 m^2/s, and land nodes were assigned a viscosity of 10 m^2/s. As mentioned above, ERDC-CHL tested and applied locally smoothing to the eddy viscosity values in order to avoid sharp gradients.

6.5.3 Primitive weighting coefficient

The generation of the Tau0 values follows the standard methodology as outlined in the ADCIRC website utility program (http://adcirc.org/home/related-software/adcirc-utility-programs/tau0_gen.f). The method for setting Tau0 is based on both depth and nodal spacing. In particular, if the average distance between a node and its adjacently connected neighbor nodes is less than 1750.0 m, then Tau0 is set to 0.030. If the average distance between a node and its adjacently connected neighbor nodes is greater than 1750.0 m and the water depth is less than 10.0 m, then Tau0 is set to 0.020, while for distances greater than 1750.0 m and depths greater than 10.0 m, the value of Tau0 is set to 0.005. In order to smooth sharp gradients in Tau0 that can exist based on the criteria above, the values of Tauo were locally averaged.

6.5.4 Canopy coefficient

The synthetic wind and pressure fields that are typically used for these types of studies are created by using a planetary boundary layer model. This model assumes that the winds and pressures are being generated over open water without land effects impacting the winds. In reality, as tropical storms move closer to land, the rotating winds are diminished after traversing over land and encountering heavily forested areas or large buildings. Due to this limitation of the modeled winds, and similarly for hindcast wind products, two nodal attributes are used by ADCIRC to make adjustments: the canopy coefficient and the directional wind reduction coefficient. In addition, the default wind drag cutoff coefficient (0.004) defined in ADCIRC was applied in this study (Garratt 1977). The canopy coefficients are based on the USGS-published land coverage types. Nodes that reside in heavily forested areas are assigned a coefficient of zero indicating no wind energy transfer to the water column whereas a coefficient of one is specified for all other areas. This has the effect of setting winds to zero in heavily forested areas.

6.5.5 Directional wind reduction

The surface directional effective roughness length makes adjustments to the winds by looking at the aggregate land use types in 12 directional bands around each node. This allows for different surface roughness values for areas over open water as compared to areas over marsh grasses or scrub bushes, etc. This nodal-based parameter is a set of 12 values assigned to each mesh node with each value corresponding to a 30 deg wedge emanating from a given node. Each wedge represents a potential direction from which winds can come towards the node. For each of the 12 wedges, a wind reduction factor is assigned to the node, based on the vegetation type in that wedge upwind of the node. Additional details can be found in Westerink et al. (2008).

6.6 High-frequency save point locations for model output

The ERDC team worked directly with District personnel in order to establish storm surge and wave save point locations where model results (i.e., time-series of water level, water and wind velocity, and wave conditions) were saved during each CSTORM-MS model simulation at a higher temporal frequency than the solution at every computational node, referred to as the global solution. Model results saved during each simulation at the save-point locations can provide useful information at District project sites and/or can be applied as boundary forcing conditions for local refined numerical models and are more easily accessible than the global solutions. Therefore, the primary goal in establishing the save-points set is to provide frequent nearshore time-series information for a smaller subset of points that would be more easily accessible than the global solution files. To accomplish this goal, District personnel provided XY locations for save points (at project locations and other areas of interest) as well as depth contour and spacing information for additional save points. The requested save-point locations were then imported into the existing ADCIRC mesh, and the local mesh resolution in the vicinity of each save-point location was provided to District personnel along with the associated mesh bathymetry/topography. District personnel were also provided with a section of the existing ADCIRC mesh (fort.14 file) for their geographic region to aid with the selection and visualization of save points. Providing the mesh helped to ensure that important District projects were included and adequately resolved within the mesh. Mesh enhancements were made based on District feedback. An example showing seven of the requested the U.S. Army District, Philadelphia (NAP) save-point locations at New Jersey in-

lets is shown in Figure 6-14. The ADCIRC mesh resolution for these inlets ranges from 70–200 m.

Figure 6-14. NAP save point locations at seven inlets in New Jersey; the ADCIRC mesh resolution for these inlets ranges from 70–200 m.

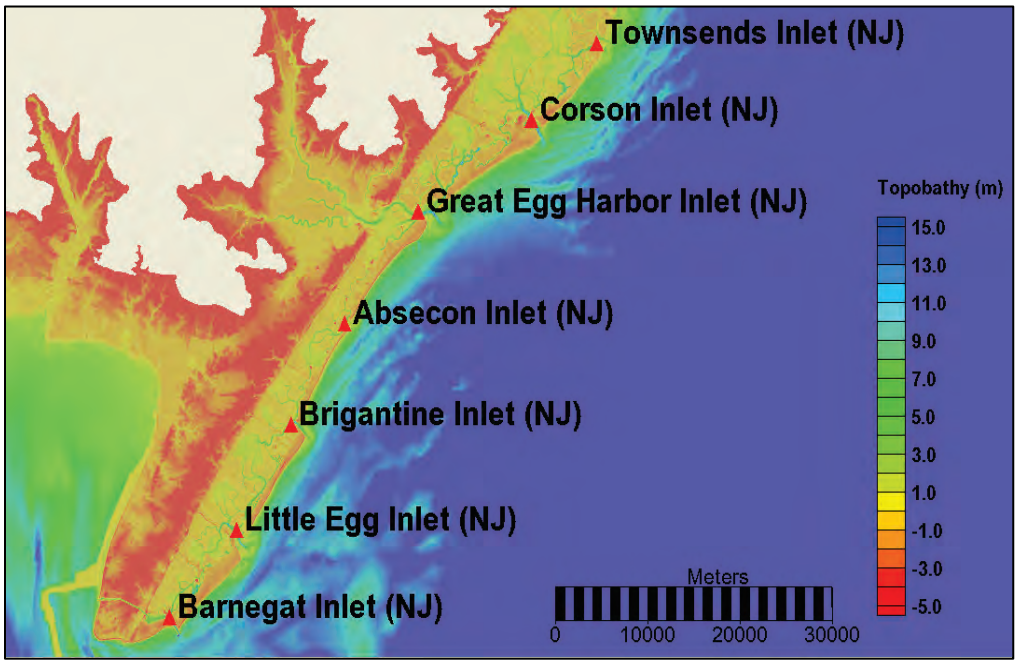

In addition to the District save-point locations, all of the regional NOAA water level gages, WIS stations (Wave Information Studies; http://chl.erdc.usace.army.mil/wis/), and NDBC buoy locations are also included in the save-points set. Table 6-2 provides information regarding the save points. The total number of save points is 18,977. Figure 6-15 through Figure 6-20 show an overview of the save points from Maine to Virginia.

Table 6-2. Save points.

Name	Number of Save Points
NAE Points	342
NAE Contour Points	3,142
NAN Points	240
NAN Contour Points	1,620
NAP Points	40
NAP Contour Points	448
NAB Points	369
NAB Contour Points	132
NAO Points	64
NAO Contour Points	383
WIS	247

Name	Number of Save Points
NERACOOS	94
NOAA	730
ERDC	11,123
Canada	3
Total	**18,977**

Figure 6-15. High-frequency save points, shown as black dots, in Maine and New Hampshire.

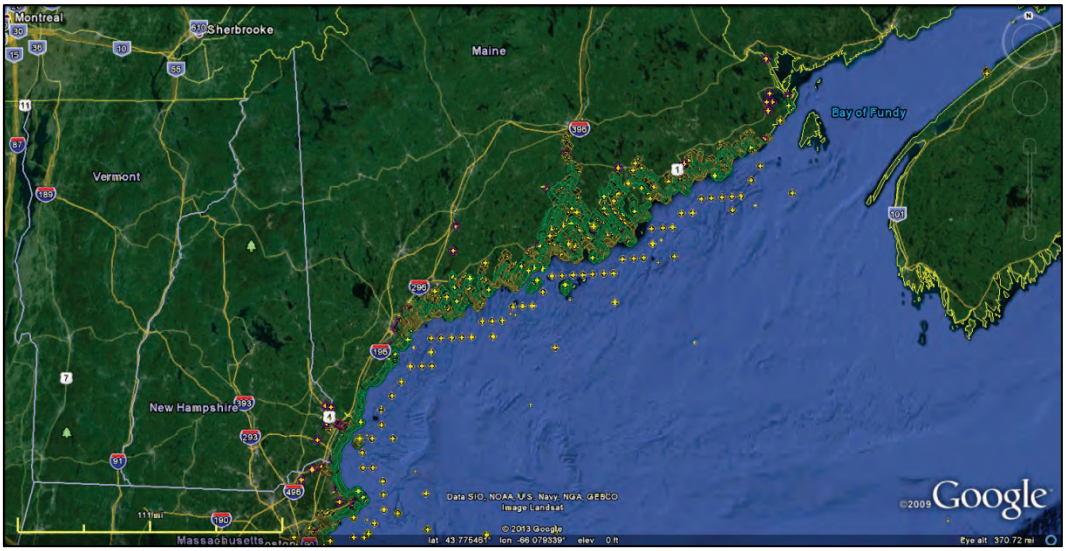

Figure 6-16. High-frequency save points, shown as black dots, in Massachusetts and Rhode Island.

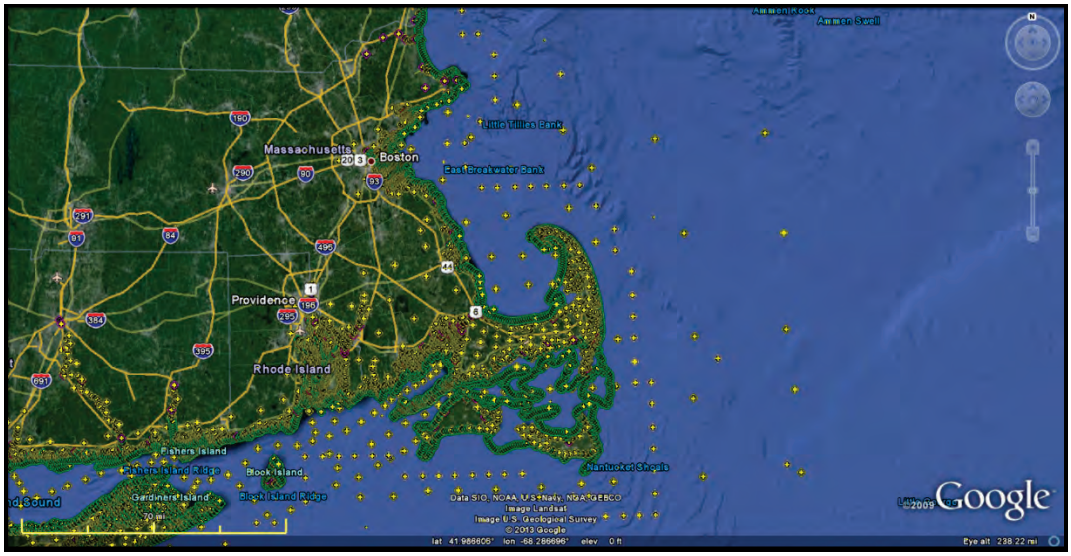

Figure 6-17. High-frequency save points, shown as black dots, in Connecticut and New York.

Figure 6-18. High-frequency save points, shown as black dots, in New Jersey.

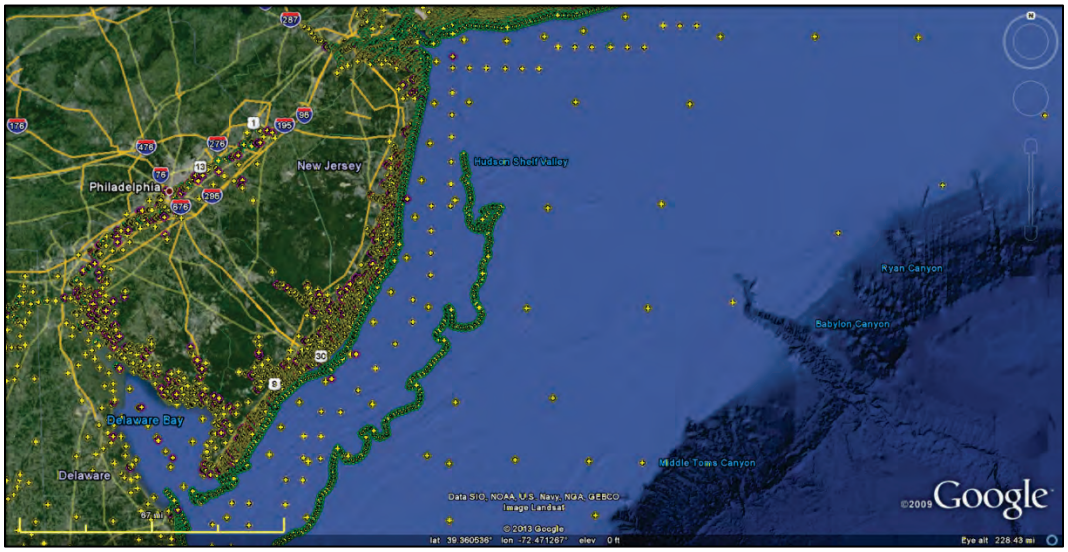

Figure 6-19. High-frequency save points, shown as black dots, in Delaware and Maryland.

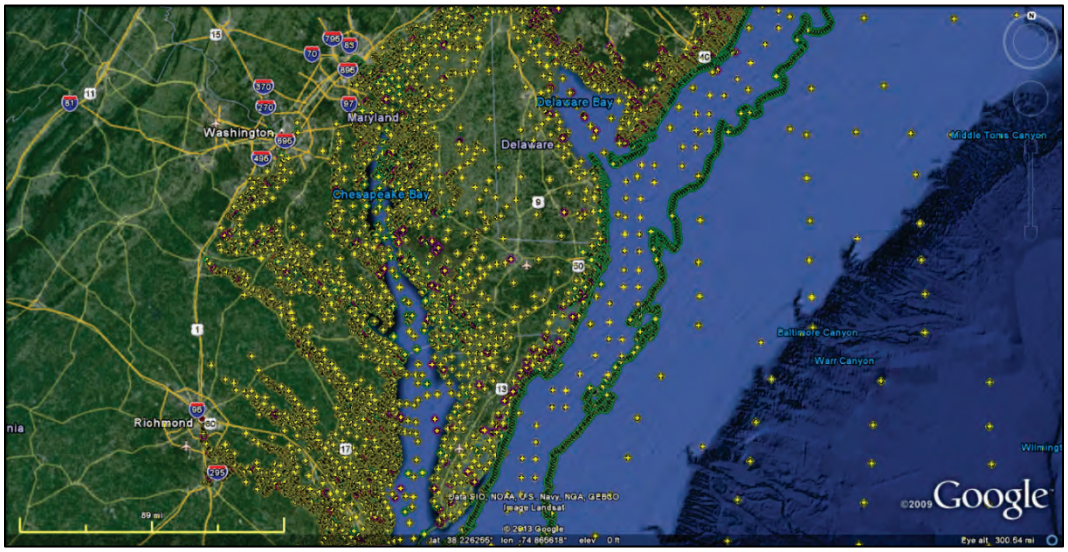

Figure 6-20. High-frequency save points, shown as black dots, in Virginia.

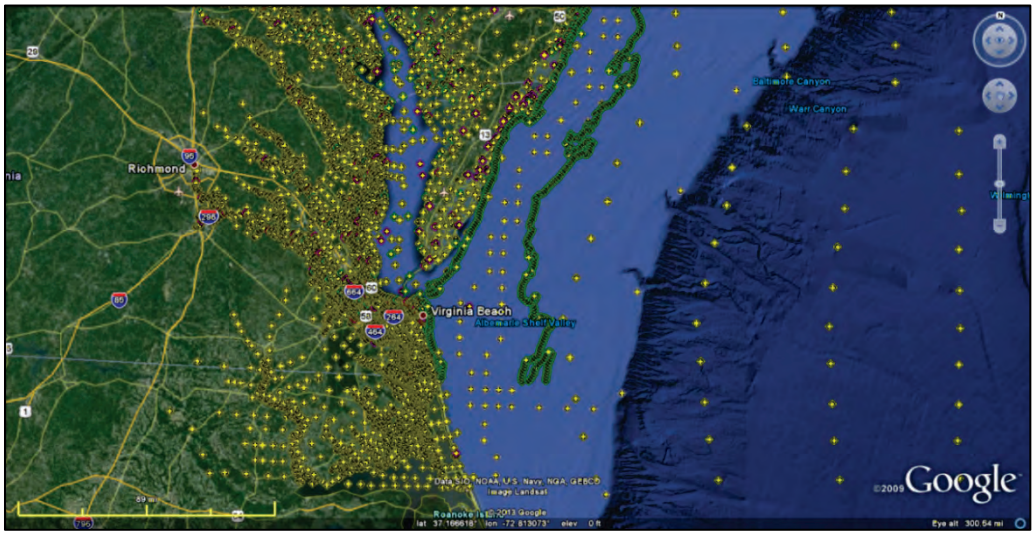

Approximately 11,000 additional save points along the shorelines and main channels of the Atlantic coast from Virginia to Maine are also included within the save-points set, referred to in Table 6-2 as the “ERDC” save points. As previously mentioned, this smaller subset of points provides frequent nearshore time-series information that is more easily accessible than the global solution files. This data is expected to be useful for applications involving future projects and further statistical analyses. The ERDC save points were placed along bathymetric elevation contours of 1 m, 2 m, and 3 m with the majority focus on the 3 m contour.

6.7 Model validation

6.7.1 General considerations

Validation was performed to ensure ADCIRC adequately predicts the hydrodynamics of the study area. Accuracy of a model is influenced by the accuracy of the forcing functions specified at open-water boundaries, representation of the geometry of the study area (i.e., bathymetry and shoreline), and by errors induced by the truncated terms associated with the governing equations as well as to values selected for model parameters, such as the bottom friction and lateral eddy coefficients. A satisfactory comparison between predictions and measurements in the validation procedure provides confidence that the model adequately replicates hydrodynamic processes. The validation procedure accomplished for this study included a harmonic analysis to ensure that the model is responding correctly to astronomical forcing and a comparison of model to measurements for seven storm conditions to ensure that the model is responding to meteorological forcing.

6.7.2 Harmonic analysis

With the initial version of the ADCIRC mesh completed, the hydrodynamic model underwent preliminary testing to ensure model stability and general performance when forced with only tidal conditions.

A tidal forcing boundary condition was defined at the offshore boundary, all island and mainland boundaries were developed, and a long-term (60-day) tidal simulation was performed on the Cray Xe6 (Garnet) supercomputer. Time-varying tidal elevations specified at nodes along the open ocean boundaries were synthesized using the M_2, S_2, N_2, K_1, O_1, Q_1, P_1, and K_2 tidal constituents. Constituent information was extracted from a database developed from the TOPEX 7 satellite measurements. Because the model domain is of sufficient size that celestial attraction induces tide within the mesh proper, tide-generating potential functions were included in the simulations and correspond to the constituents listed above. The 60-day tidal simulation included a 15-day tidal spin-up time period and a 45-day time period for the harmonic analysis. The harmonic analysis of the last 45 days of the simulation was conducted to compare the NOAA-synthesized constituent amplitudes and epochs with the ADCIRC-computed amplitudes and epochs at 143 NOAA gage locations.

Based on the initial tidal harmonic analysis, the NACCS ADCIRC mesh underwent updates due to the underprediction of tides in the Gulf of Maine. A first attempt at increasing the tide range in the Gulf of Maine was to drive more water into this region by extending the offshore boundary from the initial VDATUM offshore boundary for the north portion of the mesh to the traditional East Coast ADCIRC mesh boundary, which follows the 60 deg W longitude. The additional volume of water did not produce a noticeable change in the tide range at the Gulf of Maine gage locations.

The second attempt at increasing the tide range in the Gulf of Maine was to examine the bathymetry in the Gulf of Maine and Bay of Fundy. In the early stages (June/July 2013 timeframe) of the NACCS mesh development, ERDC CHL provided input to the University of Oklahoma (UO) to improve its efforts to update the East Coast tidal database. In turn, UO contacted NOAA VDatum developers which led to a NOAA update to the Gulf of Maine bathymetry in August 2013. The update to the Gulf of Maine bathymetry was relayed back to ERDC CHL in December 2013 and incorporated into the NACCS ADCIRC mesh. Tidal prediction in the Gulf of Maine improved with the updated bathymetry as shown for the Portland, ME, station (Figure 6-21). Tidal harmonic analysis results at several other gage locations from Maine to North Carolina are shown in Figure 6-22 to Figure 6-26. Comparison of model and measurements shows excellent correlations at most locations.

Figure 6-21. Tidal harmonic analysis for Portland, ME, gage. The top two panels show the constituent amplitudes and epochs before the Gulf of Maine bathymetric correction, and the bottom two panels show the constituent amplitudes and epochs after Gulf of Maine bathymetric correction.

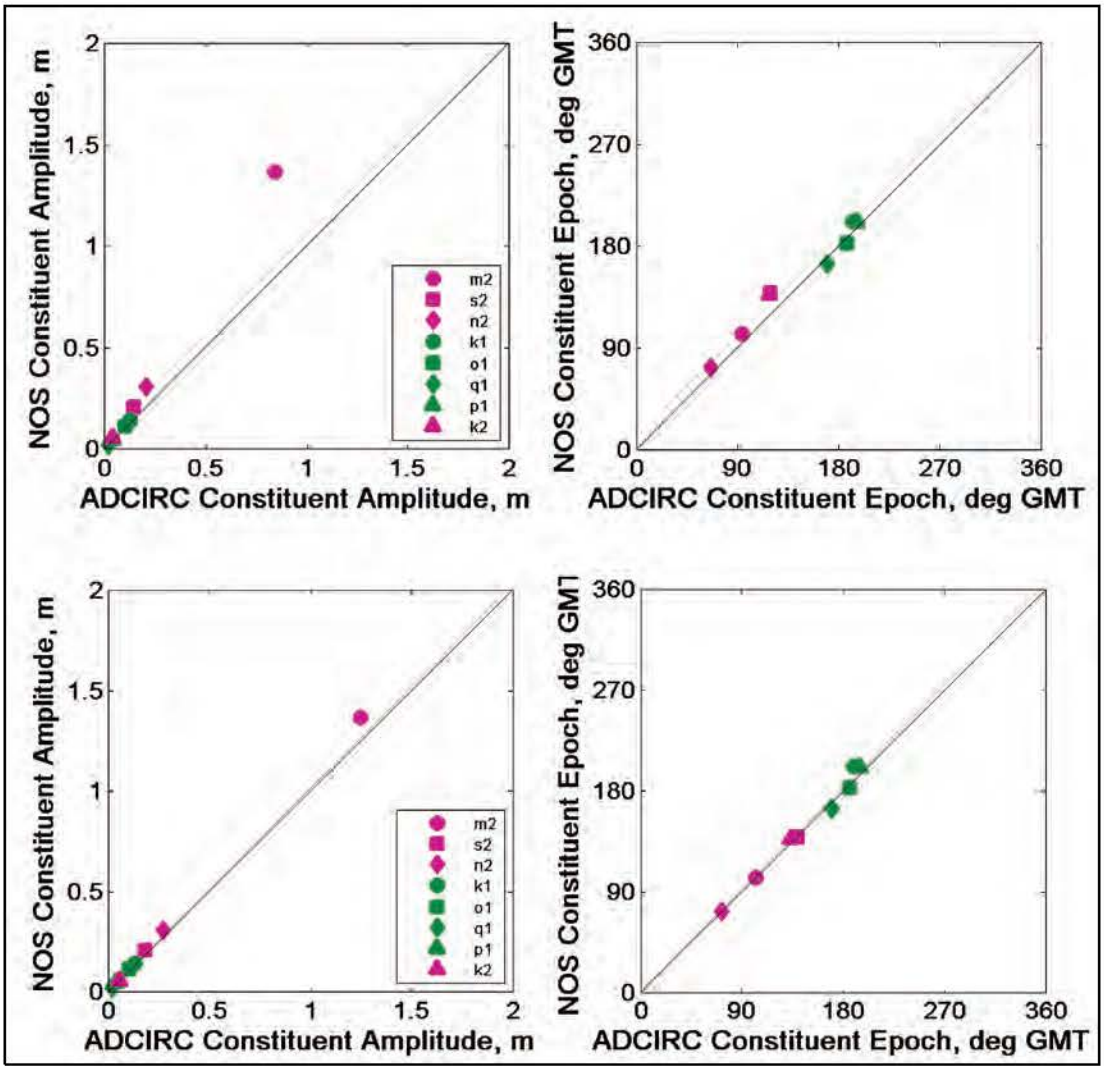

Figure 6-22. Tidal harmonic analysis for Thomaston, ME.

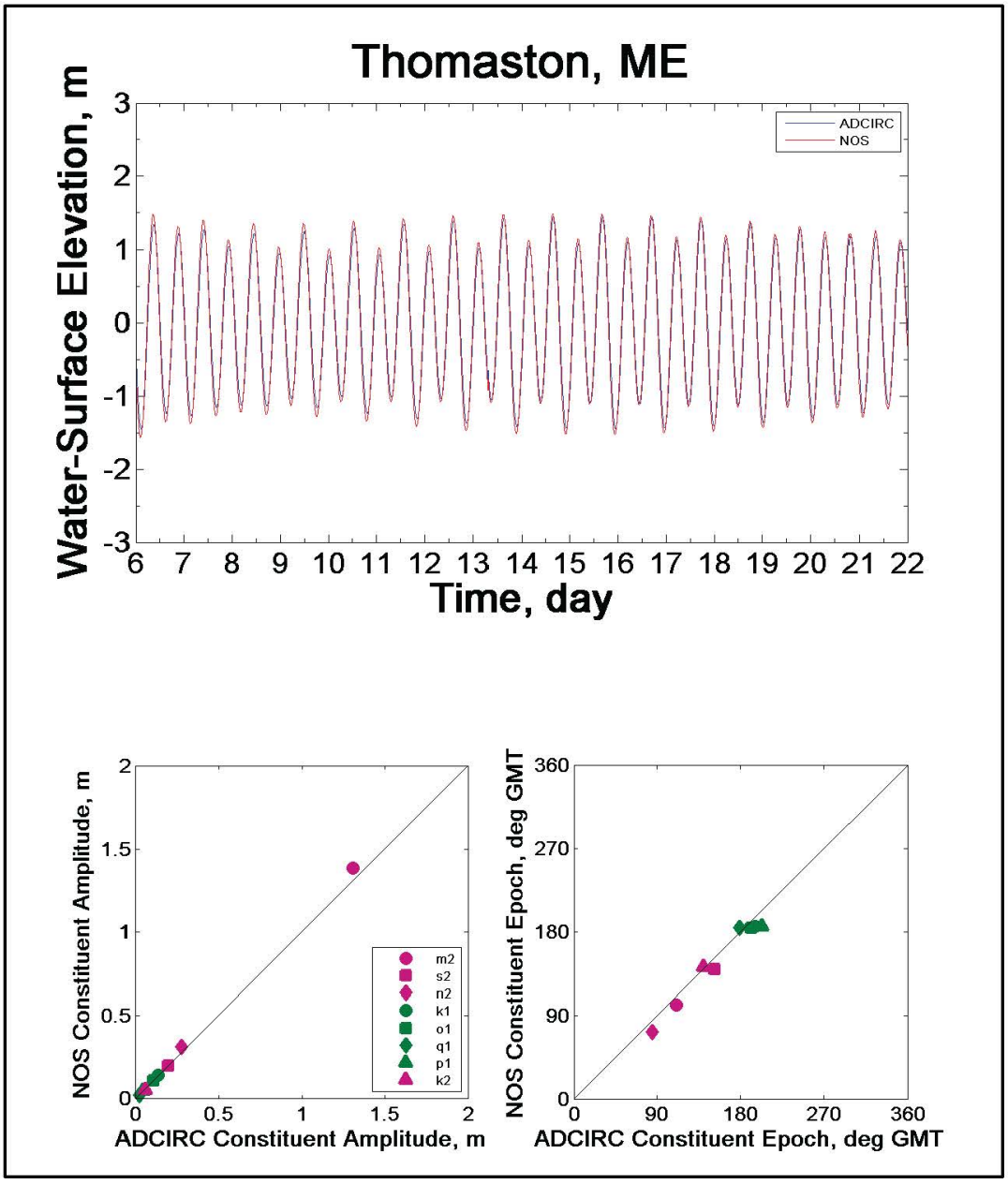

Figure 6-23. Tidal harmonic analysis for The Battery, NY.

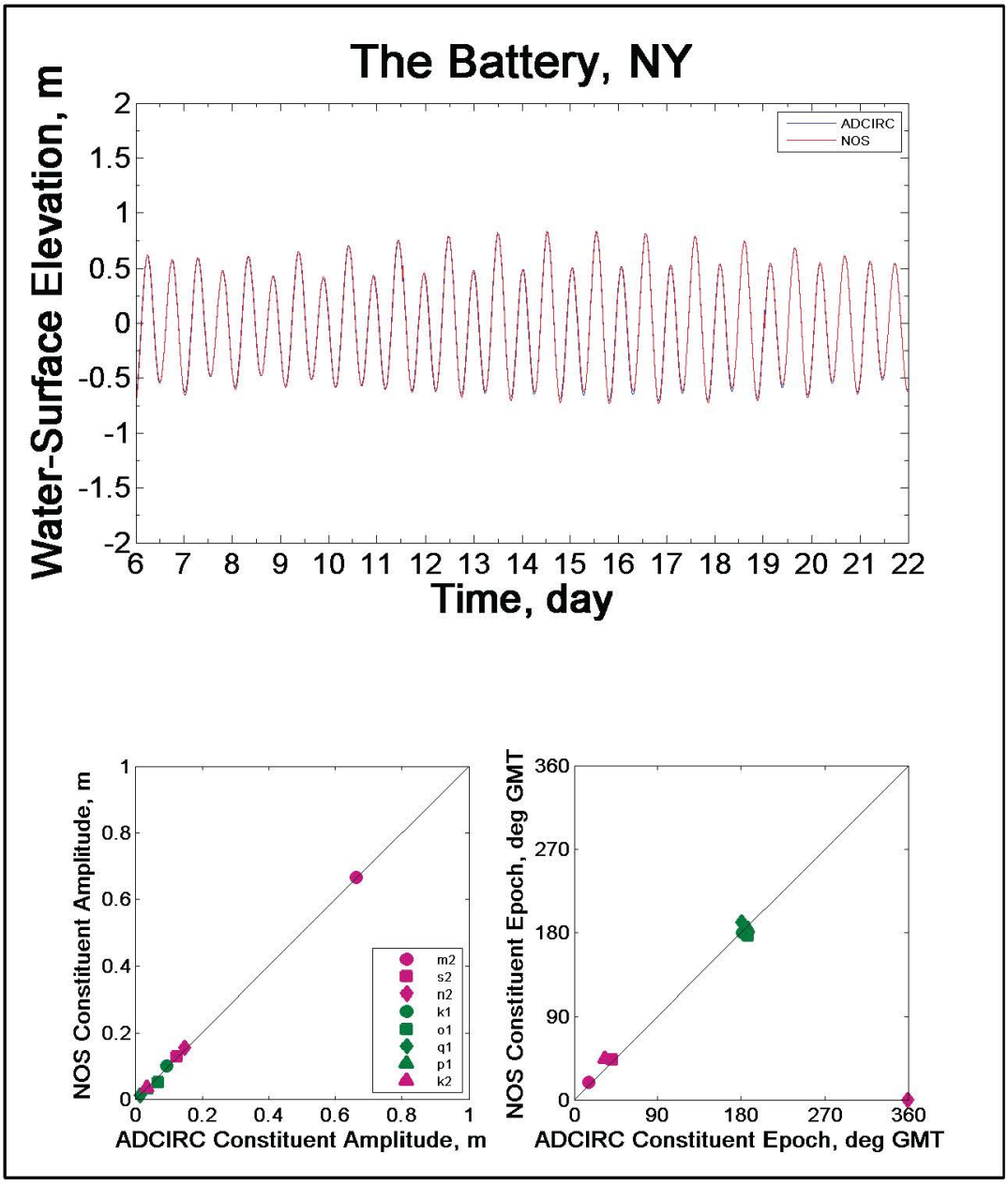

Figure 6-24. Tidal harmonic analysis for Atlantic City, NJ.

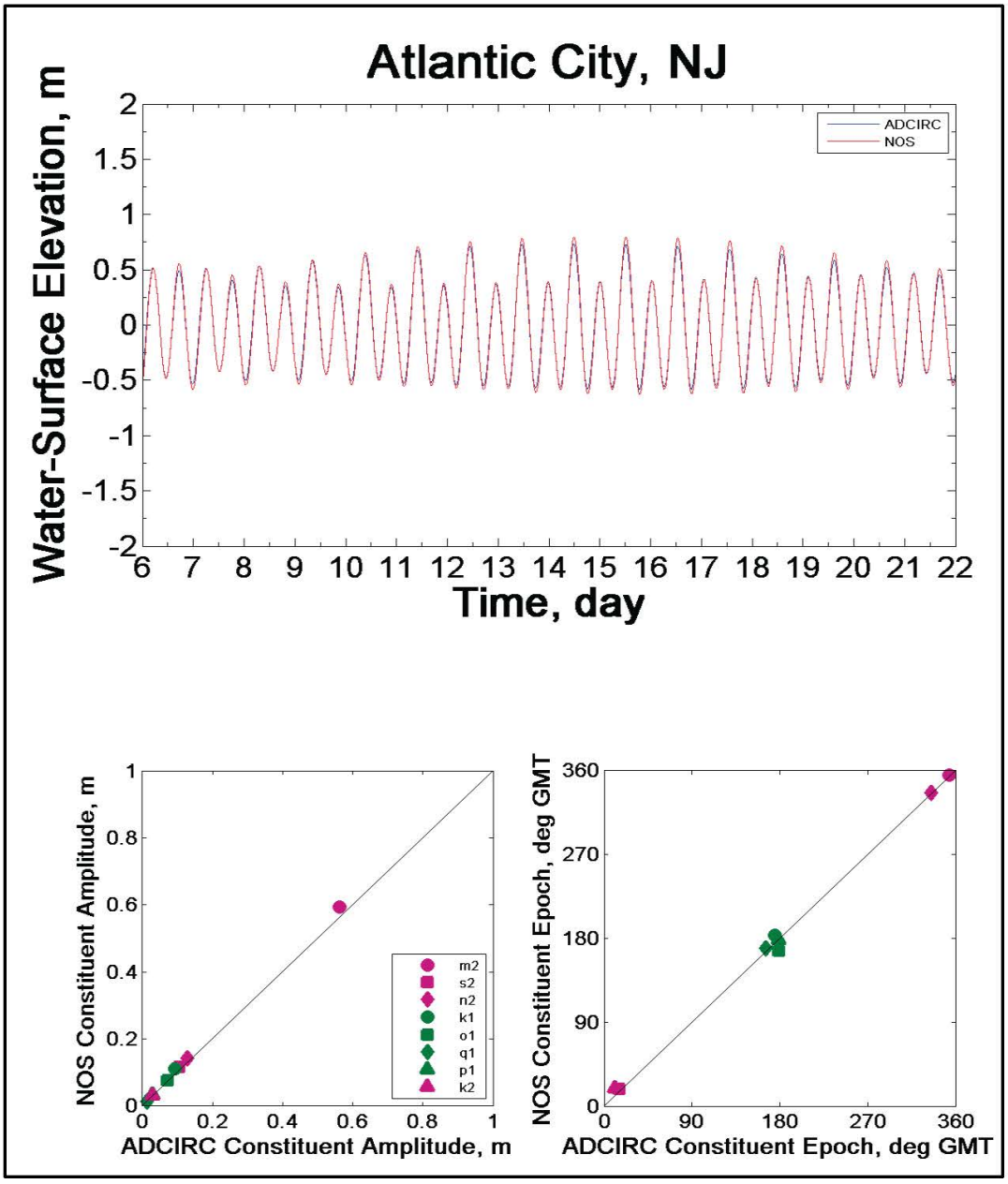

Figure 6-25. Tidal harmonic analysis for Lewes, DE.

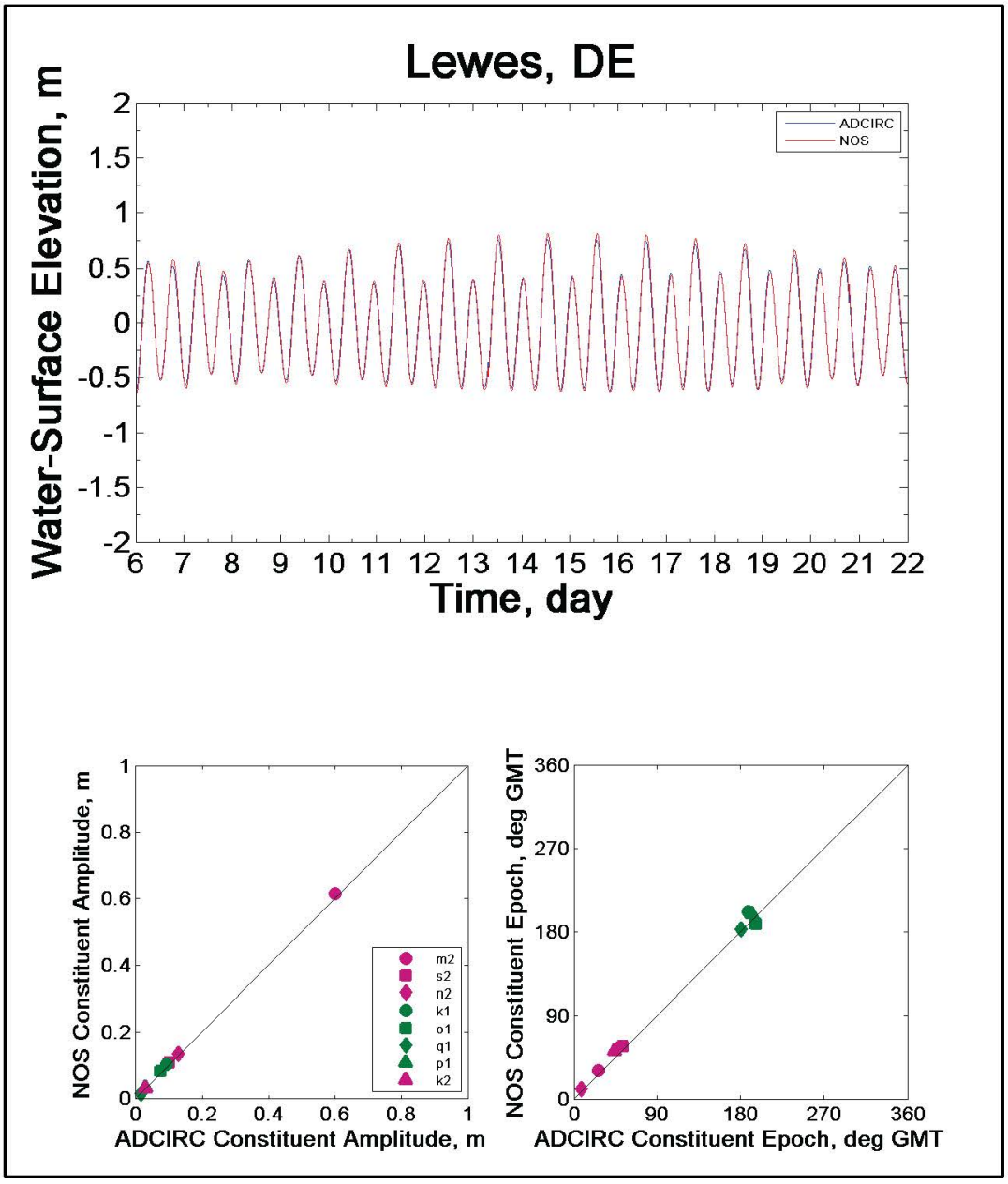

Figure 6-26. Tidal harmonic analysis for the U.S. Coast Guard (USCG) Station, Hatteras, NC.

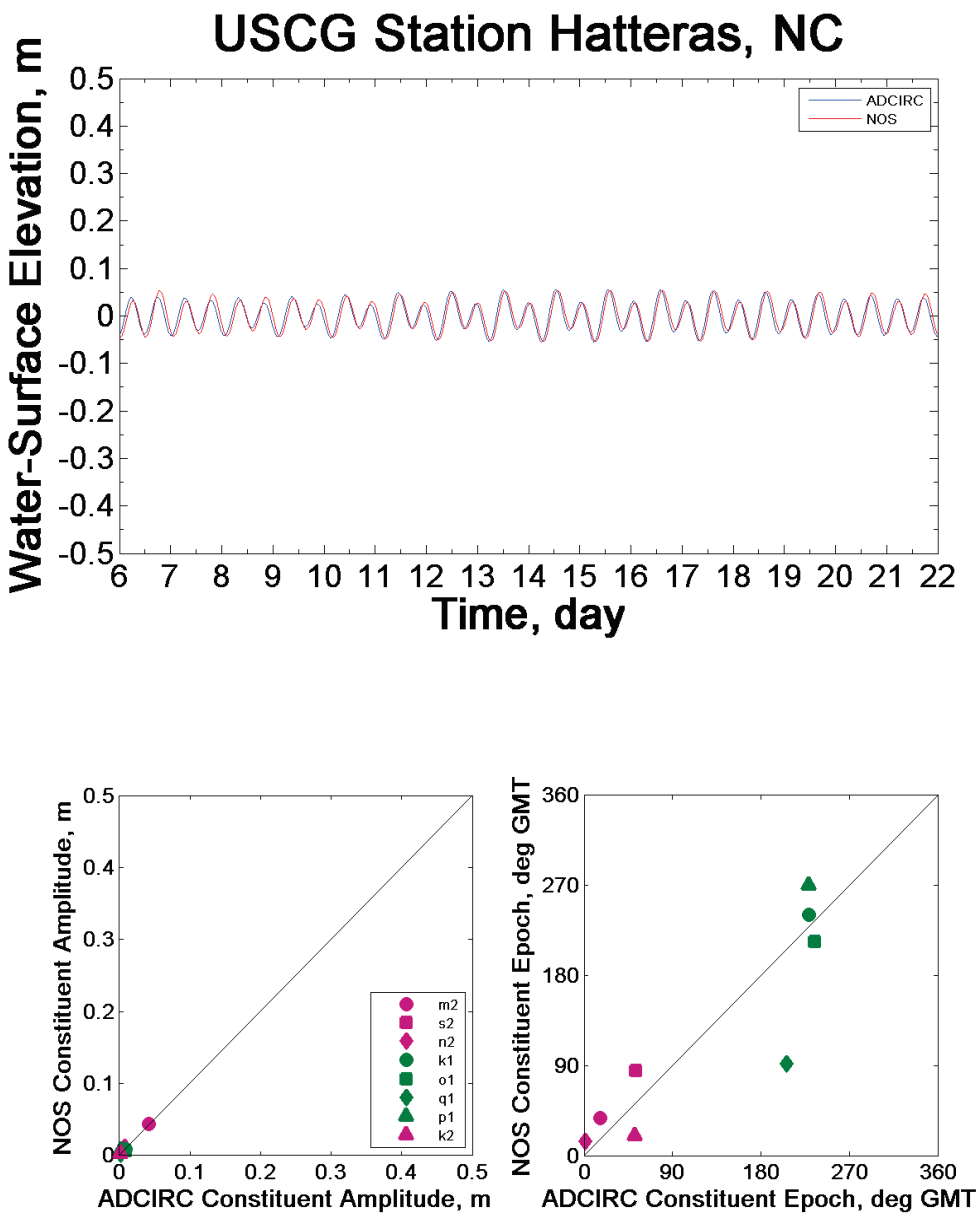

6.7.3 Model validation

Validation storms were selected based on the availability of wind and pressure fields along with sufficient measured water level and wave data in order to compare with model results. Storm wind and pressure fields for eight tropical validation simulations were obtained from available sources/studies including an in-house project (Isabel), a University of

North Carolina project (Irene), directly from OWI (Sandy), FEMA Region II (1938, 1944, Donna, and Gloria) and FEMA Region III (Josephine) studies. The green box in Figure 6-27 shows the extent of the fine resolution winds for the FEMA Region II tropical storms (1938, 1944, Donna, and Gloria). The blue box indicates the limits of the fine resolution winds for Josephine and Isabel. The orange and black boxes indicate the limits of the fine resolution winds for Irene and Sandy, respectively. For the NACCS, fine resolution winds were developed by OWI within the red box and covered the entire area from Virginia to Maine. Basin scale winds (latitude range: 22 to 48 deg N; longitude range: 58 to 82 deg W) were also provided by OWI for every storm and are discussed in the OWI contractor report and the "Winds" section of this report.

Figure 6-27. Fine resolution wind domains for validation storms and NACCS.

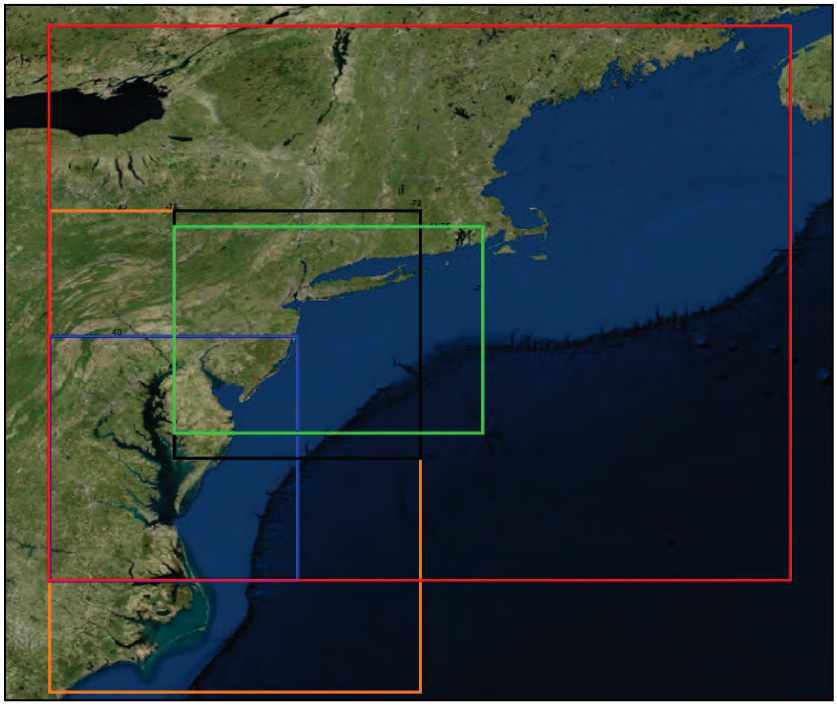

Validation of the ADCIRC mesh and input parameters was first accomplished with the simulation and analysis of the aforementioned 8 tropical storms as well as 12 extratropical storms. Not all of these storms were included as part of the model validation but were simply simulated to search for any potential model application issues. Of the 20 initial validation storms simulated for stability testing, a detailed analysis was performed with a focus on Sandy, Irene, Isabel, Josephine, and Gloria because those storms have the greatest number of water level gages available within the corresponding detailed wind domain, and they occurred most recently. In

addition, analysis of two extratropical storms (ET070 and ET073), including The North American Blizzard of 1996, was performed based on available measurements to compare with model results.

ADCIRC model simulations under combined astronomical and meteorological conditions were completed for seven hindcast simulations of tropical and extratropical events as part of the validation process. Tide, river, wind, pressure, and wave forcing contributions to water level were included in all validation simulations. Storm simulations were initiated with a 16-day tidal spin-up, with the exception of Hurricane Sandy, which had a 13.5-day tidal spin-up, and continued with the application of basin and regional-scale winds and pressures for each event. Each storm also included a steric water level adjustment for the time period of that event derived from the historic steric height adjustment values for the gages as discussed in steric height adjustment section. Details of each of the validation simulations are reported herein.

6.7.3.1 Hurricane Gloria

Hurricane Gloria was simulated for the period beginning 12 September 1985 at 12:00 Greenwich Mean Time (GMT) and concluding at 28 September 1985 at 18:00. Gloria originated from a tropical wave on 16 September 1985 in the eastern Atlantic Ocean. (Figure 6-28 shows the path of each of the validation events.) After remaining a weak tropical cyclone for several days, Gloria intensified into a hurricane on 22 September 1985. Gloria quickly intensified on 24 September 1985 and the next day reached peak winds of 145 mph (230 km/hr). The hurricane weakened before striking the Outer Banks of North Carolina on 27 September. Later that day, Gloria made two subsequent landfalls on Long Island and later western Connecticut before becoming an extratropical storm on 28 September 1985 over New England. A 1 s time-step was used in the simulation, and a 14-day ramping function was applied to the tidal signal and the wind fields at the beginning of the simulations in order to prevent generating spurious modes of oscillation by starting the model under full forcing. Time-varying tidal elevations corresponding to the 16.25-day simulation time period were specified at nodes along the open ocean boundaries and synthesized using the M_2, S_2, N_2, K_1, O_1, Q_1, P_1, and K_2 tidal constituents. Constituent information was extracted from a database developed from the TOPEX 7 satellite measurements. Wind fields available for the 26 September 85 through 28 September 85 time period were supplied to the model and were developed by OWI. This OWI data included hourly wind

components and pressures at 0.25 deg spacing for the basin scale region, bounded by latitude range 22 deg to 48 deg N and longitude range 58 deg to 82 deg W. The detailed resolution winds were at a 0.05 deg spacing, bounded by latitude range 38.4 deg to 41.75 deg N and longitude range 71 deg to 76 deg W.

Figure 6-28. Paths of tropical validation storms.

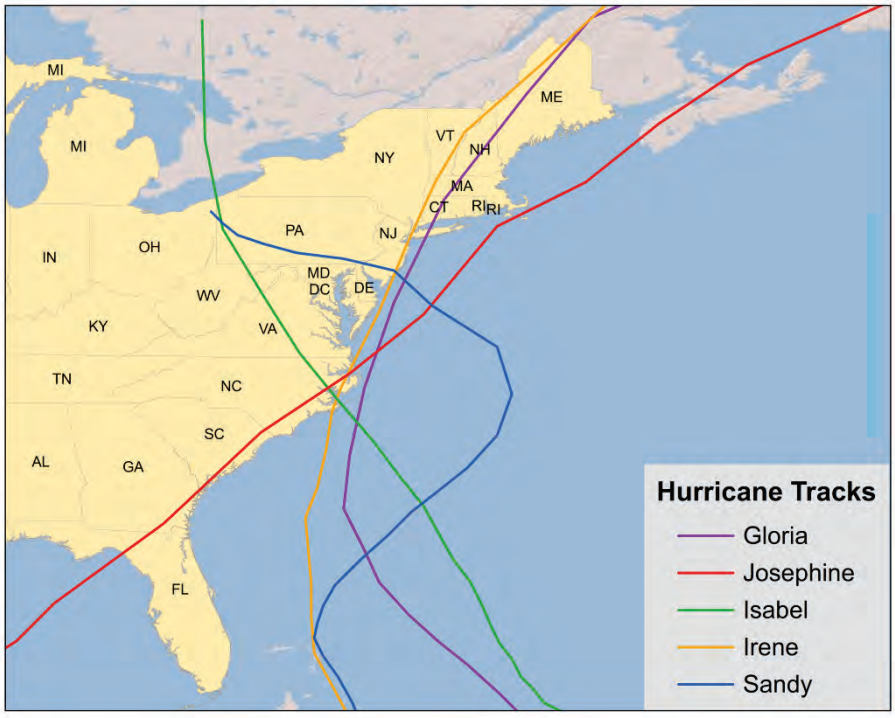

Time series of measured NOAA/NOS water-surface elevations were obtained at 39 stations for the validation time period (Figure 6-29). Figure 6-30 displays a comparison of modeled and measured time series of water-surface elevation for the Atlantic City gage (8534720) from 26–30 September 1985, which included Hurricane Gloria. The time series of measured water levels shows that wind has a significant influence on water levels in the study area. Astronomical tides at this location are approximately 1.4 m during this event whereas with wind, water levels varied 2.7 m during the validation period. Figure 6-30 shows that wind has a significant influence on water level, both amplifying and suppressing water level as storm systems pass through the region. The model-to-measurement comparisons show that ADCIRC generally performs well and reproduces the overall water level response but does not capture the fine details that would require winds and pressures being produced at a scale finer than those used in this validation simulation.

Figure 6-29. NOAA station locations.

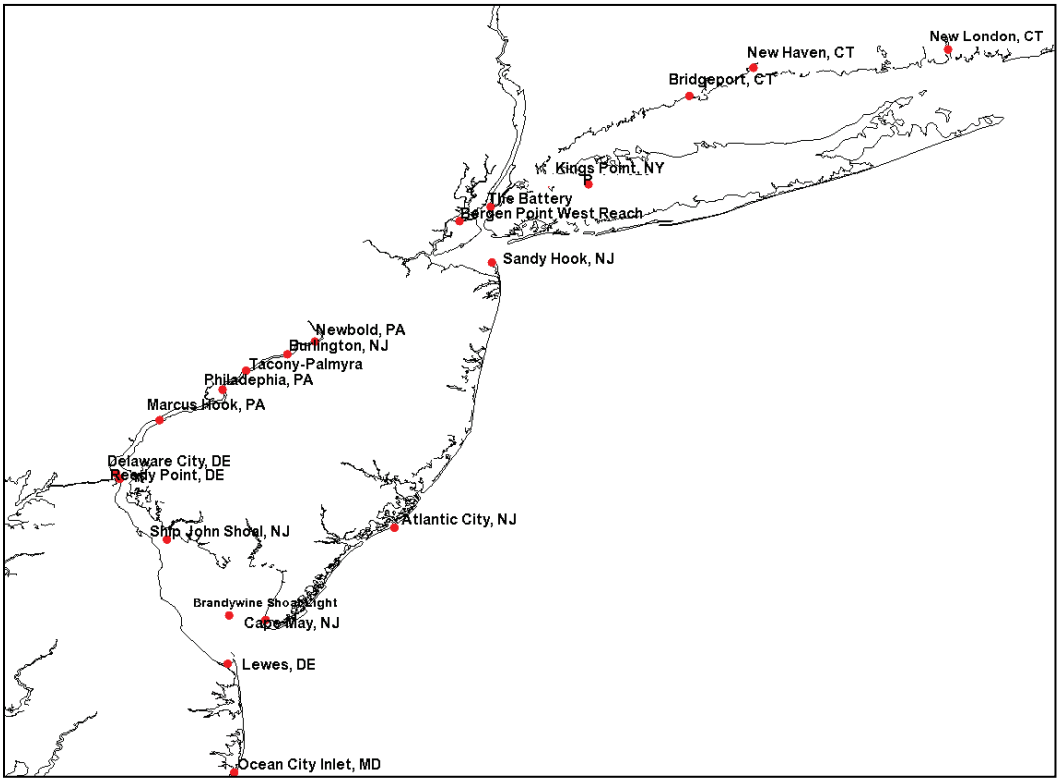

Figure 6-30. Hurricane Gloria time-series comparison at Atlantic City, NJ.

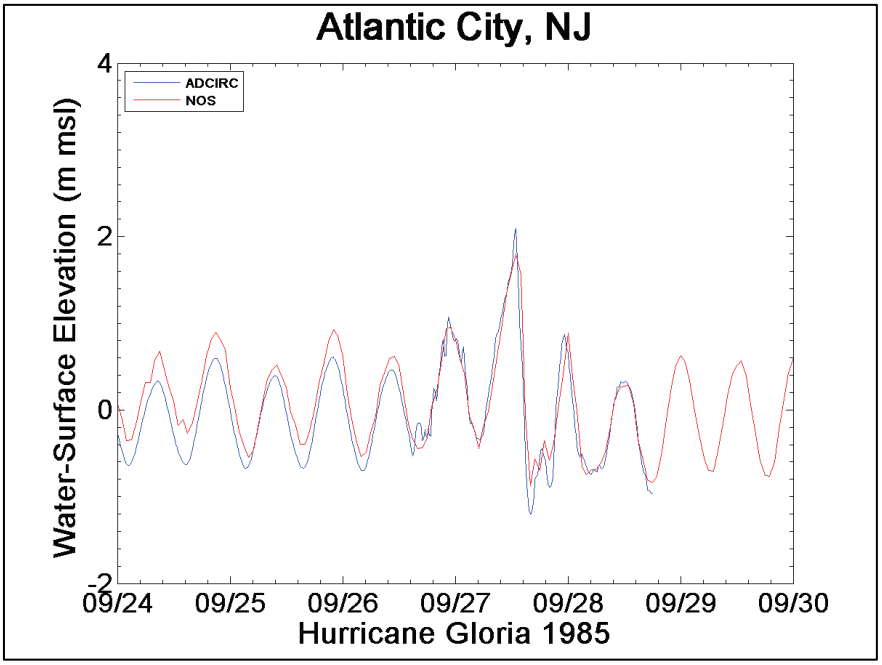

6.7.3.2 Hurricane Josephine

Hurricane Josephine was simulated for the period beginning 20 September 1996 at 00:00 GMT and concluding 12 October 1996 at 00:00. Tropical Storm Josephine was an unusual Atlantic tropical storm that moved from west to east across the Gulf of Mexico in October 1996. It formed on 4 October 1996 as a tropical depression from the remnants of a cold front. Early in its duration, the system interacted with a ridge over the central United States, which produced strong winds and high tides along the Texas coast. Moving generally to the east due to a trough, the depression intensified into a tropical storm on 6 October 1996 and the next day reached peak winds of 70 mph while approaching the west coast of Florida. Josephine made landfall in Taylor County, FL, near peak intensity early on 8 October 1996 and soon after became an extratropical event. The extratropical storm traveled over Georgia then accelerated to the northeast along the east coast of the United States with winds of 50 mph (85 km/hr) which strengthened to 77 mph (124 km/hr) near Ocean City, MD. The storm continued along a northeasterly path, eventually moving offshore, then strengthened in the northern Atlantic Ocean and merged with another extratropical storm near Iceland. A 1 s time-step was used in the simulation, and a 14-day ramping function was applied to the tidal signal and the wind fields at the beginning of the simulations in order to prevent generating spurious modes of oscillation by starting the model under full forcing. Time-varying tidal elevations corresponding to the 22-day simulation time period were specified at nodes along the open ocean boundaries, synthesized using the M_2, S_2, N_2, K_1, O_1, Q_1, P_1, and K_2 tidal constituents. Constituent information was extracted from a database developed from the TOPEX 7 satellite measurements. Wind fields for the 4 October 1996 through 12 October 1996 time period were supplied to the model and were developed by OWI. This OWI data included hourly wind components and pressures at 0.25 deg spacing for the basin scale region, bounded by latitude range 22 deg to 48 deg N and longitude range 58 deg to 82 deg W. The detailed resolution winds were at a 0.025 deg spacing, bounded by latitude range 36 deg to 40 deg N and longitude range 74 deg to 78 deg W.

Time series of measured NOAA/NOS water-surface elevations were obtained at 41 stations for the validation time period. Figure 6-31 displays a comparison of modeled and measured time series of water-surface elevation for the Lewes, DE, Station (8557380) from 5–11 October 1996, which included Hurricane Josephine. The time series of measured water levels shows that wind has a significant influence on water levels in the study ar-

ea. Astronomical tides at this location are approximately 1 m during the validation period whereas with wind, water levels varied 1.65 m during the validation period. Overall, the 1996 Hurricane Josephine model simulation reproduced measured water levels fairly well, but there is a 0.1 m positive bias in the model prior to the storm peak and a 0.1 m negative bias after the storm peak.

Figure 6-31. Hurricane Josephine time series comparison at Lewes, DE.

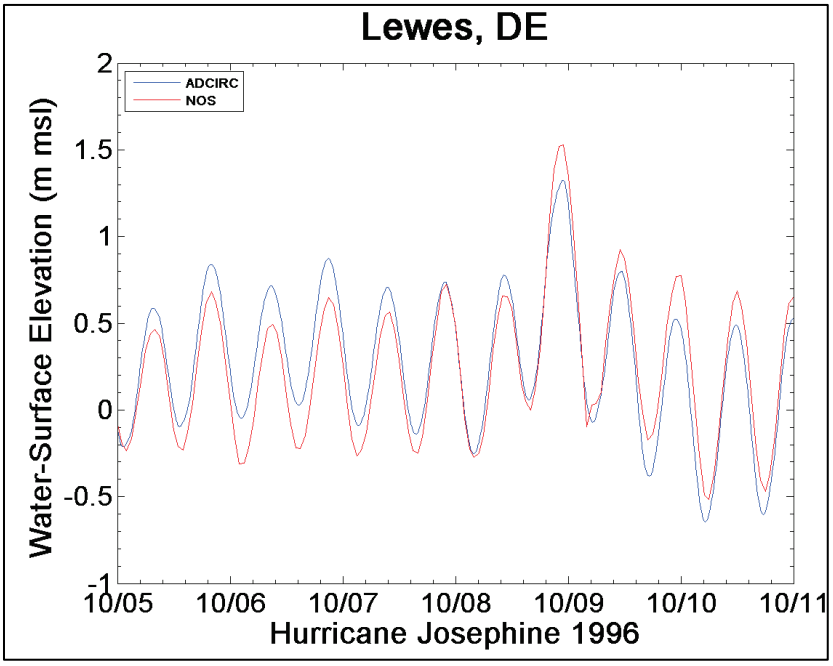

6.7.3.3 Hurricane Isabel

Hurricane Isabel was simulated for the period beginning 31 August 2013 at 00:00 GMT and concluding at 30 September 2003 at 00:00. Isabel formed near the Cape Verde Islands from a tropical wave on 6 September 2013 in the tropical Atlantic Ocean. It moved northwestward, and within an environment of light wind shear and warm waters, it steadily strengthened to reach peak winds of 165 mph (265 km/h) on 11 September 2013. After fluctuating in intensity for 4 days, Isabel gradually weakened and made landfall on the Outer Banks of North Carolina with winds of 105 mph (165 km/h) on 18 September 2013. It quickly weakened over land and became extratropical over western Pennsylvania the next day. A 1 s time-step was used in the simulation, and a 14-day ramping function was applied to the tidal signal and the wind fields at the beginning of the simulations in order to prevent generating spurious modes of oscillation by starting the model under full forcing. Time-varying tidal elevations corre-

sponding to the 20-day simulation time period were specified at nodes along the open ocean boundaries, synthesized using the M_2, S_2, N_2, K_1, O_1, Q_1, P_1, and K_2 tidal constituents. Wind fields for the 14 September 2003 through 20 September 2003 time period were supplied to the model and were developed by OWI. This OWI data included hourly wind components and pressures at 0.25 deg spacing for the basin scale region, bounded by latitude range 22 deg to 48 deg N and longitude range 58 deg to 82 deg W. The detailed resolution winds were at a 0.025 deg spacing, bounded by latitude range 36 deg to 40 deg N and longitude range 74 deg to 78 deg W.

Time series of measured NOAA/NOS water-surface elevations were obtained at 60 stations for the validation time period. Figure 6-32 displays a comparison of modeled and measured time series of water-surface elevation for the Duck, NC, Station (8651370) from the 15–21 September 2003, which included Hurricane Isabel. The time series of measured water levels shows that wind has a significant influence on water levels in the study area. Astronomical tides at this location are approximately 0.9 m during the validation time period whereas with wind, water levels varied 1.95 m during the validation period. Overall, the 2003 Hurricane Isabel model simulation reproduced measured water levels fairly well.

Figure 6-32. Hurricane Isabel time series comparison at Duck, NC.

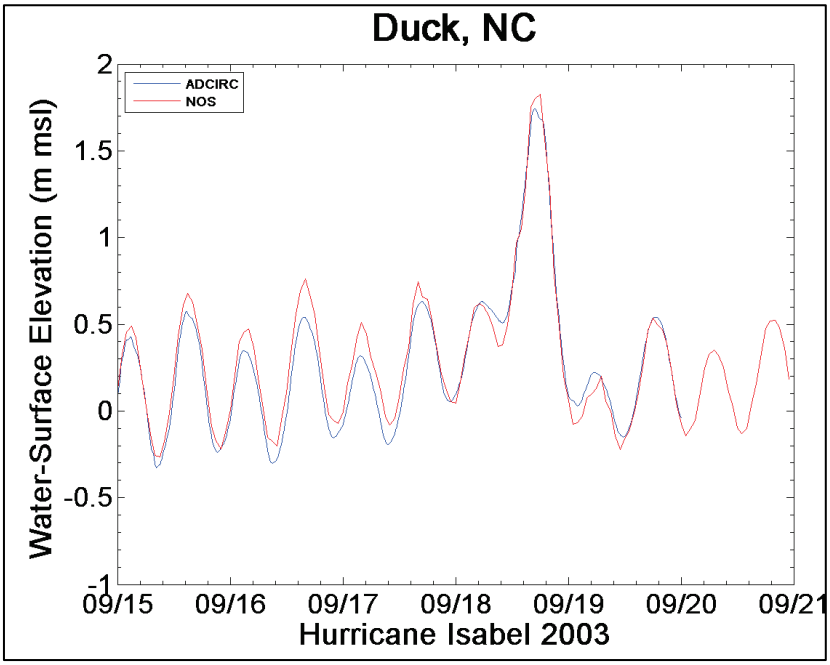

6.7.3.4 Hurricane Irene

Hurricane Irene was simulated for the period beginning 6 August 2011 at 00:00 GMT and concluding at 30 August 2011 at 00:00. Irene originated from a well-defined Atlantic tropical wave that began showing signs of organization east of the Lesser Antilles. Due to development of atmospheric convection and a closed center of circulation, the system was designated as Tropical Storm Irene on 20 August 2011. After intensifying, Irene made landfall in St. Croix as a strong tropical storm later that day. Early on 21 August, the storm made a second landfall in Puerto Rico. While crossing the island, Irene strengthened into a Category 1 hurricane. The storm paralleled offshore of Hispaniola and continued to slowly intensify in the process. Shortly before making four landfalls in the Bahamas, Irene peaked as a 120 mph (195 km/h) Category 3 hurricane. Thereafter, the storm slowly leveled off in intensity as it struck the Bahamas and then curved northward after passing east of Grand Bahama. Continuing to weaken, Irene was downgraded to a Category 1 hurricane before making landfall on the Outer Banks of North Carolina on 27 August 2013, becoming the first hurricane to make landfall in the United States since Hurricane Ike in 2008. Early on the following day, the storm re-emerged into the Atlantic from southeastern Virginia. Although Irene remained a hurricane over land, it weakened to a tropical storm while making yet another landfall in the Little Egg Inlet in southeastern New Jersey on 28 August 2013. A few hours later, Irene made its ninth and final landfall in Brooklyn, New York City. Early on 29 August 2013, Irene transitioned into an extratropical cyclone hitting Vermont/New Hampshire after remaining inland as a tropical cyclone for less than 12 hours. A 1 s time-step was used in the simulation, and a 14-day ramping function was applied to the tidal signal and the wind fields at the beginning of the simulations in order to prevent generating spurious modes of oscillation by starting the model under full forcing. Time-varying tidal elevations corresponding to the 26-day simulation time period were specified at nodes along the open-ocean boundaries, synthesized using the M_2, S_2, N_2, K_1, O_1, Q_1, P_1, and K_2 tidal constituents. Wind fields for the 20 August 2011 through 30 August 2011 time period were supplied to the model and were developed by OWI. This OWI data included hourly wind components and pressures at 0.25 deg spacing for the basin scale region, bounded by latitude range 22 deg to 48 deg N and longitude range 58 deg to 82 deg W. The detailed resolution winds were at a 0.05 deg spacing, bounded by latitude range 34 deg to 42 deg N and longitude range 72 deg to 78 deg W.

Time series of measured NOAA/NOS water-surface elevations were obtained at 60 stations for the validation time period. Figure 6-33 displays a comparison of modeled and measured time series of water-surface elevation for the Chesapeake Bay Bridge Tunnel Station (8638863) from 26–30 August 2011, which included Hurricane Irene. The time series of measured water levels shows that wind has a significant influence on water levels in the study area. Astronomical tides at this location are approximately 0.9 m during the validation time period whereas with wind, water levels varied 1.8 m during the validation period. Overall, the 2011 Hurricane Irene model simulation reproduced measured water levels well.

Figure 6-33. Hurricane Irene time series comparison at Chesapeake Bay Bridge Tunnel, Virginia.

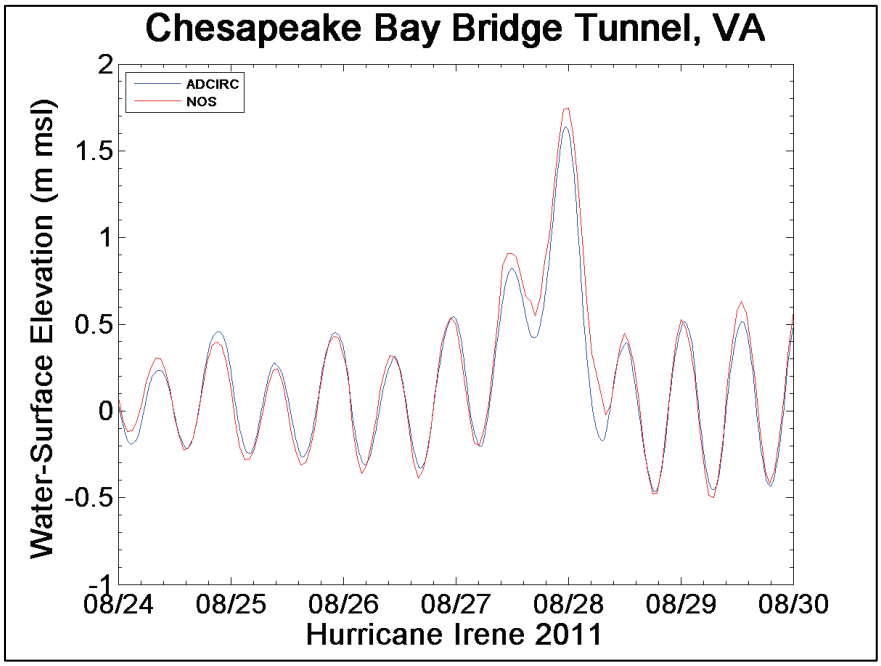

6.7.3.5 Hurricane Sandy

Hurricane Sandy was simulated for the period beginning 11 October 2012 at 12:00 GMT and concluding at 1 November 2012 at 00:00. Sandy developed from a tropical wave in the western Caribbean Sea on 22 October 2012, quickly strengthened, and was upgraded to Tropical Storm Sandy 6 hours later. Sandy moved slowly northward toward the Greater Antilles and gradually intensified. On 24 October 2012, Sandy became a hurricane, made landfall near Kingston, Jamaica, re-emerged a few hours later into the Caribbean Sea, and strengthened into a Category 2 hurricane. On 25 October 2012, Sandy hit Cuba as a Category 3 hurricane and

then weakened to a Category 1 hurricane. Early on 26 October 2012, Sandy moved through the Bahamas. On 27 October 2012, Sandy briefly weakened to a tropical storm and then restrengthened to a Category 1 hurricane. Early on 29 October 2012, Sandy curved north-northwest and then moved ashore near Brigantine, NJ, just to the northeast of Atlantic City, as a posttropical cyclone with hurricane-force winds. During the next 2 days, Sandy's remnants drifted northward and then northeastward over Ontario before merging with another low-pressure area over Eastern Canada. A 1 s time-step was used in the simulation, and a 13.5-day ramping function was applied to the tidal signal and the wind fields at the beginning of the simulations in order to prevent generating spurious modes of oscillation by starting the model under full forcing. Time-varying tidal elevations corresponding to the 20.5-day simulation time period were specified at nodes along the open ocean boundaries, synthesized using the M_2, S_2, N_2, K_1, O_1, Q_1, P_1, and K_2 tidal constituents. Wind fields for the 25 October 2012 through 1 November 2012 time period were supplied to the model and were developed by OWI. This OWI data included hourly wind components and pressures at 0.25 deg spacing for the basin scale region, bounded by latitude range 22 deg to 48 deg N and longitude range 58 deg to 82 deg W.

Time series of measured NOAA/NOS water-surface elevations were obtained at 57 stations for the validation time period. Figure 6-34 displays a comparison of modeled and measured time series of water-surface elevation for The Battery, New York Station (8518750) from 27 October–2 November 2012, which included Hurricane Sandy. The time series of measured water levels shows that wind has a significant influence on water levels in the study area. Astronomical tides at this location are approximately 1.7 m during the validation period whereas with wind, water levels varied 3.7 m during the validation period. Overall, the 2012 Hurricane Sandy model simulation reproduced measured water levels well.

Figure 6-34. Hurricane Sandy time series comparison at The Battery, NY.

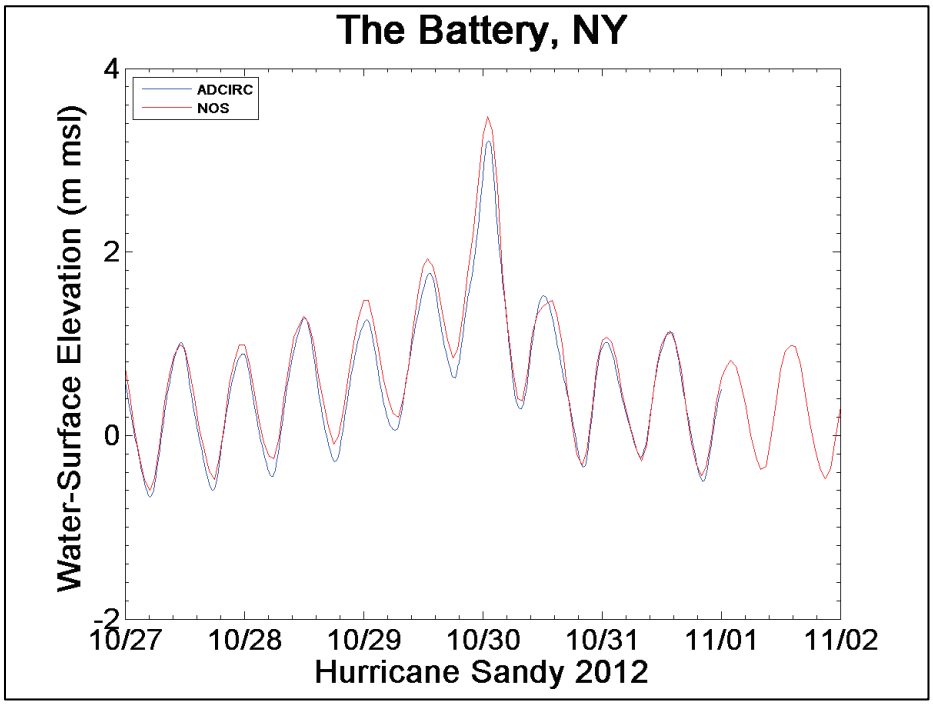

One noted exception is the overprediction of the storm peak at Atlantic City, NJ (Figure 6-35), for the Hurricane Sandy model simulation. This discrepancy in water level prediction at Atlantic City, NJ, was also reported by other researchers at the USGS Workshop (June 2014, Staten Island, NY). Because the model performs well at this location for other storms and in the tidal harmonic analysis, the mesh resolution and gage placement in the model were ruled out as potential causes of the discrepancy. Because the inferior performance is related to a specific event, the cause can be attributed to the forcing conditions or a malfunction in the measurement device. Many other gages, including two that bracket the Atlantic City gage (Sandy Hook and Brandywine Shoal Light) failed around this same time period. Because others have experienced the same discrepancy in their model-to-measurement comparison at Atlantic City, because the surrounding gages failed during the event and considering the magnitude of this event, the contention is that the discrepancy at this location is due to gage malfunction.

Figure 6-35. Hurricane Sandy time series comparison at Atlantic City, NJ.

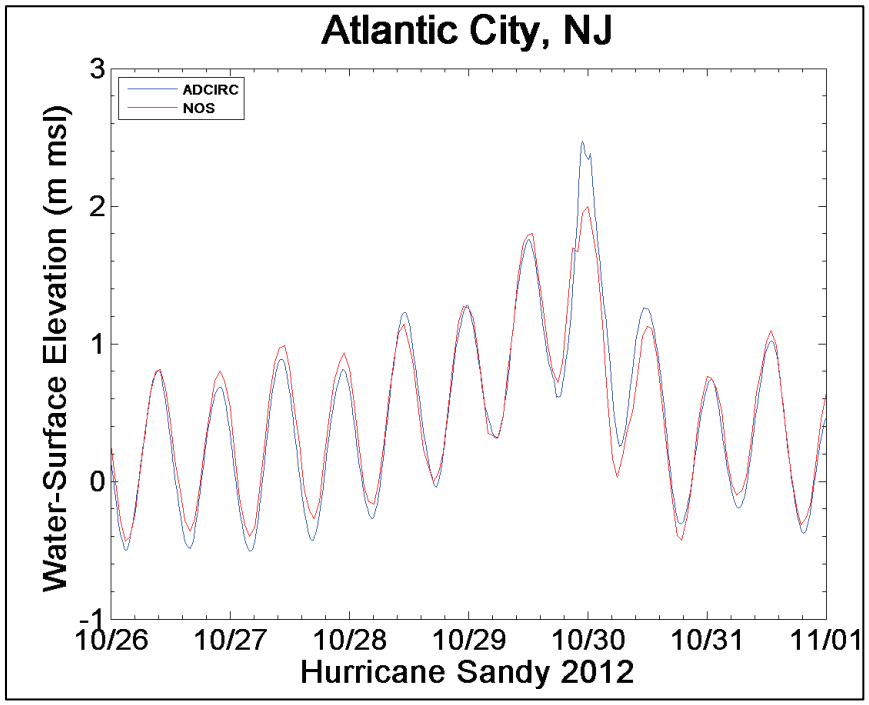

6.7.3.6 ET070

ET070, also known as, The North American Blizzard of 1996, was simulated for the period beginning 20 December 1995 at 00:00 GMT and concluding at 11 January 1996 at 00:00. A 1 s time-step was used in the simulation, and a 14-day ramping function was applied to the tidal signal and the wind fields at the beginning of the simulations in order to prevent generating spurious modes of oscillation by starting the model under full forcing. Time-varying tidal elevations corresponding to the 22-day simulation time period were specified at nodes along the open ocean boundaries, synthesized using the M_2, S_2, N_2, K_1, O_1, Q_1, P_1, and K_2 tidal constituents. Wind fields for the 3 January 1996 through 11 January 1996 time period were supplied to the model and were developed by OWI. This OWI data included hourly wind components and pressures at 0.25 deg spacing for the basin scale region, bounded by latitude range 22 deg to 48 deg N and longitude range 58 deg to 82 deg W.

Time series of measured NOAA/NOS water-surface elevations were obtained at 38 stations for the validation time period. Figure 6-36 displays a comparison of modeled and measured time series of water-surface elevation for the Lewes, DE, Station (8557380) from 3–11 January 1996, which included ET070. The time series of measured water levels shows that wind

has a significant influence on water levels in the study area. Astronomical tides at this location are approximately 1.5 m during this time period whereas with wind, water levels were elevated 0.75 m during the validation period. Overall, ET070 model simulation reproduced measured water levels fairly well.

Figure 6-36. ET070 time series comparison at Lewes, DE.

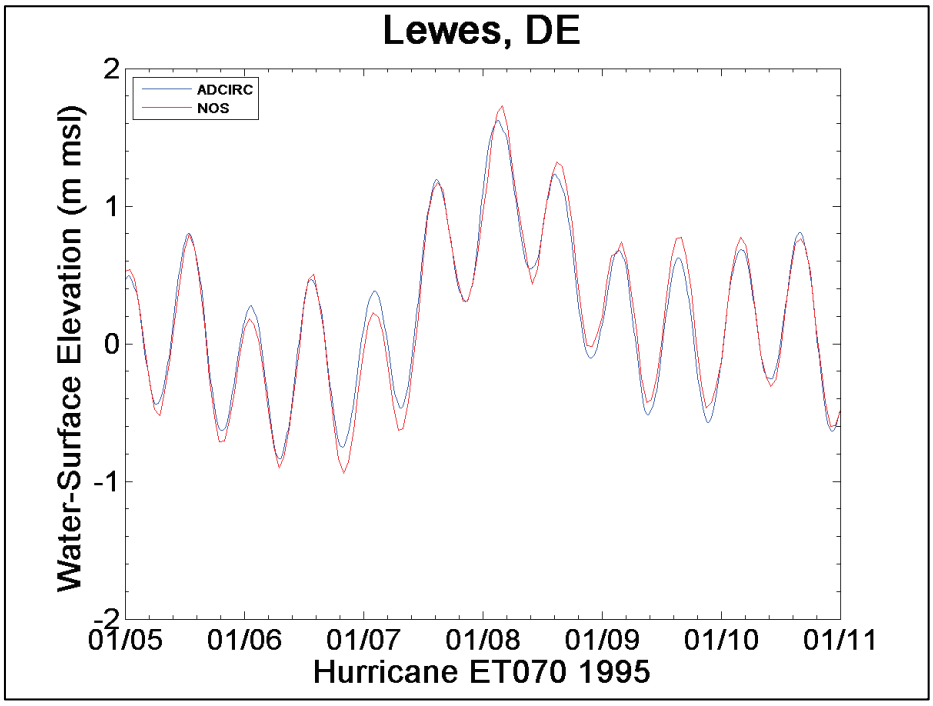

6.7.3.7 ET073

ET073 was simulated for the period beginning 17 November 1996 at 00:00 GMT and concluding at 9 December 1996 at 00:00. A 1 s time-step was used in the simulation, and a 14-day ramping function was applied to the tidal signal and the wind fields at the beginning of the simulations in order to prevent generating spurious modes of oscillation by starting the model under full forcing. Time-varying tidal elevations corresponding to the 22-day simulation time period were specified at nodes along the open ocean boundaries, synthesized using the M_2, S_2, N_2, K_1, O_1, Q_1, P_1, and K_2 tidal constituents. Wind fields for the 1 December 1996 through 9 December 1996 time period were supplied to the model and were developed by OWI. This OWI data included hourly wind components and pressures at 0.25 deg spacing for the basin scale region, bounded by latitude range 22 deg to 48 deg N and longitude range 58 deg to 82 deg W.

Time series of measured NOAA/NOS water-surface elevations were obtained at 40 stations for the validation time period. Figure 6-37 displays a comparison of modeled and measured time series of water-surface elevation for the Willets Point, NY, Station (8516990) from the 3–9 December 1996 validation simulation that included ET073. The time series of measured water levels shows that wind has a significant influence on water levels in the study area. Astronomical tides at this location are approximately 1.75 m during this time period whereas with wind, water levels increased by more than 1.0 m during the validation period. Overall, ET073 model simulation reproduced measured water levels fairly well.

Figure 6-37. ET073 time series comparison at Willets Point, NY.

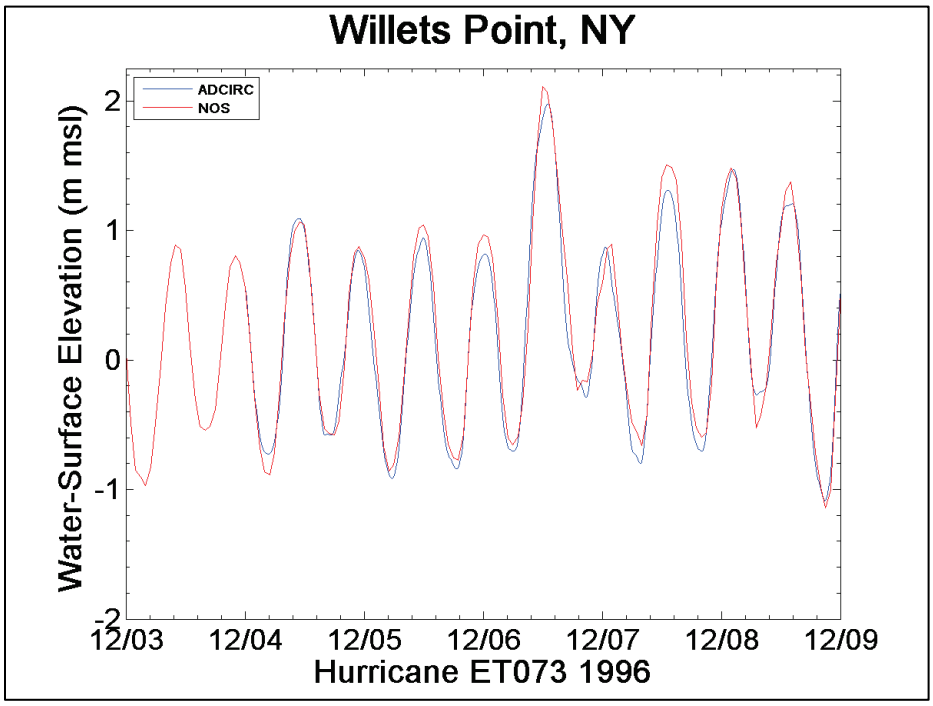

6.7.4 Interactive model evaluation and diagnostics system (IMEDS)

Comparisons between measured and modeled water levels were achieved using the IMEDS. (For additional details about IMEDS, see references at http://www.frf.usace.army.mil/morphos/imeds/ref.shtml.) The premise behind IMEDS is to determine a *performance score* or metric for the modeled event. The overall model performance score is computed by normalizing the water level metrics (statistical quantities: RMSE and bias) to mean quantities and averaging them across metrics, time, and stations with contributions weighted by sample size. The resulting nondimensional performance score

ranges from 0.0 to 1.0, with 1.0 indicating perfect model performance, and relates to the fraction of the mean that is not impacted by error.

In general, the coupled ADCIRC model performed well for the set of tropical and extratropical storm events applied in the validation series. Coupled storm simulations were initiated with a 16-day tidal spin-up and continued with the application of basin and regional-scale winds and pressures for each event. River inflow and wave forcing were also included in the validation simulations. Water level measurements from 133 NOAA NOS stations throughout the study area were queried and when available, were compared to the coupled ADCIRC-simulated water levels using IMEDS. Figure 6-38 and Figure 6-39 show the IMEDS scores for Hurricane Sandy at each available station in the northern and southern portions of the study area, respectively. Lower scores in Chesapeake Bay are attributed to the lack of detailed winds in this region. As indicated in Table 6-3, the model compares well to the measured water levels for all validation simulations as indicated by IMEDS summary performance scores of 0.83 to 0.89.

Figure 6-38. Hurricane Sandy IMEDS scores for the northern portion of the study area.

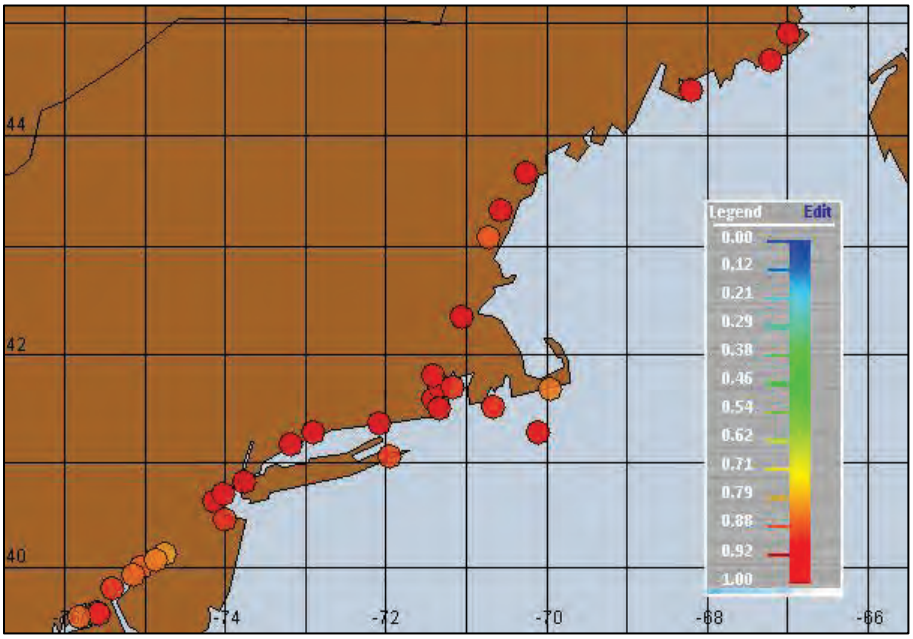

Figure 6-39. Hurricane Sandy IMEDS scores for the southern portion of the study area.

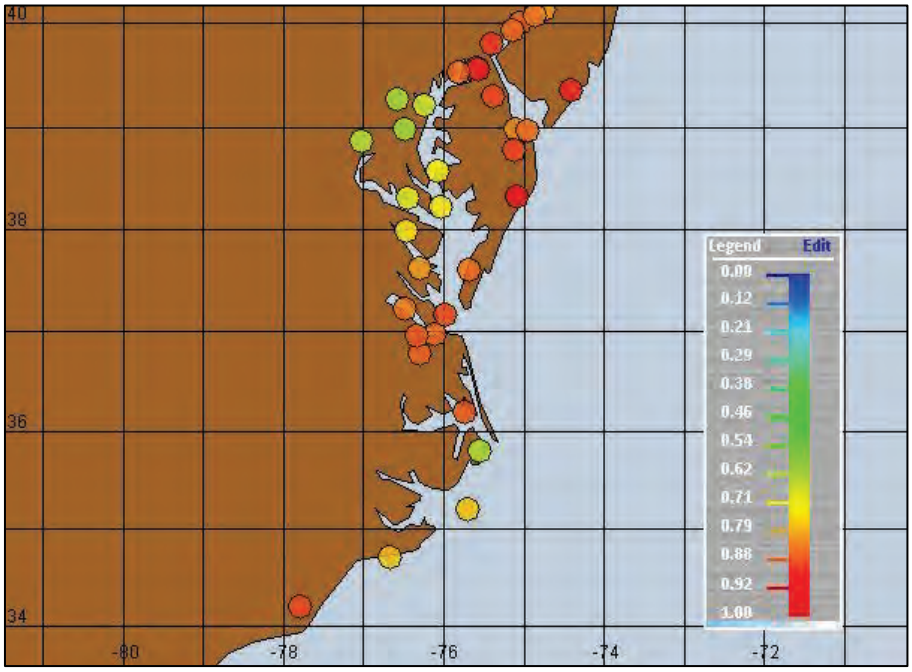

Table 6-3. Coupled ADCIRC validation IMEDS scores.

Storm Name	Year	Performance Score	Overall Bias (m)
Gloria	1985	0.838	0.014
Josephine	1996	0.834	0.014
Isabel	2003	0.89	-0.003
Irene	2011	0.868	0.005
Sandy	2012	0.868	-0.04
Extratropical 070	1996	0.841	0.015
Extratropical 073	1996	0.862	-0.004

6.7.5 High water marks comparisons

A comparison of Hurricane Sandy peak water level model results to USGS high water marks shows the ability of the model to inundate low-lying areas during storm events accurately. Comparisons were made at 314 land locations that wetted during this event. Figure 6-40 shows that 90% of the comparison locations differed by less than 0.5 m with an average error of 6.8%. Red or *hot* colors indicate an overprediction of the peak water level by the model, and blue or *cool* colors indicate an underprediction of the peak water level by the model. The average difference for these locations

was 0.2 m. Figure 6-41 shows the 10% of the comparison locations that differed by more than 0.5 m. The majority (85%) of these larger differences shown in Figure 6-41 were within 1.0 m with the remaining 15% greater than 1.0 m. The average absolute difference for all comparison locations was 0.27 m, which is comparable to errors in other large studies. (IPET 2009) reported an overall absolute error of 1.3 ft (0.4 m).) The small number of particularly poor comparisons (5 of 314 comparison locations) could be due to inaccurate measurements because the trend of the water level response was otherwise consistent and nearby comparisons were within 0.5 m. In addition, some areas that performed somewhat poorly were located in geometric constrictions, such as small channel creeks which are sometimes not well resolved in the model. Because the majority of the model and measurement differences were consistently small and comparable to differenced reported in other studies, there is confidence in the model's ability to predict water levels throughout the domain.

Figure 6-40. Differences between modeled and measured water levels of less than 0.5 m.

Figure 6-41. Differences between modeled and measured water levels of more than 0.5 m.

6.8 Summary

An ADCIRC model for simulating storm surge for the east coast region from Virginia to Maine was developed for the NACCS. The ADCIRC mesh domain encompasses the western North Atlantic, the Gulf of Mexico, and the western extent of the Caribbean Sea with 3.1 million computational nodes and 6.2 million elements. The ADCIRC mesh developed and applied to the NACCS was adapted from a combination of two previously validated FEMA model meshes and the NOAA VDATUM mesh. For the northern reaches, the combined mesh was refined, expanded, and extended into areas not included in the existing meshes. The full NACCS finite element mesh included the upland areas to allow for flooding and drying of these areas during storms and to allow for overland wind reduction in the model simulations.

ADCIRC model validation was accomplished by comparisons of model simulated water levels to NOAA/NOS-measured water-surface elevations. Model validation was conducted with the analysis of a long-term tidal simulation as well as five tropical and two extratropical storm events. Determining a *sufficient* number of storm events used in the validation process is somewhat subjective and depends upon the availability of storm wind fields to apply as model forcing conditions, the availability of meas-

ured storm data to compare to modeled water levels, as well as the overall project schedule to complete this task. For this study, the consistency in the model's ability to predict water levels for the seven validation storm events provided a level of confidence in what can be expected from the model.

From the harmonic analysis conducted for the long-term simulation, it was determined that the model accurately predicts response to tidal forcing. Model accuracy was tested for the seven validation storm events and showed that the model agrees with measured water-surface elevations (time series and high water marks) at measurement locations throughout the study domain. Model accuracy is a function of the quality of the ADCIRC mesh in resolving geometric features such as shorelines and inlets, the accuracy of the bathymetry within the mesh, the representation of bottom friction characterized in the model, and the accuracy of the wind forcing. Small differences in modeled and measured water-surface elevations for the validation storms are attributed to these factors.

7 Nearshore Wave Modeling

7.1 Introduction

The purpose of applying nearshore wave models is to describe quantitatively the change in wave parameters (wave height, period, direction, and spectral shape) between the offshore and the shoreline (typically depths of less than 40 m). Offshore wave information obtained from wave buoys or global- or regional-scale wave hindcasts and forecasts is transformed through the nearshore coastal region using these models.

The nearshore wave model Steady State spectral WAVE (STWAVE) was applied for the NACCS. Ten STWAVE grids, encompassing the East Coast from Virginia to Maine, were developed for this modeling effort.

In order to rigorously represent the underlying physical processes of the storm events, *tight* two-way coupling between ADCIRC and STWAVE was facilitated with the CSTORM-MS, a physics-based modeling capability for simulating tropical and extratropical storm, wind, wave, and water level response. During the two-way coupling process, a single instance of ADCIRC passes water elevations and wind fields to multiple instances of STWAVE. Upon completion, STWAVE passes wave radiation stress gradients to ADCIRC to drive wave-induced water level changes (e.g., wave setup and setdown). Additional detailed information about the coupling procedure is found in Chapter 8.

This chapter presents the theoretical description of STWAVE, model setup including grid develop and offshore forcing, model parameters, and validation for the NACCS application.

7.2 STWAVE Version 6.2.24

STWAVE is a steady-state, finite-difference, phase-averaged spectral wave model based on the wave action balance equation. STWAVE simulates nearshore wave transformation including depth- and current-induced refraction and shoaling, depth- and steepness-induced wave breaking, wind-wave generation and growth, and wave-wave interaction and whitecapping.

The STWAVE model uses the governing equation for steady-state conservation of spectral wave action along a wave ray (Jonsson 1990):

$$\left(C_g\right)_{\mathrm{i}} \frac{\partial}{\partial \mathrm{x_i}} \frac{C C_g \cos(\alpha) E(\omega, \alpha)}{\omega} = \sum \frac{S}{\omega} \tag{1}$$

where:

C_g = group celerity
C = wave celerity
i = tensor notation for x- and y-coordinates
α = wave orthogonal direction
E = wave energy density divided by the density of water ρ_w and the acceleration of gravity g
ω = angular frequency
S = energy source and sink terms.

Source and sink mechanisms include surf-zone breaking in the form of the Miche criterion (Miche 1951), the flux of input energy due to wind (Resio 1988; Hasselmann et al. 1973), energy distribution through wave-wave interactions (Resio and Perrie 1989), whitecapping (Resio 1987, 1988), and energy losses due to bottom friction (Hasselmann et al. 1973; Padilla-Hernandez 2001; Holthuijsen 2007). Radiation stress gradients are calculated based on linear wave theory and provide wave forcing to external circulation models.

The wave orthogonal direction for steady-state conditions is given by the following (Mei 1989; Jonsson 1990):

$$C_g \frac{D\alpha}{DR} = -\frac{Ck}{\sinh(2kd)} \frac{Dd}{Dn} \tag{2}$$

where:

R = coordinate in the direction of the wave ray
k = wave number
d = water depth
n = coordinate normal to the wave orthogonal.

The angular frequency is related to the wave number k by the dispersion relation:

$$\omega^2 = gk \tanh(kd) \tag{3}$$

with celerity, C, and group celerity, C_g, given by

$$C = \frac{\omega}{k} \tag{4}$$

$$C_g = 0.5C\left[1 + \frac{2kd}{\sinh(2kd)}\right] \tag{5}$$

Refraction and shoaling are implemented in STWAVE by applying the conservation of wave action along backward-traced wave rays. Rays are traced in a piecewise manner. The wave ray is traced back to the previous grid column or row, and the length of the ray segment DR is calculated. Derivatives of depth normal to the wave orthogonal are estimated (based on the orthogonal direction) and substituted into Equation 2 to calculate the wave orthogonal direction at the previous column. The energy is calculated as a weighted average of energy between the two adjacent grid points in the column and the direction bins. The energy density is corrected by a factor that is the ratio of the angle band width to the width of the back-traced band to account for the different angle increment in the back-traced ray. The shoaled and refracted wave energy is then calculated using Equation 1. The process is repeated for the next columns.

Readers are referred to STWAVE documentation (Massey et al. 2011; Smith 2007; Smith et al. 2001) for additional model features and technical details.

7.3 Model setup

7.3.1 Grid development

STWAVE is formulated on a Cartesian grid, with the x-axis oriented in the cross-shore direction (I) and the y-axis oriented alongshore (J), parallel with the shoreline. Angles are measured counterclockwise from the grid x-axis.

The bathymetry, topography, and bottom friction Manning's *n* values were interpolated from the ADCIRC mesh to create 10 STWAVE domains. The STWAVE grids spanned two projections, UTM Zone 18 and 19. Figure 7-1 shows the location of grids with respect to the ADCIRC mesh, with grid geometries presented in Table 7-1. The full names of the grids are based on the covered state, moving from north to south. Abbreviated grid names, also provided in Table 7-1, will be used hereafter. The grids' offshore boundaries were extended into depths of at least 30 m. Wave interactions with the bottom at this offshore extent are relatively small, particularly in comparison to the importance of wave generation. A previous validation of STWAVE for Hurricane Ike featured offshore boundaries near the 30 m contour (Bender et al. 2013). In cases of steep shorelines, such as Maine, the offshore boundaries were extended further than 30 m offshore to obtain an approximate equal number of grid cells between the offshore boundary and the shoreline as the other grids.

Figure 7-1. STWAVE grid domains.

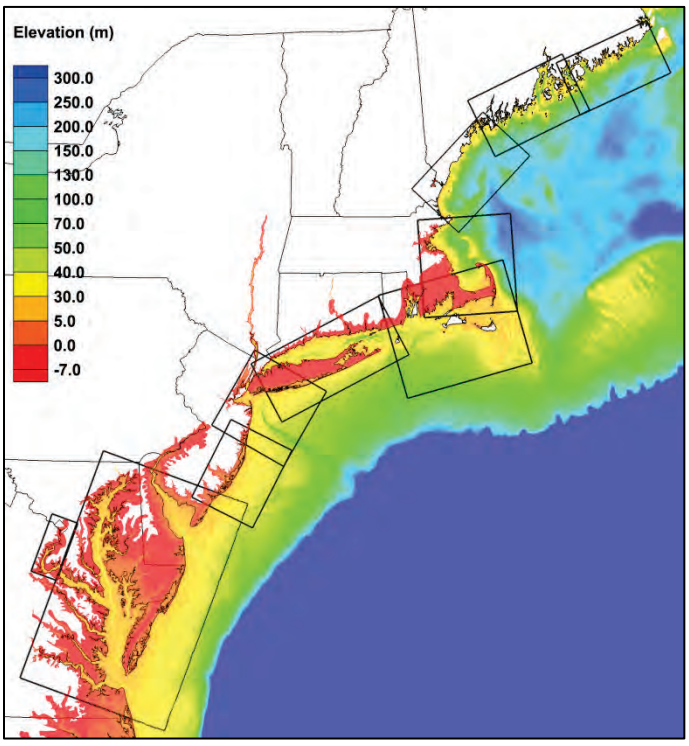

A grid resolution of 200 m was selected for all of the grids except for the grid encompassing Chesapeake Bay and Washington, DC, which had finer resolutions of 125 m and 100 m, respectively. Previous studies of Hurricanes Katrina, Rita, Gustav, and Ike in the Gulf of Mexico used similar resolutions and demonstrated good agreements between measurements

and STWAVE (Dietrich et al. 2011; Hope et al. 2008; Bunya et al. 2010; Dietrich et al. 2010; Bender et al. 2013). The resolution for coastal areas in these studies was 200 m, with 100–200 m resolution in the nested bays. A 200 m resolution was selected for the majority of the grids as these past studies showed this resolution sufficiently resolved the surf zone to capture the wave breaking processes that drive wave radiation stresses and wave setup. A finer resolution was needed in Chesapeake Bay and around Washington, DC, in order to accurately resolve the bay's smaller characteristics. A 100 m resolution within Chesapeake Bay proved to be computationally intensive; thus, the grid resolution was decreased from 100 m to 125 m. Decreasing the resolution of the Chesapeake Bay grid reduced the grid size by approximately 35% without significantly impacting the maximum wave height solution for a preliminary Sandy simulation (the absolute difference in maximum wave height within Chesapeake Bay rarely exceeded 0.1 m)

Table 7-1. STWAVE grid geometries.

Grid	Projection	Grid Origin (x,y) (m)	Azimuth (deg)	Resolution (m)	Number of Cells	
					I	J
Northern Maine (NME)	UTM 19	682704.7, 4899673.0	110.7	200.0	392	682
Central Maine (CME)	UTM 19	568406.9, 4857172.5	112.0	200.0	427	720
Southern Maine (SME)	UTM 19	482432.8, 4800937.9	133.0	200.0	439	717
Eastern Massachusetts (EMA)	UTM 19	450200.0, 4724100.0	180.0	200.0	638	670
Southern Massachusetts (SMA)	UTM 19	465575.3, 4518084.4	101.9	200.0	733	887
Long Island (LID)	UTM 18	802679.3, 4544326.0	117.9	200.0	453	986
North New Jersey (NNJ)	UTM 18	689660.5, 4494212.9	150.2	200.0	569	593
Central New Jersey (CNJ)	UTM 18	642056.1, 4413284.8	153.1	200.0	468	596
Chesapeake Bay (CPB)	UTM 18	581350.8, 4339880.0	159.8	125.0	1687	2653
Washington, DC (WDC)	UTM 18	348428.2, 4313375.1	159.9	100.0	377	837

7.3.2 Offshore boundary spectra

Spectral wave energy saved from WAM was transformed to STWAVE coordinates and applied as offshore boundary forcing for the STWAVE domains open to the Atlantic Ocean. The location of these boundary points is listed in Table 7-2 and Table 7-3, and their location on each grid, along with detailed bathymetry, is shown in Figure 7-2 to Figure 7-11. The inland

WDC grid is not listed in Table 7-3 because it was forced only by local winds as little wave energy was expected to propagate up the Potomac River system.

Table 7-2. Latitude and longitude of offshore boundary spectra for grids in UTM Zone 19.

NME	CME	SME	EMA	SMA
-68.33, 43.83	-69.25, 43.50	-69.33, 43.33	-69.58, 41.50	-69.42, 40.83
-68.17, 43.83	-69.17, 43.58	-69.25, 43.33	-69.58, 41.67	-69.58, 40.83
-68.08, 43.92	-69.00, 43.58	-69.42, 43.25	-69.58, 41.83	-69.67, 40.75
-67.92, 43.92	-68.92, 43.67	-69.50, 43.17	-69.58, 42.00	-69.83, 40.75
-67.75, 43.92	-68.75, 43.67	-69.58, 43.08	-69.58, 42.17	-70.00, 40.75
-67.67, 44.00	-68.67, 43.75	-69.67, 43.00	-69.58, 42.33	-70.17, 40.67
-67.50, 44.00	-68.50, 43.75	-69.83, 43.00	-69.58, 42.50	-70.33, 40.67
-67.42, 44.08	-68.33, 43.83	-69.92, 42.92	-69.58, 42.67	-70.50, 40.67
-67.25, 44.08	-68.17, 43.83	-70.00, 42.83		-70.58, 40.58
-67.08, 44.17	-69.42, 43.50	-70.08, 42.75		-70.75, 40.58
-66.92, 44.17	-69.58, 43.50	-70.17, 42.67		-70.92, 40.58
-66.75, 44.25	-69.67, 43.42	-70.25, 42.67		-71.00, 40.50
		-70.33, 42.58		-71.17, 40.50
		-70.42, 42.50		-71.33, 40.50
		-70.50, 42.50		-71.50, 40.42

Table 7-3. Latitude and longitude of offshore boundary spectra for grids in UTM Zone 18.

LID	NNJ	CNJ	CPB
-71.42, 41.00	-72.75, 40.58	-73.33, 39.83	36.42, -75.42
-71.50, 41.00	-72.83, 40.50	-73.42, 39.75	36.50, -75.33
-71.58, 40.92	-72.92, 40.42	-73.50, 39.67	36.58, -75.25
-72.58, 40.58	-73.00, 40.33	-73.58, 39.58	36.75, -75.25
-72.42, 40.58	-73.08, 40.25	-73.58, 39.50	36.83, -75.17
-72.33, 40.67	-73.08, 40.17	-73.67, 39.42	36.92, -75.08
-72.17, 40.67	-73.17, 40.08	-73.67, 39.33	37.08, -75.08
-72.08, 40.75	-73.25, 40.00	-73.75, 39.25	37.17, -75.00
-71.92, 40.75	-73.33, 39.92	-73.83, 39.17	37.33, -75.00
-71.83, 40.83	-73.33, 39.83	-73.83, 39.08	37.42, -74.92
-71.75, 40.92	-73.42, 39.75	-73.92, 39.00	37.50, -74.83
-72.75, 40.50	-73.50, 39.67	-74.00, 38.92	37.67, -74.83
-72.83, 40.42			37.75, -74.75
-73.00, 40.42			37.83, -74.67
-73.08, 40.33			38.00, -74.67
-73.25, 40.33			38.17, -74.58

LID	NNJ	CNJ	CPB
-73.33, 40.25 -73.50, 40.25			38.25, -74.50 38.42, -74.50 38.50, -74.42 38.58, -74.33 38.75, -74.33 38.83, -74.25 38.92, -74.17 39.08, -74.17 39.17, -74.08

The number and values of the discrete frequency bands, as well as the starting and ending bands, were the same as those defined in WAM. The number and value of the frequency bands were defined as

$$f(n+1) = 1.1 * f(n) \text{ where } n = 1{,}28$$

and the starting and ending bands were 0.0314 Hz (T = 31.8 s) and 0.4114 Hz (T = 2.4 s), respectively. The resolved frequency range for the WDC domain was narrower. The frequency distribution was defined as 0.125 Hz (T = 8 s) to 0.975 Hz (T = 1.03 s) with a constant frequency increment of 0.025 Hz. The number of angle bands was constant at 72, resulting in an angular resolution of 5 deg. For full-plane mode, the wave directions begin at 0 deg and increase in angular resolution (5 deg increments) to 355 deg. Morphic interpolation was applied along the boundary between input spectra and 1D transformation performed along the lateral boundaries to preserve the shape of the directional distribution (Smith and Smith 2002).

Figure 7-2. WAM offshore spectra locations and bathymetry of NME.

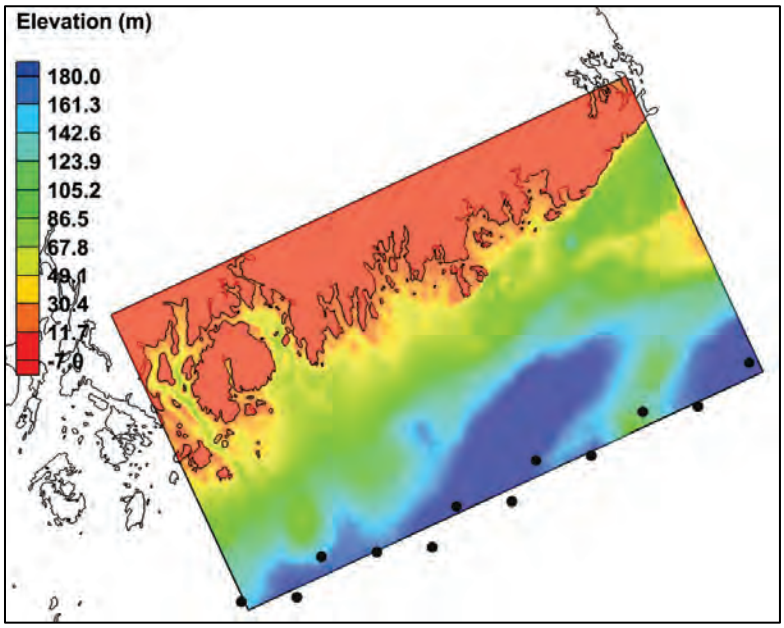

Figure 7-3. WAM offshore spectra locations and bathymetry of CME.

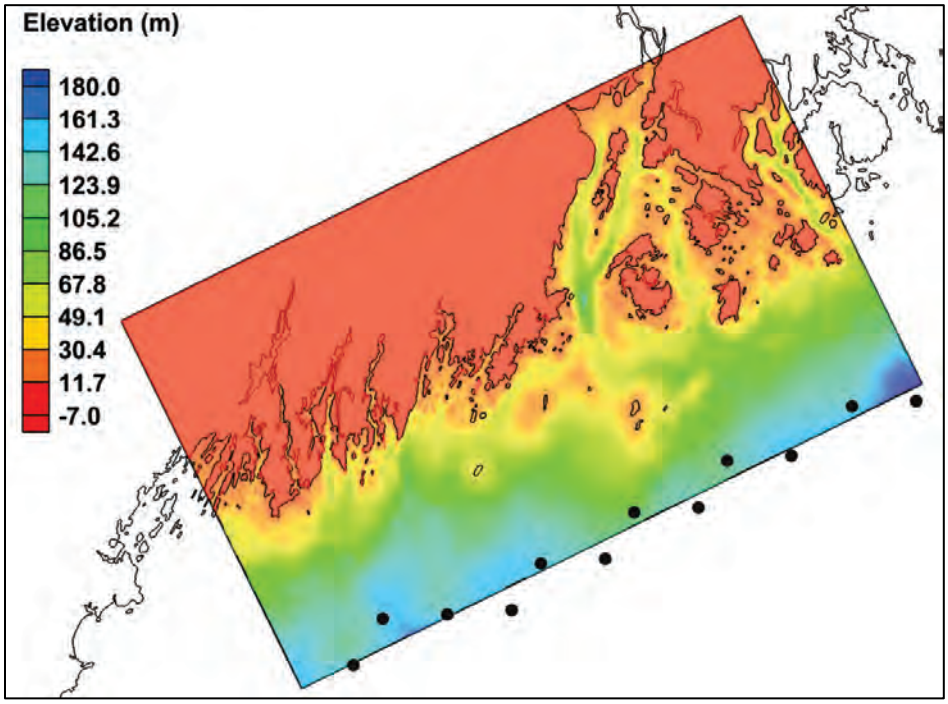

Figure 7-4. WAM offshore spectra locations and bathymetry of SME.

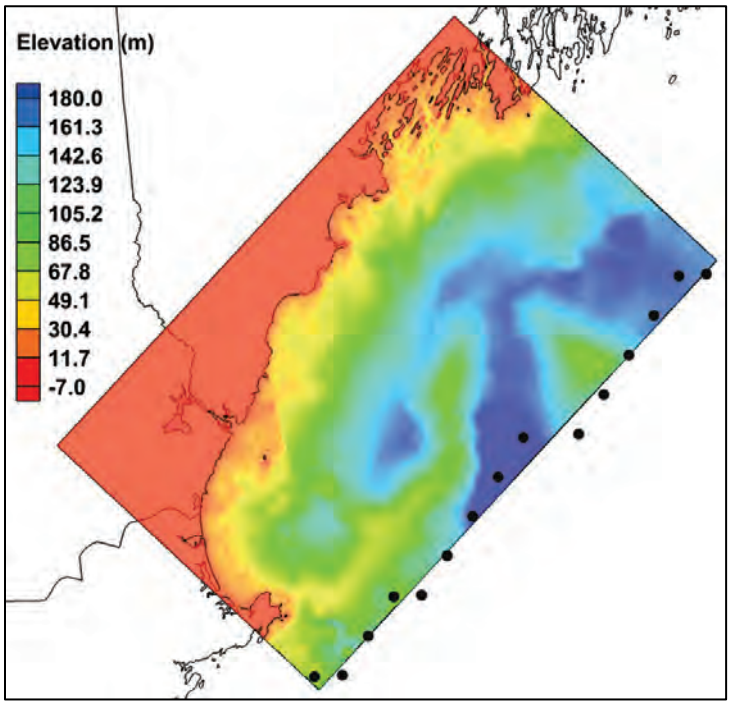

Figure 7-5. WAM offshore spectra locations and bathymetry of EMA.

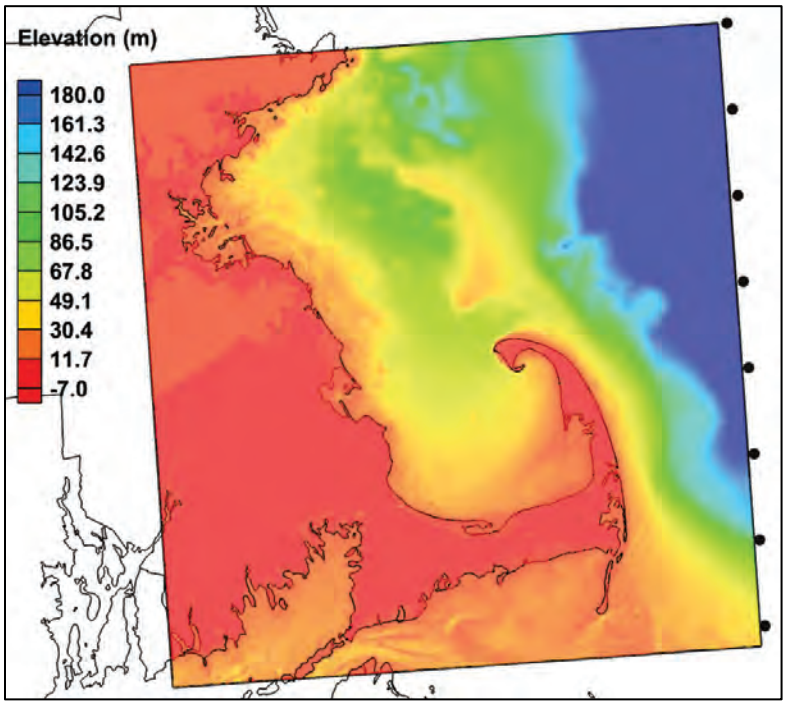

Figure 7-6. WAM offshore spectra locations and bathymetry of SMA.

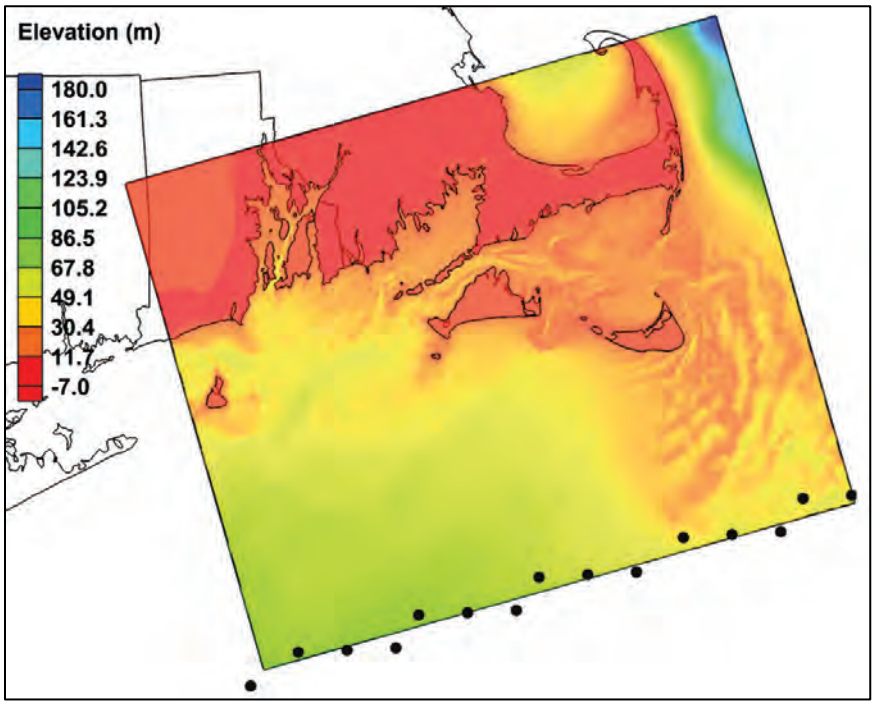

Figure 7-7. WAM offshore spectra locations and bathymetry of LID.

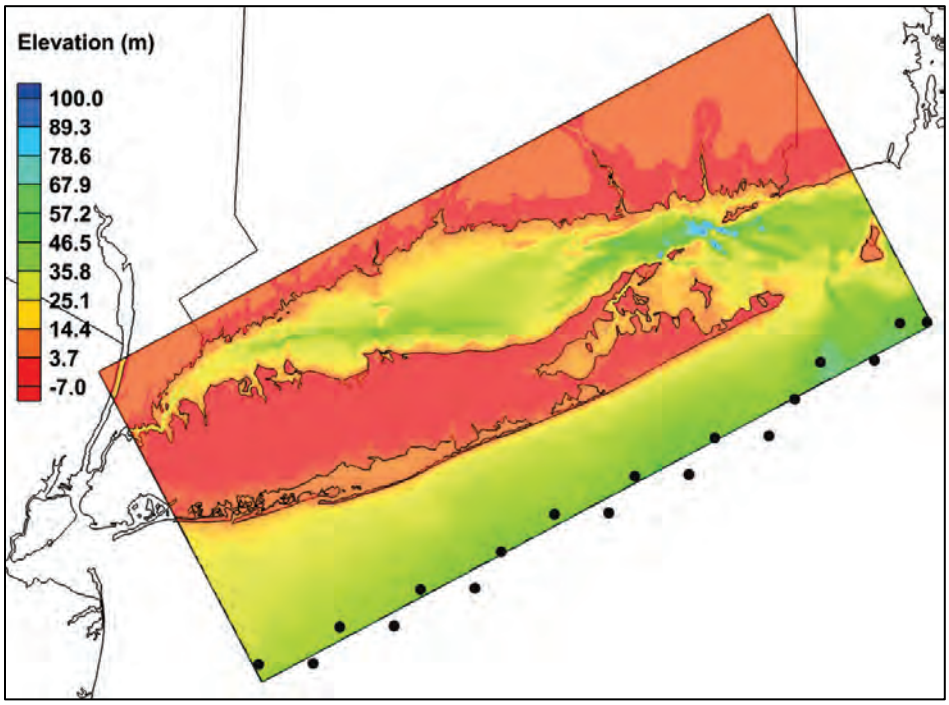

Figure 7-8 WAM offshore spectra locations and bathymetry of NNJ.

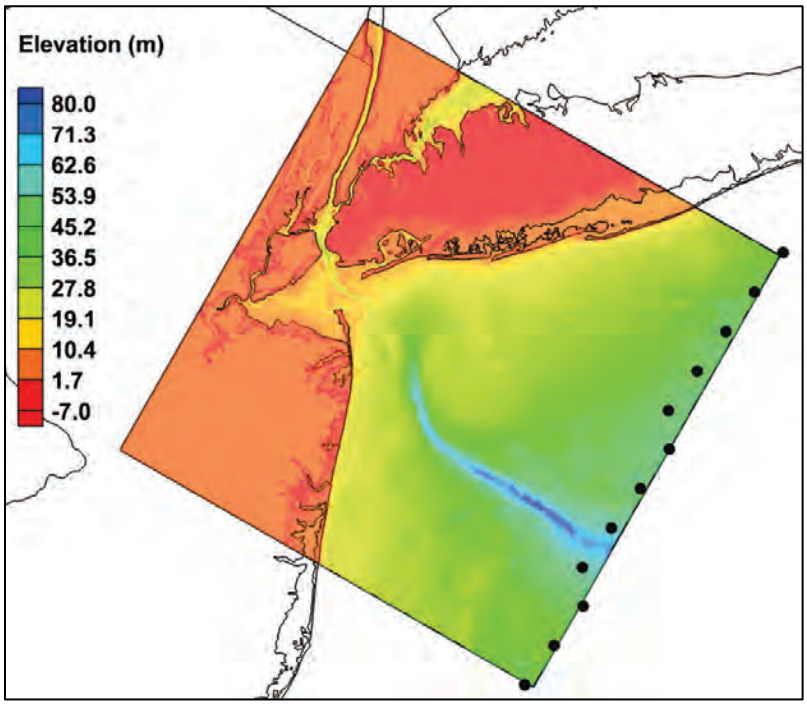

Figure 7-9. WAM offshore spectra locations and bathymetry of CNJ.

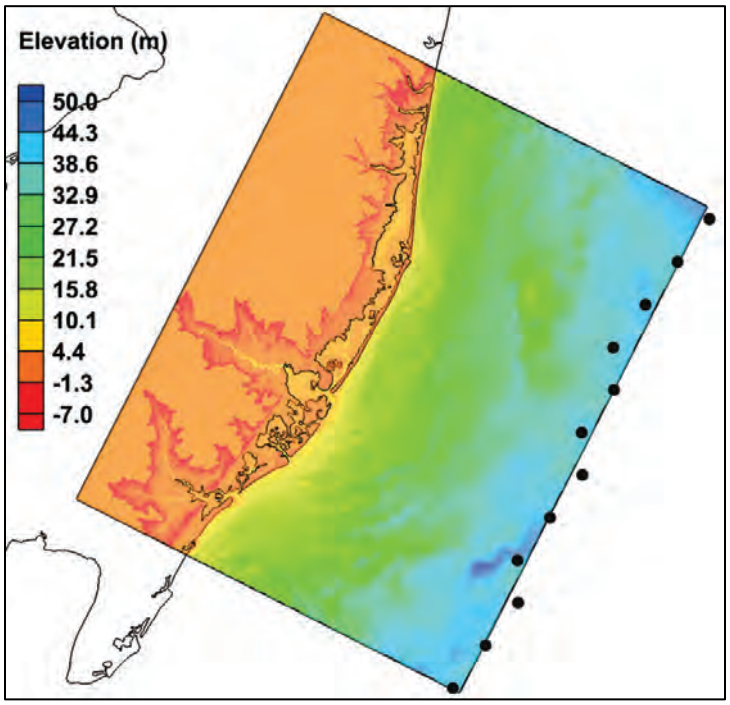

Figure 7-10. WAM offshore spectra locations and bathymetry of CPB.

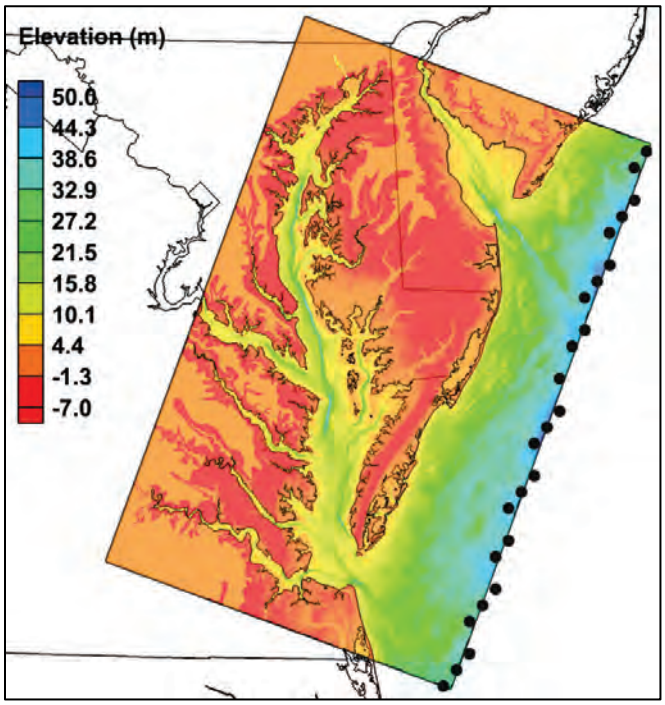

Figure 7-11. Bathymetry of WDC. No spectral points are shown since waves were locally generated within the domain.

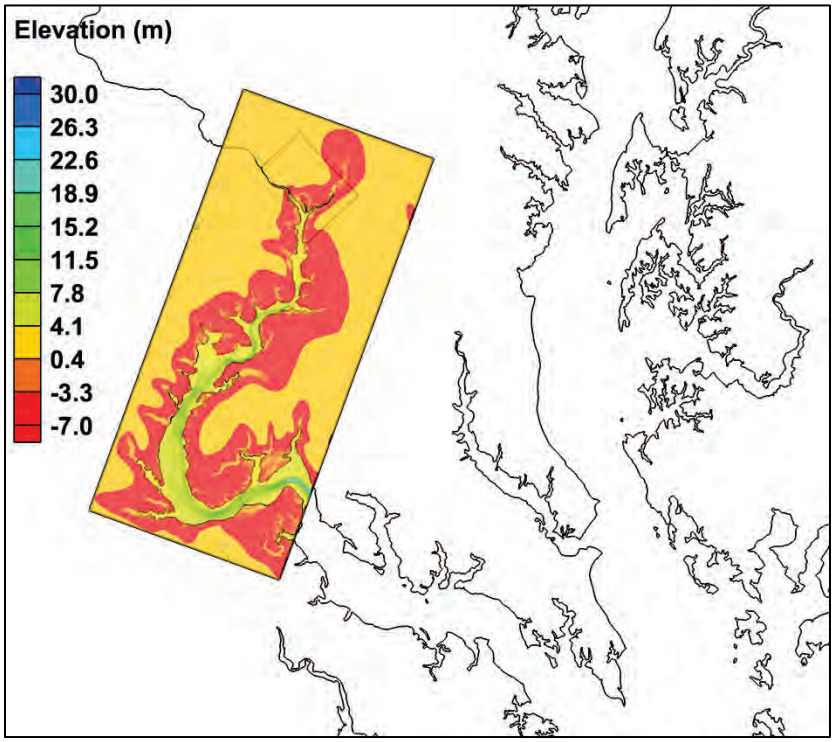

7.3.3 High-frequency save points

Storm conditions were exported at selected (x, y) locations during each time-step. The output information consists of the following: time-step identifier, x-location (in grid projection), y-location (in grid projection), significant wave height (m), mean wave period (s), mean wave direction (deg), peak wave period (s), wind magnitude (m/s), wind direction (deg), and water elevation (m). This information was stored in the *.station.out files. The location of these save points can be referenced in Section 6.6.

7.4 Model parameters

7.4.1 Half-plane versus full-plane

STWAVE has two modes available, half-plane and full-plane. Half-plane mode allows wave energy to propagate only from the offshore towards the nearshore (± 87.5 deg from the x-axis of the grid), and grids are typically aligned with the dominant wave direction. All waves traveling in the negative x-direction, such as those generated by offshore-blowing winds, are neglected in half-plane simulations. Full-plane mode allows wave transformation and generation on the full 360 deg plane. During grid development, simulations were executed in both half-plane and full-plane mode to quantify any differences in the wave field. Local differences in the maximum wave height solution existed in all the grids, particularly those near the landfall location and with complex shorelines and features (bays, islands, barrier islands, etc.). Because determining and aligning the grids with the dominant wave direction is not feasible given the extensive number of production storms, all simulations were executed in full-plane mode, allowing wave generation in all directions and a more realistic representation of the wave climate.

7.4.2 Model execution

The full-plane version of STWAVE uses an iterative solution process that requires user-defined convergence criteria to signal a suitable solution. Boundary spectra information is propagated from the boundary throughout the domain during the initial iterations. Once this stage converges, winds and surges are added to the forcing, and this final stage iteratively executes until it also reaches a convergent state. The convergence criteria for both stages include the maximum number of iterations to perform per time-step, the relative difference in significant wave height between iterations, and the minimum percent of cells that must satisfy the convergence

criteria (i.e., have values less than the relative difference). Convergence parameters were selected based on a previous study by Massey et al. (2011) in which the sensitivity of the solution to the final convergence criteria was examined.

Full-plane mode required considerable memory requirements and run times, particularly the CPB domain due to its large size. STWAVE was set up with parallel in-space execution whereby each computational grid was divided into different partitions (in both the *x*- and *y*-direction), with each partition executing on a different computer processor. Because energy can only cross one grid partition at a time during a single iteration, the maximum number of initial and final iterations was set to a value 5 and 20 times higher than the largest grid partition, respectively. Testing to optimize both the total number of processors and the number of processors assigned to each grid was performed to maximize computational efficiency and reduce execution time. The convergence criteria and partitions for each grid are listed in Table 7-4.

Table 7-4. Full-plane runtime parameters.

Grid	Maximum Iterations		Relative Difference		Minimum Cell Percentage		Number of Cells per partition	Partitions		Processors
	Initial	Final	Initial	Final	Initial	Final		I	J	
NME	14	29	0.1	0.05	100	99.8	80	5	9	45
CME	15	30	0.1	0.05	100	99.8	70	6	10	60
SME	15	30	0.1	0.05	100	99.8	70	6	10	60
EMA	14	29	0.1	0.05	100	99.8	76	8	9	72
SMA	18	33	0.1	0.05	100	99.8	70	10	13	130
LID	21	36	0.1	0.05	100	99.8	60	8	16	128
NNJ	11	26	0.1	0.05	100	99.8	95	6	6	36
CNJ	11	26	0.1	0.05	100	99.8	95	4	6	24
CPB	58	73	0.1	0.05	100	99.8	50	34	53	1802
WDC	13	28	0.1	0.05	100	99.8	100	4	8	32

7.5 STWAVE validation

The validation storms selected consist of five tropical events: Gloria (1985), Josephine (1996), Isabel (2003), Irene (2011), and Sandy (2012)

and two extratropical events: ET070 (January 1996) and ET073 (December 1996). Forcing conditions from WAM and ADCIRC were applied every 30 min. Upon completion of the run, the simulations were checked for consistency, and when applicable, the performance of STWAVE was evaluated by comparing existing point source measurements and model results.

7.5.1 QA/QC

The maximum significant wave height envelope was plotted to identify erroneous estimates or discontinuities in the wave height solution for a given simulation. Figure 7-12 color contours the maximum wave height field for the LID grid for Sandy. Although some offshore wave energy penetrates into Long Island Sound, waves within the bay are largely locally generated.

The convergence of the final wave solution was also checked for each domain. To satisfy the final convergence criteria, at least 99.8% of the cells had to have a relative difference in wave height of 0.05 m or less. The number of time-steps that did not meet the final convergence criteria is provided in Table 7-5.

Figure 7-12. Maximum significant wave height color contour of LID grid for Sandy.

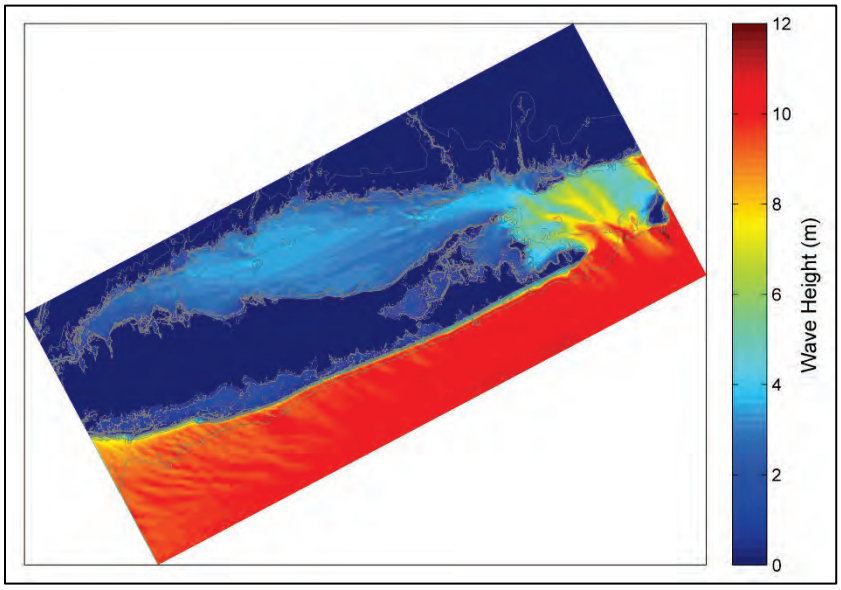

The tropical events had fewer unconverged time-steps across the 10 simulation domains than the extratropical events. The WDC grid accounted for nearly all of the unconverged time-steps for the tropical simulations. The unconverged time-steps closely approached the 99.8% criterion, with 73 of the 150 total unconverged steps exceeding 99.6%. The lowest percentage

was 99.0%. The NME and CME grids, with the addition of the LID grid for ET070, accounted for a large majority of the unconverged time-steps for the extratropical simulations. Like the tropical storms, nearly all the unconverged time-steps achieved percentages close to 99.8%. Out of 228 total unconverged time-steps for ET070 and ET073, only 7 did not exceed 99.6%. The lowest percentage for the extratropicals was 97.3%.

Table 7-5. Unconverged time-steps for validation storms.

Storm	Number of Days Modeled	Number of Unconverged Time-Steps									
		NME	CME	SME	EMA	SMA	LID	NNJ	CNJ	CPB	WDC
ET070	3	27	45	10	0	0	43	0	16	0	12
ET073	2	24	42	0	0	0	0	0	0	6	3
Gloria	2.25	0	0	0	0	0	0	0	0	0	2
Josephine	2	0	0	0	0	0	0	0	0	0	14
Isabel	2	0	0	0	0	0	0	0	0	0	5
Irene	3	0	0	0	3	0	0	0	0	25	30
Sandy	4	0	0	0	2	0	0	0	0	0	69

7.5.2 Model evaluation

Thirty buoys were identified within the STWAVE domains. Sources included NDBC, National Oceanographic Data Center (NODC), Northeastern Regional Association of Coastal Ocean Observing Systems (NERACOOS), Coastal Data Information Program (CDIP), Long Island Sound Integrated Coastal Observing System (LISICOS), Chesapeake Bay Interpretive Buoy System (CBIBS), USACE, Martha's Vineyard Coastal Observatory (MVCO), and personal communication. The locations and names of the identified buoys are shown in Figure 7-13. The number of operational buoys increased with more recent storms (Gloria: 1; ET070: 5; Josephine: 4; ET073: 4; Isabel: 13; Irene: 26; Sandy: 26).

Figure 7-13. Location of identified buoys.

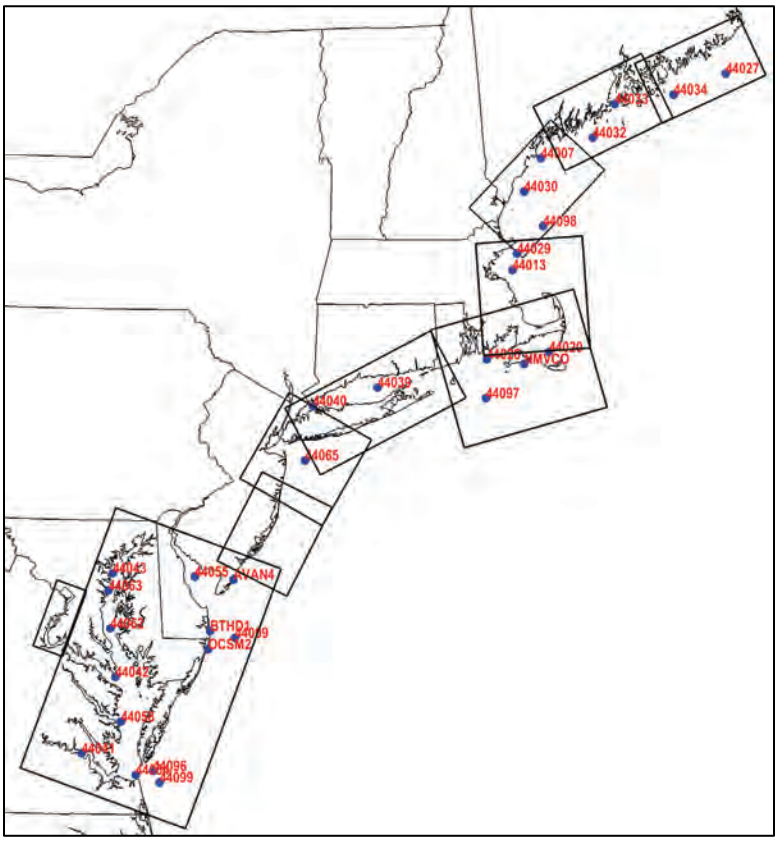

STWAVE results were compared to existing measurements both graphically and statistically. Graphical products included time-paired scatter plots and Taylor diagrams (Taylor 2001). Statistical calculations include bias (modeled-measured), RMSE, linear regression (both symmetric slope where the intercept is forced to be zero and correlation coefficient), and index of agreement (Willmott et al. 1985). Buoys with measurement periods shorter than 20% of the simulated duration were omitted.

An example of a model-measurement comparison is shown in Figure 7-14 for 44013 during Sandy. For this example, STWAVE shows excellent agreement with measurements of significant wave height (H_s), mean wave period (T_m), and mean wave direction (θ_{wave}). As observations of T_p are shown to be highly variable, T_m is often considered a more stable comparison parameter. STWAVE captures the growth and decay sequence of the storm, with the peak wave height well represented in the model results.

Figure 7-14. Time plot of model results versus measurements at 44013 for Sandy.

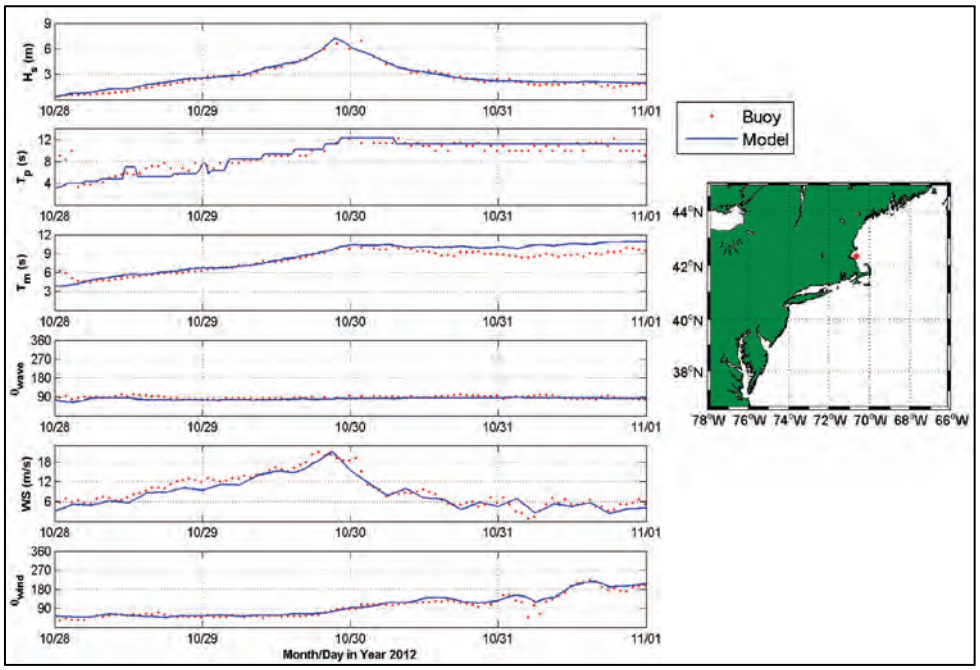

The skill of STWAVE in predicting the wave height at each operational buoy is evaluated using Taylor diagrams. A 2D Taylor diagram can represent three different statistics simultaneously (the centered RMSE, the correlation, and the standard deviation). In the following figures, the solid black contours represent the normalized standard deviation, the dash-dot blue line represents the correlation coefficient, and the dash green lines represent the RMSE. Normalized statistics were used to collapse the buoy measurements to a single point on the plot. The measured data are indicated by the black dot, which lies at a correlation coefficient and normalized standard deviation of 1 and an RMSE of 0. The closer the data lie to this reference point, the better the model agrees with the measurements. Note that although some model-measurement comparisons have approximately the same correlation, the model results closer to the reference point simulate the amplitude of the variations (i.e., the standard deviation) much better and result in a smaller RMSE. Outlying model-measurement comparisons are easily identified using Taylor diagrams. Taylor diagrams for the extratropical events are shown in Figure 7-15 and Figure 7-16.

Figure 7-15. Taylor diagram for ET070.

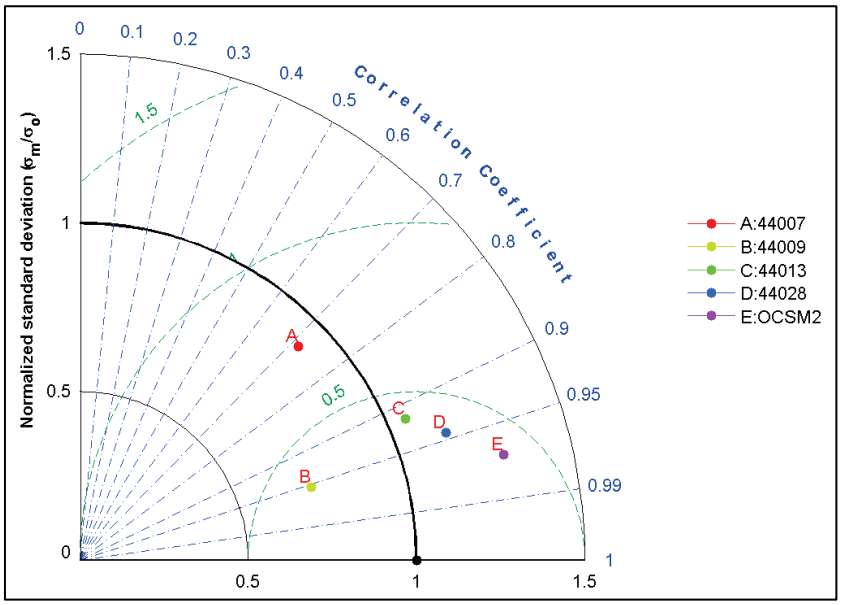

Figure 7-16. Taylor diagram for ET073.

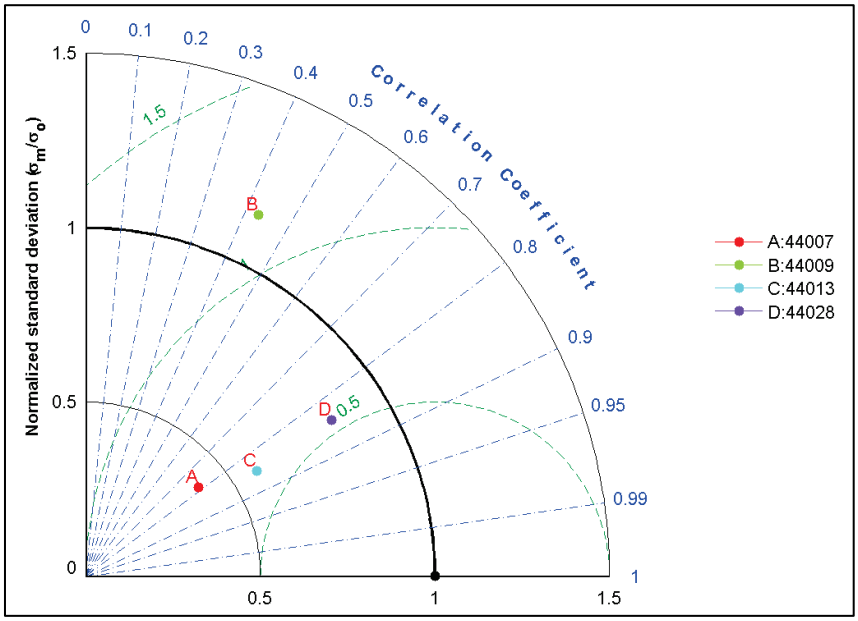

STWAVE performs better for ET070 than ET073. Figure 7-15 shows a correlation greater than 0.9 and a normalized RMSE less than 0.5 at three of four sites for ET070. Figure 7-17 shows scatter on both sides of the line of perfect fit although a slight negative bias is evident for ET070. STWAVE consistently underestimated wave heights, particularly the largest, for ET073.

Figure 7-17. Scatter plots of validation extratropical storms.

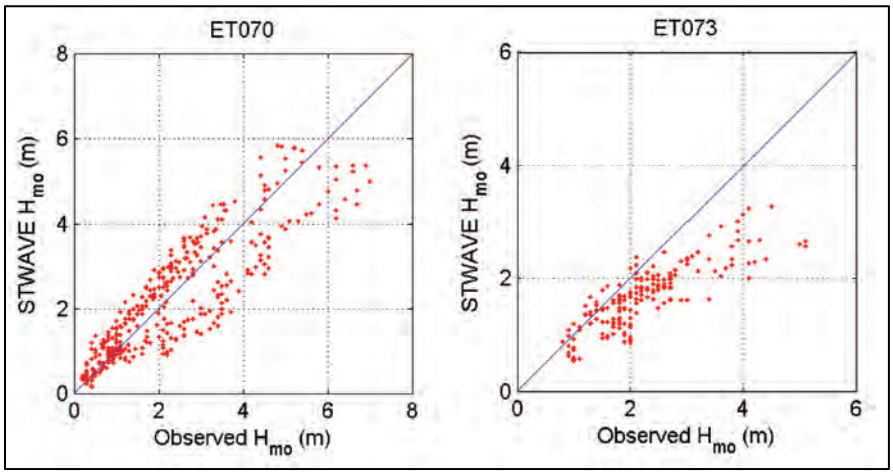

Looking at Figure 7-18 to Figure 7-22 for the tropical events, STWAVE improved with more recent storms as more buoys lie near the reference point. This may be a result of the development of improved wind and offshore forcings as well as enhancements in in situ measurement techniques. For example, tracking 44007 shows STWAVE's performance at this location improving with time. For storms prior to Irene, STWAVE's best performance is seen at buoys within the detailed wind boundaries. However, to say this is the definite reason for this improved performance is difficult as measurements are extremely limited for these early storms.

Figure 7-18. Taylor diagram for Gloria.

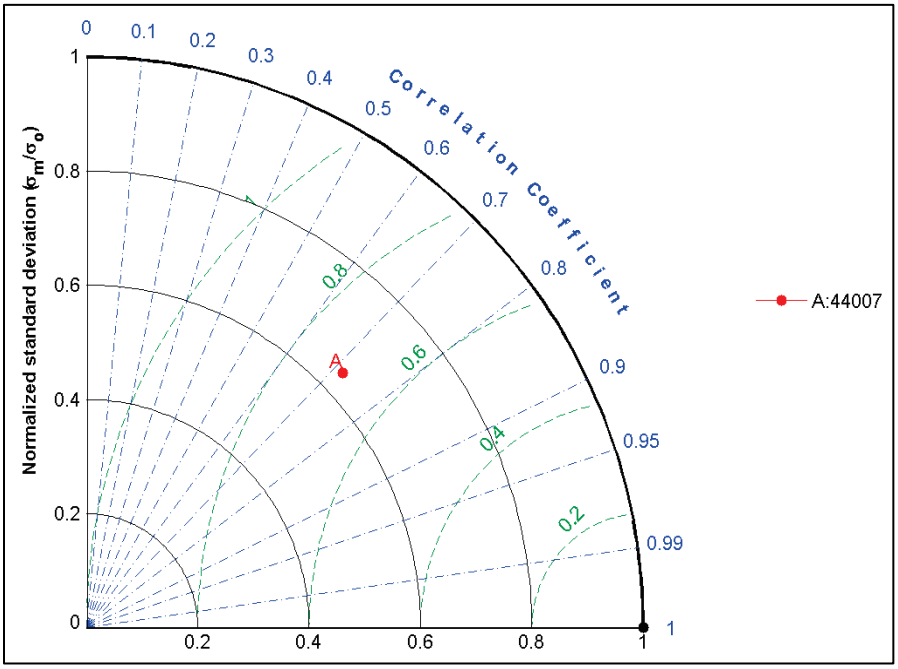

Figure 7-19. Taylor diagram for Josephine.

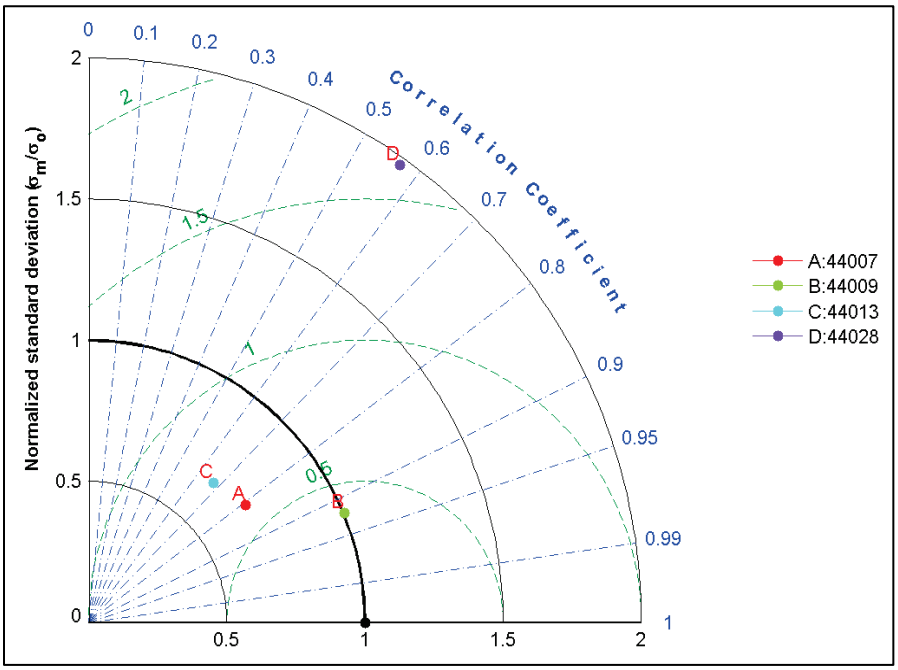

Figure 7-20. Taylor diagram for Isabel.

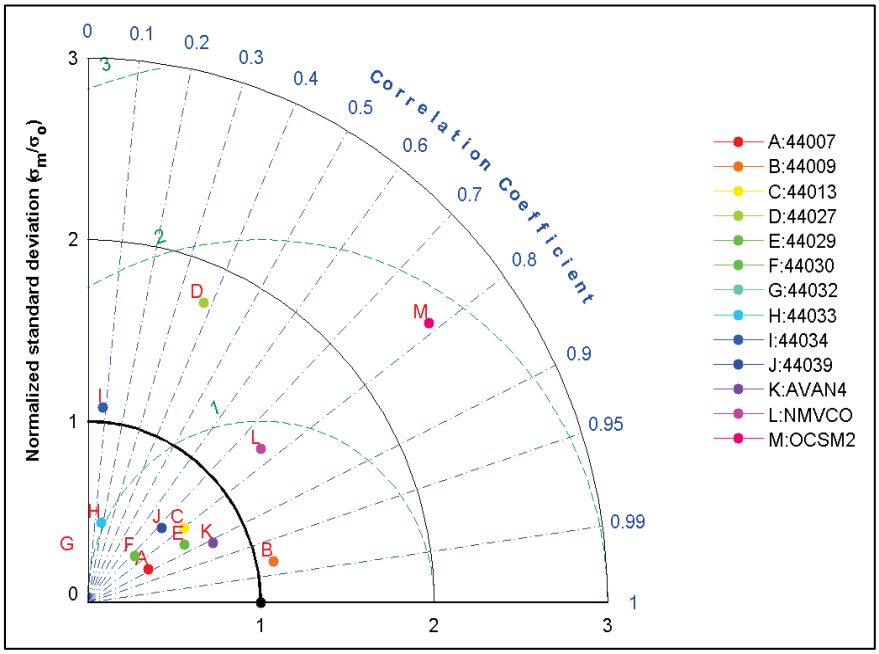

The performance of STWAVE for Irene and Sandy are similar (Figure 7-21 and Figure 7-22), with the majority of the sites within a normalized RMSE of 0.5 and correlation greater than 0.8. STWAVE generally performs better outside the detailed wind boundaries than it did for the earlier storms,

particularly for the northern buoys. Although model results compared poorly at two northern sites, MVCO and 44033, for Irene, performance at MVCO improved significantly during Sandy. Buoy 44033 cannot be discussed further as it was inoperational during Sandy. Southern measurement sites are mainly located within or near Chesapeake Bay. STWAVE performed average within the bay for both storms, as indicated by the cluster of bluish points. Having detailed winds for Irene did not significantly improve model results in Chesapeake Bay compared to the coarse winds for Sandy.

Two USACE coastal stations, BTHD1 and OCSM2, and one CBIBS station, 44064, demonstrated persistent poor performance. Further inspection showed STWAVE significantly overestimated the storm growth sequence while accurately simulating the decay at these sites. Comparing modeled spectra to measured spectra at OCSM2 and BTHD1 during Sandy, revealed few details as the STWAVE spectra looked relatively similar in shape but amplified at the peak. Truncating the modeled spectra at 0.25 Hz to match the measured spectra reduced the wave height by a few centimeters, which was not enough to significantly improve model-measurement wave height comparisons. Spectra for 44064 were unavailable. Diagnosing the reasons for disappointing model performance is difficult as it could be due to issues in the model formulations, the forcing conditions, or the buoy measurements themselves.

Figure 7-21. Taylor diagram for Irene.

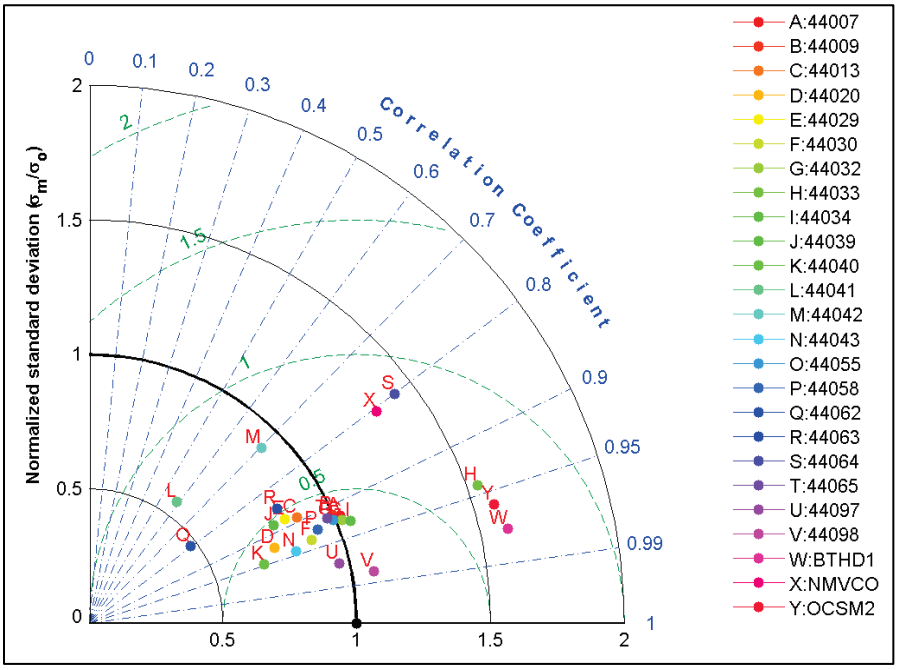

Figure 7-22. Taylor diagram for Sandy.

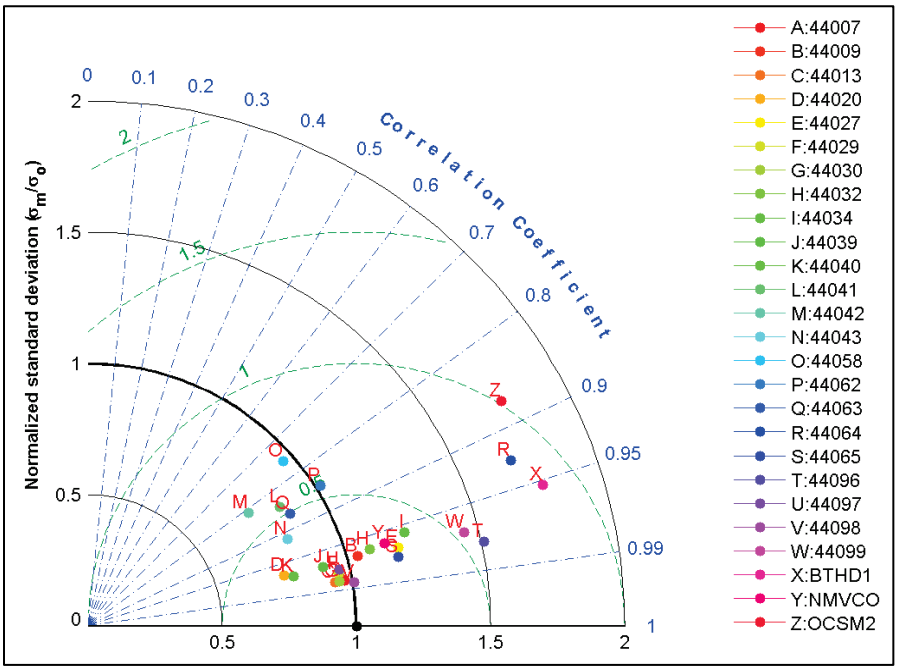

Looking at the scatter plots presented in Figure 7-23, one can see a noticeable decrease in scatter with more recent storms. Both Gloria and Josephine have far fewer observations than the other storms (< 200). For Isabel, STWAVE generally underestimated wave heights less than 2 m but overestimated the 2–4 m wave height range. The extreme wave heights were captured well by STWAVE. There is a slight positive bias in the model results for Irene and Sandy compared to the measurements. STWAVE does a good job estimating the peak waves for Irene. For Sandy, there are some noticeable outliers lying above the line of perfect, and further inspection revealed these points to be an overestimation of the storm peak at one buoy (44065). Again, the modeled spectral generally compared well to the measured spectra but with simply more energy at the peak frequency.

Figure 7-23. Scatter plots of validation tropical storms.

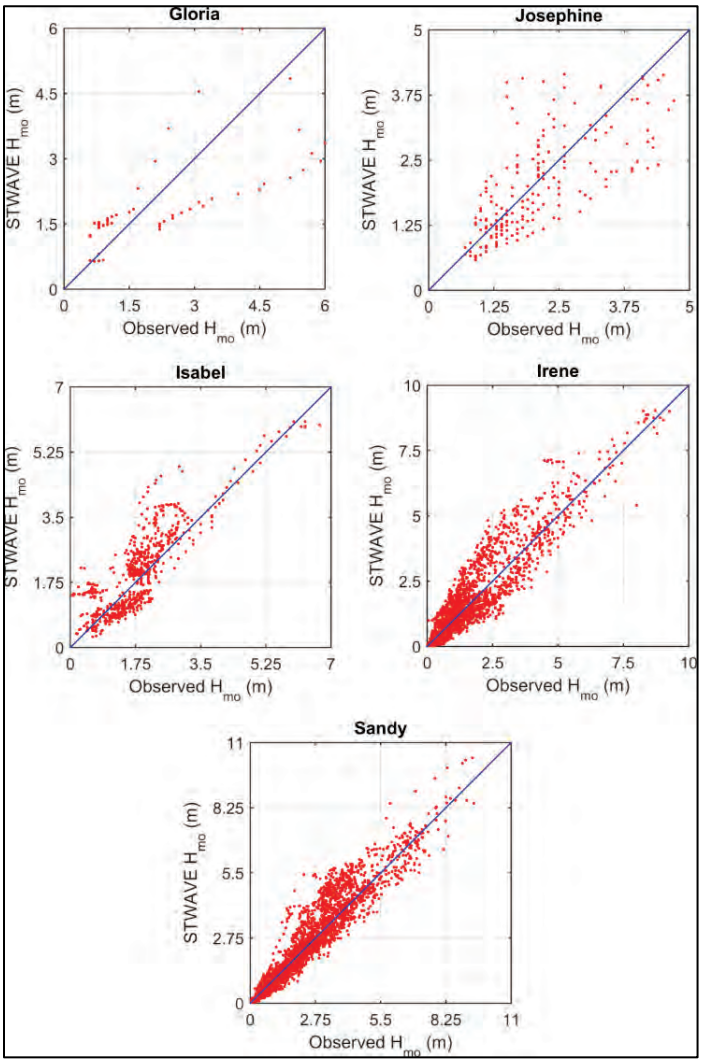

To evaluate STWAVE's performance for each individual storm simulation, statistical tests were run on the time-paired measurement and model results. The tests were performed on the significant wave height and mean wave period. The statistical results for significant wave height are presented in Table 7-6. Based on Willmott's index of agreement, the lowest performing storms were Gloria and ET073. Both of these storms had indices of agreement less than 0.6 and significantly higher biases compared to the other storms. The biases were -0.58 m and -0.27 m for Gloria and ET073, respectively, indicating an underestimation of the mean significant wave height. STWAVE's performance in terms of wave height increased with more recent storm events, approaching 0.7 for Josephine and Isabel and exceeding 0.8 for Irene and Sandy. Note that population size increased with more recent storms, allowing for more model-measurement comparisons. These more recent storms demonstrated very low biases (-0.09 m to

0.18 m), suggesting STWAVE accurately captured the mean wave trend. The RMSE results were somewhat disappointing and exceeded 0.5 m for all the storms. Exceeding 1.0 m, the RMSE for Gloria is poor; however, note that only one buoy was operational. The symmetric slope (i.e., linear regression defined with a zero intercept) indicates average negative errors of 6%, 27%, 20%, and 4% for ET070, ET073, Gloria, and Josephine, and positive errors of 11%, 8%, and 6% for Isabel, Josephine, and Sandy in modeled significant wave height.

Table 7-6. Summary statistics for validation storm significant wave height.

Storm	Gauges	Observations	Mean (m)		Bias (m)	RMS error (m)	Linear Reg		Index of Agreement
			Obs	STW			Corr	Sym slope	
ET070	5	355	2.23	2.16	-0.08	0.74	0.88	0.94	0.77
ET073	4	183	2.25	1.67	-0.58	0.53	0.83	0.73	0.55
Gloria	1	55	2.2	1.92	-0.27	1.17	0.72	0.80	0.59
Josephine	4	188	2.07	1.99	-0.09	0.74	0.71	0.96	0.65
Isabel	13	697	1.76	1.95	0.18	0.58	0.85	1.11	0.69
Irene	26	2301	1.56	1.66	0.10	0.63	0.92	1.08	0.80
Sandy	26	3516	2.19	2.29	0.10	0.55	0.95	1.06	0.86

The summary for the mean wave period is presented in Table 7-7. Model performance for wave period was worse than for wave heights, as indicated by the lower indices of agreement. Again, model performance generally improved with more recent storms. The bias trend matched those of the wave heights, where pre-Isabel storms saw negative biases and post-Isabel storms saw positive biases. The RMSE was somewhat high and varied from slightly over 0.8 s (ET073) to slightly over 2.5 s (Isabel). The symmetric slope indicated negative errors of 6%, 12%, 20%, and 10% for ET070, ET073, Gloria, and Josephine, and positive errors of 19%, 18%, and 21% for Isabel, Josephine, and Sandy in modeled mean wave period relative to the measured mean wave period.

Table 7-7. Summary statistics for validation mean wave period.

Storm	Gauges	Observations	Mean (s)		Bias (s)	RMS error (s)	Linear Reg		Index of Agreement
			Obs	STW			Corr	Sym slope	
ET070	5	290	7.31	6.89	-0.42	1.24	0.85	0.94	0.75
ET073	4	183	8.22	7.20	-1.03	0.87	0.68	0.88	0.49
Gloria	1	55	9.19	7.26	-1.93	1.66	0.22	0.80	0.33
Josephine	4	188	8.34	7.52	-0.83	1.10	0.65	0.90	0.51
Isabel	13	378	8.59	9.86	1.28	2.52	0.79	1.19	0.60
Irene	26	1632	5.59	6.54	0.95	1.96	0.83	1.18	0.72
Sandy	26	2786	6.11	7.50	1.31	1.41	0.91	1.21	0.75

In order to evaluate overall model performance, this battery of statistics was then applied to time-paired measurements and model results concatenated across all validation events. Time-paired, color scatter plots of significant wave height and mean wave period are shown in Figure 7-24. STWAVE estimates show good agreement to wave height measurements throughout the measurement range as the scatter rarely exceeds the 95% confidence limits. The scatter above and below the line of perfect fit is fairly well balanced, resulting in an overall error slightly biased positively at 5.0%. Wave heights less than 2.0 m comprise a large percentage of the wave climate. The mean wave period estimates compared to the buoy measurements show far more scatter than the wave heights; however, the bulk of these time-paired data sets remains, in general, within the 95% confidence limits. The overall error is biased positively at approximately 15%.

Figure 7-24. Color contour of time-paired significant wave height (top) and mean wave period (bottom) for all validation storms.

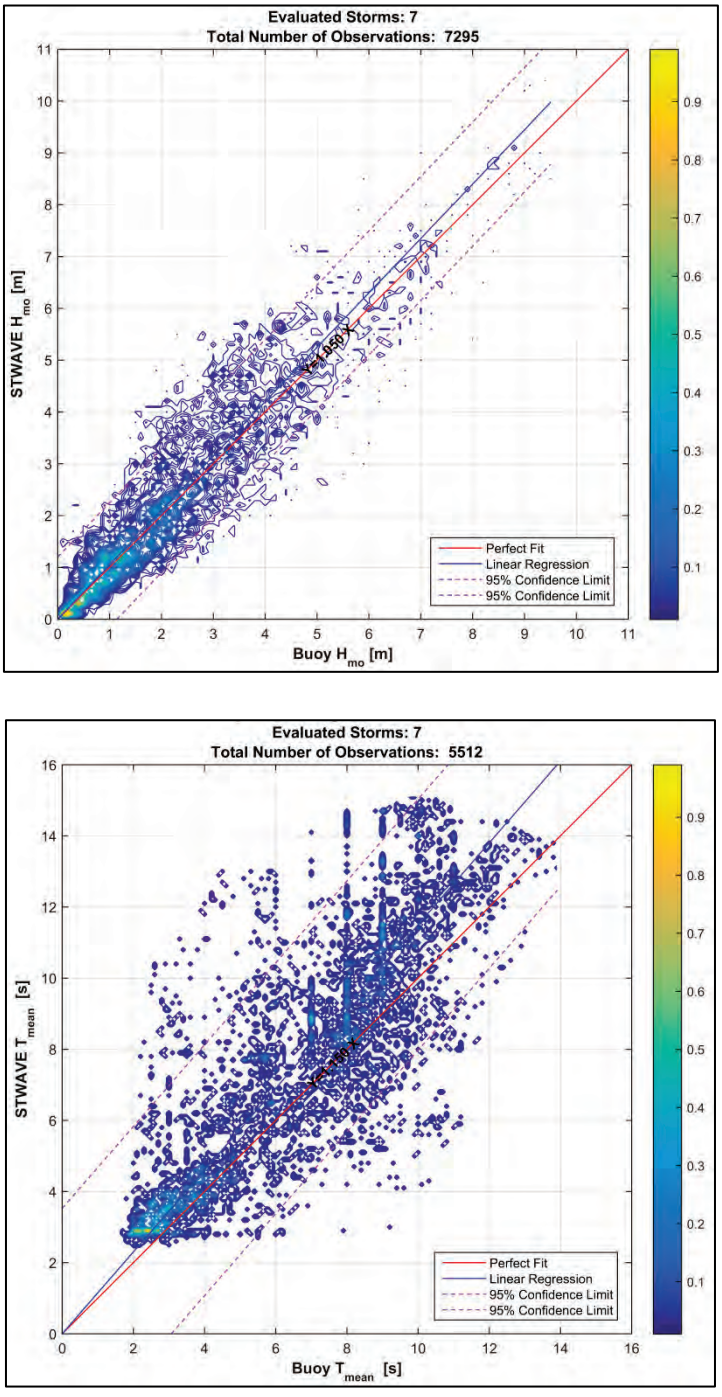

STWAVE's overall statistical performance is presented in Table 7-8. While STWAVE performed poorly for the earlier validation events, it did a good job modeling the more recent storms, particularly Irene and Sandy. This is likely due to a combination of factors, such as development of more accurate wind and offshore forcing, more advanced buoy technology, and larg-

er measurement population size. A bias of 0.07 m for significant wave height and 0.93 s for mean wave period are reasonable. The RMSE of both parameters are somewhat disappointing considering the magnitude of the mean. However, given the extent and complexity of the modeled region and that detailed wind forcing was not available for all the domains, STWAVE performed reasonably and even excellently at many buoys, despite some persistent issues at others.

Table 7-8. Statistical summary of STWAVE's overall performance.

Parameter	Observations	Mean		Bias	RMSE	Linear Reg.		Index of Agreement
		Obs	STW			Corr	Sym slope	
H_{m0} [m]	7295	1.96	2.03	0.07	0.61	0.93	1.05	0.82
T_{mean} [s]	5512	6.40	7.33	0.93	1.80	0.84	1.15	0.73

7.6 Summary

Nearshore wave transformation for the NACCS was accomplished using the spectral wave model STWAVE. Extensive grid creation and development was undertaken along the East Coast, resulting in 10 STWAVE grids encompassing coastal Virginia to Maine. All of the grids except those in Chesapeake Bay had 200 m resolution; the Chesapeake Bay and Washington, DC, grids had resolutions of 125 m and 100 m, respectively. Finer grid resolution for these areas assured that the smaller geographic features were better represented within the model domain. The wave climate provided by WAM was interpolated onto the STWAVE domains to serve as offshore forcing. Two-way coupling with ADCIRC was facilitated by CSTORM-MS, where ADCIRC passed wind and water levels to STWAVE and STWAVE passed wave radiation stress gradients to ADCIRC to drive wave-induced water level changes. Prior to the production phase, STWAVE results were evaluated against measurements for five tropical (Gloria, Josephine, Isabel, Irene, and Sandy) and two extratropical storms. The evaluation consisted of time, scatter, Taylor diagrams, and a suite of statistics. STWAVE comparisons with measurements improved with more recent storms. This is likely due to a combination of factors, such as, but not limited to, development of more accurate wind and offshore forcing, more advanced buoy technology, and larger measurement population size. STWAVE was also more accurate in estimating wave height than mean wave period. Although some sites did demonstrate persistent poor performance, STWAVE provided overall good wave estimates compared to

measurement sites given the large extent and complexity of the modeled regions.

8 CSTORM-MS Production

This chapter summarizes the application of the USACE ERDC CSTORM-MS as applied in the NACCS numerical modeling study, including the CSTORM-PS, the CSTORM Production Visualization (CSTORM-PVz), and first-level QA/QC reporting. Additional topics include a discussion of the frequency of evaluation of steady state nearshore wave conditions in relation to the forward speed of the storm and a discussion of the three water level conditions used for the CSTORM-MS production simulations. These water level conditions are

- the base conditions which do not include tides
- the with-tides condition
- the with-tides and sea level change condition.

8.1 Coupling overview

The CSTORM-MS coupling framework is written in modern FORTRAN 90 and uses the Message Passing Interface (MPI) (MPI 2014) in order to operate in a parallel computing environment. The system has a main controller or driver that operates on a single processor and acts as the *conductor*, instructing the individual models when to run, pause, and exchange information through the couplers. The driver also controls the coupler processors that are used to receive, interpolate, and send information between the individual models. There is one coupler processor dedicated for each STWAVE domain. Figure 8-1 is a schematic showing the interconnection of processes within the CSTORM-MS framework. In Figure 8-2, the ADCIRC and STWAVE models are shown separated to illustrate the flow of information even though both models use the same computer processors to perform computations. The entire system is contained in a single executable file.

Figure 8-1. A schematic showing the major components of the CSTORM-MS coupling paradigm and the flow of information.

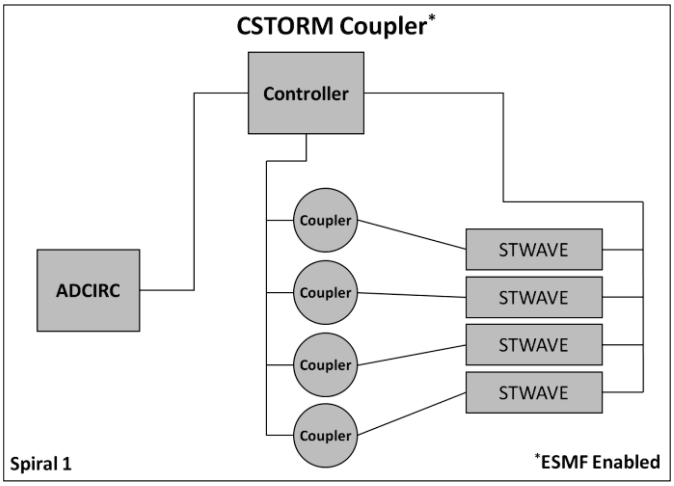

ADCIRC and STWAVE models operate sequentially, with ADCIRC starting the process and running for a designated period of time then pausing and waiting to receive updated information from STWAVE (Figure 8-2).

Figure 8-2. A workflow schematic showing the order of operation between ADCIRC and STWAVE within the CSTORM-MS coupling framework. Red and blue alternating patterns are used for visual effects only to show separation of individual run periods.

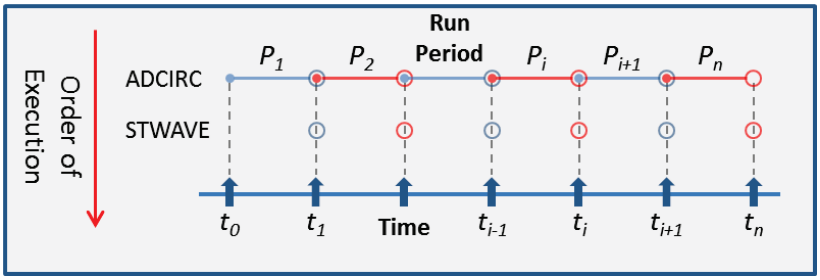

When ADCIRC pauses, the controller directs ADCIRC to send the latest sea-surface elevation and wind to the coupler processors, which in turn perform linear interpolation of those fields onto the STWAVE computational domains. Once mapped, those fields are sent to the individual STWAVE domains for use in computing the updated nearshore wave fields. The controller processor next instructs STWAVE to update the wave field, after which the couplers reverse the flow of information and collects from STWAVE the gradients of surface wave radiation stresses. The couplers then perform a linear interpolation of those surface-wave stress gradients onto the ADCIRC domain.

When multiple STWAVE domains are involved, the driver processor collects the interpolated gradients of wave stresses from all STWAVE domains and combines them into a single wave stress gradient field prior to sending it to ADCIRC. By default, when two or more STWAVE domains overlap, the CSTORM-MS coupling system selects the surface wave stress gradient with the largest magnitude from among the individual STWAVE domains. With this definition of the default option, no smoothing of possible disjoint gradients is performed, and no adverse results have been observed in any storm simulations. Once ADCIRC receives the updated gradients of surface wave stresses from the couplers, it resumes its forward progression in time, applying the same wave stresses until the next time for it to exchange information with STWAVE.

ADCIRC computational nodes that lie outside of the STWAVE domains receive a default value of zero for radiation stress gradients. In a similar way, STWAVE cell center points that lie outside of the ADCIRC domain have nothing to interpolate; however, an attempt is made to extrapolate STWAVE neighboring cell information. In this case, a search algorithm examines a maximum of 10 neighboring cells to the logical left, right, above, and below the target cell for a nonzero value. If a nonzero value is found, then it is used; otherwise, appropriate default values are used, with a zero value for surge and zero value for wind magnitudes.

The time period between each evaluation of STWAVE is constant throughout the coupled simulation. In fact, each *run period*, as shown in Figure 8-2, is for the same length of time except possibly for the first and last period, which may have had longer ADCIRC run lengths. The first ADCIRC run period can be longer to allow for spinning up the surge model. The last ADCIRC time period can be longer for continued evaluation of water elevations and circulation after the main thrust of the storm has passed in order to allow for modeling of the drainage of inundated areas. Prior to STWAVE being executed the first time, ADCIRC uses zero values for the wave surface stress gradients. Likewise after STWAVE stops execution, ADCIRC uses a zero value for the gradients of surface wave radiation stresses.

Since ADCIRC and STWAVE operate in a sequential pattern, they do not run at the same time and can therefore share computer processors to perform their computations within the CSTORM-MS framework. If more than one STWAVE domain is used, each one is contained on a unique collection

of computer processors that do not overlap with other STWAVE domains, but all of which can be shared with ADCIRC. Different STWAVE domains are not allowed to overlap on a single computer processor due to the use of global variables within STWAVE and the possibility of memory overlapping between instances.

ADCIRC is configured to use tightly coupled wave radiation stress gradients by setting the ADCIRC wind wave input variable NWS parameter in the ADCIRC control input file (fort.15) to have a value of 400 plus whatever wind/pressure options are being used. For example, all the NACCS wind/pressure files are stored in what ADCIRC calls a type 12 format, indicating an OWI formatted data set, which would mean that a coupled ADCIRC-STWAVE wave/surge simulation would be indicated by setting NWS equal to 412. Similarly, STWAVE is configured to use tightly coupled water surface elevations and winds by setting the ISURGE parameter to 101 and the IWIND parameter to 101 in the STWAVE simulation control input file *.sim. This indicates to STWAVE that it is using globally spatially varying surge and wind fields that are being passed to it via the CSTORM-MS coupler. Finally, the CSTORM-MS controller uses a single-text ASCII coupler file for ADCIRC-STWAVE tightly coupled simulations which is named mf_config.in in the CSTORM-MS version 1.1.07+. The purpose of this file is to define the necessary input parameters for coupling ADCIRC and STWAVE. In this version of the coupler application, ADCIRC is considered the primary component, and time values are listed relative to ADCIRC time-step numbers. When the ADCIRC mesh is given in geographic coordinates and the STWAVE grids are supplied in either State Plane or UTM coordinates, the coupler can perform the necessary coordinate transformation between those coordinate systems automatically. There is also an option to have both the ADCIRC mesh and all the STWAVE grids in the same local (meters) coordinate systems, in which case no coordinate mappings have to take place. The coupler file makes use of FORTRAN namelists (Adams et al. 1992) constructs, and currently there are three namelists in the mf_config file: the first is “service”, the second is “adc_def”, and the third is “stw_def”. A brief introduction to each of these namelists is given in the following.

The “service” FORTRAN namelist in the mf_config.in file describes the type of coupling to perform and the datasets to share, along with the number of STWAVE grids and the starting and ending time of the STWAVE simulation. The FORTRAN namelist “adc_def” within the mf_config.in file

describes run time information related to the ADCIRC model only (the ADCIRC mesh file [fort.14] name, the number of computer processors to apply to the ADCIRC model simulation and when to start and end the ADCIRC portion of the simulation). A FORTRAN namelist "stw_def" within the mf_config.in file is listed once for each of the STWAVE grids and defines needed run time values related to each of the STWAVE model domains. A detailed description of each of these namelists as well as a sample CSTORM-MS coupler control file (mf_config.in) is provided in Appendix D: mf_config.in Details.

8.2 CSTORM production system

The SMS GUI is a convenient tool for setting up an initial CSTORM simulation and for viewing small numbers of the results. However, with the need to perform approximately 3500 CSTORM simulations, a semiautomated process was needed to efficiently and accurately set up and execute the simulations. To this end, two main semiautomated production scripts for setting up CSTORM-MS simulations (ADCIRC+STWAVE) were created, tested, and verified for historical extratropical storms, historical tropical storms, and synthetic tropical storms and have been executed for all production simulations. These scripts are written principally in BASH and make calls to Python functions, both of which are readily available on Linux and Unix systems and all the Department of Defense (DoD) Defense Shared Resource Center's (DSRC) high performance computing (HPC) systems. A description of the purpose and functionality of the two scripts follows.

8.2.1 Conversion of WAM output to STWAVE boundary input (Wam2Stwave)

Once the offshore, deep-water wave model WAM has been successfully executed and results verified, the WAM special point location output files (.SPE2D) are made available to provide input boundary spectral information for the STWAVE model domains. A FORTRAN 90 code (wam_to_stwave_for_v6p0.f) is applied to postprocess the WAM *.SPE2D files for each of the STWAVE model domains that require boundary spectra information. In the NACCS production case, this process is required for nine STWAVE domains. The FORTRAN code requires user input files for each STWAVE domain and storm simulation. The input files provide the following necessary information: Start and end date/times for the WAM outputs, frequency of the WAM output in each SPE2D file in

minutes, the desired start and end date/times for the STWAVE boundary spectra (*.eng file) information along with the frequency of sampling in minutes. This information is storm-simulation specific, so these inputs need to be specified in an automated fashion. As such, a BASH script called proc_wam2stave.sh is used to actually supply the needed information for the input files, copy files into the correct locations for production use, and execute the FORTRAN codes to produce the STWAVE boundary spectra files (*.eng). Upon execution of the shell script, the user supplies the following information: Storm Type (Historical or Synthetic), Storm Class (Tropical or ExtraTropical), storm number, and the name of the CSTORM grid configuration templates. From this information, the script accesses the run parameters table associated with the particular Storm Class and Storm Type and reads in the storm information for the particular storm number supplied. The run parameters table is discussed in more detail below. The information from the run parameters table necessary for this script to function properly is the start and end dates/times of the STWAVE portion of the simulation and the STWAVE execution frequency in minutes. All the WAM SPE2D files are stored in a central location within the CSTORM-PS directory hierarchy and have a unique name identifying results by storm class, storm type, and storm number. All the STWAVE *.ENG spectral energy boundary files are also stored in a central location within the CSTORM-PS directory hierarchy and have unique names that identify them by Storm Type, Storm Class, Storm Number, and associated STWAVE domain name. The proc_wam2stwave.sh script creates the STWAVE output directories, copies the correct WAM SPE2D files into that directory, copies the CSTORM grid configuration templates into that directory, fills in the input templates needed for the wam_to_stwave_for_v6p0.f routine with the correct information (Dates/Times and Frequency of input/output), then executes the FORTRAN code for processing the WAM2STWAVE results. Finally, the script performs a *cleanup* step where temporary working files are removed, run parameters and run log files are renamed and archived together with the STWAVE *.ENG files for production use.

8.2.2 CSTORM-MS model setup and execution script (master_01.sh)

In a similar fashion to the WAM2STWAVE script described above, the CSTORM-MS master setup script is written in BASH with calls to Python functions. The function of this script is to completely set up all the necessary inputs for a single CSTORM-MS simulation (coupled

ADCIRC+STWAVE). The required inputs for a single simulation are the following:

1. For ADCIRC–the mesh file (fort.14), the model control file (fort.15), the nodal attribute file (fort.13), and the wind and pressure files (fort.22, fort.221, fort.222, fort.223, fort.224)
2. For each STWAVE domain–the grid depth file (*.dep), the friction file (*.friction.in), the model control files (*.sim), and the boundary spectra file (*.eng) where used
3. For the CSTORM-MS coupling configuration, an mf_config.in file that specifies when each model (ADCIRC and STWAVE) is to run, when they are to exchange information, and what information they are to exchange
4. Inputs for preparing (*prepping*) ADCIRC for parallel execution using the ADCPREP code
5. Queue submission scripts for executing ADCPREP and the coupled CSTORM-MS (ADCIRC+STWAVE) simulation. The script requires the following information for each storm:
   a. Storm type (historical or synthetic)
   b. Storm class (tropical or extratropical)
   c. Storm number
   d. The name of the cstorm grid configuration templates
   e. Tidal scenario number
   f. River input conditions
   g. Sea level change configuration number
   h. Cold or hot starting ADCIRC
   i. Estimated simulation (CSTORM-MS) run time in hours
   j. An email address for the user submitting the job.

From this input, the script finds and reads the user-specified run parameters table based on the storm class and storm type, finds the user-specified storm number in the table, and reads in the specific storm information from the table, as described later. Next, a run directory is created within the production area of the file disk space, and all the temporally static files are copied to the run directory including grids, meshes, friction files, the storm-specific wind and pressure files, and the storm-specific STWAVE boundary spectra files. In addition, all of the model input templates that require updating with the storm-specific, time-dependent run information supplied in the run parameters table were copied to the storm-specific run directory. The script fills in the ADCIRC fort.15 file template, all the

STWAVE *.sim file templates, and the mf_config.in file template, including determining the tidal potential factors if required for ADCIRC's input file for the specific storm selected for simulation. The script also copies all the necessary model executable codes into the directory (adcprep.exe and cpadcirc.exe – the single executable for the coupled ADCIRC+STWAVE). The script creates several Portable Batch System (PBS) and BASH script files for

6. submitting the ADCPREP step
7. executing the CSTORM-MS coupled ADCIRC+STWAVE simulation
8. renaming all the generic ADCIRC outputs with unique run identification information
9. launching the CSTORM-PVz
10. compressing and tarring the results
11. storing all the results to long term archive.

The script also constructs the ADCIRC fort.22 file needed for specifying the number of wind and pressure files and synchronizing those files within the ADCIRC simulation period by using information from the run parameters table. Figure 8-3 illustrates the cascading process initiated by the CSTORM-PS master script. The CSTORM-PS master script also creates a metadata run log that contains all the inputs for the particular simulation it just created. At the end of the setup process, the master script submits the first batch script to the computer queue for execution. After successful completion of each batch script, the next script is automatically submitted for execution using the appropriate computer resources (processors and queue types) for that particular job. This process reduces the hands-on human interaction in the simulation process, thus reducing potential for human error. The QA/QC process, however, includes qualified scientists reviewing model settings, files, and results for accuracy and completeness.

Figure 8-3. Schematic showing the sequence of operations performed during the CSTORM-PS process.

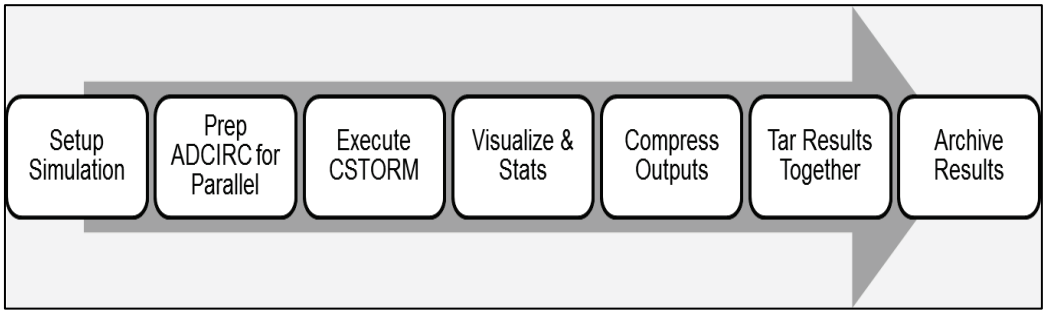

8.3 Model coupling timing

8.3.1 Run parameter table

There are three distinct run parameter tables which correspond to

- historical extratropical storms
- historical tropical storms
- synthetic tropical storms.

The run parameters tables specify timing information for each storm and include

12. start and end dates/times for winds/pressure files along with the time frequency of the data supplied in those files (dates/times are supplied as a 4-digit year, 2-digit month, 2-digit day, 2-digit hour)
13. the start and end dates/times for nearshore STWAVE model execution and the time frequency of the STWAVE snaps
14. the start and end dates/times for when winds/pressures are to be applied to ADCIRC
15. the tidal/river spin-up times for the ADCIRC portion of the simulation
16. five times per storm for random tidal hot-starting
17. three potential sea level change/steric height adjustment values.

A portion of the run parameters table for historical extratropical storms is provided in Table 8-1.

Table 8-1. Excerpt from the run parameters table for historical extratropical storms 29-35.

Storm ID	Met Start Date	Met End Date	Met Int (min)	STW Start Date	STW End Date	STW Int (min)
29	1972121200	1972122000	60	1972121418	1972121718	60
30	1973012500	1973020200	60	1973012802	1973013102	60
31	1974112800	1974120600	60	1974113021	1974120321	60
32	1976012900	1976020600	60	1976013122	1976020322	60
33	1977010600	1977011400	60	1977010907	1977011207	60
34	1977101000	1977101800	60	1977101307	1977101607	60
35	1978011600	1978012400	60	1978011908	1978012208	60

ADC Wind Start Date	ADC Wind End Date	Tidal Spin (days)	Random Tide/IHOT Val 1	Random Tide/IHOT Val 2	Random Tide/IHOT Val 3	Random Tide/IHOT Val 4
1972121200	1972122000	14.0	2433000	2500920	1355400	1482300
1973012500	1973020200	14.0	3364620	1432140	2051100	2594520
1974112800	1974120600	14.0	2892300	2401020	1819860	3067200
1976012900	1976020600	14.0	1756800	2935200	2763180	2773620
1977010600	1977011400	14.0	3229320	2259960	1425060	3099780
1977101000	1977101800	14.0	1662900	3696180	2828940	2623140
1978011600	1978012400	14.0	2783040	2610120	2446200	1662180

Random Tide/IHOT Val 5	SLC/Steric Val 0 (m)	SLC/Steric Val 1 (m)	SLC/Steric Val 2 (m)
3085740	0.095	1.095	0.595
2197740	0.096	1.096	0.596
1418160	0.105	1.105	0.605
3297060	0.096	1.096	0.596
1713360	0.090	1.090	0.590
2175420	0.182	1.182	0.682
3382140	0.090	1.090	0.590

8.3.2 Specific information for the historical extratropical storms run parameters

The wind and pressure files for the historical extratropical storms were all based upon a peak water level date/time from measurements, and the time frequency for those wind and pressure files were all provided by OWI as hourly data. The peak water level date/time is used to center the nearshore STWAVE simulations times. Specifically, STWAVE simulations are started 36 hours prior to the peak water level date and continue until 36 hours after the peak water level date and occur on an hourly basis. STWAVE is a steady-state wave model, and since the wind fields are changing hourly, it was determined that computing updated wave snaps at the same frequency as the wind updates was sufficient. Each ADCIRC simulation applied the entire supplied wind/pressure file time period and for tidal simulations included an additional 14-day tidal spin-up period to adequately allow for the circulation solution to evolve from an at-rest state to a fully

evolved and transient-free state prior to applying the winds, pressures, and waves.

8.4 CSTORM-PS data organization and description

The CSTORM storm simulations are divided into two types: synthetic and historical, then further divided into two classes: tropical and extratropical storms developed for this study. Note that there are no synthetic extratropical storms. Each storm class/type combination has a number assigned starting at 1. Each simulation is further identified based on additional run parameters, including Tides (no tides, real tides, random tides), Rivers (no river, constant river, real river flows), and Sea Level Change (no change; option 1: 1 m of rise; option 2: 0.5 m of rise). Each output file is named with a prefix (RNAME) that uniquely identifies the simulation. The RNAME value is constructed based on six simulation characteristics as listed below in Table 8-2.

RNAME =
NACCS_CLASS_RNUM_TYPE_Tides_TN_SLC_SN_RFC_RN_

Table 8-2. A listing of the simulation characteristics and their description used in constructing a Unix prefix name for simulation results.

Characteristic	Description
CLASS	Storm classification: TP – Tropical or ET – Extratropical
RNUM	Storm Number – Ranges from 0001 to 1050
TYPE	Storm Type: SYN – Synthetic or HIS – Historical
TIDES_TN	Tidal Scenario Option. TN ranges from 0 to 5 0=no tide; 1-specific tide, 2-random tide
SLC_SN	Sea Level Change/Steric Adjustment Scenario. SN ranges from 0 to 2 (0-steric adjustment only, 1- steric adjustment + 1 m SLR; 2 – steric adjustment + 0.5 m SLR
RFC_RN	River Forcing Conditions. RN ranges from 0 to 2 0 – no inflow or default inflows, 1 – specific (real) inflows, 2 – random inflows

An example of RNAME for a Tropical Synthetic storm number 1043 using the first random tide hot-start value described in the run parameter table and the default sea level condition/steric adjustment (steric adjustment only) and default river forcing conditions would be given as

NACCS_TP_1043_SYN_Tides_2_SLC_0_RFC_0_.

For each CSTORM-MS run, the input and output files that are to be stored long term are compressed using gzip and then are combined (*tarred*) together into a few *tar ball* files grouped in a meaningful way. Each tar file also uses the prefix naming convention (RNAME). For the NACCS numerical modeling study, there are 10 STWAVE domains applied in the CSTORM-MS simulations, each archived with two tar files: "Outputs" and "SurgeWind." There are four ADCIRC tar files, one STWAVE station tar file, one CSTORM-MS tar file, plus five additional tar files resulting from the visualization process. A PDF report of all the QA/QC plots and statistics is also archived. A detailed description of the tarred contents and the individual files for a CSTORM-MS simulation is provided in Appendix E: Tar Ball Details and Appendix F: Model and CSTORM File Descriptions, respectively.

Files are stored by class/type, configuration, and run number (RNC) in a base directory for a given computer system (e.g., basedir/NACCS/CSTORM_Sims/).

Figure 8-4. A schematic description of the general directory structure for simulation classifications.

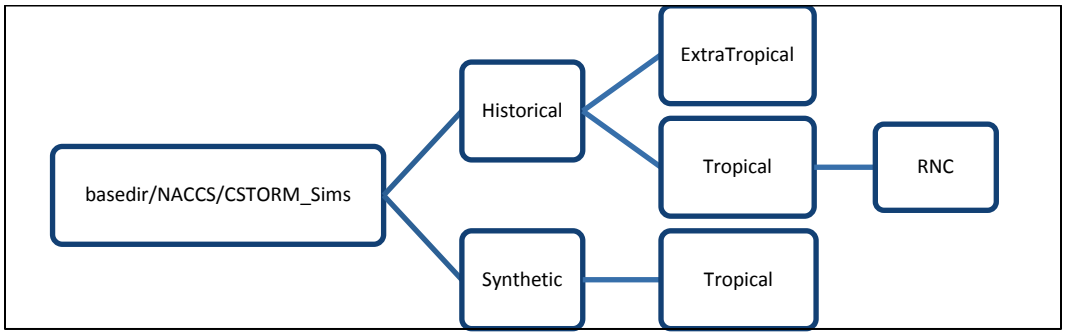

Within a given storm type and class, the simulation directory, represented as RNC in Figure 8-4 , is named according to simulation properties as follows:

RNC = Run_NM_Tides_TN_SLC_SN_RFC_RN_WAV_WN_GCP_PN_UID_IDV

where:

- Run_NM = Storm Number, NM = 0001 to 1050
- Tides_TN = Tidal Scenario, TN = 0 to 2

- SLC_SN = Sea Level Change/Steric Adjustment Scenario, SN = 0 to 2
- RFC_RN = River Forcing Conditions, RN = 0 to 2
- WAV_WN= Waves Off/On, WN = 0 or 1 (Note that WAV_WN was not used in the NACCS modeling project)
- GCP_PN = Grid Configuration Packet Name
- UID_IDV = User Identification, IDV = person performing simulation.

8.5 Storm speed and evaluation frequency

The wind and pressure files for the synthetic tropical storms were all supplied at 5 min time increments in order to better represent some very fast moving storms. Each of the 1050 storms is designed for a particular region (Region 1, 2, or 3) for which it is included for statistical purposes in the context of the JPM-OS. Region 3 covers the area between latitudes 36.5 deg and 39.0 deg north, Region 2 covers the area between latitudes 39.0 deg and 41.5 deg north, and Region 1 covers the area between latitudes 41.5 deg and 45.0 deg north. Each of the storms is also classified as either a landfalling or bypassing storm. A storm definition table was provided by OWI that details several key pieces of information for each of the 1050 synthetic tropical storms.

For the purpose of determining the CSTORM-MS run parameters table, the key information from that table is the landfalling/bypassing classification, the region of impact, the landfall location coordinates if a landfalling storm, and the reference location coordinates for the storm and the forward speed of the storm. The reference location coordinates for landfalling storms is 250 km away from the landfall location of the storm. The reference location coordinates for bypassing storms is the location when the storm exits the impact region (e.g., at latitudes 39.0 [for Region 3], 41.5 [for Region 2] and 45.0 [for Region 1] deg north). The forward speed of the storms ranged from a slow-moving 6.5 knots to a very fast-moving 47.5 knots with the mean forward speed over all storms being 21.96 knots with a standard deviation of 9.0985 knots. Figure 8-5 shows the distribution of the storms based on forward speed. The storms were then grouped into three speed categories (slow, moderate, and fast) with slow storms having a forward speed of between 6.5 knots and 12.9 knots, moderate storms having a forward speed of between 12.9 and 31.1 knots, and fast storms having a forward speed greater than 31.1 knots. The range of forward speeds in the moderate category falls within +/- one standard deviation about the mean forward speed. Figure 8-6 shows the number of storms for each category.

Figure 8-5. Distribution of synthetic tropical storms by their forward speed.

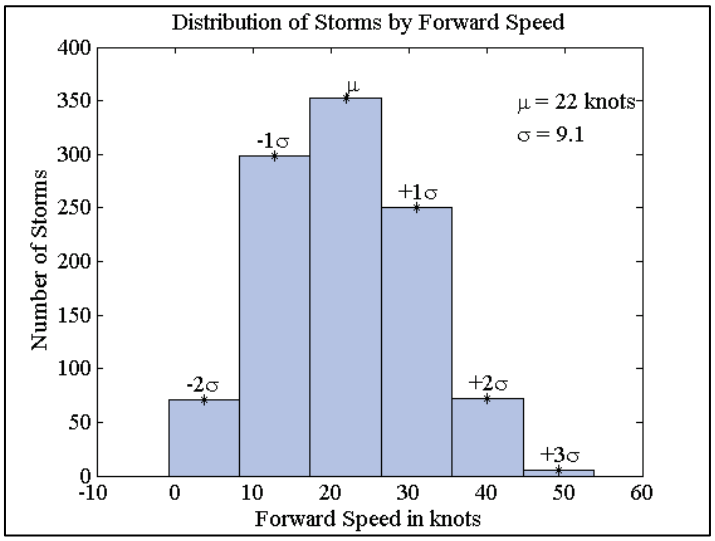

Figure 8-6. Grouping of synthetic tropical storms into three forward-speed categories and the number of storms in each category.

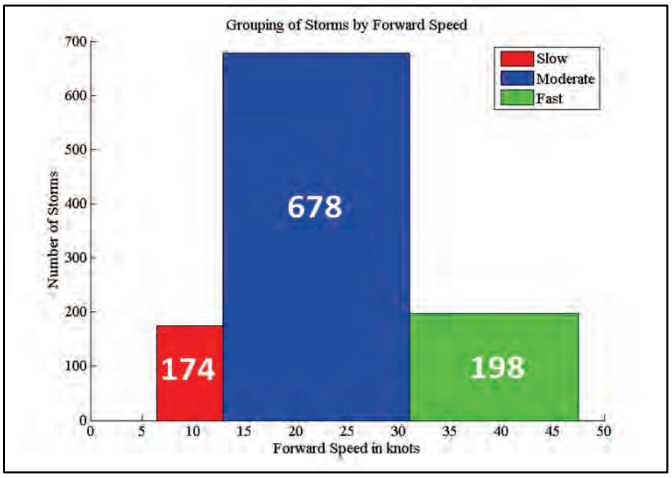

The timing frequency of STWAVE snaps for the CSTORM-MS solution is based on the forward-speed classification of the storm. Slowly moving storms have STWAVE snaps computed every 60 min, moderately forward-speed storms have wave snaps every 30 min, and the fast-moving storms have wave snaps computed every 15 min. Based on the forward speed and the time increment between snaps, the approximate distance the storm travels between wave snaps is between 18 and 20 km. For each synthetic tropical storm, a total of 97 STWAVE snaps are computed, with 66 snaps occurring before the landfall/region exit location time, 1 snap at landfall, and 30 snaps after landfall. This corresponds to 4 days, 2 days, and 1 day of STWAVE wave snaps for the slowly, moderately, and fast-moving storms respectively.

The wind/pressure domains are larger than the ADCIRC domain. The ADCIRC domain boundary starts at -60.0 deg west longitude. In order to avoid model instabilities and to reduce overall model execution times, the CSTORM-MS-coupled ADCIRC+STWAVE simulations start using winds and pressure when the storm track crosses the -62.0 deg west longitude. The STWAVE simulations start-and-end dates/times are keyed off either the landfall time for landfalling storms or the reference time indicating when the storm leaves the impact region for bypassing storms. Figure 8-7 and Figure 8-8 show two example storm tracks, one landfalling and one bypassing, and indicate when the ADCIRC and STWAVE simulations are started and ended along the track.

Figure 8-7. Synthetic Tropical Storm Number 2 track (a landfalling storm) and indicators for ADCIRC-only (blue) computations and ADCIRC+STWAVE (red) computations along the track.

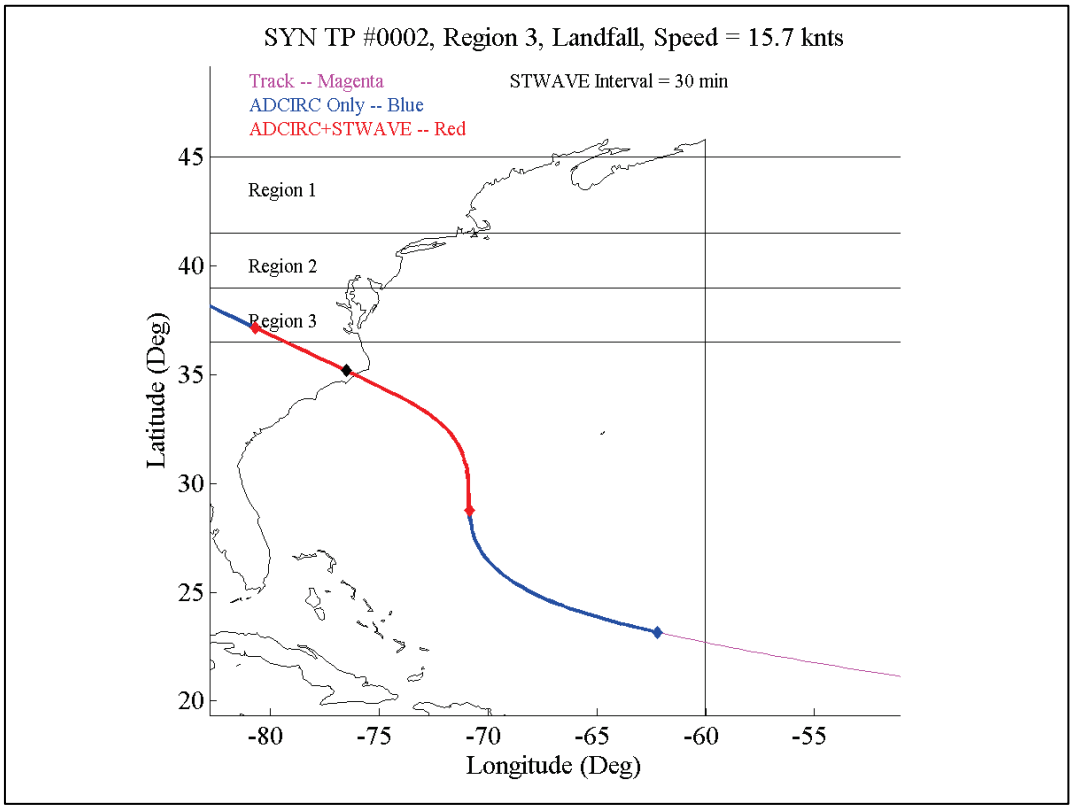

Figure 8-8. The track for Synthetic Tropical Storm Number 990 (a bypassing storm for Region 1) and indicators for ADCIRC-only (blue) computations and ADCIRC+STWAVE (red) computations along the track.

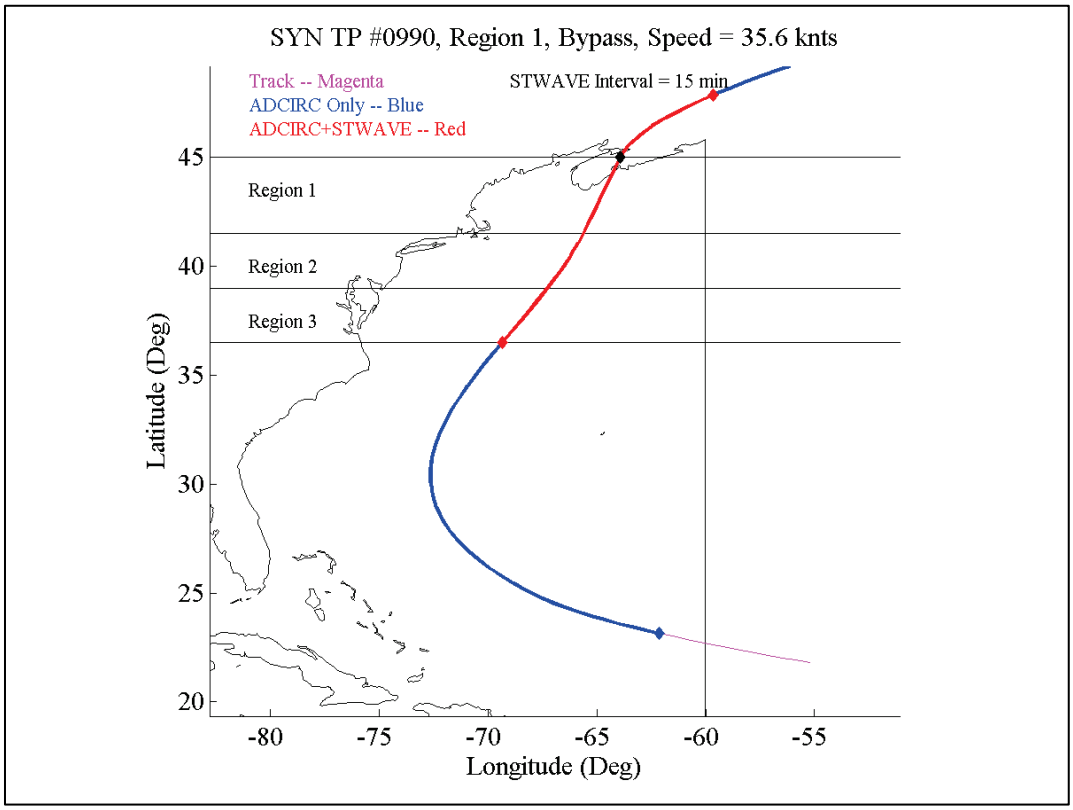

8.6 CSTORM production visualization

Visualization tasks are integrated throughout the workflow in physics-based numerical modeling such as the models used in the CSTORM-MS. Hands-on methods using desktop software are usually employed for building and creation of individual models with a small number of simulation requirements. The SMS software provides an appropriate framework and GUI for performing visualization tasks associated for these small-scale efforts. However, the NACCS requirements of simulation and execution of over 3500 events necessitates an automated solution for viewing model data sets and results for which manual methods could not be completed within reasonable time frames. Thus, a visualization component (CSTORM-PVz) was created within the CSTORM-MS framework and automation scripts to produce graphics, descriptive statistics, and digital reports for all NACCS results. Visualization scripts are written in Python with one primary script which controls initiation and all aspects and products of the visualization workflow.

Creating graphics on HPC systems can be challenging as the primary focus has traditionally been on computations rather than visualization. Traditional HPC systems devoted to computations (no graphics processors) are separated from systems whose emphasis is visual products (with many graphics processors). These configurations detailed the needs for data transfers and creation of specialized software tools for viewing model results and creating graphics. However, computer scientists have long developed tools for *off screen* rendering that create graphics entirely through software, circumventing the need for graphic hardware components. Albeit, these tools are not as fast as direct hardware rendering; the resultant products are of the same high quality.

The open source ParaView software was selected as the tool to render the NACCS CSTORM-MS visualization products. ParaView is a fully parallelized code that is open source and readily available on most of the DoD HPC systems. ParaView can perform both hardware-accelerated (using graphics processors if available) as well as off-screen, software-based rendering. All of the NACCS CSTORM-MS simulations were performed on DoD HPC systems that did not use dedicated graphic processors.

The main CSTORM-PVz Visualization Python scripts creates and builds a hierarchy of ParaView Python scripts which drive ParaView and create all graphic results. These scripts will automatically generate peak plots of both ADCIRC and STWAVE results including peak surge, wave heights, and wave periods for all NACCS storms. The following is a description of the functionality and purposes of the primary Python script and the subsequent ParaView scripts.

8.6.1 CSTORM-PVz preconfiguration setup

Several items, codes, templates, grid files, etc., must be created and exist in the CSTORM project directory structure before CSTORM-PVz scripts can be executed. ParaView can read large and diverse data sets and formats as well as imagery and raster image files. Spatial geometry formats both 2D and 3D include point sets, rectilinear grids, polygonal meshes, and time-series data. However, Paraview does not have a native reader for directly importing ADCIRC and STWAVE geometry. Therefore, a C-program (adc2vtk.x) must be manually executed to convert the ADCIRC mesh to an ASCII ParaView format called VTK which stands for Visualization Toolkit. The VTK format is a historic format created by the Paraview software creator, Kitware, Inc. The VTK version of the NACCS ADCIRC

mesh is created and stored in the project "Codes/Vizscripts/grids/ADCIRC" subfolder. Each of the STWAVE grids must also be converted to VTK format. This is done using the interactive version of ParaView. The VTK version of each NACCS STWAVE mesh is created and stored in the project "Codes/Vizscripts/grids/STWAVE" subfolder. Additionally, two VTK files for each STWAVE grid are required, one in the default rectilinear projection, which for the NACCS study were all UTM, and one in the Geodetic Latitude and Longitude coordinate system.

The large project spatial domain covering the Atlantic coast from southern Virginia to northern Maine was partitioned into six regions for creation and review of ADCIRC results. The spatial extents and region names are coded in a file called "options.viz". This file also contains the STWAVE grid names, given by a three letter code, and titles to be used for labeling STWAVE plots.

8.6.2 CSTORM-PVz script initiation and creation

Once the VTK format files and the options.viz files are created, the CSTORM-PVz script can be initiated. The main script can be initiated interactively and from the CSTORM-MS automation bash scripts by entering "python naccs_vizPlots_3.py" followed by optional and required arguments. Primary options are scenario, run check, units, and to plot or not to plot waves (Appendix G: CSTORM-Pvz Options).

The script assumes the ADCIRC results will be plotted (unless only a run check is entered), and the stormNumber(s) are expressed in the full run directory names. There must be at least one run directory (storm) to plot. An example command would be "python naccs_vizPlots_3.0.py –u feet –w Run_0120_Tides_2_SLC_0_RFC_0_GCP_NAC11_UID_xxxxxxxx".

Given these options, the script will create a subfolder called "vizout" in the storm run directory and build ADCIRC and STWAVE Paraview batch scripts in this subfolder. The main script will check to ensure that all required files are present as well as copy and convert the ADCIRC peak surge file (maxele.63) to a VTK format. There are two template ParaView batch Python scripts (one for ADCIRC and one for STWAVE rendering) in the project "Vizscripts" folder which are copied and modified with the specific storm run ADCIRC and STWAVE information and specific run name files.

Three storm-specific ParaView Python batch scripts are created for each ADCIRC *zoom* region. The first script reads the VTK format maxele.63 file and *clips* this according to the bounding coordinates specified in the options.viz file. This script also converts elevation units to feet (if specified) and computes and extracts the zero contour line (the coast line) for the region. The second script plots the region-specific peak surges, coast line, as well as the storm track (if the track crossed within this region). The color scales for this plot span the full range of the peak surge elevations. The second script plots the same data sets but at a standard color scale across all NACCS storms (range from 0 to 20 ft). Figure 8-9 shows an example ADCIRC Chesapeake Bay peak-surge contour plot.

Four storm-specific ParaView Python batch scripts are autogenerated for each STWAVE grid. Two of the scripts plot the maximum significant wave heights (H_s) (over the entire storm event) in two color ranges: the first for the entire data range and the second uses a standard color range (0 to 10 ft) across all NACCS storms. Two separate scripts plot the peak wave period (T_p) (over the entire storm event) in two color ranges: one for the data range and one standard across all NACCS storms. Figure 8-10 and Figure 8-11 show example contour plots of maximum significant wave heights (H_s) and peak wave periods (T_p) for NACCS synthetic tropical storm number 180.

Figure 8-9. Chesapeake Bay region ADCIRC peak-surge contour plot for synthetic tropical storm number 180.

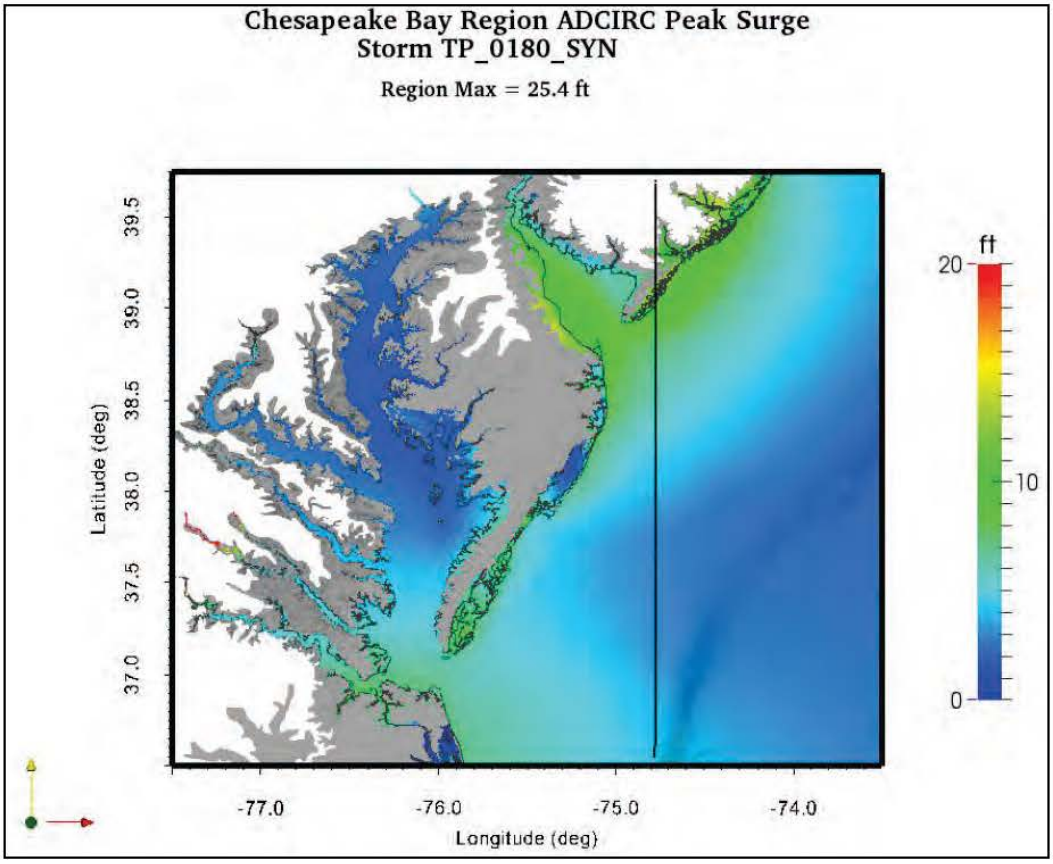

Figure 8-10. Chesapeake Bay STWAVE significant wave heights contour plot for synthetic tropical storm number 180.

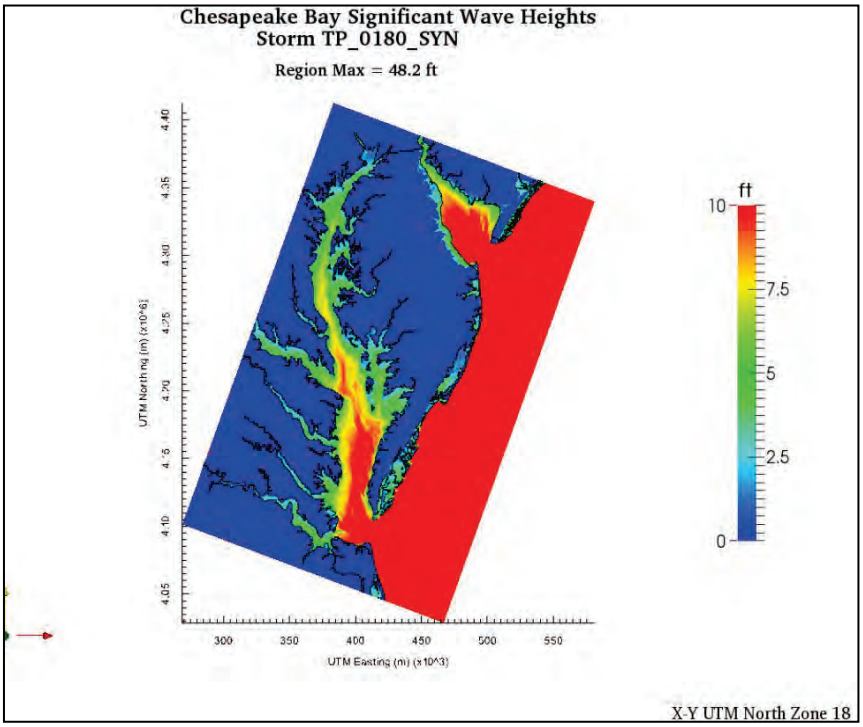

Figure 8-11. Chesapeake Bay STWAVE peak wave periods contour plot for synthetic tropical storm number 180.

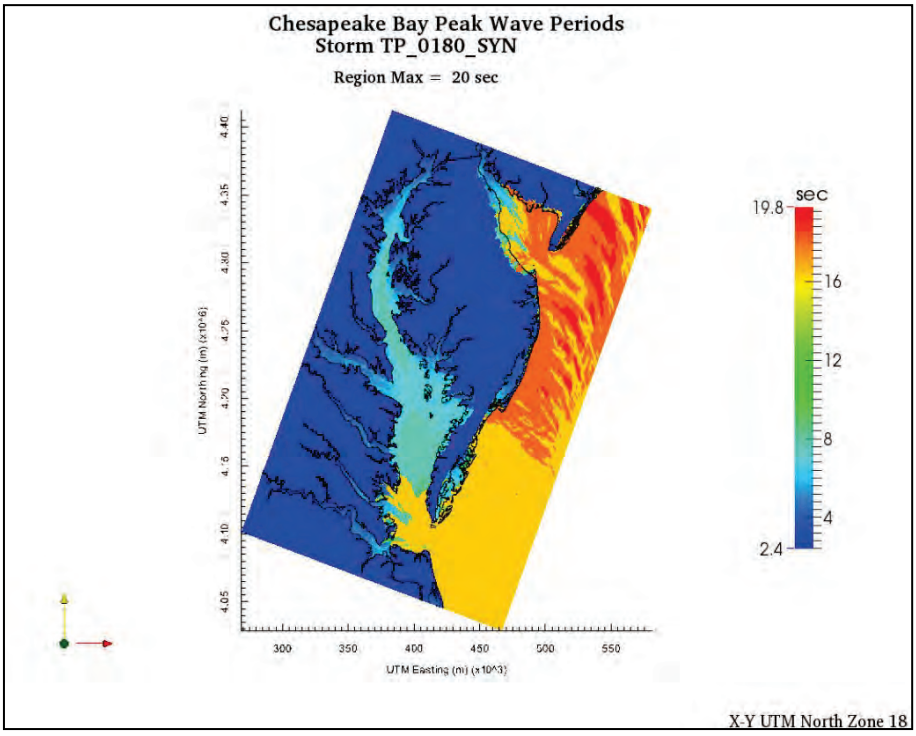

One additional run-specific ParaView Python batch script is automatically generated to create one overview plot of the maximum significant wave heights (Hs) for all 10 STWAVE grids. The image provides insight on wave results for the entire project area produced by all of the STWAVE grids. Figure 8-12 shows an example of this contour plot for synthetic tropical storm number 180. Graphics generated from individual STWAVE grids are rendered from south to north, overlaying the previously rendered images in the overlap regions. Recall that STWAVE results in the overlap regions are selected based on maximum radiation stress gradients in the CSTORM-MS computations, which is not reflected in these static diagnostic images.

8.6.3 CSTORM-PVz script execution workflow and parallelization

The ParaView Python scripts are executed and controlled by two PBS scripts (one for ADCIRC and one for STWAVE) along with supplemental BASH shell scripts. The ADCIRC PBS visualization script is submitted first and is configured to run each of the ParaView Python scripts in parallel (14 total with 2 scripts for each region), with each script using 16 CPUs. The STWAVE PBS script is submitted after the ADCIRC PBS script. This script in combination with separate BASH shell scripts assembles the needed STWAVE files for each grid into temporary folders. The maximum overall snaps of significant wave heights and peak wave periods are extracted for each STWAVE grid in parallel. These peak files are then moved to the "vizout" folder and appended to the grid-specific STWAVE VTK format file. All these tasks are performed in parallel. Once these tasks are completed, the four ParaView Python batch scripts for each STWAVE grid, and the final script to plot the overview of maximum wave heights contours for all grids, are executed in parallel, each using 16 CPUs.

Figure 8-12. STWAVE peak wave heights combined overview contour plot for Synthetic Tropical Storm Number 180.

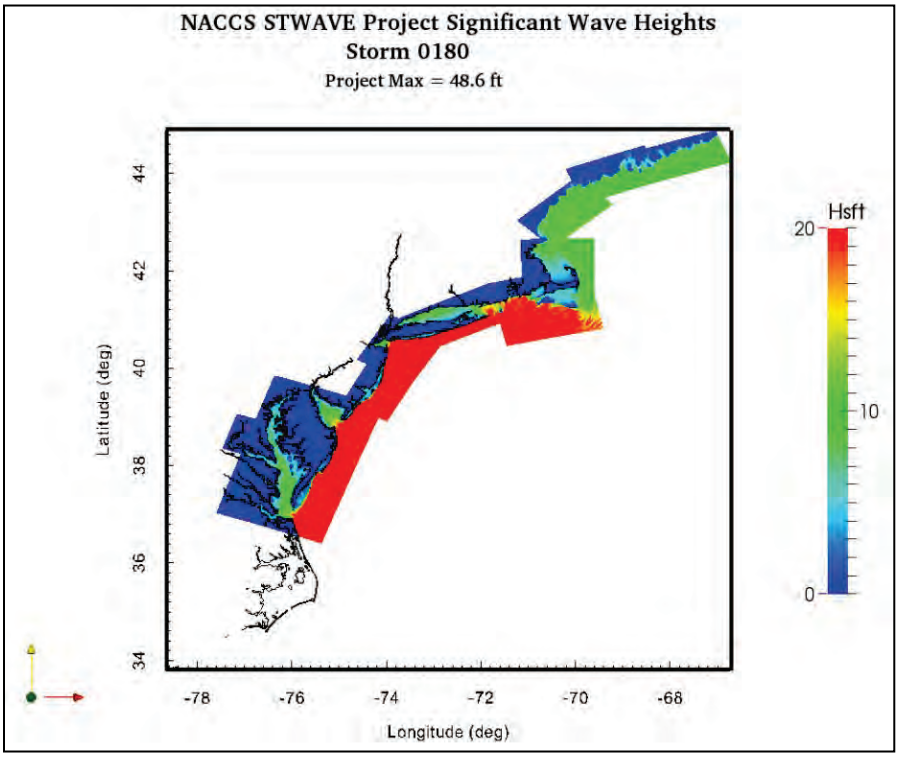

8.6.4 CSTORM-PVz reports and tar files creation

Once both the ADCIRC and STWAVE graphic products are created, a final Python script is executed which compiles all graphics and diagnostics text files into a report in PDF format. These individual storm reports are collected and reviewed for all NACCS storms as part of the full QA/QC process. Following creation of the PDF report, all files are compressed and collected into appropriate TAR files for archiving.

8.6.5 CSTORM-PVz QA/QC data and reports

In addition to the graphic products, the CSTORM-PVz scripts perform automated simulation completion diagnostics for QA/QC of all storms. The diagnostics include an indication of a successfully completed simulation, tabulation of maximum and minimum water levels, and for each STWAVE grid, wave heights and peak wave periods.

ADCIRC information includes the total number of wet nodes and the maximum, minimum, and mean water levels. The time-to-peak maximum is also extracted, and the average times of wetting are computed for nodes greater than 15, 20, 25, 30, and 35 ft. The latitude and longitude location

of the maximum water level over the entire simulation is also listed in the report. A sample of ADCIRC information is shown in Figure 8-13.

Figure 8-13. Example ADCIRC QA/QC diagnostics and information.

ADCIRC Grid/Run/Info			Mean Time to Peak (Hours)		
Total Number of Nodes	=	3110470			
Number of Wet Nodes	=	1581649	100.1		
Maximum maxeta (feet)	=	22.8826	0		
Minimum maxeta (feet)	=	0.3576	40.9		
Mean maxeta (feet)	=	4.9455	100.1		
Number Nodes maxeta > 15 ft	=	2107	39.4		
Number Nodes maxeta > 20 ft	=	57	79.5		
Number Nodes maxeta > 25 ft	=	0	0		
Number Nodes maxeta > 30 ft	=	0	0		
Number Nodes maxeta > 35 ft	=	0	0		
Location of maxeta	=	927289	-77.151	37.889	-5.00

STWAVE diagnostics information includes the maximum peak wave height over the entire storm event over the entire grid domain, along with the maximum and minimum average wave heights. Additionally, the percent of "Final Convergence Sweeps" (%FCS) over all snaps is listed to ascertain model convergence. Example STWAVE diagnostics information is shown in Figure 8-14.

Figure 8-14. Example STWAVE QA/QC diagnostics and information.

SIM	Max Max Wave Ht	Max Avg Wave Ht	Min Avg Wave Ht	%FCS
EMA.sim	11.2	5.0	2.5	100.0
CME.sim	13.9	5.2	2.2	100.0
SMA.sim	31.2	12.6	5.0	100.0
SME.sim	14.5	7.7	3.1	100.0
LID.sim	40.5	11.2	3.1	100.0
NNJ.sim	45.0	19.2	4.5	100.0
NME.sim	14.8	6.5	2.9	100.0
WDC.sim	3.6	0.2	0.1	96.9
CNJ.sim	48.2	22.1	4.0	100.0
CPB.sim	48.4	8.3	1.3	100.0

8.7 CSTORM-MS base simulations

The original scope of work considered 1000 production storms to be simulated, analyzed, and incorporated into the CHS. This included 900 synthetic tropical storms and 100 historical extratropical events. However, the NACCS team included an additional 150 synthetic tropical storms to fill out the statistical parameter space more completely and to allow for a 5% loss rate if some storms did not run to completion, meaning that a 95% completion rate would be sufficient for performing statistical analysis. The final total number of storms to be simulated (1150) then included 1050 synthetic tropical storms and 100 historical extratropical events.

To maintain organization of the thousands of simulations being run, several Excel spreadsheets were created using Google docs which allowed for the members of the production team to edit and share simulation status information in one location. The two main spreadsheets were for the (1) 100 extratropical storm simulations and (2) 1050 tropical storm simulations with each spreadsheet including the three forcing conditions (base, with tide, and with tide/sea level change). These spreadsheets allowed the production team leader to organize the run assignments to members of the NACCS team and create columns to mark completion of each step for every simulation with the date completed. Up to six members of the NACCS team were assigned storms to run at a given time. Organization was imperative for this project when coordinating completion of over 3000 simulations in order to prevent duplication of efforts and aid in minimization of errors.

After receipt of the 1150 wind and pressure fields from OWI, production began with the storm wind and pressure fields applied to the *base* condition. Base conditions were run on the HPC Garnet CRAYXE6 within a special *nonpurge* area of 175 Tb allocated specifically for the NACCS team. The base condition simulations do not include tides, river inflows, or sea level change. All 100 historical extratropical and 1031 of the 1050 synthetic tropical storm simulations were successfully completed. The successful completion of a simulation is verified by assuring that the simulation *log file* exists and checking it for errors and that peak water level and wave files have been created. In addition, the visualization tool developed for this study is used in the postprocessing phase as part of the quality control process and involved inspecting the 55 plots created for each of the simulations for any *abnormalities*.

After a simulation successfully completed, it was necessary to clean and compress all model input files and model results in order to maintain enough disk space to run the remaining simulations. A single storm simulation would typically require approximately 300 GB of disk space, and with limited space on Garnet, it was not feasible to store all the simulations and files on the machine at one time. To clean the nonpurge area on Garnet, a script was created to remove files that were only temporarily needed and not required for permanent storage for a simulation (e.g., the ADCIRC grid that was common to all simulations). Subsequent to the cleaning procedure, a compression script was submitted to zip or compress the remaining model result files thus creating more usable disk space. The clean and compress log file was then checked for successful completion and errors. The additional tar and archive scripts would then run after the completion of compression, to combine and store the files, respectively. Once again the log file is checked for successful completion and errors. The number of files and file sizes archived (on the HPC Gold storage utility) are then compared to the number of files and file sizes on Garnet to make sure that all files for each simulation are properly stored. The steps described here for processing and postprocessing model simulations were completed for all 3000+ model simulations.

8.8 CSTORM-MS With Tides simulations and With Tides and Sea Level Change simulations

In order to complete the With Tide and With Tide and SLC simulations, the production team explored other means for increasing production throughput. Allowances were made to grant the NACCS production team access to special computational resources to complete these two sets of 1150 storm simulations in an efficient manner. The With Tide condition simulations include tides and river inflows. Details about the river inflows are in Chapter 6. The total With Tide simulations completed were 1114 of the 1150 storms received. The With Tide and SLC conditions include tides, river inflows, and a 1 m increase in sea level. The total With Tide and SLC simulations completed were 1084 of the 1150 storms received.

9 Summary

This chapter summarizes the application of a suite of high-fidelity numerical models for the NACCS. The effort was conducted to provide information for computing the joint probability of coastal storm forcing parameters for the North Atlantic Coast of the United States because this information is critical for effective flood risk management project planning, design, and performance evaluation. The numerical modeling study was performed using the high-fidelity models within the CSTORM-MS. The NACCS numerical modeling study produced nearshore wind, wave, and water level estimates and the associated marginal and joint probabilities. Documentation of the statistical evaluation is provided in a companion report (Nadal-Caraballo et al., in preparation).

The first major step in the numerical modeling effort was to select a suite of storms to simulate that are statistically significant to the region of interest. The NACCS coastal region is primarily affected by tropical, extratropical, and transitional storms. It is common to group the storms into statistical families of tropical and extratropical with transitional storms that were once tropical being mostly categorized as tropical. In this study, both tropical and extratropical storms were strategically selected to characterize the regional storm hazard. Extratropical storms were selected using the method of Nadal-Caraballo and Melby (2014) using an observation screening process. The tropical storm suite was developed using a modified version of the JPM methodology (Ho and Myers 1975) with optimized sampling (JPM-OS) methods from Resio et al. (2007) and Toro et al. (2010). In this process, synthetic tropical storms are defined from a JPM of tropical cyclone parameters. The cyclone parameters describe the storm size, intensity, location, speed, and direction. This approach to statistical sampling is specifically designed to produce coastal hydrodynamic responses that efficiently span practical parameter and probability spaces to the study area.

With the storms selected, OWI generated extratropical wind and pressure fields for the 100 historical extratropical events identified in the storm selection process for the NACCS effort for two working grids: the original WIS Level II domain as well as a 0.125 deg domain covering 36 deg to 45 deg N and 78 deg to 66 deg W (NACCS domain covering Virginia to

Maine). OWI performed a reanalysis of the storm core of winds generating the maximum ocean response and included the assessment/assimilation of coastal station data such as National Weather Service reporting stations and National Ocean Service stations not considered as part of the WIS effort. Background fields were sourced from the NCEP/NCAR reanalysis for the 1948–2012 periods, preserving the enhancements applied in the WIS effort. Storms prior to 1948 were developed from the NCEP 20th Century Reanalysis project. Matching pressure fields on both grids were sourced from reanalysis products and interpolated onto the WIS/NACCS grids. Each extratropical storm event produced by OWI contains 8 days of wind/pressure fields with the majority of the reanalysis effort concentrated on the coastal domain of the storm with high wind forcing.

In addition to the extratropical storm wind and pressure fields developed by OWI for the NACCS study, OWI provided developmental support and analysis associated with the generation of synthetic tropical storm wind and pressure fields. ERDC provided OWI with storm parameters associated with 1050 tropical synthetic events, and OWI was responsible (with input from ERDC) to expand these landfall parameters into a full storm track time history for each event. The development of a track path both pre- and postlandfall followed the same basic methodology as was applied in OWI's contribution to the FEMA Region IV Georgia/North Florida Surge Study. Storm speed remained constant for the storm duration by applying the landfall speed specification supplied by ERDC. Postlandfall, the storm heading was preserved for a suitable amount of time (usually 24 hours) to allow sufficient spin-down time for the response (surge and wave) models. Prior to landfall, an analysis of mean track paths for three regional stratifications supplied by ERDC was evaluated to recommend a suitable turning rate (by stratification, if needed) of storm heading so that synthetic track paths were consistent with the historical record. Generation of synthetic tropical storm wind and pressure fields from 3–5 days prior to landfall/closest approach to 1 day postlandfall was accomplished with a tropical PBL model. Wind (WIN) and pressure (PRE) output files of 10 m wind and sea level pressures were made on two target grids. The same WIS Level II and NACCS domains described in the extratropical wind and pressure field development were applied with the synthetic tropical storms.

With the storms selected and wind and pressure fields generated, the next major step was to apply CSTORM-MS to each event because this system

provides a comprehensive methodology to simulate coastal storms and produce accurate surge and waves in the coastal zone. CSTORM-MS was applied with WAM for producing offshore deep water waves mainly intended for providing boundary conditions to the nearshore steady-state wave model STWAVE, ADCIRC to simulate the surge and circulation response to the storms, and STWAVE to provide the nearshore wave conditions including local wind-generated waves. The CSTORM-MS coupling framework options used for the NACCS numerical modeling study tightly links the ADCIRC and STWAVE models in order to allow for dynamic interaction between surge and waves. Each model was validated separately prior to going into production mode.

An evaluation was conducted to assess the quality of the offshore wave model WAM estimates for several historical extratropical and tropical events. The testing also provided a means to evaluate the grid system, model resolutions, and forcing conditions. Validation was conducted by simulating 5 tropical and 17 extratropical storms based on high water level measurements and extreme wave-dominated events and comparing to measured wave conditions for each event. The wave model results were evaluated at as many as 30 point-source measurements in the Atlantic basin. The evaluation consisted of time, scatter, Q-Q graphics, and a battery of statistical tests performed at each site for each grid level and for each of the 22 selected storm events. These results indicated that WAM provided high-quality wave estimates compared to the measurement sites. From these tests, the need to initiate the Level 1 WAM historic storm simulations at a minimum of 10 days prior to the occurrence of the storm peak was also determined. This assured the nearshore wave climate contained sufficient far-field wave energy generated by synoptic-scale events in the entire Atlantic Ocean basin. The preproduction assessment also provided a means to develop and test the fully automated system, generation of boundary condition information for STWAVE, and tools for quality checking the final model results used in the production portion of the work.

The ADCIRC mesh developed for the NACCS study encompasses the western North Atlantic, the Gulf of Mexico and the western extent of the Caribbean Sea with 3.1 million computational nodes and 6.2 million elements. Validation of this mesh was accomplished by comparisons of model simulated water levels to NOAA/NOS-measured water-surface elevations. Model validation was conducted with the analysis of a long-term tidal simulation as well as five tropical and two extratropical storm events.

From the harmonic analysis conducted for the long-term simulation, it was determined that the model accurately predicts response to tidal forcing. Model accuracy was tested for the seven validation storm events and showed that the model agreed with measured water-surface elevations (time-series and high-water marks) at measurement locations throughout the study domain. Model accuracy was a function of the quality of the ADCIRC mesh, the accuracy of the bathymetry within the mesh, the representation of bottom friction characterized in the model, and the accuracy of the wind forcing. Small differences in modeled and measured water surface elevations for the validation storms are attributed to these factors.

Nearshore wave transformation for the NACCS was accomplished using the spectral wave model STWAVE applied to 10 domains encompassing coastal Virginia to Maine. Prior to the production phase, STWAVE results were evaluated against measurements for the same five tropical and two extratropical storms used in the evaluation of ADCIRC. The evaluation consisted of time, scatter, Taylor diagrams, and a suite of statistics. Comparisons were most favorable for the most recent storms, likely due to development of more accurate wind and offshore forcing, more advanced buoy technology, and a larger measurement population size in recent time. STWAVE was also more accurate in estimating wave height than mean wave period. Although some sites did demonstrate persistently poor performance, STWAVE provided overall good wave estimates compared to measurement sites given the large extent and complexity of the model region.

Once the models were validated, NACCS production began on the suite of 1150 storms for three conditions. With the 3450 CSTORM-MS simulation requirement, a semiautomated process was needed to efficiently and accurately set up and execute this large simulation suite. Therefore, semiautomated production scripts for setting up CSTORM-MS simulations (CSTORM-PS) were created, tested, and verified for historical extratropical storms, historical tropical storms, and synthetic tropical storms and were executed for all production simulations. Because of the magnitude of this study, a visualization component (CSTORM-PVz) was created within the CSTORM-MS framework, and automation scripts were generated to produce graphics, descriptive statistics, and digital reports for all NACCS results.

Products of this study are intended to close data gaps required for flood risk management analyses by providing statistical wave and water level information for the North Atlantic Coast (NAC) within the CHS. The CHS is expected to provide cost and study-time efficiencies and a level of regional standardization for project studies compared to developing individual, project-specific coastal storm hazard information as is the current practice. The CSTORM-MS platform provides the raw model data (winds, waves, and water levels) as well as processed data (visualization products and statistics), which are available through the internet-based CHS. These data are available for engineering analyses and project design for coastal projects from Maine to Virginia.

References

Adams, J. C., W. S. Brainerd, J. T. Martin, B. T. Smith, and J. L. Wagener. 1992. *FORTRAN 90 handbook: Complete ANSI/ISO reference*. New York, NY: Intertext Publications, McGraw-Hill Book Company.

ADCIRC (2014) *User's manual*. http://adcirc.org.

Bender, C., J. M. Smith, A. Kennedy, and R. Jensen. 2013. STWAVE simulation of Hurricane Ike: Model results and comparison to data. *Coastal Engineering* 73: 58–70.

Bunya, S., J. Westerink, J. C. Dietrich, H. J. Westerink, L. G. Westerink, J. Atkinson, B. Ebersole, J. M. Smith, D. Resio, R. Jensen, M. A. Cialone, R. Luettich, C. Dawson, H. J. Roberts, and J. Ratcliff. 2010. A high-resolution coupled riverine flow, tide, wind, wind wave and storm surge model for Southern Louisiana and Mississippi: Part I-Model development and validation. *Monthly Weather Review* 138:345–377.

Cardone, V. J., C. V. Greenwood, and J. A. Greenwood. 1992. *Unified program for the specification of hurricane boundary layer winds over surfaces of specified roughness*. Contract Report CERC-92-1. Vicksburg, MS: U.S. Army Engineer Research and Development Center.

Cardone, V. J., and J. A. Greenwood. 1993. *Final report: Development and initial test against SWADE of an interactive objective kinematic analysis program for marine surface wind field analysis*. Submitted to U.S. Army Engineer Research and Development Center, Vicksburg, MS.

Cardone, V. J., R. E. Jensen, D. T. Resio, V. R. Swail, and A. T. Cox. 1996. Evaluation of contemporary ocean wave models in rare extreme events: the "Halloween Storm" of October 1991 and the "Storm of the Century" of March 1993. *Journal of Atmospheric and Oceanic Technology* 13:198–230.

Cox, A. T., J. A. Greenwood, V. J. Cardone, and V. R. Swail. 1995. An interactive objective kinetic analysis system. In *The 4th International Workshop on Wave Hindcasting and Forecasting, Banff, Alberta, Canada*.

Dietrich, J. C., J. J. Westerink, A. B. Kennedy, J. M. Smith, R. Jensen, M. Zijlema, L. H. Holthuijsen, C. Dawson, R. A. Luettich, Jr., M. D. Powell, V. J. Cardone, A. T. Cox, G. W. Stone, H. Pourtaheri, M. E. Hope, S. Tanaka, L. G. Westerink, H. J. Westerink, Z. Cobell. 2011. Hurricane Gustav (2008) waves, storm surge and currents: Hindcast and synoptic analysis in Southern Louisiana. *Monthly Weather Review* 139:2488–2522.

Dietrich, J. C., S. Bunya, J. J. Westerink, B. A. Ebersole, J. M. Smith, J. H. Atkinson, R. Jensen, D. T. Resio, R. A. Luettich, C. Dawson, V. J. Cardone, A. T. Cox, M. D. Powell, H. J. Westerink, and H. J. Roberts. 2010. A high-resolution coupled riverine flow, tide, wind, wind wave and storm surge model for Southern Louisiana and Mississippi: Part II-Synoptic description and analysis of Hurricanes Katrina and Rita. *Monthly Weather Review* 138:378–404.

Federal Emergency Management Agency (FEMA). 2012. *Operating guidance No. 8-12 for use by FEMA staff and flood mapping partners: Joint probability – optimal sampling method for tropical storm surge*. Washington, DC: Federal Emergency Management Agency, U.S. Department of Homeland Security.

———. 2014. *Region II storm surge project–Joint probability analysis of hurricane and extratropical flood hazards*. Federal Emergency Management Agency, U.S. Department of Homeland Security, Washington DC.

Flather, R. A. 1988. A numerical model investigation of tides and diurnal-period continental shelf waves along Vancouver Island. *Journal of Physical Oceanography* 18:115–139.

Garratt, J. R. 1977. Review of drag coefficients over oceans and continents. *Monthly Weather Review 105:*915–929.

Gunkel, B. L., T. O. McAlpin, and N. C. Nadal-Caraballo. 2015. North Atlantic coast comprehensive study (NACCS) storm simulation and statistical analysis: Part V – River inflows. In *Coastal Sediments Conference, San Diego, CA, 2015*.

Hagen, S. C., J. J. Westerink, R. L. Kolar, and O. Horstmann. 2001. Two-dimensional, unstructured mesh generation for tidal models. *International Journal for Numerical Methods in Fluids* 35:669–686.

Hasselmann, K., T. P. Barnett, E. Bouws, H. Carlson, D. E. Cartwright, K. Enke, J. A. Ewing, H. Gienapp, D. E. Hasselmann, P. Kruseman, A. Meerburg, P. Muller, D. J. Olbers, K. Richter, W. Sell, and H. Walden. 1973. Measurement of wind-wave growth and swell decay during the Joint North Sea Wave Project (JONSWAP). *Deutches Hydrographisches Institut Suppl. A* 8(12):1–95

Hesser, T. J., M. A. Cialone, and M. E. Anderson. 2013. *Lake St. Clair: Storm wave and water level modeling*. ERDC/CHL TR-13-5. Vicksburg, MS: U.S. Army Engineer Research and Development Center.

Ho, F. P., and V. A. Myers. 1975.. NOAA Technical Report NWS 18. Washington, DC: National Weather Service.

Holland, G. J. 1980. An analytic model of the wind and pressure profiles in hurricanes. *Monthly Weather Review* 108(8):1212–1218.

Holthuijsen, L. H. 2007. *Waves in ocean and coastal waters*. United Kingdom: Cambridge University Press.

Hope, M. E., J. J. Westerink, A. B. Kennedy, P. C. Kerr, J. C. Dietrich, C. Dawson, C. Bender, J. M. Smith, R. E. Jensen, M. Zijlema, L. H. Holthuijsen, R. A. Luettich, M. D. Powell, V. J. Cardone, A. T. Cox, H. Pourtaheri, H. J. Roberts, J. H. Atkinson, S. Tanaka, H. J. Westerink, and L. G. Westerink. 2013. Hindcast and validation of Hurricane Ike (2008) waves, forerunner, and storm surge. *Journal of Geophysical Research* 118(9):4424–4460.

Interagency Performance Evaluation Task Force. (IPET). 2009. *Performance evaluation of the New Orleans and Southeast Louisiana hurricane protection system*. Final Report of the Interagency Performance Evaluation Task Force. Washington, DC: Department of the Army, U.S. Army Corps of Engineers.

Irish, J. L., B. P. Williams, A. Militello, and D. J. Mark. 2005. Regional-scale storm-surge modeling of Long Island, New York, USA. In *29th International Conference on Coastal Engineering, Lisbon, Portugal*, 1565–1577.

Jensen, R. E., M. A. Cialone, R. S. Chapman, B. A. Ebersole, M. E. Anderson, and L. Thomas. 2012. *Lake Michigan: Storm wave and water level modeling.* ERDC/CHL TR-12-26. Vicksburg, MS: U.S. Army Engineer Research and Development Center.

Jonsson, I. G. 1990. Wave-current interactions. In *The Sea*, Chapter 3, Vol. 9, Part A, B, ed. LeMehaute and D. M. Hanes. New York: John Wiley & Sons, Inc.

Kolar, R. L., W. G. Gray, J. J. Westerink, and R. A. Luettich. 1994. Shallow water modeling in spherical coordinates: Equation formulation, numerical implementation, and application. *Journal of Hydraulic Research* 32(1):3–24.

Komen, G. J., L. Cavaleri, M. Donelan, K. Hasselmann, S. Hasselmann, and P. A. E. M. Janssen. 1994. *Dynamics and modeling of ocean waves*. United Kingdom: Cambridge University Press.

Landsea, C. W., and J. L. Franklin. 2013. Atlantic hurricane database uncertainty and presentation of a new database format. *Monthly Weather Review* 141(10):3576–3592.

Luettich, R. A., Jr., J. J. Westerink, and N. W. Scheffner. 1992. *ADCIRC: An advanced three-dimensional circulation model for shelves, coasts, and estuaries*. Technical Report DRP-92-6. Vicksburg, MS: U.S. Army Engineer Research and Development Center.

Massey, T. C., T. V. Wamsley, and M. A. Cialone. 2011a. Coastal storm modeling – System integration. In *Proceedings of the 2011 Solutions to Coastal Disasters Conference, Anchorage, Alaska*, 99–108.

Massey, T. C., M. E. Anderson, J. M. Smith, J. Gomez, and R. Jones. 2011b. *STWAVE: Steady-state spectral wave model user's manual for STWAVE, ersion 6.0*. ERDC/CHL SR-11-1. Vicksburg, MS: U.S. Army Engineer Research and Development Center.

Mei, C. C. 1989. *The applied dynamics of ocean surface waves*. Singapore: World Scientific Publishing.

Message Passing Interface (MPI). 2014. http://www.mcs.anl.gov/research/projects/mpi/index.htm

Miche, M. 1951. Le pouvoir reflechissant des ouvrages maritimes exposes a l'action de la houle. *Annals des Ponts et Chaussess* 121e Annee, 285–319. Translated by Lincoln and Chevron. University of California, Berkeley: Wave Research Laboratory, Series 3, Issue 363, June 1954.

Nadal-Caraballo, N. C., J. A. Melby, and B. A. Ebersole. 2012. *Statistical analysis and storm sampling approach for Lakes Michigan and St. Clair*. ERDC/CHL TR-12-19. Vicksburg, MS*:* U.S. Army Engineer Research and Development Center.

Nadal-Caraballo, N. C., and J. A. Melby. 2014. *North Atlantic Coast comprehensive study – phase I: Statistical analysis of historical extreme water levels with sea level change*. ERDC/CHL TR-14-7. Vicksburg, MS: U.S. Army Engineer Research and Development Center.

Nadal-Caraballo, N. C., J. A. Melby, V. M. Gonzalez, and A. T. Cox. In preparation. *North Atlantic coast comprehensive study – Coastal storm hazards from Virginia to Maine*. ERDC/CHL Technical Report. Vicksburg, MS: U.S. Army Engineer Research and Development Center.

Oceanweather, Inc. 2014. *Development of wind and pressure forcing for the North Atlantic Coast comprehensive study (NACCS).* Submitted to U.S. Army Engineer Research and Development Center, Vicksburg, MS.

Padilla-Hernandez, R., and J. Monbaliu. 2001. Energy balance of wind-waves as a function of the bottom friction formulation. *Coastal Engineering* 43:131–148.

Phillips, O. M. 1957. On the generation of waves by turbulent wind. *Journal of Fluid Mechanics* 2:417–465.

Pierson, W. J., and L. Moskowitz. 1964. A proposed spectral form for fully developed wind seas based on the similarity theory of S.A. Kitaigorodskii. *Journal of Geophysical Research* 69:5181–5190.

Resio, D. T. 1987. Shallow-water waves. I: Theory. *Journal of Waterway, Port, Coastal, and Ocean Engineering* 113(3):264–281.

Resio, D.T. 1988. Shallow-water waves. II: Data comparisons. *Journal of Waterway, Port, Coastal, and Ocean Engineering* 114(1):50–65.

Resio, D. T., and W. Perrie. 1989. Implications of an f^{-4} equilibrium range for wind-generated waves. *Journal of Physical Oceanography* 19:193–204.

Resio, D. T., V. R. Swail, R. E. Jensen, and V. J. Cardone. 1999. Wind speed scaling in fully developed seas. *Journal of Atmospheric and Oceanic Technology* 29:1801–1811.

Resio, D. T., S. J. Boc, L. Borgman, V. Cardone, A. T. Cox, W. R. Dally, R. G. Dean, D. Divoky, E. Hirsh, J. L. Irish, D. Levinson, A. Niedoroda, M. D. Powell, J. J. Ratcliff, V. Stutts, J. Suhada, G. R. Toro, and P. J. Vickery. 2007. *White Paper on estimating hurricane inundation probabilities*. Consulting Report prepared by USACE for FEMA. Vicksburg, MS: U.S. Army Engineer Research and Development Center, Coastal and Hydraulics Laboratory.

Smith, J. M., and C. L. Vincent. 1992. Shoaling and decay of two wave trains on beach, *Journal of Waterway, Port, Coastal, and Ocean Engineering* 10(106):517–533.

Smith, J. M., A. R. Sherlock, and D. T. Resio. 2001. *STWAVE: Steady-state spectral wave model user's manual for STWAVE, version 3.0*. ERDC/CHL SR-01-1.Vicksburg, MS: U.S. Army Engineer Research and Development Center.

Smith, J. M., and Smith, S. J. 2002. *Grid nesting with STWAVE*. ERDC/CHL CHETN I-66. Vicksburg, MS: U.S. Army Engineer Research and Development Center. http://chl.wes.army.mil/library/publications/chetn/

Smith, J. M. 2007. *Full-plane STWAVE with bottom friction: II. Model overview*. ERDC/CHL CHETN-I-75. Vicksburg, MS: U.S. Army Engineer Research and Development Center.

SWAN Team. 2014. *SWAN scientific and technical documentation SWAN Cycle III version 41.01*. The Netherlands: Delft university of Technology. http://swanmodel.sourceforge.net/

Taylor, K. E. 2001. Summarizing multiple aspects of model performance in a single diagram. *Journal of Geophysical Research* 106:7183–7192. (also PCMDI Report 55, http://www-pcmdi.llnl.gov/publications/ab55.html)

Thompson, E. F. 1980. *Energy spectra in shallow U.S. coastal waters*. Technical paper No. 80-2. Fort Belvoir, VA: Coastal Engineering Research Center, U.S. Army Corps of Engineers.

Thompson, E. F., and V. J. Cardone. 1996. Practical modeling of hurricane surface wind fields. *Journal of Waterway, Port, Coastal, and Ocean Engineering* 122(4):195–205.

Tolman, H. L. 2014. *User manual and system documentation of WAVEWATCH III version 4.18*. Technical Note 316. NOAA/NWS/NCEP/ MMAB.

Toro, G. R. 2008. *Joint probability analysis of hurricane flood hazards for Mississippi – Final URS group report in support of the FEMA-HMTAP flood study of the State of Mississippi*. Boulder CO: Risk Engineering.

Toro, G. R., D. T. Resio, D. Divoky, A. W. Niedoroda, and C. Reed. 2010. Efficient joint-probability methods for hurricane surge frequency analysis. *Ocean Engineering* 37:125–134.

United States Army Corps of Engineers (USACE). 2006. *Louisiana coastal protection and restoration (LACPR) preliminary technical report*. Provided to United States Congress.

Vickery, P. J. 2005. Simple empirical models for estimating the increase in the central pressure of tropical cyclones after landfall along the coastline of the United States. *Journal of Applied Meteorology* 44:1807–1826.

Walsh, E. J., C. W. Wright, D. Vandemark, W. B. Krabill, A. W. Garcia, S. H. Houston, S. T. Murillo, M. D. Powell, P. G. Black, and F.D. Marks, Jr. 2002. Hurricane directional wave spectrum spatial variation at landfall. *Journal of Physical* Oceanography 32:1667–1684.

Wamsley, T. V., E. S. Godsey, B. W. Bunch, R. S. Chapman, M. B. Gravens, A. S. Grzegorzewski, B. D. Johnson, D. B. King, R. L. Permenter, D. H. Tillman, and M. W. Tubman. 2013. *Mississippi coastal improvement program; Evaluation of barrier island restoration efforts.* ERDC TR-13-12. Vicksburg, MS: U.S. Army Engineer Research and Development Center.

Westerink, J. J., R. A. Luettich, Jr., A. M. Baptista, N. W. Scheffner, and P. Farrar. 1992. Tide and storm surge predictions using finite element model. *Journal of Hydraulic Engineering* 118(10):1373–1390.

Westerink, J. J., R. A. Luettich, Jr., J. C. Feyen, J. H. Atkinson, C. Dawson, H. J. Roberts, M. D. Powell, J. P. Dunion, E. J. Kubatko, and H. Portaheri. 2008. A basin- to channel-scale unstructured grid hurricane storm surge model applied to southern Louisiana. *Monthly Weather Review* 136:833–864.

Willmott C. J., S. G. Ackleson, R. E. Davis, J. J. Feddema, K. M. Klink, D. R. Legates, J. O'Donnell, C. M. Rowe. 1985. Statistics for the evaluation of model performance. *Journal of Geophysical Research* 90(C5):8995–9005.

Appendix A: NACCS Historical Extratropical Cyclones

The following table lists the 100 historical extratropical cyclones that were identified for the NACCS study area. The "Number of Water Level Stations" column indicates the amount of NOAA gages where each storm was identified as a top-50 water level event. "Rank" is the highest ranking achieved by each storm's water level response at any one NOAA gage. For each storm, the "NOAA Station ID" indicates the gage where the highest response was observed, as well as the "NACCS Subregion" where each NOAA station is located.

Storm ID	yyyy	mm	dd	hh	Number of Water Level Stations	NACCS Subregion	NOAA Station ID	Rank	Water Level (m)
1	1938	1	25	13	2	3	8574680	11	1.03
2	1940	2	15	3	3	1	8443970	8	1.22
3	2010	2	6	9	4	3	8638863	17	0.97
4	1943	10	27	3	2	2	8518750	6	1.67
5	1945	11	30	8	3	1	8443970	3	1.46
6	1947	3	3	6	2	1	8443970	11	1.17
7	1950	11	25	21	4	2	8531680	1	2.50
8	1952	3	11	18	2	3	8574680	8	1.13
9	2000	12	17	21	2	3	8571892	17	0.86
10	1952	11	21	22	3	3	8594900	8	1.66
11	1953	11	7	10	4	2	8518750	10	1.40
12	1958	2	16	20	3	1	8443970	17	1.06
13	1960	2	19	7	4	1	8452660	15	0.93
14	1960	3	4	15	2	1	8443970	14	1.12
15	1961	2	4	10	4	2	8534720	10	1.12
16	1961	4	14	0	2	1	8443970	6	1.32
17	1962	3	7	6	6	3	8557380	1	1.77
18	1962	12	6	16	3	2	8534720	13	1.04
19	1964	1	13	18	4	2	8534720	9	1.12
20	1966	1	23	10	5	2	8536110	15	1.06
21	1966	1	30	16	3	2	8510560	16	1.04
22	1968	11	12	12	4	3	8557380	2	1.58
23	1970	12	17	14	4	2	8516945	16	1.66

Storm ID	yyyy	mm	dd	hh	Number of Water Level Stations	NACCS Subregion	NOAA Station ID	Rank	Water Level (m)
24	1971	3	4	16	2	1	8452660	9	1.02
25	1971	11	25	11	5	2	8531680	16	1.39
26	1972	2	4	6	3	1	8452660	11	1.00
27	1972	2	19	12	6	2	8534720	5	1.32
28	1972	11	9	2	3	2	8516945	9	1.82
29	1972	12	16	6	3	2	8510560	12	1.12
30	1973	1	29	14	2	1	8452660	14	0.94
31	1974	12	2	9	5	2	8531680	6	1.66
32	1976	2	2	10	3	1	8447930	9	0.97
33	1977	1	10	19	4	1	8447930	13	0.90
34	1977	10	14	19	2	2	8536110	14	1.06
35	1978	1	20	20	3	2	8510560	17	1.01
36	1978	1	26	18	5	3	8574680	7	1.16
37	1978	2	7	1	3	2	8510560	3	1.28
38	1978	4	26	23	2	3	8638610	7	1.23
39	1978	12	25	16	3	1	8413320	12	0.71
40	1979	1	21	23	8	1	8413320	7	0.81
41	1980	10	25	21	7	1	8454000	12	1.15
42	1982	10	25	10	2	3	8638863	4	1.22
43	1983	2	11	18	5	3	8638863	9	1.12
44	1983	3	19	6	6	3	8577330	7	0.79
45	1983	11	25	23	4	1	8413320	5	0.84
46	1983	12	12	21	4	3	8577330	10	0.70
47	1983	12	23	2	2	1	8410140	9	0.87
48	1983	12	29	3	3	1	8454000	7	1.29
49	1984	2	29	5	3	1	8413320	16	0.68
50	1984	3	29	21	4	1	8449130	3	1.03
51	1985	2	13	1	6	3	8574680	17	0.98
52	1985	11	5	7	6	3	8577330	1	1.04
53	1987	1	2	7	4	3	8557380	11	1.17
54	1987	1	23	6	9	1	8418150	3	1.05
55	1988	4	13	17	3	3	8638863	13	1.03
56	1988	11	2	12	3	1	8413320	9	0.79
57	1990	11	11	4	3	1	8413320	11	0.72
58	1991	10	30	20	9	1	8449130	1	1.41
59	1992	1	4	16	3	3	8577330	9	0.71
60	1992	12	11	22	4	2	8516945	2	2.26
61	1993	3	5	1	4	3	8571892	10	0.88
62	1993	3	14	0	6	2	8510560	2	1.29

Storm ID	yyyy	mm	dd	hh	Number of Water Level Stations	NACCS Subregion	NOAA Station ID	Rank	Water Level (m)
63	1993	11	28	15	5	3	8571892	4	0.98
64	1993	12	21	22	2	1	8413320	8	0.80
65	1994	1	4	13	5	2	8536110	7	1.11
66	1994	3	2	23	7	2	8531680	2	2.23
67	1994	12	24	12	4	2	8516945	4	2.00
68	1995	2	5	0	4	1	8418150	5	0.94
69	1995	11	15	3	4	2	8516945	10	1.73
70	1996	1	8	6	7	2	8536110	1	1.54
71	2003	10	15	16	2	1	8413320	17	0.68
72	1996	10	20	2	3	2	8516945	14	1.69
73	1996	12	8	11	3	1	8418150	9	0.83
74	1997	1	10	9	5	1	8454000	15	1.08
75	1997	4	19	12	2	1	8449130	9	0.95
76	1998	1	28	21	4	3	8638863	3	1.36
77	1998	2	5	1	8	3	8557380	3	1.53
78	2000	1	25	12	4	3	8638863	10	1.10
79	2001	3	7	10	3	1	8449130	11	0.93
80	2003	12	11	13	4	3	8577330	15	0.70
81	2003	12	18	5	4	1	8418150	10	0.83
82	2006	10	7	6	2	3	8638863	15	0.99
83	2006	10	28	19	6	1	8454000	11	1.16
84	2006	11	17	1	4	3	8575512	13	0.90
85	2006	11	22	17	2	3	8638863	6	1.15
86	2007	4	16	5	7	1	8454000	8	1.24
87	2008	5	12	4	6	3	8577330	5	0.87
88	2008	12	22	5	2	1	8410140	2	0.97
89	2009	11	13	2	5	3	8638863	1	1.57
90	2009	12	9	22	3	1	8418150	16	0.78
91	2009	12	19	18	5	3	8638863	11	1.09
92	2009	12	26	10	5	3	8577330	16	0.69
93	2010	2	26	4	7	1	8443970	1	1.84
94	2010	3	13	7	3	3	8594900	10	1.52
95	2010	10	1	4	2	3	8577330	14	0.70
96	2010	10	15	13	2	1	8418150	11	0.82
97	2010	12	27	6	6	1	8418150	14	0.80
98	2011	4	17	3	4	3	8571892	6	0.95
99	2012	12	21	12	6	3	8571892	3	1.09
100	2012	12	27	7	4	2	8516945	12	1.72

Substitute historical extratropical storms for OWI generation of wind and pressure fields.

Storm ID	yyyy	mm	dd	hh	Number of Water Level Stations	Region	Station ID	Rank	Water Level (m)
101	2010	2	6	9	4	3	8638863	17	0.97
102	2000	12	17	21	2	3	8571892	17	0.86
103	2003	10	15	16	2	1	8413320	17	0.68
104	1960	12	12	8	2	3	8557380	18	1.09
105	1990	10	26	11	2	3	8638863	18	0.96
106	1988	10	22	17	3	1	8418150	18	0.76
107	1977	3	23	1	2	2	8516945	19	1.53
108	2011	1	12	18	3	1	8413320	19	0.67
109	1986	12	3	1	2	3	8577330	19	0.66
110	2008	2	14	0	2	1	8454000	20	1.02
111	1998	3	9	16	4	3	8574680	20	0.93
112	1942	12	2	8	2	1	8452660	20	0.90
113	1942	12	30	22	3	3	8575512	20	0.81
114	2010	1	25	20	5	3	8577330	20	0.65
115	1969	12	27	11	3	1	8443970	21	1.04
116	2011	3	11	1	5	3	8574680	21	0.92
117	1951	3	14	17	4	3	8575512	21	0.80
118	2005	4	3	0	3	3	8577330	21	0.65
119	2007	12	16	18	2	2	8516945	22	1.51
120	1961	2	26	3	3	3	8594900	22	1.18
121	1942	3	3	13	2	1	8461490	22	1.02
122	2009	3	2	10	3	2	8534720	22	0.96
123	1983	4	3	8	3	3	8571892	22	0.81
124	1982	4	7	0	2	1	8449130	22	0.81
125	1998	2	25	10	4	1	8410140	22	0.74

Appendix B: Synthetic Tropical Cyclone Master Tracks

Following are the 130 master tracks developed for the NACCS synthetic tropical cyclones.

Master Track ID	NACCS Subregion	Heading Direction, θ (deg)	Reference Latitude (deg North)	Reference Longitude (deg West)
1	3	-60	34.05	74.18
2	3	-60	34.39	73.57
3	3	-60	34.89	73.30
4	3	-60	35.64	73.57
5	3	-60	36.22	73.48
6	3	-60	36.65	73.09
7	3	-60	37.08	72.71
8	3	-60	37.74	72.81
9	2	-60	38.06	72.19
10	2	-60	38.52	71.73
11	2	-60	39.07	71.50
12	2	-60	39.49	70.96
13	2	-60	39.71	69.97
14	2	-60	40.12	69.42
15	2	-60	40.19	68.12
16	1	-60	40.53	67.40
17	1	-60	41.49	68.00
18	1	-60	42.16	67.94
19	1	-60	42.66	67.48
20	1	-60	42.90	66.42
21	1	-60	43.21	65.53
22	1	-60	42.56	62.38
23	1	-60	43.02	61.82
24	1	-60	43.31	60.88
25	3	-40	33.64	74.75
26	3	-40	33.83	74.06
27	3	-40	34.67	74.08
28	3	-40	35.52	74.09
29	3	-40	36.03	73.75
30	3	-40	36.50	73.38
31	3	-40	37.52	73.59
32	2	-40	37.58	72.69
33	2	-40	38.12	72.30

Master Track ID	NACCS Subregion	Heading Direction, θ (deg)	Reference Latitude (deg North)	Reference Longitude (deg West)
34	2	-40	38.84	72.11
35	2	-40	38.97	71.29
36	2	-40	39.14	70.51
37	2	-40	39.60	70.05
38	2	-40	39.75	69.26
39	1	-40	39.89	68.44
40	1	-40	41.22	68.85
41	1	-40	41.79	68.43
42	1	-40	42.14	67.76
43	1	-40	42.30	66.88
44	1	-40	42.73	66.31
45	1	-40	42.89	65.42
46	1	-40	41.95	63.30
47	1	-40	42.33	62.67
48	1	-40	42.76	62.10
49	1	-40	42.98	61.28
50	3	-20	33.23	75.34
51	3	-20	33.64	74.82
52	3	-20	35.21	74.80
53	3	-20	35.80	74.36
54	3	-20	37.15	74.28
55	2	-20	37.26	73.55
56	2	-20	37.94	73.07
57	2	-20	38.50	72.55
58	2	-20	38.65	71.83
59	2	-20	38.84	71.14
60	2	-20	39.25	70.55
61	1	-20	39.51	69.88
62	1	-20	40.88	69.74
63	1	-20	41.57	69.23
64	1	-20	41.76	68.45
65	1	-20	42.34	67.86
66	1	-20	42.29	66.97
67	1	-20	42.51	66.22
68	1	-20	41.59	64.90
69	1	-20	41.58	64.03
70	1	-20	42.07	63.42
71	1	-20	42.33	62.67
72	3	0	32.45	76.88
73	3	0	33.11	76.10
74	3	0	35.62	75.44
75	3	0	36.79	74.78

Master Track ID	NACCS Subregion	Heading Direction, θ (deg)	Reference Latitude (deg North)	Reference Longitude (deg West)
76	2	0	37.80	74.05
77	2	0	38.43	73.31
78	2	0	38.59	72.57
79	2	0	39.06	71.84
80	2	0	39.29	71.10
81	1	0	41.33	70.30
82	1	0	41.63	69.48
83	1	0	41.90	68.66
84	1	0	42.31	67.85
85	1	0	42.52	67.04
86	1	0	42.11	66.22
87	1	0	41.23	65.41
88	1	0	41.82	64.60
89	1	0	42.22	63.78
90	1	20	45.00	70.55
91	1	20	45.00	69.60
92	1	20	45.00	68.66
93	1	20	45.00	67.71
94	1	20	45.00	66.76
95	1	20	45.00	65.82
96	1	20	45.00	64.87
97	1	20	45.00	63.93
98	2	20	41.50	74.08
99	2	20	41.50	73.25
100	2	20	41.50	72.43
101	2	20	41.50	71.60
102	2	20	41.50	70.78
103	2	20	41.50	69.95
104	2	20	41.50	69.13
105	2	20	41.50	68.30
106	2	20	41.50	67.47
107	3	20	39.00	75.37
108	3	20	39.00	74.65
109	3	20	39.00	73.94
110	3	20	39.00	73.22
111	3	20	39.00	72.51
112	3	20	39.00	71.79
113	1	40	45.00	68.33
114	1	40	45.00	67.17
115	1	40	45.00	66.01
116	1	40	45.00	64.85
117	1	40	45.00	63.69

Master Track ID	NACCS Subregion	Heading Direction, θ (deg)	Reference Latitude (deg North)	Reference Longitude (deg West)
118	1	40	45.00	62.53
119	2	40	41.50	72.55
120	2	40	41.50	71.54
121	2	40	41.50	70.53
122	2	40	41.50	69.51
123	2	40	41.50	68.50
124	2	40	41.50	67.49
125	3	40	39.00	74.90
126	3	40	39.00	74.03
127	3	40	39.00	73.15
128	3	40	39.00	72.27
129	3	40	39.00	71.40
130	3	40	39.00	70.52

Appendix C: NACCS Synthetic Tropical Cyclones

Following is a list of the 1,050 synthetic tropical cyclones that were developed for the NACCS study area. Storm parameters assigned to each cyclone include heading direction, θ; central pressure deficit, Δp; radius of maximum winds RMW; and forward speed, V_f.

NACCS Synthetic Tropical Cyclone ID	NACCS Subregion	Master Track ID	θ (deg)	Δ*P* (hPa)	R_{max} (km)	V_f (km/h)
1	3	1	-60	88	39	18
2	3	1	-60	78	108	29
3	3	1	-60	68	62	42
4	3	1	-60	58	47	32
5	3	1	-60	48	64	12
6	3	1	-60	38	72	19
7	3	1	-60	28	26	39
8	3	2	-60	88	114	25
9	3	2	-60	78	51	30
10	3	2	-60	68	26	31
11	3	2	-60	58	37	12
12	3	2	-60	48	77	44
13	3	2	-60	38	72	13
14	3	2	-60	28	39	39
15	3	3	-60	88	105	24
16	3	3	-60	78	50	30
17	3	3	-60	68	39	12
18	3	3	-60	58	26	29
19	3	3	-60	48	82	44
20	3	3	-60	38	68	15
21	3	3	-60	28	42	40
22	3	4	-60	88	50	40
23	3	4	-60	78	51	29
24	3	4	-60	68	107	26
25	3	4	-60	58	65	12
26	3	4	-60	48	28	34
27	3	4	-60	38	37	13
28	3	4	-60	28	75	38
29	3	5	-60	88	77	37
30	3	5	-60	78	35	26
31	3	5	-60	68	62	12

NACCS Synthetic Tropical Cyclone ID	NACCS Subregion	Master Track ID	θ (deg)	Δ*P* (hPa)	R_{max} (km)	V_f (km/h)
32	3	5	-60	58	109	25
33	3	5	-60	48	49	25
34	3	5	-60	38	58	40
35	3	5	-60	28	25	35
36	3	6	-60	88	72	31
37	3	6	-60	78	38	27
38	3	6	-60	68	53	35
39	3	6	-60	58	105	28
40	3	6	-60	48	64	14
41	3	6	-60	38	25	28
42	3	6	-60	28	61	46
43	3	7	-60	88	50	37
44	3	7	-60	78	78	12
45	3	7	-60	68	104	35
46	3	7	-60	58	41	12
47	3	7	-60	48	25	31
48	3	7	-60	38	48	20
49	3	7	-60	28	71	33
50	3	8	-60	88	47	18
51	3	8	-60	78	75	40
52	3	8	-60	68	104	21
53	3	8	-60	58	41	39
54	3	8	-60	48	67	36
55	3	8	-60	38	25	19
56	3	8	-60	28	58	13
57	3	25	-40	88	53	20
58	3	25	-40	78	105	21
59	3	25	-40	68	29	22
60	3	25	-40	58	73	41
61	3	25	-40	48	51	40
62	3	25	-40	38	38	36
63	3	25	-40	28	65	12
64	3	26	-40	88	54	30
65	3	26	-40	78	104	30
66	3	26	-40	68	37	12
67	3	26	-40	58	29	38
68	3	26	-40	48	80	13
69	3	26	-40	38	63	47
70	3	26	-40	28	50	23
71	3	27	-40	88	44	24
72	3	27	-40	78	66	45
73	3	27	-40	68	117	25

NACCS Synthetic Tropical Cyclone ID	NACCS Subregion	Master Track ID	θ (deg)	Δ*P* (hPa)	R_{max} (km)	V_f (km/h)
74	3	27	-40	58	52	17
75	3	27	-40	48	26	20
76	3	27	-40	38	39	41
77	3	27	-40	28	74	23
78	3	28	-40	88	69	43
79	3	28	-40	78	53	16
80	3	28	-40	68	37	42
81	3	28	-40	58	103	23
82	3	28	-40	48	29	19
83	3	28	-40	38	62	38
84	3	28	-40	28	60	25
85	3	29	-40	88	53	35
86	3	29	-40	78	79	22
87	3	29	-40	68	32	22
88	3	29	-40	58	105	28
89	3	29	-40	48	55	12
90	3	29	-40	38	31	47
91	3	29	-40	28	59	39
92	3	30	-40	88	53	21
93	3	30	-40	78	42	22
94	3	30	-40	68	115	40
95	3	30	-40	58	25	33
96	3	30	-40	48	83	24
97	3	30	-40	38	50	45
98	3	30	-40	28	46	13
99	3	31	-40	88	65	16
100	3	31	-40	78	54	44
101	3	31	-40	68	104	31
102	3	31	-40	58	44	17
103	3	31	-40	48	27	32
104	3	31	-40	38	46	25
105	3	31	-40	28	74	21
106	3	50	-20	98	66	38
107	3	50	-20	88	76	12
108	3	50	-20	78	42	21
109	3	50	-20	68	113	32
110	3	50	-20	58	25	23
111	3	50	-20	48	37	49
112	3	50	-20	38	62	30
113	3	51	-20	98	48	26
114	3	51	-20	88	117	29
115	3	51	-20	78	68	42

NACCS Synthetic Tropical Cyclone ID	NACCS Subregion	Master Track ID	θ (deg)	Δ*P* (hPa)	R_{max} (km)	V_f (km/h)
116	3	51	-20	68	47	24
117	3	51	-20	58	72	12
118	3	51	-20	48	33	41
119	3	51	-20	38	31	12
120	3	52	-20	98	63	28
121	3	52	-20	88	38	22
122	3	52	-20	78	115	26
123	3	52	-20	68	70	38
124	3	52	-20	58	25	25
125	3	52	-20	48	44	43
126	3	52	-20	38	63	12
127	3	53	-20	98	59	19
128	3	53	-20	88	116	33
129	3	53	-20	78	27	36
130	3	53	-20	68	37	20
131	3	53	-20	58	56	46
132	3	53	-20	48	75	21
133	3	53	-20	38	45	20
134	3	54	-20	98	49	33
135	3	54	-20	88	100	17
136	3	54	-20	78	87	44
137	3	54	-20	68	28	20
138	3	54	-20	58	50	12
139	3	54	-20	48	65	27
140	3	54	-20	38	38	46
141	3	72	0	88	42	31
142	3	72	0	83	53	12
143	3	72	0	78	77	35
144	3	72	0	73	133	26
145	3	72	0	68	40	16
146	3	72	0	63	26	13
147	3	72	0	58	29	38
148	3	72	0	53	55	21
149	3	72	0	48	51	48
150	3	72	0	43	71	15
151	3	72	0	38	59	39
152	3	72	0	33	98	35
153	3	72	0	28	33	20
154	3	73	0	88	53	27
155	3	73	0	83	39	12
156	3	73	0	78	145	20
157	3	73	0	73	49	46

NACCS Synthetic Tropical Cyclone ID	NACCS Subregion	Master Track ID	θ (deg)	Δ*P* (hPa)	R_{max} (km)	V_f (km/h)
158	3	73	0	68	79	29
159	3	73	0	63	27	28
160	3	73	0	58	42	12
161	3	73	0	53	87	12
162	3	73	0	48	76	42
163	3	73	0	43	39	33
164	3	73	0	38	25	13
165	3	73	0	33	50	12
166	3	73	0	28	83	24
167	3	74	0	88	93	28
168	3	74	0	83	59	31
169	3	74	0	78	41	31
170	3	74	0	73	64	12
171	3	74	0	68	40	16
172	3	74	0	63	25	25
173	3	74	0	58	69	47
174	3	74	0	53	114	25
175	3	74	0	48	78	21
176	3	74	0	43	45	36
177	3	74	0	38	67	26
178	3	74	0	33	25	53
179	3	74	0	28	53	16
180	3	75	0	88	51	24
181	3	75	0	83	29	38
182	3	75	0	78	140	32
183	3	75	0	73	64	25
184	3	75	0	68	59	51
185	3	75	0	63	73	12
186	3	75	0	58	38	14
187	3	75	0	53	42	40
188	3	75	0	48	25	25
189	3	75	0	43	52	22
190	3	75	0	38	92	32
191	3	75	0	33	71	21
192	3	75	0	28	39	36
193	3	107	20	88	63	29
194	3	107	20	83	33	26
195	3	107	20	78	140	29
196	3	107	20	73	71	49
197	3	107	20	68	60	12
198	3	107	20	63	56	12
199	3	107	20	58	73	28

NACCS Synthetic Tropical Cyclone ID	NACCS Subregion	Master Track ID	θ (deg)	Δ*P* (hPa)	R_{max} (km)	V_f (km/h)
200	3	107	20	53	31	46
201	3	107	20	48	35	48
202	3	107	20	43	88	21
203	3	107	20	38	25	17
204	3	107	20	33	41	22
205	3	107	20	28	59	35
206	3	108	20	88	59	33
207	3	108	20	83	104	35
208	3	108	20	78	46	24
209	3	108	20	73	53	12
210	3	108	20	68	31	29
211	3	108	20	63	47	37
212	3	108	20	58	142	13
213	3	108	20	53	69	17
214	3	108	20	48	43	59
215	3	108	20	43	27	12
216	3	108	20	38	73	34
217	3	108	20	33	25	27
218	3	108	20	28	55	33
219	3	109	20	88	40	27
220	3	109	20	83	75	18
221	3	109	20	78	106	50
222	3	109	20	73	63	36
223	3	109	20	68	135	21
224	3	109	20	63	25	38
225	3	109	20	58	48	12
226	3	109	20	53	54	27
227	3	109	20	48	38	45
228	3	109	20	43	34	33
229	3	109	20	38	79	34
230	3	109	20	33	31	12
231	3	109	20	28	40	29
232	3	110	20	88	54	15
233	3	110	20	83	140	18
234	3	110	20	78	66	25
235	3	110	20	73	56	44
236	3	110	20	68	79	19
237	3	110	20	63	29	18
238	3	110	20	58	33	44
239	3	110	20	53	33	19
240	3	110	20	48	51	33
241	3	110	20	43	100	35

NACCS Synthetic Tropical Cyclone ID	NACCS Subregion	Master Track ID	θ (deg)	ΔP (hPa)	R_{max} (km)	V_f (km/h)
242	3	110	20	38	25	34
243	3	110	20	33	74	12
244	3	110	20	28	46	29
245	3	111	20	88	44	18
246	3	111	20	83	104	19
247	3	111	20	78	25	42
248	3	111	20	73	95	36
249	3	111	20	68	55	19
250	3	111	20	63	71	23
251	3	111	20	58	86	52
252	3	111	20	53	49	45
253	3	111	20	48	67	12
254	3	111	20	43	25	12
255	3	111	20	38	41	29
256	3	111	20	33	32	29
257	3	111	20	28	71	27
258	3	112	20	88	67	23
259	3	112	20	83	85	16
260	3	112	20	78	44	16
261	3	112	20	73	62	49
262	3	112	20	68	44	38
263	3	112	20	63	137	33
264	3	112	20	58	28	31
265	3	112	20	53	27	26
266	3	112	20	48	47	28
267	3	112	20	43	79	27
268	3	112	20	38	60	12
269	3	112	20	33	38	49
270	3	112	20	28	45	19
271	3	125	40	98	76	28
272	3	125	40	93	51	23
273	3	125	40	88	68	46
274	3	125	40	83	89	20
275	3	125	40	78	139	30
276	3	125	40	73	26	20
277	3	125	40	68	55	12
278	3	125	40	63	41	28
279	3	125	40	58	35	35
280	3	125	40	53	25	34
281	3	125	40	48	61	35
282	3	125	40	43	79	21
283	3	125	40	38	47	27

NACCS Synthetic Tropical Cyclone ID	NACCS Subregion	Master Track ID	θ (deg)	ΔP (hPa)	R_{max} (km)	V_f (km/h)
284	3	126	40	98	92	33
285	3	126	40	93	45	35
286	3	126	40	88	34	27
287	3	126	40	83	125	23
288	3	126	40	78	62	26
289	3	126	40	73	61	30
290	3	126	40	68	74	15
291	3	126	40	63	25	31
292	3	126	40	58	25	31
293	3	126	40	53	83	44
294	3	126	40	48	42	59
295	3	126	40	43	35	12
296	3	126	40	38	63	47
297	3	127	40	98	68	20
298	3	127	40	93	132	22
299	3	127	40	88	55	37
300	3	127	40	83	50	12
301	3	127	40	78	40	50
302	3	127	40	73	30	27
303	3	127	40	68	98	31
304	3	127	40	63	60	17
305	3	127	40	58	90	21
306	3	127	40	53	34	13
307	3	127	40	48	43	12
308	3	127	40	43	38	21
309	3	127	40	38	26	40
310	3	128	40	98	92	40
311	3	128	40	93	44	27
312	3	128	40	88	60	42
313	3	128	40	83	75	18
314	3	128	40	78	67	39
315	3	128	40	73	126	30
316	3	128	40	68	62	12
317	3	128	40	63	30	39
318	3	128	40	58	26	42
319	3	128	40	53	58	51
320	3	128	40	48	25	15
321	3	128	40	43	39	17
322	3	128	40	38	73	26
323	3	129	40	98	61	27
324	3	129	40	93	71	46
325	3	129	40	88	121	22

NACCS Synthetic Tropical Cyclone ID	NACCS Subregion	Master Track ID	θ (deg)	Δ*P* (hPa)	R_{max} (km)	V_f (km/h)
326	3	129	40	83	46	22
327	3	129	40	78	25	34
328	3	129	40	73	70	15
329	3	129	40	68	50	54
330	3	129	40	63	42	12
331	3	129	40	58	48	38
332	3	129	40	53	27	16
333	3	129	40	48	88	34
334	3	129	40	43	64	33
335	3	129	40	38	57	12
336	3	130	40	98	104	12
337	3	130	40	93	87	31
338	3	130	40	88	46	12
339	3	130	40	83	40	25
340	3	130	40	78	61	36
341	3	130	40	73	79	12
342	3	130	40	68	28	35
343	3	130	40	63	103	31
344	3	130	40	58	56	19
345	3	130	40	53	42	33
346	3	130	40	48	45	57
347	3	130	40	43	53	32
348	3	130	40	38	26	14
349	2	9	-60	78	125	65
350	2	9	-60	68	52	26
351	2	9	-60	58	56	61
352	2	9	-60	48	57	25
353	2	9	-60	38	29	43
354	2	9	-60	28	93	37
355	2	10	-60	78	51	36
356	2	10	-60	68	127	55
357	2	10	-60	58	88	28
358	2	10	-60	48	67	64
359	2	10	-60	38	31	52
360	2	10	-60	28	47	25
361	2	11	-60	78	125	43
362	2	11	-60	68	61	26
363	2	11	-60	58	69	62
364	2	11	-60	48	39	53
365	2	11	-60	38	35	35
366	2	11	-60	28	82	39
367	2	12	-60	78	50	45

NACCS Synthetic Tropical Cyclone ID	NACCS Subregion	Master Track ID	θ (deg)	Δ*P* (hPa)	R_{max} (km)	V_f (km/h)
368	2	12	-60	68	139	48
369	2	12	-60	58	79	31
370	2	12	-60	48	75	67
371	2	12	-60	38	41	24
372	2	12	-60	28	34	64
373	2	13	-60	78	47	29
374	2	13	-60	68	77	56
375	2	13	-60	58	127	49
376	2	13	-60	48	56	61
377	2	13	-60	38	80	27
378	2	13	-60	28	30	52
379	2	14	-60	78	55	28
380	2	14	-60	68	126	42
381	2	14	-60	58	79	65
382	2	14	-60	48	48	58
383	2	14	-60	38	30	38
384	2	14	-60	28	76	32
385	2	15	-60	78	66	60
386	2	15	-60	68	44	30
387	2	15	-60	58	127	48
388	2	15	-60	48	81	23
389	2	15	-60	38	33	62
390	2	15	-60	28	65	50
391	2	32	-40	78	47	57
392	2	32	-40	68	130	42
393	2	32	-40	58	74	25
394	2	32	-40	48	26	45
395	2	32	-40	38	46	33
396	2	32	-40	28	76	59
397	2	33	-40	78	67	63
398	2	33	-40	68	126	45
399	2	33	-40	58	74	22
400	2	33	-40	48	44	38
401	2	33	-40	38	29	68
402	2	33	-40	28	78	50
403	2	34	-40	78	67	61
404	2	34	-40	68	42	32
405	2	34	-40	58	80	25
406	2	34	-40	48	127	50
407	2	34	-40	38	33	65
408	2	34	-40	28	63	50
409	2	35	-40	78	44	28

NACCS Synthetic Tropical Cyclone ID	NACCS Subregion	Master Track ID	θ (deg)	Δ*P* (hPa)	R_{max} (km)	V_f (km/h)
410	2	35	-40	68	64	60
411	2	35	-40	58	125	51
412	2	35	-40	48	67	55
413	2	35	-40	38	79	24
414	2	35	-40	28	33	58
415	2	36	-40	78	46	25
416	2	36	-40	68	62	62
417	2	36	-40	58	126	61
418	2	36	-40	48	94	30
419	2	36	-40	38	30	55
420	2	36	-40	28	59	41
421	2	37	-40	78	82	59
422	2	37	-40	68	61	24
423	2	37	-40	58	44	60
424	2	37	-40	48	128	36
425	2	37	-40	38	31	29
426	2	37	-40	28	70	48
427	2	38	-40	78	52	23
428	2	38	-40	68	126	40
429	2	38	-40	58	45	55
430	2	38	-40	48	81	69
431	2	38	-40	38	72	33
432	2	38	-40	28	26	34
433	2	55	-20	88	55	62
434	2	55	-20	78	82	27
435	2	55	-20	68	126	50
436	2	55	-20	58	28	52
437	2	55	-20	48	48	29
438	2	55	-20	38	76	57
439	2	56	-20	88	47	36
440	2	56	-20	78	130	42
441	2	56	-20	68	50	68
442	2	56	-20	58	73	23
443	2	56	-20	48	79	56
444	2	56	-20	38	36	44
445	2	57	-20	88	60	45
446	2	57	-20	78	129	43
447	2	57	-20	68	43	29
448	2	57	-20	58	75	63
449	2	57	-20	48	37	58
450	2	57	-20	38	72	28
451	2	58	-20	88	43	38

NACCS Synthetic Tropical Cyclone ID	NACCS Subregion	Master Track ID	θ (deg)	Δ*P* (hPa)	R_{max} (km)	V_f (km/h)
452	2	58	-20	78	82	29
453	2	58	-20	68	66	64
454	2	58	-20	58	128	52
455	2	58	-20	48	29	64
456	2	58	-20	38	51	32
457	2	59	-20	88	58	34
458	2	59	-20	78	50	35
459	2	59	-20	68	126	48
460	2	59	-20	58	68	66
461	2	59	-20	48	34	48
462	2	59	-20	38	80	29
463	2	60	-20	88	67	56
464	2	60	-20	78	126	41
465	2	60	-20	68	34	26
466	2	60	-20	58	66	22
467	2	60	-20	48	40	54
468	2	60	-20	38	78	57
469	2	76	0	78	74	38
470	2	76	0	73	89	79
471	2	76	0	68	112	14
472	2	76	0	63	35	36
473	2	76	0	58	62	50
474	2	76	0	53	25	54
475	2	76	0	48	58	47
476	2	76	0	43	42	66
477	2	76	0	38	126	47
478	2	76	0	33	52	19
479	2	76	0	28	71	60
480	2	77	0	78	58	75
481	2	77	0	73	61	32
482	2	77	0	68	143	30
483	2	77	0	63	36	33
484	2	77	0	58	97	59
485	2	77	0	53	60	29
486	2	77	0	48	49	58
487	2	77	0	43	98	39
488	2	77	0	38	25	56
489	2	77	0	33	61	54
490	2	77	0	28	60	18
491	2	78	0	78	117	38
492	2	78	0	73	73	62
493	2	78	0	68	42	43

NACCS Synthetic Tropical Cyclone ID	NACCS Subregion	Master Track ID	θ (deg)	Δ*P* (hPa)	R_{max} (km)	V_f (km/h)
494	2	78	0	63	76	21
495	2	78	0	58	56	68
496	2	78	0	53	25	30
497	2	78	0	48	45	29
498	2	78	0	43	80	50
499	2	78	0	38	132	45
500	2	78	0	33	39	66
501	2	78	0	28	61	40
502	2	79	0	78	82	47
503	2	79	0	73	46	42
504	2	79	0	68	96	68
505	2	79	0	63	74	18
506	2	79	0	58	130	32
507	2	79	0	53	33	14
508	2	79	0	48	94	45
509	2	79	0	43	28	55
510	2	79	0	38	64	38
511	2	79	0	33	58	66
512	2	79	0	28	46	39
513	2	80	0	78	71	26
514	2	80	0	73	76	56
515	2	80	0	68	140	50
516	2	80	0	63	44	44
517	2	80	0	58	52	88
518	2	80	0	53	25	56
519	2	80	0	48	51	50
520	2	80	0	43	83	69
521	2	80	0	38	37	14
522	2	80	0	33	99	35
523	2	80	0	28	62	38
524	2	98	20	78	73	38
525	2	98	20	73	86	82
526	2	98	20	68	83	32
527	2	98	20	63	50	55
528	2	98	20	58	37	34
529	2	98	20	53	137	39
530	2	98	20	48	59	22
531	2	98	20	43	28	49
532	2	98	20	38	92	51
533	2	98	20	33	59	58
534	2	98	20	28	45	35
535	2	99	20	78	41	33

NACCS Synthetic Tropical Cyclone ID	NACCS Subregion	Master Track ID	θ (deg)	Δ*P* (hPa)	R_{max} (km)	V_f (km/h)
536	2	99	20	73	69	61
537	2	99	20	68	108	22
538	2	99	20	63	145	50
539	2	99	20	58	26	50
540	2	99	20	53	70	17
541	2	99	20	48	58	39
542	2	99	20	43	41	77
543	2	99	20	38	50	47
544	2	99	20	33	41	39
545	2	99	20	28	100	49
546	2	100	20	78	70	34
547	2	100	20	73	36	60
548	2	100	20	68	144	52
549	2	100	20	63	73	22
550	2	100	20	58	70	56
551	2	100	20	53	44	39
552	2	100	20	48	60	60
553	2	100	20	43	25	41
554	2	100	20	38	103	42
555	2	100	20	33	50	74
556	2	100	20	28	61	23
557	2	101	20	78	77	32
558	2	101	20	73	62	65
559	2	101	20	68	33	42
560	2	101	20	63	138	49
561	2	101	20	58	62	27
562	2	101	20	53	93	58
563	2	101	20	48	101	23
564	2	101	20	43	42	14
565	2	101	20	38	48	46
566	2	101	20	33	61	48
567	2	101	20	28	33	84
568	2	102	20	78	60	44
569	2	102	20	73	96	33
570	2	102	20	68	57	73
571	2	102	20	63	145	43
572	2	102	20	58	32	55
573	2	102	20	53	31	24
574	2	102	20	48	90	51
575	2	102	20	43	35	39
576	2	102	20	38	85	14
577	2	102	20	33	57	46

NACCS Synthetic Tropical Cyclone ID	NACCS Subregion	Master Track ID	θ (deg)	Δ*P* (hPa)	R_{max} (km)	V_f (km/h)
578	2	102	20	28	57	46
579	2	103	20	78	44	34
580	2	103	20	73	78	33
581	2	103	20	68	139	65
582	2	103	20	63	65	61
583	2	103	20	58	111	29
584	2	103	20	53	30	49
585	2	103	20	48	58	29
586	2	103	20	43	50	53
587	2	103	20	38	42	60
588	2	103	20	33	41	14
589	2	103	20	28	95	51
590	2	104	20	78	68	57
591	2	104	20	73	141	37
592	2	104	20	68	58	26
593	2	104	20	63	32	55
594	2	104	20	58	79	44
595	2	104	20	53	33	43
596	2	104	20	48	39	14
597	2	104	20	43	83	17
598	2	104	20	38	54	50
599	2	104	20	33	55	60
600	2	104	20	28	100	54
601	2	105	20	78	68	48
602	2	105	20	73	128	60
603	2	105	20	68	67	22
604	2	105	20	63	66	56
605	2	105	20	58	62	78
606	2	105	20	53	56	24
607	2	105	20	48	32	53
608	2	105	20	43	38	28
609	2	105	20	38	62	63
610	2	105	20	33	100	37
611	2	105	20	28	52	47
612	2	106	20	78	118	25
613	2	106	20	73	61	51
614	2	106	20	68	36	28
615	2	106	20	63	58	36
616	2	106	20	58	74	29
617	2	106	20	53	50	59
618	2	106	20	48	93	57
619	2	106	20	43	126	34

NACCS Synthetic Tropical Cyclone ID	NACCS Subregion	Master Track ID	θ (deg)	Δ*P* (hPa)	R_{max} (km)	V_f (km/h)
620	2	106	20	38	27	62
621	2	106	20	33	57	27
622	2	106	20	28	51	62
623	2	119	40	88	66	31
624	2	119	40	83	94	43
625	2	119	40	78	76	60
626	2	119	40	73	46	45
627	2	119	40	68	45	88
628	2	119	40	63	129	56
629	2	119	40	58	98	29
630	2	119	40	53	29	50
631	2	119	40	48	46	14
632	2	119	40	43	66	53
633	2	119	40	38	52	34
634	2	120	40	88	69	39
635	2	120	40	83	137	57
636	2	120	40	78	47	14
637	2	120	40	73	64	79
638	2	120	40	68	60	45
639	2	120	40	63	33	29
640	2	120	40	58	34	56
641	2	120	40	53	102	41
642	2	120	40	48	54	41
643	2	120	40	43	72	17
644	2	120	40	38	64	67
645	2	121	40	88	105	33
646	2	121	40	83	67	59
647	2	121	40	78	46	36
648	2	121	40	73	50	53
649	2	121	40	68	33	76
650	2	121	40	63	126	38
651	2	121	40	58	68	21
652	2	121	40	53	28	31
653	2	121	40	48	85	49
654	2	121	40	43	88	69
655	2	121	40	38	54	54
656	2	122	40	88	146	44
657	2	122	40	83	54	27
658	2	122	40	78	63	71
659	2	122	40	73	67	36
660	2	122	40	68	87	14
661	2	122	40	63	25	28

NACCS Synthetic Tropical Cyclone ID	NACCS Subregion	Master Track ID	θ (deg)	Δ*P* (hPa)	R_{max} (km)	V_f (km/h)
662	2	122	40	58	63	44
663	2	122	40	53	43	29
664	2	122	40	48	115	44
665	2	122	40	43	32	59
666	2	122	40	38	68	45
667	2	123	40	88	75	58
668	2	123	40	83	48	35
669	2	123	40	78	136	40
670	2	123	40	73	37	73
671	2	123	40	68	92	33
672	2	123	40	63	27	34
673	2	123	40	58	54	47
674	2	123	40	53	76	28
675	2	123	40	48	105	58
676	2	123	40	43	53	52
677	2	123	40	38	40	14
678	2	124	40	88	158	62
679	2	124	40	83	46	51
680	2	124	40	78	62	49
681	2	124	40	73	51	16
682	2	124	40	68	90	17
683	2	124	40	63	70	45
684	2	124	40	58	62	80
685	2	124	40	53	29	71
686	2	124	40	48	27	34
687	2	124	40	43	105	56
688	2	124	40	38	51	46
689	1	16	-60	68	153	58
690	1	16	-60	58	51	36
691	1	16	-60	48	75	66
692	1	16	-60	38	95	35
693	1	16	-60	28	36	66
694	1	17	-60	68	53	48
695	1	17	-60	58	151	53
696	1	17	-60	48	89	33
697	1	17	-60	38	83	70
698	1	17	-60	28	28	51
699	1	18	-60	68	50	60
700	1	18	-60	58	154	46
701	1	18	-60	48	78	35
702	1	18	-60	38	92	68
703	1	18	-60	28	35	29

NACCS Synthetic Tropical Cyclone ID	NACCS Subregion	Master Track ID	θ (deg)	Δ*P* (hPa)	R_{max} (km)	V_f (km/h)
704	1	19	-60	68	69	66
705	1	19	-60	58	151	61
706	1	19	-60	48	98	37
707	1	19	-60	38	33	60
708	1	19	-60	28	53	34
709	1	20	-60	68	152	44
710	1	20	-60	58	52	60
711	1	20	-60	48	78	33
712	1	20	-60	38	92	67
713	1	20	-60	28	36	32
714	1	21	-60	68	79	61
715	1	21	-60	58	153	53
716	1	21	-60	48	48	37
717	1	21	-60	38	40	71
718	1	21	-60	28	91	28
719	1	22	-60	68	54	51
720	1	22	-60	58	154	49
721	1	22	-60	48	86	31
722	1	22	-60	38	88	68
723	1	22	-60	28	30	44
724	1	23	-60	68	50	61
725	1	23	-60	58	150	46
726	1	23	-60	48	79	36
727	1	23	-60	38	93	71
728	1	23	-60	28	38	28
729	1	24	-60	68	52	62
730	1	24	-60	58	150	42
731	1	24	-60	48	77	33
732	1	24	-60	38	96	67
733	1	24	-60	28	36	34
734	1	39	-40	68	51	49
735	1	39	-40	58	152	49
736	1	39	-40	48	86	31
737	1	39	-40	38	85	68
738	1	39	-40	28	26	50
739	1	40	-40	68	151	44
740	1	40	-40	58	77	35
741	1	40	-40	48	50	62
742	1	40	-40	38	37	30
743	1	40	-40	28	93	68
744	1	41	-40	68	54	64
745	1	41	-40	58	151	40

NACCS Synthetic Tropical Cyclone ID	NACCS Subregion	Master Track ID	θ (deg)	Δ*P* (hPa)	R_{max} (km)	V_f (km/h)
746	1	41	-40	48	70	29
747	1	41	-40	38	94	61
748	1	41	-40	28	35	40
749	1	42	-40	68	51	34
750	1	42	-40	58	151	59
751	1	42	-40	48	74	65
752	1	42	-40	38	96	34
753	1	42	-40	28	36	63
754	1	43	-40	68	51	37
755	1	43	-40	58	151	55
756	1	43	-40	48	78	64
757	1	43	-40	38	94	30
758	1	43	-40	28	37	67
759	1	44	-40	68	68	66
760	1	44	-40	58	152	65
761	1	44	-40	48	101	39
762	1	44	-40	38	54	32
763	1	44	-40	28	34	57
764	1	45	-40	68	51	65
765	1	45	-40	58	150	43
766	1	45	-40	48	76	36
767	1	45	-40	38	95	67
768	1	45	-40	28	37	34
769	1	46	-40	68	48	36
770	1	46	-40	58	151	55
771	1	46	-40	48	79	61
772	1	46	-40	38	42	71
773	1	46	-40	28	91	29
774	1	47	-40	68	52	65
775	1	47	-40	58	151	41
776	1	47	-40	48	71	30
777	1	47	-40	38	92	61
778	1	47	-40	28	36	41
779	1	48	-40	68	50	61
780	1	48	-40	58	153	45
781	1	48	-40	48	78	34
782	1	48	-40	38	91	67
783	1	48	-40	28	38	29
784	1	49	-40	68	48	60
785	1	49	-40	58	80	36
786	1	49	-40	48	151	47
787	1	49	-40	38	89	69

NACCS Synthetic Tropical Cyclone ID	NACCS Subregion	Master Track ID	θ (deg)	Δ*P* (hPa)	R_{max} (km)	V_f (km/h)
788	1	49	-40	28	40	29
789	1	61	-20	78	52	36
790	1	61	-20	68	76	66
791	1	61	-20	58	154	54
792	1	61	-20	48	93	33
793	1	61	-20	38	36	64
794	1	62	-20	78	49	37
795	1	62	-20	68	150	52
796	1	62	-20	58	79	65
797	1	62	-20	48	87	32
798	1	62	-20	38	40	66
799	1	63	-20	78	63	35
800	1	63	-20	68	103	57
801	1	63	-20	58	150	30
802	1	63	-20	48	58	72
803	1	63	-20	38	33	48
804	1	64	-20	78	52	64
805	1	64	-20	68	75	35
806	1	64	-20	58	151	41
807	1	64	-20	48	97	67
808	1	64	-20	38	37	35
809	1	65	-20	78	51	63
810	1	65	-20	68	150	45
811	1	65	-20	58	78	35
812	1	65	-20	48	92	69
813	1	65	-20	38	39	33
814	1	66	-20	78	51	36
815	1	66	-20	68	78	63
816	1	66	-20	58	152	55
817	1	66	-20	48	94	30
818	1	66	-20	38	37	67
819	1	67	-20	78	51	36
820	1	67	-20	68	79	66
821	1	67	-20	58	153	53
822	1	67	-20	48	37	66
823	1	67	-20	38	91	34
824	1	68	-20	78	59	69
825	1	68	-20	68	166	50
826	1	68	-20	58	34	49
827	1	68	-20	48	93	49
828	1	68	-20	38	58	29
829	1	69	-20	78	52	61

NACCS Synthetic Tropical Cyclone ID	NACCS Subregion	Master Track ID	θ (deg)	Δ*P* (hPa)	R_{max} (km)	V_f (km/h)
830	1	69	-20	68	151	43
831	1	69	-20	58	95	67
832	1	69	-20	48	36	32
833	1	69	-20	38	78	34
834	1	70	-20	78	49	60
835	1	70	-20	68	81	35
836	1	70	-20	58	150	48
837	1	70	-20	48	87	68
838	1	70	-20	38	42	32
839	1	71	-20	78	38	67
840	1	71	-20	68	156	55
841	1	71	-20	58	92	33
842	1	71	-20	48	77	65
843	1	71	-20	38	49	37
844	1	81	0	68	89	43
845	1	81	0	63	55	49
846	1	81	0	58	154	54
847	1	81	0	53	32	60
848	1	81	0	48	86	52
849	1	81	0	43	74	73
850	1	81	0	38	70	18
851	1	81	0	33	44	43
852	1	81	0	28	104	42
853	1	82	0	68	64	51
854	1	82	0	63	84	62
855	1	82	0	58	156	46
856	1	82	0	53	28	58
857	1	82	0	48	80	25
858	1	82	0	43	43	33
859	1	82	0	38	49	64
860	1	82	0	33	104	55
861	1	82	0	28	61	60
862	1	83	0	68	72	60
863	1	83	0	63	162	50
864	1	83	0	58	58	72
865	1	83	0	53	49	31
866	1	83	0	48	32	53
867	1	83	0	43	100	26
868	1	83	0	38	72	38
869	1	83	0	33	105	59
870	1	83	0	28	51	58
871	1	84	0	68	80	59

NACCS Synthetic Tropical Cyclone ID	NACCS Subregion	Master Track ID	θ (deg)	ΔP (hPa)	R_{max} (km)	V_f (km/h)
872	1	84	0	63	57	48
873	1	84	0	58	107	70
874	1	84	0	53	153	49
875	1	84	0	48	32	41
876	1	84	0	43	100	34
877	1	84	0	38	42	73
878	1	84	0	33	54	27
879	1	84	0	28	73	57
880	1	85	0	68	85	30
881	1	85	0	63	52	51
882	1	85	0	58	154	47
883	1	85	0	53	103	54
884	1	85	0	48	78	35
885	1	85	0	43	83	72
886	1	85	0	38	36	38
887	1	85	0	33	38	79
888	1	85	0	28	59	48
889	1	86	0	68	79	25
890	1	86	0	63	151	48
891	1	86	0	58	80	67
892	1	86	0	53	52	46
893	1	86	0	48	45	83
894	1	86	0	43	33	43
895	1	86	0	38	98	59
896	1	86	0	33	99	40
897	1	86	0	28	57	53
898	1	87	0	68	104	68
899	1	87	0	63	70	29
900	1	87	0	58	54	53
901	1	87	0	53	163	40
902	1	87	0	48	32	52
903	1	87	0	43	97	42
904	1	87	0	38	56	65
905	1	87	0	33	49	29
906	1	87	0	28	79	56
907	1	88	0	68	83	56
908	1	88	0	63	50	44
909	1	88	0	58	168	43
910	1	88	0	53	80	28
911	1	88	0	48	42	79
912	1	88	0	43	59	67
913	1	88	0	38	104	61

NACCS Synthetic Tropical Cyclone ID	NACCS Subregion	Master Track ID	θ (deg)	ΔP (hPa)	R_{max} (km)	V_f (km/h)
914	1	88	0	33	36	38
915	1	88	0	28	71	42
916	1	89	0	68	76	61
917	1	89	0	63	83	41
918	1	89	0	58	170	52
919	1	89	0	53	48	46
920	1	89	0	48	26	53
921	1	89	0	43	64	25
922	1	89	0	38	101	44
923	1	89	0	33	75	74
924	1	89	0	28	50	56
925	1	90	20	68	50	41
926	1	90	20	63	94	37
927	1	90	20	58	66	78
928	1	90	20	53	162	47
929	1	90	20	48	57	54
930	1	90	20	43	30	55
931	1	90	20	38	72	20
932	1	90	20	33	93	61
933	1	90	20	28	59	60
934	1	91	20	68	89	40
935	1	91	20	63	60	47
936	1	91	20	58	31	54
937	1	91	20	53	174	45
938	1	91	20	48	102	72
939	1	91	20	43	56	69
940	1	91	20	38	38	32
941	1	91	20	33	98	38
942	1	91	20	28	54	30
943	1	92	20	68	87	51
944	1	92	20	63	101	31
945	1	92	20	58	52	50
946	1	92	20	53	50	45
947	1	92	20	48	155	51
948	1	92	20	43	27	45
949	1	92	20	38	87	61
950	1	92	20	33	49	81
951	1	92	20	28	75	28
952	1	93	20	68	55	50
953	1	93	20	63	112	16
954	1	93	20	58	35	54
955	1	93	20	53	165	52

NACCS Synthetic Tropical Cyclone ID	NACCS Subregion	Master Track ID	θ (deg)	ΔP (hPa)	R_{max} (km)	V_f (km/h)
956	1	93	20	48	75	45
957	1	93	20	43	67	79
958	1	93	20	38	51	17
959	1	93	20	33	102	49
960	1	93	20	28	48	53
961	1	94	20	68	100	38
962	1	94	20	63	82	74
963	1	94	20	58	59	47
964	1	94	20	53	151	53
965	1	94	20	48	64	59
966	1	94	20	43	34	71
967	1	94	20	38	41	35
968	1	94	20	33	78	25
969	1	94	20	28	94	49
970	1	95	20	68	62	42
971	1	95	20	63	92	57
972	1	95	20	58	156	29
973	1	95	20	53	35	57
974	1	95	20	48	113	57
975	1	95	20	43	50	46
976	1	95	20	38	61	69
977	1	95	20	33	74	36
978	1	95	20	28	42	26
979	1	96	20	68	109	71
980	1	96	20	63	88	28
981	1	96	20	58	52	57
982	1	96	20	53	28	51
983	1	96	20	48	152	46
984	1	96	20	43	77	51
985	1	96	20	38	50	29
986	1	96	20	33	88	54
987	1	96	20	28	55	73
988	1	97	20	68	85	59
989	1	97	20	63	83	25
990	1	97	20	58	40	66
991	1	97	20	53	68	66
992	1	97	20	48	150	36
993	1	97	20	43	59	34
994	1	97	20	38	108	50
995	1	97	20	33	30	38
996	1	97	20	28	62	65
997	1	113	40	78	82	56

NACCS Synthetic Tropical Cyclone ID	NACCS Subregion	Master Track ID	θ (deg)	Δ*P* (hPa)	R_{max} (km)	V_f (km/h)
998	1	113	40	73	156	48
999	1	113	40	68	45	34
1000	1	113	40	63	82	23
1001	1	113	40	58	34	64
1002	1	113	40	53	69	83
1003	1	113	40	48	58	52
1004	1	113	40	43	113	52
1005	1	113	40	38	69	45
1006	1	114	40	78	117	64
1007	1	114	40	73	58	51
1008	1	114	40	68	73	19
1009	1	114	40	63	56	54
1010	1	114	40	58	152	39
1011	1	114	40	53	29	57
1012	1	114	40	48	40	29
1013	1	114	40	43	73	77
1014	1	114	40	38	87	43
1015	1	115	40	78	157	53
1016	1	115	40	73	55	23
1017	1	115	40	68	71	45
1018	1	115	40	63	51	73
1019	1	115	40	58	74	48
1020	1	115	40	53	96	75
1021	1	115	40	48	31	49
1022	1	115	40	43	113	36
1023	1	115	40	38	57	48
1024	1	116	40	78	65	47
1025	1	116	40	73	154	47
1026	1	116	40	68	39	67
1027	1	116	40	63	35	27
1028	1	116	40	58	100	26
1029	1	116	40	53	70	79
1030	1	116	40	48	104	58
1031	1	116	40	43	71	36
1032	1	116	40	38	53	45
1033	1	117	40	78	83	67
1034	1	117	40	73	88	27
1035	1	117	40	68	156	45
1036	1	117	40	63	45	52
1037	1	117	40	58	33	28
1038	1	117	40	53	73	44
1039	1	117	40	48	64	42

NACCS Synthetic Tropical Cyclone ID	NACCS Subregion	Master Track ID	θ (deg)	ΔP (hPa)	R_{max} (km)	V_f (km/h)
1040	1	117	40	43	53	81
1041	1	117	40	38	107	53
1042	1	118	40	78	174	43
1043	1	118	40	73	77	62
1044	1	118	40	68	58	66
1045	1	118	40	63	39	61
1046	1	118	40	58	74	32
1047	1	118	40	53	39	33
1048	1	118	40	48	69	32
1049	1	118	40	43	114	50
1050	1	118	40	38	59	57

Appendix D: CSTORM-MS mf_config.in Details

service namelist

Note that all STWAVE simulations must start and end at the same time during the overall coupled simulation. A list and description of the variables in the **service** namelist in the CSTORM-MS coupler file (mf_config.in) are given below.

Variable Name	Description	
wsid	Wave Coupling Service Identification Tag	
	Value	Coupling Type and Data to Share
	1	Tight one-way coupling ADCIRC → STWAVE (ADCIRC sends surge and wind to STWAVE)
	2	Tight one-way coupling ADCIRC → STWAVE (ADCIRC sends surge, wind, and currents to STWAVE)
	3	Tight two-way coupling ADCIRC ←→ STWAVE (ADCIRC sends surge and wind; STWAVE sends non-zero wave radiation stress gradients)
	4	Tight two-way coupling ADCIRC ←→ STWAVE (ADCIRC sends surge, currents, and wind; STWAVE sends non-zero wave radiation stress gradients)
	5	Tight one-way coupling ADCIRC → STWAVE (ADCIRC sends surge, wind and ice to STWAVE)
	6	Tight two-way coupling ADCIRC ←→ STWAVE (ADCIRC sends surge, wind, and ice; STWAVE sends non-zero wave radiation stress gradients)
stwgrids	The number of STWAVE grids in the application. A non-negative integer value.	
stwstart	An integer value that corresponds to the starting time for all the STWAVE simulations relative to the ADCIRC simulation start time. This value is the ADCIRC time-step number for which the first STWAVE snap is to be computed and can be calculated by taking the selected STWAVE start time in seconds and dividing by the ADCIRC time step size also given in seconds.	
stwfinish	An integer value that corresponds to the ending time for all the STWAVE simulations relative to the ADCIRC simulation start time. This value is the ADCIRC time-step number when STWAVE calculations stop. It can be computed by taking the selected STWAVE end time in seconds and dividing by the ADCIRC time-step size also given in seconds.	
stwtiminc	The number of ADCIRC time-steps that occur between STWAVE snaps.	
geo_and_stpl_coord	A logical value of ".true." or ".false." True indicates that ADCIRC is in Geographic coordinates and STWAVE is either in State Plane or UTM coordinates. False indicates both ADCIRC and all STWAVE grids are in the same local (meters) coordinate system.	

adc_def namelist

A description of the **adc_def** namelist contained in the CSTORM-MS coupler file (mf_config.in) is given below.

Variable Name	Description
adcgrid	The file name of the ADCIRC mesh file (fort.14)
adcprocs	The number of compute processors to apply to ADCIRC. This is the same number used during the "adcprep" ADCIRC domain decomposition phase of the CSTORM-MS set up process.
writerprocs	The number of dedicated writer processors to use for ADCIRC. These are in addition to the compute processors (adcprocs).
adcstart	The time-step number when the ADCIRC simulation starts.
adcfinish	The time-step number when the ADCIRC simulation ends.

stw_def namelist

Only two variables are required in this namelist, the "simfile" and "stwprocs". All others variables are read from the STWAVE simulation file (*.sim). However, "coord_sys", "spzone", and "hemisphere" are not required in the *.sim file, so if they are not present in the *.sim file, they will be required in the mf_config.in file. If these variables are supplied in both locations, the values given in the STWAVE *.sim file will supercede those supplied in the mf_config.in file. See below for a complete description of the variables contained in the **stw_def** namelist contained in the CSTORM-MS coupler file (mf_config.in).

Variable Name	Description
simfile	The file name of the STWAVE simulation file (*.sim)
stwprocs	The number of processors to use for a given STWAVE grid
coord_sys *(optional)*	"Local", "STATEPLANE", or "UTM" – Grid specification coordinate system
Spzone *(optional)*	A four- digit STATE PLANE zone code. Use the FIPS code or the two-digit UTM zone code.
hemisphere *(optional)*	"NORTH" or "SOUTH" – Used for UTM coordinates to distinguish between the grid being located in the northern or southern hemisphere.

Sample mf_config.in

A sample CSTORM-MS coupler control file (mf_config.in) from synthetic tropical storm number 1050 using random tide sampling is given below. In this example, 2400 CPUs are applied to run the coupled simulation. One processor is the driver or *boss*, 10 processors are used for couplers, 1 for each STWAVE domain. ADCIRC uses the remaining 2389 processors to perform computations. The total of all STWAVE processor applied to this simulation (sum of the individual 10 domains) is also 2389 CPUs. The coupled simulation starts by *hot starting* ADCIRC at time-step number 2,091,600 to incorporate random tides. Waves start at time-step number 2,174,400 and continuing every 1800 time-steps (30 min in this case) until time-step number 2,347,200.

```
#
# CSTORM-MS Input Parameters File
#    Compatible with CSTORM-MS Version 1.0.0
#
# Adcirc Grid
&adc_def adcgrid     = "NAC2014_P42_Rivers.grd",
         adcprocs    = 2389,
         writerprocs = 0,
         adcstart    = 2091600,
         adcfinish   = 2347200
/
# Wave Service
&service wsid  = 3,
         stwgrids    = 10,
         stwstart    = 2174400,
         stwfinish   = 2347200,
         stwtiminc   = 1800,
         geo_and_stpl_coord = .true.,
/
# Stwave Grid 1
&stw_def simfile = "NME.sim", stwprocs = 45,
         coord_sys = "UTM", hemisphere = "NORTH", spzone = 19 /
# Stwave Grid 2
&stw_def simfile = "CME.sim", stwprocs = 60,
         coord_sys = "UTM", hemisphere = "NORTH", spzone = 19 /
# Stwave Grid 3
&stw_def simfile = "SME.sim", stwprocs = 60,
         coord_sys = "UTM", hemisphere = "NORTH", spzone = 19 /
# Stwave Grid 4
&stw_def simfile = "EMA.sim", stwprocs = 72,
         coord_sys = "UTM", hemisphere = "NORTH", spzone = 19 /
# Stwave Grid 5
&stw_def simfile = "SMA.sim", stwprocs = 130,
         coord_sys = "UTM", hemisphere = "NORTH", spzone = 19 /
# Stwave Grid 6
&stw_def simfile = "LID.sim", stwprocs = 128,
         coord_sys = "UTM", hemisphere = "NORTH", spzone = 18 /
# Stwave Grid 7
&stw_def simfile = "NNJ.sim", stwprocs = 36,
         coord_sys = "UTM", hemisphere = "NORTH", spzone = 18 /
# Stwave Grid 8
&stw_def simfile = "CNJ.sim", stwprocs = 24,
         coord_sys = "UTM", hemisphere = "NORTH", spzone = 18 /
# Stwave Grid 9
&stw_def simfile = "CPB.sim", stwprocs = 1802,
         coord_sys = "UTM", hemisphere = "NORTH", spzone = 18 /
# Stwave Grid 10
&stw_def simfile = "WDC.sim", stwprocs = 32,
         coord_sys = "UTM", hemisphere = "NORTH", spzone = 18 /
```

Appendix E: Tar Ball Details

For the NACCS numerical modeling study, there are 10 STWAVE domains applied in the CSTORM-MS simulations, each archived with two tar files: "Outputs" and "SurgeWind". There are four ADCIRC tar files, one STWAVE station tar file, one CSTORM-MS tar file, plus five additional tar files resulting from the visualization process (indicated below by red text).

ADCIRC

RNAME_ADCIRC_GBL_Hydro.tar -- fort.63.gz, fort.64.gz, *properties.log.gz
RNAME_ADCIRC_GBL_Met.tar -- fort.73.gz, fort.74.gz, rads.64.gz, *properties.log.gz
RNAME_ADCIRC_MaxMins.tar – maxele.63.gz, maxvel.63.gz, maxwvel.63.gz, maxrs.63.gz, minpr.63.gz, *properties.log.gz
RNAME_ADCIRC_Stations.tar -- fort.61.gz, fort.62.gz, fort.71.gz, fort.72.gz, station locations (*stat.151.gz), *properties.log.gz
RNAME_Viz_ADCIRC_pngs.tar.gz – ADCIRC graphics (png files) from Viz

STWAVE – per grid (GNAME)

RNAME_STWAVE_GNAME_Outputs.tar -- Waves.out.gz, TP.out.gz, break.out.gz, selh.out.gz, obse.out.gz, nest.out.gz, station.out.gz, station.in.gz, *properties.log.gz
RNAME_STWAVE_GNAME_SurgeWind.tar -- Wind.in.gz, Surge.in.gz, *properties.log.gz
RNAME_Viz_STWAVE_MaxMins.tar – Postprocessed comma separated ASCII files for the maximum wave height, period, peak period over all STWAVE snaps for each STWAVE grid
RNAME_Viz_STWAVE_pngs.tar.gz – STWAVE graphics (png files) from Viz

STWAVE – All Stations in One Tar File

RNAME_STWAVE_All_Stations.tar -- *station.in*, *station.out*, *properties.log.gz

Run Info for CSTORM

RNAME_CSTORM_Data.tar -- MF.log.gz, MF####, adcirc.log.gz, stwave.logs.gz, fort.15.gz, *.sim.gz, mf_config.in.gz, *stat.151.gz, *station.in.gz, submit*, run_*, *.sh, *properties.log.gz

Visualization

RNAME_Viz_Data.tar – Visualization python scripts, run logs, etc.
RNAME_Viz_VTK.tar – VTK files for the ADCIRC and STWAVE grids

Report PDF File

RNAME_Report.pdf – Auto generated report containing graphics and statistics for the model simulation (ADCIRC and STWAVE)

Appendix F: Model and CSTORM File Descriptions

ADCIRC

Global Time-Series Files: *Global* means that there is a value given for each finite element node in the ADCIRC mesh. These files can be very large in size.

a. Fort.63 – the global time-series file for sea surface elevations above and below the geoid. Stored in units of meters.
b. Fort.64 – the global time-series file for the depth-averaged water velocities. Stored in units of meters/second.
c. Fort.73 – the global time-series file for the atmospheric pressure at sea level. Stored in units of meters of water.
d. Fort.74 – the global time-series file for wind velocities. Stored in units of meters/second.
e. Rads.64 – the global time-series of the *x*- and *y*-components of surface gradient stress tensors.

Global Max/Min Files: These files contain the maximum or minimum value over the entire model simulation time stored at each node location. Max/Min is over time.

f. Maxele.63 – maximum sea surface elevation. Stored in units of meters relative to the vertical datum of the ADCIRC mesh (fort.14, or *.grd) file used.
g. Maxvel.63 – maximum depth-integrated water velocity. Stored in units of meters/second.
h. Maxwvel.63 – maximum wind speed. Stored in units of meters/second.
i. Maxrs.63 – maximum magnitude of surface gradient stress tensor.
j. Minpr.63 – minimum atmospheric pressure. Stored in units of meters of water.

Station Files: These files contain time-series data at selected point locations (stations).

k. Fort.61 – station time-series file for the sea surface elevations above and below the geoid as defined by the vertical datum of the ADCIRC mesh. Stored in units of meters.

l. Fort.62 – station-time series file for the depth-integrated water velocities (u-,v- components). Stored in units of meters/second.
m. Fort.71 – station time-series file for atmospheric surface pressure. Stored in units of (meters of water).
n. Fort.72 – station time-series file for wind velocity (u- and v- components). Stored in units of meters/second.
o. Elev_stat.151 – file that defines the *x*- and *y*- (longitude and latitude) locations of the elevation stations.
p. Vel_stat.151 -- file that defines the *x*- and *y*- (longitude and latitude) locations of the water current (velocity) stations.
q. Met_stat.151 -- file that defines the *x*- and *y*- (longitude and latitude) locations of the meteorological (winds and pressures) stations.

STWAVE

Global Time-Series Output Files:

r. Break.out – global time-series file that contains the wave breaking indices information.
s. Rads.out – global time-series file that contains the x- and y-components of the gradients of surface stress tensor.
t. Tp.out – global time-series file that contains the peak wave period.
u. Wave.out – global time-series file that contains the significant wave height (meters), mean wave period (seconds) and mean wave direction (degrees).

Global Time-Series Input Files:

v. Surge.in – global time series file that contains the sea surface elevation adjustments. Units of meters.
w. Wind.in – global time series file that contains the wind speed (meters/second) and direction (degrees).

Local Time-Series Output Files:

x. Station.out – time-series file that contains the following data at specified *x*/*y* locations within the STWAVE domain which are specified in either the STWAVE *.sim file or in an external station location specification file (station.in):
   (1) Snap IDD – Time stamp or snap identification
   (2) X-location – station *x*-coordinate location (meters)
   (3) Y-location – station *y*-coordinate location (meters)
   (4) Significant Wave Height (meters)

(5) Mean Wave Period (seconds)
(6) Mean Wave Direction (degrees)
(7) Peak Wave Period (seconds)
(8) Wind Magnitude (meters/second)
(9) Wind Direction (degrees)
(10) Water Elevation (meters)

y. Selh.out – select height file that contains the following data at specified STWAVE i/j cell locations which are specified in the STWAVE *.sim file in the select point data section:
(1) Snap IDD – Time stamp or snap identification
(2) I-cell – STWAVE i-cell number
(3) J-cell – STWAVE j-cell number
(4) Significant Wave Height (meters)
(5) Mean Wave Period (seconds)
(6) Mean Wave Direction (degrees)

z. Obse.out – time-series file that contains the spectral energy values at the same STWAVE i/j cell locations contained in the selh.out file.

aa. Nest.out – time-series file that contains the spectral energy values at specified Nesting point locations (i/j cell locations). These locations are specified in the STWAVE sim file in the Nest Point Data section.

External Station Location Specification Files: Instead of a separate file, this information can also be stored in the STWAVE *.sim file in the Station Locations Data section.

bb. Station.in – File that contains the *x*- and *y*-locations of output stations where the output data will be stored in station.out. The coordinate values are in the same local coordinate system as specified in the STWAVE *.sim file.

CSTORM Data

STWAVE Run Log Files:

cc. Log.out.0000 – For a full-plane STWAVE simulation, this file contains the convergence data for every iteration performed during the solution process and is useful for debugging purposes. For the half-plane version, it contains the summary information for each snap showing the average wave height over the entire grid.

dd. Log.out.cmpct.0000 – Only produced by the full-plane version of STWAVE and contains a summary of the snap solution iteration and average wave height over the entire grid for that snap.

ADCIRC Run Log File:

ee. Adcirc.log – contains summary data at a specified time-step interval that shows the maximum water surface elevation and water current velocity as well as information about wind data being read in, etc.

CSTORM Run Log Files:

ff. MF.log – CSTORM coupler log file that shows the number of ADCIRC/STWAVE data exchanges and when they occur. Also contains simulation timing information.

gg. MF#### -- Directories produced by the CSTORM coupler (one for each STWAVE domain). Files contained in these directories:

(1) Fort.99 – run log for the coupler handling data between ADCIRC and the assigned STWAVE domain

(2) Adcstp.grd – ASCII file that contains the *x*- and *y*-locations of the ADCIRC mesh nodes in the local coordinate system used by STWAVE (e.g., StatePlane or UTM).

(3) Interp_tables – ASCII file that contains the interpolation weights used for interpolating between ADCIRC and STWAVE

(4) Offgrid.dat – ASCII file that contains interpolation weights for interpolating STWAVE points not contained in the ADCIRC mesh.

(5) Stwgeo.grd – ASCII file that contains the STWAVE cell center *x*-*y*-locations in geographic coordinates (degrees longitude and latitude).

(6) Stwstp.grd – ASCII file that contains the STWAVE cell center *x*-*y*-locations in the local STWAVE coordinate system. Typically StatePlane or UTM with units of meters.

CSTORM Control Files:

hh. Mf_config.in – ASCII file that contains the coupler information including the number of STWAVE grids, the number of computational processors to use, coordinate systems, and timing for ADCIRC and STWAVE starts, exchanges, and completions.

ii. STWAVE Sim Control File(*.sim) – ASCII STWAVE control file

jj. ADCIRC Control File (fort.15) – ASCII file that contains the ADCIRC simulation specific information

Appendix G: CSTORM-Pvz Options

The user can get help on options arguments by typing “python naccs_vizPlots_3.py –h”.

```
python naccs_vizPlots_3.0.py -h
Usage: naccs_vizPlots_3.0.py [options] stormNumber1 stormNumber2 ...

Options:
 -h, --help        show this help message and exit
 -p PROJDIR, --project directory=PROJDIR
                   full path of project directory
 -f FILETYPES, --files=FILETYPES
                   -f maxele.63, [default is ['maxele.63']]
 -d, --depth       Flag to plot depth of surge
 -c SCENARIO, --scenario=SCENARIO
                   scenario sub dir under project dir
 -o PLOTOPTSFILE, --plot optsf=PLOTOPTSFILE
                   plot options full path and filename
 -g ADCIRCGRID, --grid=ADCIRCGRID
                   Adcirc fort.14 grid filename in vtk format
 -m EMAILADDR, --mail=EMAILADDR
                   email address
 -q QUEUE, --queue=QUEUE
                   queue name
 -A ALLOCATION, --allocation=ALLOCATION
                   allocation code
 -u FEETMETERS, --units=FEETMETERS
                   units of results -> enter 'feet' or meters
 -r, --runCheck    Flag to check if run successful completion
 -z, --compress    Flag to submit compress_clean pbs script after viz
                   completion
 -s CSCRIPT, --script=CSCRIPT
                   name of compress_clean pbs script to submit
 -w, --waves       Flag to plot wave files set in optioins.viz file
 -a, --allwaves    Flag to NOT plot all wave files overlay
```

REPORT DOCUMENTATION PAGE

Form Approved
OMB No. 0704-0188

1. REPORT DATE (DD-MM-YYYY)	2. REPORT TYPE	3. DATES COVERED (From - To)
August 2015	Final	

4. TITLE AND SUBTITLE
North Atlantic Coast Comprehensive Study (NACCS) Coastal Storm Model Simulations: Waves and Water Levels

5a. CONTRACT NUMBER

5b. GRANT NUMBER

5c. PROGRAM ELEMENT NUMBER

6. AUTHOR(S)
Mary A. Cialone, T. Chris Massey, Mary E. Anderson, Alison S. Grzegorzewski, Robert E. Jensen, Alan Cialone, David J. Mark, Kimberly C. Pevey, Brittany L. Gunkel, Tate O. McAlpin, Norberto C. Nadal-Caraballo, Jeffrey A. Melby, and Jay J. Ratcliff

5d. PROJECT NUMBER
401426

5e. TASK NUMBER

5f. WORK UNIT NUMBER

7. PERFORMING ORGANIZATION NAME(S) AND ADDRESS(ES)
U.S. Army Engineer Research and Development Center
Coastal and Hydraulics Laboratory
3909 Halls Ferry Road
Vicksburg, MS 39180-6199

8. PERFORMING ORGANIZATION REPORT NUMBER
ERDC/CHL TR-15-14

9. SPONSORING / MONITORING AGENCY NAME(S) AND ADDRESS(ES)
USAE District, Baltimore
10 S. Howard Street
Baltimore, MS 21201

10. SPONSOR/MONITOR'S ACRONYM(S)

11. SPONSOR/MONITOR'S REPORT NUMBER(S)

12. DISTRIBUTION / AVAILABILITY STATEMENT
Approved for public release; distribution is unlimited.

13. SUPPLEMENTARY NOTES

14. ABSTRACT

This document summarizes the coastal storm wave and water level modeling effort performed in support of the North Atlantic Coast Comprehensive Study (NACCS). This effort involved the application of a suite of high-fidelity numerical models within the Coastal Storm Modeling System (CSTORM-MS). The study was conducted to provide information for computing the joint probability of coastal storm environmental forcing parameters for the U.S. North Atlantic Coast (NAC) because this information is critical for effective flood risk management project planning, design, and performance evaluation. CSTORM-MS modeling produced nearshore wind, wave, and water level estimates and the associated marginal and joint probabilities. Documentation of the statistical evaluation is provided in the companion report *North Atlantic Coast Comprehensive Study (NACCS) Coastal Storm Hazards from Virginia to Maine* (Nadal-Caraballo et al. 2015). In this study, both tropical and extratropical storms were strategically selected to characterize the regional storm hazard. CSTORM-MS was then applied with the wave generation and propagation model WAM, providing offshore, deep-water waves to apply as boundary conditions to the nearshore steady-state wave model STWAVE, ADCIRC to simulate the surge and circulation response to the storms, and STWAVE to provide nearshore wave conditions including local wind -generated waves. Products of this study are intended to close data gaps required for flood risk management analyses by providing statistical wave and water level information for the NAC within the Coastal Hazards System (CHS). The CHS is expected to provide cost and study time efficiencies and a level of regional standardization for project studies.

15. SUBJECT TERMS
Hurricane Sandy, Hydrodynamic modeling, NACCS, Numerical modeling, Statistical analysis, Water levels, Waves

16. SECURITY CLASSIFICATION OF:			17. LIMITATION OF ABSTRACT	18. NUMBER OF PAGES	19a. NAME OF RESPONSIBLE PERSON
a. REPORT	b. ABSTRACT	c. THIS PAGE			Mary Cialone
Unclassified	Unclassified	Unclassified	SAR	252	19b. TELEPHONE NUMBER (include area code) 601-634-2139